A computer based technique for predicting changes in bone properties with applications in pre-clinical testing of hip implants

Taylor, William R.

Award date:
1999

Awarding institution:
University of Bath

A computer based technique for predicting changes in bone properties with applications in pre-clinical testing of hip implants

Submitted by:
William R Taylor

For the degree of PhD
of the University of Bath 1999

ProQuest LLC
789 East Eisenhower Parkway
P.O. Box 1346
Ann Arbor, MI 48106-1346

Summary

Bone remodelling is an equilibrium process that occurs continually throughout the mature skeleton and is known to be a function of the loading environment. The replacement of a hip produces abrupt changes in the localised loading conditions in the proximal femur and will cause preferential remodelling. The resulting changes in bone mass can lead to the loosening of the implant over long periods of time.

A technique to model the long-term adaptation process of bone has been developed using the Finite Element Method. This approach used the standard ABAQUS Finite Element software to produce swelling strains within the cortical bone to represent remodelling growth and resorption. The method has been validated against the remodelling seen in the avian ulna experimental model (Brown et al. 1995), and the results demonstrated good agreement with the remodelling patterns in the ulna mid-shaft sections. Under the conditions presented by Brown et al, it was concluded that remodelling using the most tensile principal stress stimulus produced the best agreement. In addition, the remodelling of cancellous bone has been demonstrated in this study by altering the stiffness of the material in response to the applied stimulus.

A Finite Element model of the human proximal femur has been constructed from CT scan data and implanted with an Exeter stem. The resulting remodelling showed resorption in the calcar region of the bone under both strain energy density and most compressive principal strain stimuli. The predictions demonstrated good agreement with the current evidence regarding the stimulus to which bone remodels (Weinans et al. 1993, Rubin et al. 1990).

Acknowledgements

Without the opportunities presented to me, I would have undoubtedly been unable to remain in the beautiful City of Bath. My stay here has been both enormously constructive and immensely enjoyable, and there are a number of people I would like to thank for their contributions.

Perhaps most importantly, I would like to thank the Arthritis and Rheumatism Campaign (ARC) who have been more than generous to me in their financial support, which has been gratefully received. Their provision has made the entire study possible.

My family have managed to be supportive throughout the duration of my studies, and I must thank them all. They have experienced all aspects of my education, and endured very much the worse in me. They all deserve medals. My housemates also come into this category.

I would also like to acknowledge the following people, who have all helped with, and contributed to the work, each in their own way. HKS for the use of their software. Jon Dunn, who has managed to contribute from more angles than a very angular thing. Paul Everall, who has a remarkable ability to spot FORTRAN errors. Greg Starke, whose initial input gave significant momentum to the project. David Barker, who has put in a immense amount of time on the computers. Andrew Rees, Andrew Goldsmith, Ahmer Wadee, various members of BLDC, Biomob, and office.

There are, however, two people I must mention, without whose help this study would never have been completed. Their contribution has been outstanding. Matt Warner has assisted me with more than any normal friend would be able. His time has been given totally unselfishly, and his humour has kept more than just me laughing. I am proud to have worked with him. Lastly, and far, far from being least, I would like to thank Sally Clift, whose dedication and enthusiasm has been an inspiration. Her ability to nurture and to teach has been given in a manner in which only the best supervisors are able. I only hope that one day I may be able to repay their kindness. Thank you both.

I raise my glass to you all. Thank you.

Nomenclature

A	displacement
c	co-ordinate position
D	stiffness matrix
DDSDDE	Jacobian matrix
E	Young's modulus
G	shear modulus
K	attenuation coefficient
N	time increments
NN	number of different loading conditions
PS(n)	principal stress/strain (n=1 to 3)
S	compliance matrix
S(n)	stress/strain (n=1 to 6)
$\Delta\varepsilon$	stress increment
$\Delta\sigma$	strain increment
ε	strain
ρ	density
μ_t	relative attenuation of tissue
μ_w	relative attenuation of water
σ	stress
υ	Poisson's ratio
$\{F\}^n$	force vector
$[k]^n$	stiffness matrix
$\{\delta\}^n$	nodal displacement matrix

Abbreviations

CART	Computer Assisted Radio Tomography
CDH	congenital dislocation of the hip
CT	Computed Tomography
FE	Finite Element
FEM	Finite Element Method
FV	field variable
HKS	Hibbitt, Karlsson and Sorensen, Inc.
HU	Houndsfield Unit
PMMA	polymethylmethacrylate
SDV	solution dependent variables
SED	strain energy density
STATEV	state variable
THA	total hip arthroplasty

Glossary of medical terminology

Location within the human body is described using a number of terms to define orientation and position. The torso is assumed to take the so-called 'anatomical position' for the description of these terms, in which the body is upright with the head facing forward. The feet are together and arms are placed at the sides with the palms also directed inwards. The body is divided into three planes, the *frontal*, *sagittal* and *transverse* planes (Figure i), which are used to define the movement ability of joints. The *sagittal* or *median* plane divides the body longitudinally into right and left halves. Hence any structure which is described as *medial* to another is nearer the midline of the body. Likewise, *lateral* denotes the areas furthest from the centre line of the body, the hands, for example, are lateral relative to the elbows.

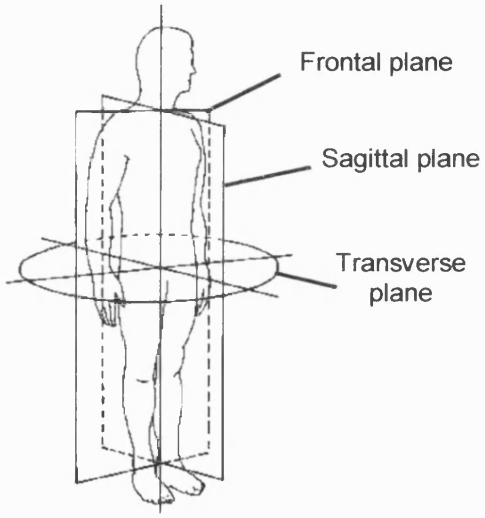

Figure i - Three planes of the human body [Frankel and Nordin 1980]

The *frontal* plane separates the front from the back of the torso. Objects that are described as being *anterior* or *ventral* are closer to the front of the body, and objects indicated as *posterior* or *dorsal* are towards the back of the body. The third plane, *transverse* plane, sections the body parallel to the ground. The term *superior* indicates a structure nearer the head, and *inferior* denotes away from the head, or towards the feet.

The terms *proximal* and distal are used when describing bones of the limbs. The *proximal* end of the bone is the one closest to the point of attachment whilst the *distal* end is furthest away.

Other medical terms used include;

acetabulum	concave indentation in the pelvic girdle
aseptic loosening	loosening without infection
cancellous bone	(also called trabecular bone) soft, honeycombed interior bone
condyle	smooth rounded projection at the end of the bone that contributes to a joint
cortical bone	(also called compact bone) hard, exterior bone
endosteal	inner surface of a long bone
in vitro	description of a procedure outside the body
in vivo	description of a procedure within the body
osteoarthritis	progressive degeneration of articular cartilage
osteon	cylindrical unit of compact bone structure built around a central vascular canal and composed of concentric bony layers
periosteal	outer surface of a long bone
physiological	of the body
rheumatoid arthritis	systematic disease of the immune system causing cartilage damage
trabecular bone	see cancellous bone
trauma	incident resulting in damage to a tissue
trochanter	roughened bony projection usually for the attachment of muscles or ligaments
voxel	volume element (3D pixel)

Contents

List of Tables and Figures

Tables

Figures

Chapter 1 Introduction

1.1 Introduction

There are a multitude of musculoskeletal disorders and degenerative diseases, such as rheumatoid arthritis and osteoarthritis, that can cause lack of movement, inflammation and perhaps worst, pain. Fracture or injury to bones can be caused by relatively low levels of trauma, especially in elderly patients, often predisposing abnormal loads in joints, and secondary arthritis. Due to the weight bearing ability of the joint, the hip tends to become one of the worst affected regions of the body, and whilst surgical intervention can attempt to diminish the problems, there is often the requirement to completely replace the joint. Total Hip Arthroplasty (THA) is the process of total replacement of the hip joint with the insertion of a femoral prosthetic implant and acetabular cup and it has, in recent years, become an increasingly popular procedure. In 1995, a total of 134,000 hips were replaced in the U.S.A. alone (AAOS, 1999).

The surgical replacement of the hip joint involves the insertion of an implant, usually down the shaft of the femur, most often using bone cement for fixation. The socket of the joint is reamed out and replaced with an acetabular cup that forms the bearing surface of the reconstructed joint. The head of the femoral implant is then seated in the cup, producing the ball and socket configuration joint (Semlitsh 1989).

For optimal design of artificial implants, a considerable understanding of the *in vivo* hip environment is required, and a good appreciation of the differences in conditions imposed by the body from general engineering situations must be gained. It has been estimated that the average person experiences approximately 300,000 loading cycles per year (Bundy, 1989). A prosthesis is generally considered a success after it reaches a ten year period, hence demanding over 3 million loading cycles. Additional problems can occur with tissue reactions to wear debris, generated as a result of friction within the reconstructed joint (Mathiesen *et al.* 1987). Perhaps most importantly of all, however, is an effect called bone remodelling which can lead to the loss of bone mass. Both of these problems can lead to eventual aseptic loosening of the prosthesis.

Bone is laid down in two distinct forms. The skeleton comprises primarily of cortical bone, which forms the hard shell like exterior surface. Cortical bone, or compact bone, is one of the hardest materials in the body. Cancellous bone (often called trabecular or spongy bone), on the other hand, is constructed in a honeycomb formation and is both less dense and has lower structural rigidity than cortical bone. It is found mainly within the cavities of long bones such as the femur and tibia.

The geometry of specific bones is believed to be both the result of genetic influences and the influence of local loading conditions. Bone has an innate ability for self-adaptation to its surrounding loading conditions. In his most famous work, 'The Law of Bone Transformation', published in 1892, Wolff observed that changes in the function of a bone were followed by certain definite changes in architecture, and he went on to suggest that the process was in accordance with mathematical laws (Treharne, 1981). The local stress-strain environment is now believed to be the primary factor underlying this mechanical adaptation process referred to as bone remodelling. Bone remodelling describes the process of continuous growth and resorption of cancellous and cortical bone in response to appropriate mechanical and chemical stimuli. It occurs by continual cell activity, both depositing and removing bone matrix, forming an equilibrium bone mass. This simultaneous process of bone growth and resorption allows replacement of old bone cells, healing of micro-fractures and cracks, and permits the bone structure to become more or less stiff in response to changes in the normal load bearing requirement. The bone thus adopts an optimum structure, compromising weight with required usage and strength.

The process of remodelling is similar in the two types of bone, and involves the laying down or removal of bone matrix from the surfaces of the bone. When viewed on a macro scale, however, the remodelling in the two different materials can be considered independent processes. Compared with trabecular bone, cortical bone is remarkably dense, and can be regarded as a solid structure (Figure 3.1). Cortical remodelling therefore only occurs on the shell or surface of the bone, resulting in an overall change in the thickness of the wall. The resulting change in the thickness of the cortical bone ensures an overall alteration in the stiffness of the structure.

Unlike cortical bone, cancellous bone has a large internal free surface area due to its honeycomb configuration (Figure 3.2). Remodelling in cancellous bone occurs through the deposition and resorption of bone matrix from the free surfaces of the individual trabeculae.

The resulting process varies the overall stiffness of the structure by becoming more or less dense. These internal changes due to remodelling can be viewed as an alteration to the stiffness of the bone.

There are currently a great number of theories regarding the aspect of loading that activates bone remodelling, but many remain based upon what has become widely known as Wolff's Law. Researchers continue to search for the exact mathematical laws eluded to by Wolff, but the stimulus is widely believed to be a function of strain rather than stress (Weinans *et al.* 1992, Davy and Hart 1983). Many alternative theories have been put forward including remodelling in response to strain energy density (Reitbergen *et al.* 1993), micro-fracture damage (Martin and Burr, 1982), and electromechanical effects (as discussed in Hart and Davy, 1989). Further discussion of the stimulus that invokes remodelling can be found in Chapter 4.

Whatever the exact signal, the occurrence of bone remodelling has several major implications after replacement of the hip joint. As a result of bone's ability to grow and resorb, the effects of bone loss due to a process called stress shielding have become of considerable interest. The effect involves the relatively rigid prosthetic implant sheltering or shielding the less stiff bone from the majority of stresses and strains normally seen by the natural femur under normal physiological loading conditions. As a result, the potential for the surrounding bone to remodel is reduced causing localised bone resorption leading to possible loosening of the implant.

Few researchers have modelled the process of long-term bone adaptation, with the majority concentrating on the reconstruction of the trabecular bone (Goldstein *et al.* 1991, Orr *et al.* 1990). The remodelling associated with cortical bone provides additional difficulties with alterations in the model geometry. With the exception of Mattheck (1994), who has studied simple two dimensional cortical remodelling with thermal expansion, Finite Element models until now have been based upon changing the nodal positions of the elements (Stülpner et al. 1997, Reitbergen *et al.* 1993). The strengths and limitations of these studies are discussed in Chapter 4.

The ability to mathematically model the long-term changes that occur in bone due to the effects of remodelling would allow predictions of long term prosthesis performance. Design improvement proposals can then be made. In addition, support can be given to theoretical and

experimental results, contributing evidence towards unknown variables such as loading environments and remodelling stimuli.

1.2 Project aims

This study aims to:

- Develop novel bone remodelling methodology using swelling routines which, integrated with commercial finite element code, would predict the long-term changes that occur due to remodelling in both cortical and cancellous bone

- Validate the code developed against previously published experimental data

- Develop F.E. models of a natural femur and a postoperative THA femur using CT scan data. Use these models together with the bone remodelling prediction software to both confirm the stress - strain environment in a human femur and predict the long-term bone geometry and density changes associated with THA. Compare predictions with published clinical evidence.

Chapter 2 Total hip replacement

2.1 Introduction

Since the pioneering work of Sir John Charnley in the early 1960's, total hip replacement has become a highly successful procedure with long term failure rates as low as 5% (Marston *et al.* 1996, Fowler *et al.* 1988, Eftekhar 1987). Long-term failures of implants are still, however, of major concern for younger patients, who may have several revision operations in their lifetime.

This chapter discusses the anatomy of the hip, including the tendons, ligaments and muscles that govern the movement of the joint (Section 2.2.1). The loading of the hip joint is then reviewed in Section 2.3, in order to establish the forces undergone by the hip. Finally, an examination is made of some types of implants and the main causes of their failure (Sections 2.5 and 2.7).

2.2 Anatomy of the hip joint

The hip joint is one of the largest joints in the body, and allows a wide range of movement to the leg. It is a ball and socket joint, and hence intrinsically stable, consisting of the rounded proximal end of the femur, or femoral head, and the concave indentation in the pelvic girdle, called the acetabulum (Figure 2.1). It has a high degree of mobility, allowing hip flexion of at least 120° and 20° extension (Frankel and Nordin 1980). In addition it allows at least 20° adduction and abduction.

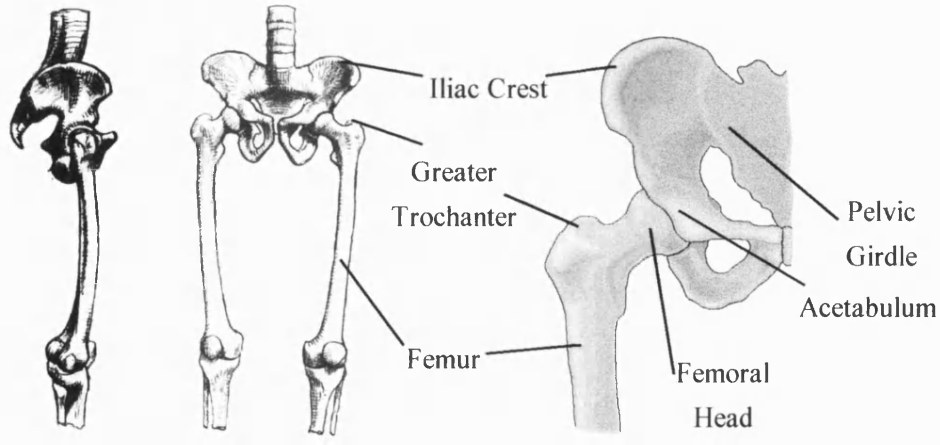

Figure 2.1 - Anatomy of the hip joint (Grundy 1982, Corel Corporation 1992)

The femoral head, which is approximately two thirds of a sphere, is covered in cartilage, except for the *fovea* where the ligament of the head of the femur, or *ligamentum teres* is attached (Figure 2.2). Blood vessels also enter into the femur at this point. Whilst the ligament is not of great strength, is does give a great deal of stability to the hip, and aids in holding the femoral head in the acetabular socket. Additional stability is given to the joint by the *labrum acetabulare*, a fibrocartilaginous ring inserted into the acetabular rim, which deepens the acetabulum considerably. Synovial fluid is located within the joint capsule, providing a lubricant to limit friction and reduce wear of the natural components (as described by Dowson, 1990).

2.2.1 Ligaments surrounding the hip

The periarticular ligaments are essential for the stability of the joint. The femoral head is enclosed by the *capsule* or *capsular ligament*, a form of cylindrical sleeve that surrounds the joint to retain the cartilaginous layers and synovial fluid. It is attached to the iliac bone at one end and the upper end of the femoral shaft at the other. It is composed of four distinct sets of fibres that give the joint stability in all articulating directions.

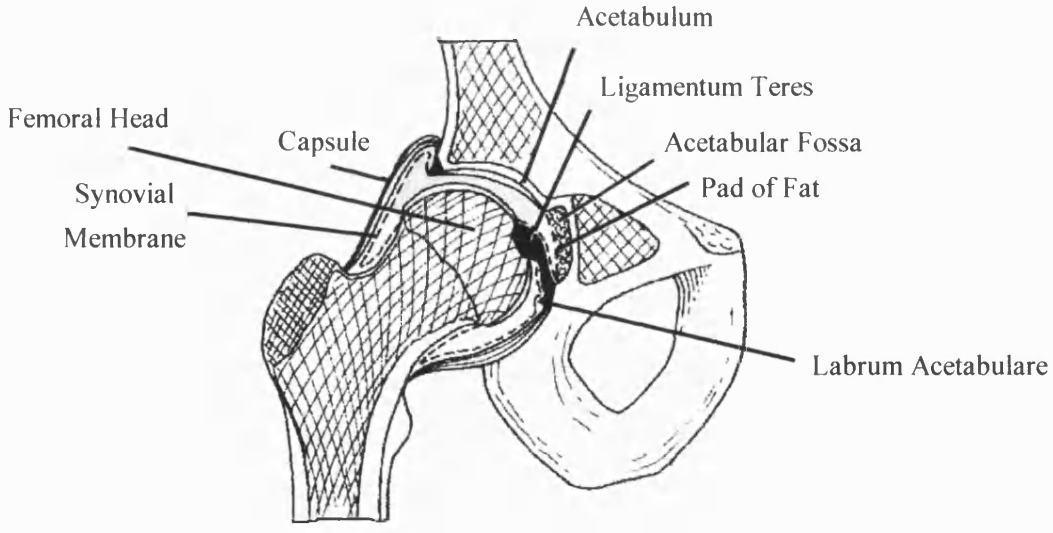

Figure 2.2 - Anatomy of the hip joint (redrawn from Grundy 1982)

Three main ligaments surround the capsule of the hip both anteriorly and posteriorly (Figure 2.3 & Figure 2.4). The *iliofemoral ligament* forms an inverted Y shape, splitting into two distinct bands joining at the anterior inferior iliac spine. The *superior, or iliotrochanteric band*, is the strongest of the ligaments of the joint, and measures 8 - 10 mm in thickness (Green and Silver 1981). It is laterally attached to the upper part of the trochanteric line (an

imaginary line connecting the femoral neck to the upper shaft of the femur), close to the greater trochanter. The *inferior band,* which forms the lower section of this ligament, connects to the lower part of the trocanteric line limits the extension of the hip in the erect, anatomical position. Together, the two parts of this ligament allow posture to be maintained without the requirement for flexor or extens

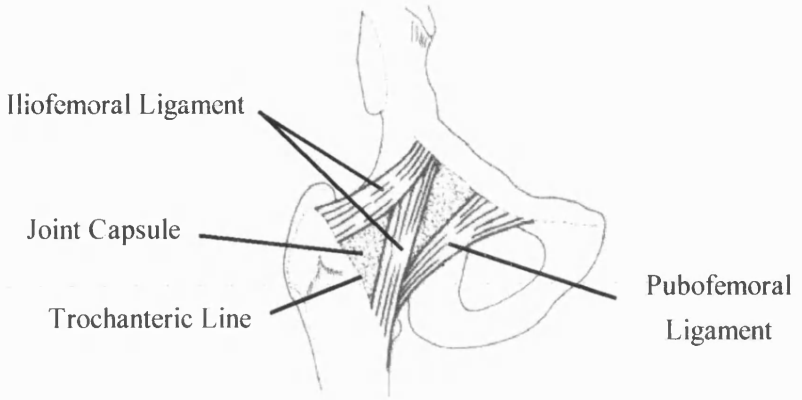

Figure 2.3 : Anterior aspect of hip ligaments (redrawn from Green, 1981)

The *pubofemoral ligament* is attached medially to the pubis and joins to the inferior part of the capsule. The *ischiofemoral ligament* is the only posterior ligament of the hip, and is connected at the posterior surface of the acetabular rim, joining to the inner surface of the greater trochanter. Since the ligaments all possess a slight natural rotation around the capsule, extension of the hip produces tension throughout. Likewise, flexion relaxes the ligaments due to the uncoiling action of the ligaments around the capsule.

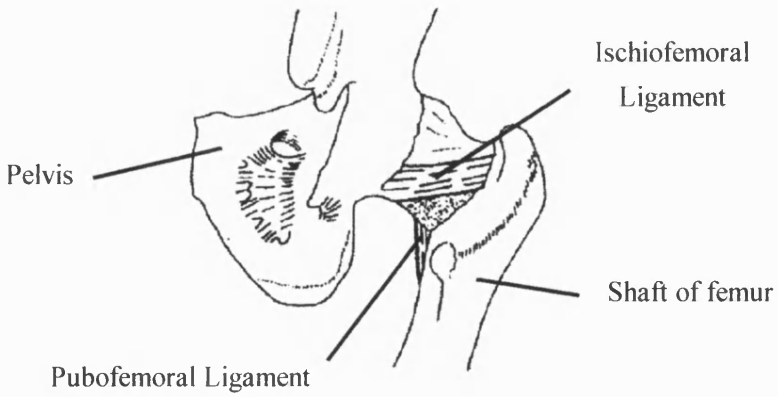

Figure 2.4 : Posterior View of Hip Ligaments (redrawn from Green, 1981)

2.2.2 Muscles surrounding the hip joint

The hip joint is encompassed by a number of muscles that enable movement in a variety of directions. Combinations of musculature actions give additional twisting and rotational movements. Figure 2.5 shows both the anterior and posterior views of the main muscles in the leg. Whilst the major muscles are described below, further information can be found in the literature [Green and Silver 1981, Kapandji 1970, Wilson 1990]

Extension of the hip is primarily caused by the *gluteus maximus*, the coarsest and the strongest muscle in the body. It has an approximate contraction length of 150 mm and is relaxed when the centre of gravity of the body falls behind the hip joint, when the iliofemoral ligament is in tension. Its action in straightening the bent thigh is assisted by the hamstring muscles (*biceps femoris, semitendinosus,* and *semiembranosus*), whose efficiency is dependent upon the angle of flexion.

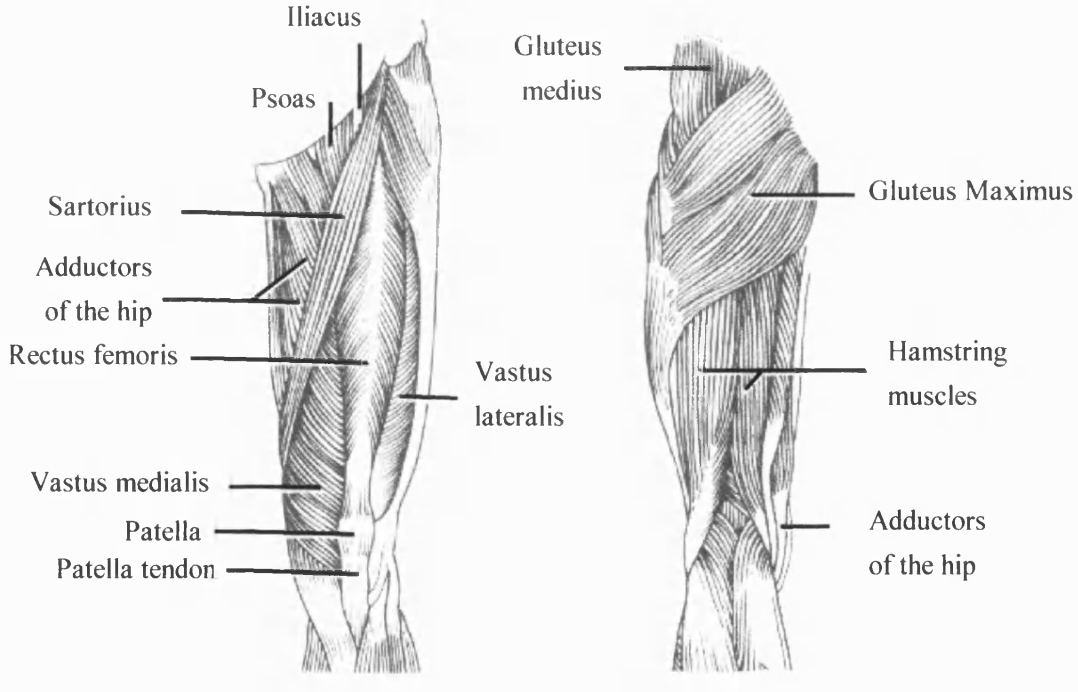

Figure 2.5 - Anterior and Posterior view of the main muscles of the lower limb (redrawn from Wilson, 1990)

The groups of muscle that lie anterior to the frontal plane though the hips centre cause flexion. They consist of the *psoas, iliacus, sartorius, rectus femoris*, *pectineus*, *adductor longus* and *gracilis*. Some of the forces created are not necessarily in complete flexion,

causing some secondary twisting or rotation, although the primary components produce lifting of the thigh.

The main muscle that causes abduction is the *gluteus medius*, which inserts into the lateral surface of the greater trochanter, and connects to the iliac crest. It has a direction of action almost perpendicular to its lever arm and is hence highly efficient. It is helped by the action of the *gluteus minimus* and the *tensor fasciae latae.* Although numerous muscles are able to pull the leg towards the body centre line, adduction is primarily caused by the action of the *adductor magnus,* which attaches to the inferior surface of the pubis.

All of the normal ranges of hip motions are obtained through forces applied by one or more of the muscles that surround the hip. Many of these muscles remain redundant during certain actions of the hip, and combinations of muscles are used throughout the gait cycle (Paul 1967). It is the action of these muscles, however, that produces the stress and strain environment described in Section 2.3, and that has been shown to be so important in the remodelling of bone (described further in Chapter 3).

2.3 Hip joint loading

Many of the muscles that influence the position of the hip and leg have been discussed in the previous section (2.2.2), but it is the loading environment that they transfer to the proximal femur that is of most interest to this study. There is still a great deal of discussion in the literature regarding the loading conditions on the proximal femur during recognised actions such as one-legged stance and stair climbing. There is, however, general agreement that the hip withstands loads of many multiples of body weight during these simple tasks (Adams and Swanson 1985, Paul 1967, Lu 1997). Figure 2.6 shows the general trends of force variation that occurs in the hip of a normal male during walking. The values of hip joint load were adapted from Paul (1967).

In terms of the longevity of implants, one of the most significant studies into the loading of the hip was conducted by Lu *et al.* (1997) who examined the influence of muscle activity on the loads measured by *in vivo* prostheses. Massive femoral implants in two patients were capable of relaying force data, with additional information being provided by force plates and EMG signals from surface electrodes attached to the muscle groups. The subjects were exposed to isometric and gait tests and the results showed that the force in the femoral implant was up to

3.5 times as large as that seen by the force plates. Corresponding axial forces of up to 2715N were seen by the prosthesis.

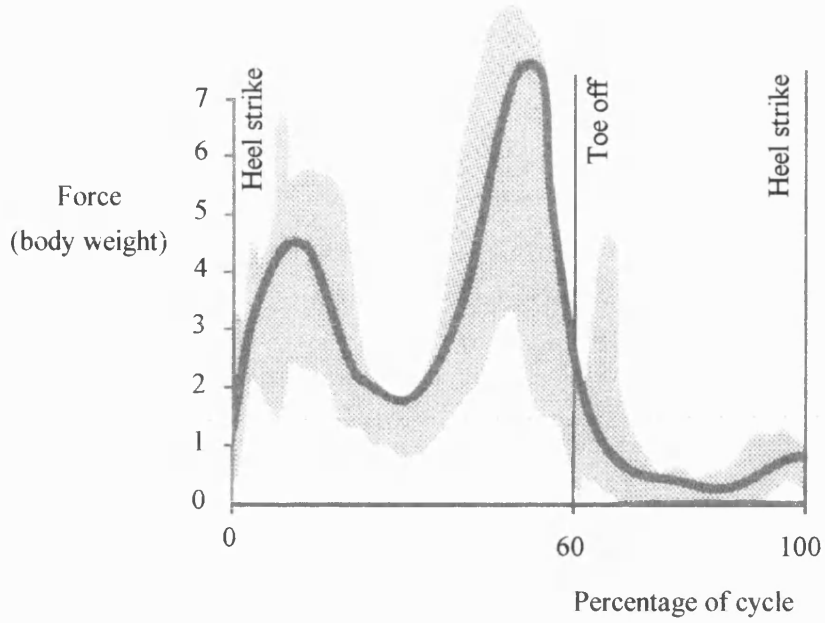

Figure 2.6 - Variation in hip joint loading during walking (redrawn from Frankel and Nordin 1980)

The importance of these results is that an implant must be capable of carrying several magnitudes of body weight in order to perform the most basic of tasks demanded of it. Further examination of the modelling of the exact mechanical loading environment to which the hip joint is exposed is discussed in Chapter 4.

2.4 Failure of natural hip joints

The human hip joint is susceptible to failure through a wide variety of reasons. The majority of problems, however, are associated with two main groups of disorders. The first, trauma of the joint, is primarily seen in severance of the femoral neck. This outcome is most frequent in the elderly, whose bones are subject to mechanical decline, including brittleness and a reduction in ultimate stress and strain (McCalden *et al.* 1993). The age related loss of bone matrix was cited as the major reason for the reduction in the materials properties, linked directly with the increasing porosity of the bone. The increasing brittleness was associated with large changes in the post-yield behaviour of bone.

The occurrences of a number of bone diseases, especially osteoporosis, also increase the chances of traumatic failure. The disorder involves an alteration in the relative rates of deposition and resorption of bone matrix, resulting in a decrease in bone mass (Wilson 1990). The consequence of the condition, which is primarily seen in post-menopausal women, is a reduction in structural strength of the bone.

Trauma of the joint has considerable consequences in young patients who may have experienced a motoring accident, for example. Total reconstruction of the joint provides one of the only solutions, but the demanded life span of the implants is far greater than in the elderly. Preservation of the bone stock under these conditions is essential.

Perhaps the predominant surgical group requiring total hip arthroplasty, however, are patients suffering arthritis, particularly rheumatoid arthritis, which is usually associated with ageing. The disease is a chronic inflammatory condition that affects the synovial membrane, leading to cumulative damage of the joints. The condition leads to increasing pain, deformity and inflammation of the joint, often leading to loss of function. Secondary effects of the disease include erosion of the articular cartilage and atrophy of muscles (Wilson 1990). Surgical intervention can often diminish these problems, but ultimately replacement of the joint may be required. In addition, the procedure can provide a corrective technique for a wide range of skeletal disorders and abnormalities. Total replacement of the joint provides a complete solution to what might otherwise be irreparable.

2.5 Implant design

The concept of totally replacing the hip joint was first pioneered over thirty-five years ago when Charnley began implanting his design of stem into human patients. The design of implants has changed remarkably little since then, with various aspects being developed, but still based on the idea of a femoral stem and acetabular cup. A wide variety of implant designs are currently available. Whilst some more unusual designs such as the Trust Plate Prosthesis (Bereiter *et al.* 1991) exist, two main types are most commonly used; cemented implants and uncemented, press-fit stems.

2.5.1 Non-cemented implants

Without cement, implant fixation depends wholly upon the tight apposition of the metal to bone interference fit. The majority of stems are straight, and as a result, the contact with the curved femoral shaft is incongruent and occurs unevenly at points of contact. The force with which they are initially compressed into the shaft of the femur is aimed to create the tight interference fit required for integration with bone. An implant designed for cementless mechanical press-fit hold within the proximal femur is shown in Figure 2.7.

Several techniques are used to increase the long-term stability of cementless prostheses. Rough surfaces are designed to allow boney in-growth of the cancellous matrix and many use a coating of hydroxyappitite to encourage bone apposition. In addition, the shafts of some implants are produced with cavities or holes to allow the bone to fully integrate into the prosthesis.

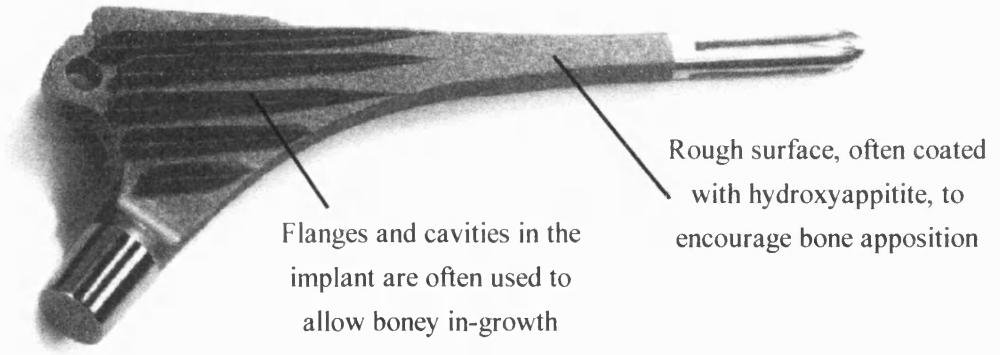

Figure 2.7 - Press fit cementless hip prostheses

Cement and metal to bone contacts are not mutually exclusive, however. Some stems, the Muller straight stem, for example, are designed to use cement as a grouting to areas not occupied by metal to bone contact. Each of the designs have relative merits which will be discussed further in the chapter.

2.5.2 Cemented prostheses

The majority of hip implants use cement fixation techniques. Cemented prostheses are seated within the femoral shaft surrounded by a mantle of bone cement, composed of polymethylmethacrylate (PMMA), for fixation. The cement mantle is designed both as a load-

mediating compliant layer between the bone and the rigid prosthesis, and as a method of accommodating any geometrical inconsistencies.

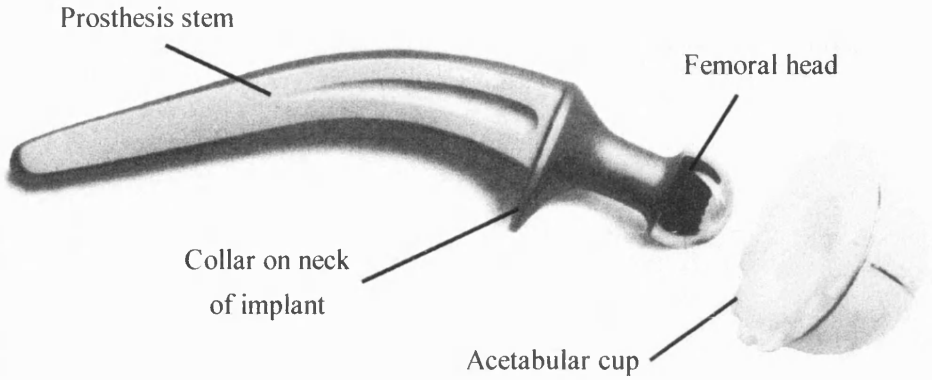

Figure 2.8 - Charnley hip prosthesis

It has been suggested that the cement mantle provides greater ability to transfer load from the femoral implant to the surrounding endosteal bone (Fowler *et al.* 1988). In addition, creep or stress relaxation of the acrylic cement may accommodate long-term variations in the geometry of the bone due to remodelling or age related effects. Uniform load distribution can therefore be achieved over long periods of time.

2.5.3 The Exeter Hip System

Total hip replacement using the Exeter stem (Figure 2.9) was first performed in the autumn of 1970 in the Princess Elizabeth Orthopaedic Hospital, Exeter. When released, it was unique in respect to a number of design features. Primarily, it was the first implant without any form of collar on the femoral component, but it also included a double tapering stem section to allow extrusion of the cement mantle during insertion into the femoral canal (Fowler *et al.* 1988).

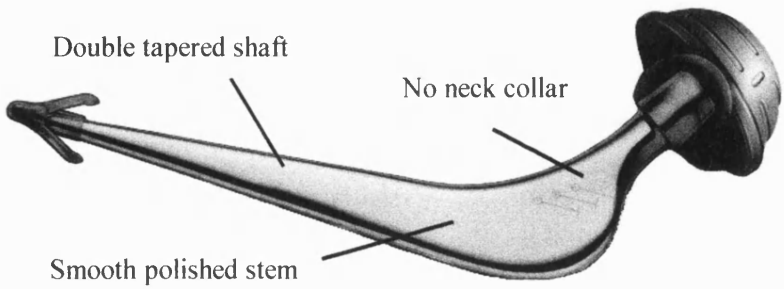

Figure 2.9 - The Exeter Hip System

Since these original operations, several design modifications have been made. In 1976 the stem changed to a matt finish, although this was later regarded as retrograde, and the polished stem was reintroduced in 1986 (Fowler *et al.* 1988). The stem is now available in a series of sizes, with stem midline to head centre offset ranging from 37.5 mm through to 50 mm, each set with a number of stem thicknesses. Two stems are also made specifically for cases of Congenital Dislocation of the Hip (CDH) with offsets of 35.5 mm and 37.5 mm. In addition, the implant now has interchangeable heads on a Morse taper stem, varying in diameter from 22 mm to 32 mm. The stem is made from Orthinox, a high strength, low corrosion stainless steel, with fatigue properties similar to that of high strength vitallium.

2.6 Surgical procedure

Total replacement of the hip joint initially involves taking pre-operative X-rays of the proximal femur and acetabulum region of the patient. From these, the surgeon is able to select the appropriate implant size from transparent templates that allow a range of component profiles to be compared to the patient's hip. The profile templates are laid over the X-rays such that the femoral head centre and the midpoint of the prosthesis head are coincident. The centreline of the shaft of the implant must then lie along the imaginary midline of the proximal femur. Allowances must be made for the thickness of the cement mantle, and the component is selected based upon the closest fit. Occasionally, it may be necessary to pick the implant based on the contralateral hip due to severe deformation.

After incision, the hip is dislocated to expose the full proximal femur, and the femoral head is removed by sectioning at the neck of the femur. Although the location of this cut is essential for correct post-operative leg length in collared implants, resection position using the Exeter stem is not critical since the device has no features which affect the line of resection (Howmedica 1992).

The long axis of the medullary canal is then manually reamed, removing the majority of the trabecular bone from within the calcar until a thin layer of approximately 2-3 mm remains. Less bone is removed if cementless stems are being used. In the case of cemented implants, this layer provides a strong foundation for interface micro-interlocking between the cement mantle and the bone.

The acetabulum is then drilled out in a similar manner using grater reamers to remove all remnants of articular cartilage and to shape the cavity. The cement is then mixed and left until stiffening commences. The cavity is washed, cleaned and dried to remove remaining blood before the cement is inserted into the recess. The acetabular cup is positioned under considerable pressure in order to overcome the viscosity of the cement.

A trial femoral component is implanted into the proximal femur and comparing the relative positions of the femoral condyles assesses correct restoration of leg length. Alteration can occur by compensation of the level of stem insertion. The femoral shaft is cleaned to extract remaining bone marrow and blood in order to prevent contamination of the cement. An intramedullary plug is driven into the femoral shaft, approximately 170 - 180 mm distal to the tip of the greater trochanter, in order to restrain the cement from free flow down the medullary canal. Cement is then introduced into the femur using a cement gun, and the implant is carefully driven into the canal. In the case of cementless implants, no cement is introduced, and the prosthesis is press fitted under considerable pressure.

The appropriate size femoral head is then placed over the stem spigot, the joint is reconstructed with the head carefully inserted into the acetabular cup, and the surrounding tissue repositioned.

2.7 Failure of replacement hips

Although the success rates of hip replacements are high, a small percentage, some 4 - 8 % still fail within ten years post-operatively (Eftekhar, 1987, Bannister 1988, Griss, 1982).

Failure of implants can be categorised into short and long-term failures. Initial, short-term failures are considered over a period of weeks or months postoperatively. They are most often due to infection, surgical technique, poor initial cementing, and thermal necrosis of the bone from the high temperatures created by the cement.

More significantly in terms of this study, however, are the long-term failures of the joint, which necessitate revision surgery. A wide variety of factors including bone quality, levels of physical activity, age and obesity of the patient, and design of the implant all influence the long-term integrity of the reconstructed joint. Most long term failures, however, can be

attributed to two main factors. Firstly, fatigue of the cement mantle or the acetabular cup cause particles of PMMA or polyethylene wear debris to be generated, leading to bone necrosis, and eventually loss of stability of the joint. The other main mode of failure concerns the maintenance of sufficient bone density around the implant. Abrupt changes in the local loading conditions can alter the growth patterns of the bone: This effect often occurs around implants by altering the density of the surrounding bone, and is referred to as bone remodelling. Over longer periods of time, this effect plays a crucial role in bone loss and can lead to loss of support and therefore loosening of the prosthesis. If the process continues, total failure of the joint can occur.

Figure 2.10 demonstrates both lysis and hypertrophy around an Exeter stem. It is important to notice the deposition of bone matrix on both the periosteal and endosteal surfaces of the medial femoral shaft. This is a result of long-term remodelling often seen around this design of stem (Bannister 1993). It is possible to use the evidence of this sclerosis to validate the clinical relevance of modelling predictions. In addition, cortical resorption is seen in the areas surrounding the greater trochanter.

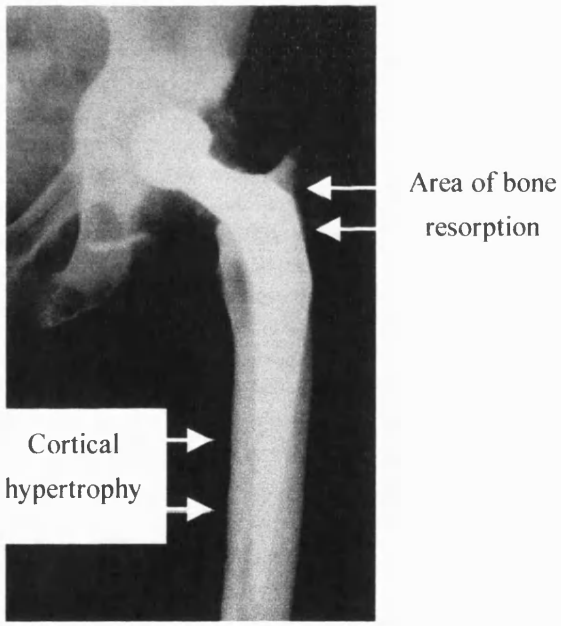

Figure 2.10 - Radiograph showing results of long-term remodelling (Bannister 1993)

This remodelling effect is especially significant in the modes of failure of modern implants. Reduction in bone mass around, or total resorption away from the surface of an implant can affect or even initiate tipping or pivoting of the prosthesis. Figure 2.11 shows cortical

resorption at the end of the Mark 3 Ring prosthesis allowing tipping of the implant at the femoral collar.

Figure 2.11 - Tipping of the mark III Ring prosthesis (Bannister 1993)

Bannister (1988) compared the modes of failure of the Muller straight stem (small collar), the Muller curved stem (larger collar) and the Exeter (collarless) prosthesis that had survived a 10 year or greater period. The most notable difference in the stem designs concerned the neck of the femoral component. It was found that the integrity of the stem was directly related to the X-Ray lucency at the bone - cement interface. The formation of osteolytic cysts and migration of the implant into the varus position were strongly associated with the need for revision surgery. In addition, the occurrence of cement mantle subsidence within the bone (or pistoning of the cement mantle at the bone - cement interface) was five times as frequent in the revision hips. Perhaps the most notable observation, however, was that subsidence of the implants within the cement mantle (at the stem - cement interface) was five times as common in the prostheses that survived.

It was suggested that the allowance of this subsidence of the stem influenced the modes of failure of the implants. The analysis showed that failure due to pistoning of both the implant and cement within the bone was observed in three times as many revision cases as controls. This mode of failure was seen 6 – 7 times more frequently in the Muller curved stems as the Exeter prosthesis.

This observation is supported by Fowler *et al.* (1988) who examined the history of the Exeter stem. Subsidence of the implant within the cement mantle appeared to benefit the long-term integrity of the joint. It was suggested that the capability of the implant to transfer load to the surrounding bone was improved by the movement of the implant within the cement. The taper of the stem appeared to induce lateral creep of the proximal cement, resulting in continued engagement of the cement mantle with the bone. Experiments went on to show that the stem - cement interface friction in the matt version of the stem was over double that of the polished counterpart. The reduced performance of the matt stem was attributed to the resulting lack of subsidence of the implant. As a result, the smooth polished finish replaced the implant matt surface. The study went on to imply that any device which might interfere with the subsidence of the stem at the stem - cement interface, and prevent distal movement from occurring (e.g. collars, flanges, texturing of the surface) would alter the engagement of the taper. As a result, reduction of the load transfer capability would occur, especially in the proximal regions.

Marston *et al.* (1996) carried out a long-term study evaluating the differences between the Charnley and the Stanmore cemented prostheses in order to investigate, amongst other things, the effect of the femoral head size on longevity. A sample of 213 Stanmore and 200 Charnley implants were reviewed at 5 to 10 years (mean 6.5) post-operatively. No statistically significant difference in the rate of revision surgery was recorded between the stems (both resulted in a revision rate of 4.0%), and no difference was found in the effect of the size of the femoral head. Surprisingly, approximately equal subsidence was reported in both stems, despite the large collar on the Stanmore. The mode of failure was not studied.

In his PhD thesis, Bannister (1993) made a number of observations relating to the integrity of the replaced joint. He concluded that surgical technique alone demonstrated the potential to reduce rates of revision in cemented femoral components by 28%. He went on to suggest that a combination of good surgical technique and a prosthesis that elicits a favourable biological response should reduce aseptic loosening by some 55%.

One important observation was made by Sochart *et al.* (1998), who studied the long-term results of THA using the Charnley implant in patients aged less than 30 years. The study showed implant survival rates of 70% after 25 years postoperatively, but importantly, implant loosening was strongly associated with the occurrence of bone resorption.

2.8 Summary

This chapter has highlighted the procedure and methods involved in the total replacement of a human hip. Some of the problems associated with the long-term stability of the implants have been discussed, emphasising the continuing need for improvement in the longevity of the reconstructed joint.

The geometrical design of the implant plays an important role in the remodelling response of the bone. The most obvious difference is seen in the study of the performance of prostheses with collars against those that have none. The examination and possible prediction of the long-term performance of various geometries of stem could provide a tool to aid in design analysis and eventually reduce the surgical revision rates.

Chapter 3 Biomechanics of bone

3.1 Function of bone

The human skeleton is primarily made up of three components: bone, muscle and connective tissues (including tendons, ligaments and body organs such as the heart and liver etc.). Neither muscle nor any of the connective tissues have any significant stiffness in shear (Currey 1984), so the primary structural support for the body is provided by bone. Its highly calcified composition gives the material immense rigidity whilst its lightweight makeup yields a high strength to weight ratio, allowing it to become a principal component for all forms of vertebrates.

In addition to providing structural support for the body, bone performs a multitude of functions. It supplies attachment sites for muscles, tendons and ligaments, acting as a rigid lever system allowing effective muscle action and hence functional movement. In addition, bone aids in protection of the vital internal organs such as the brain and heart and serves as a reservoir for numerous ions. The skeleton is also important metabolically as it regulates fluids in the body.

3.2 Macro structure of bone

Bone is formed in two distinct configurations in the mature human skeleton (Figure 3.1). Cortical or compact bone is the hard dense exterior surface that generally surrounds the marrow cavities in the shafts of the long bones. With the exception of microscopic channels, it can be considered of solid, dense construction.

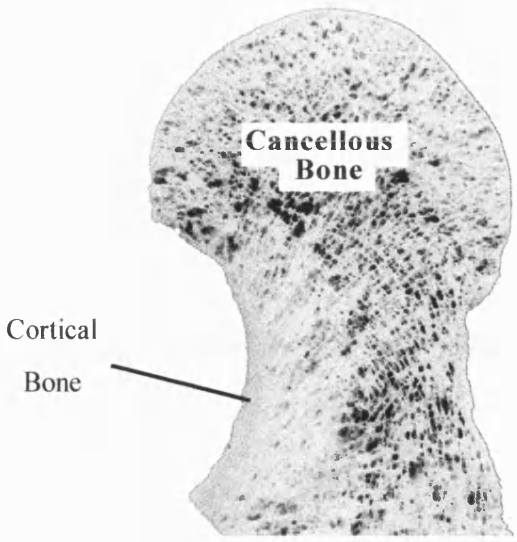

Figure 3.1 - Cortical and cancellous bone (Bouvier 1989)

Cancellous or trabecular bone, in contrast, is organised in a lattice structure, joined by rods and plates known as trabeculae (Figure 3.2). This honeycomb type arrangement gives the bone a spongy appearance. Unlike cortical bone, which accounts for approximately 80% of the adult skeletal mass, cancellous bone is primarily confined to the central cavities within the cortical shell, generally in the long bones of the body.

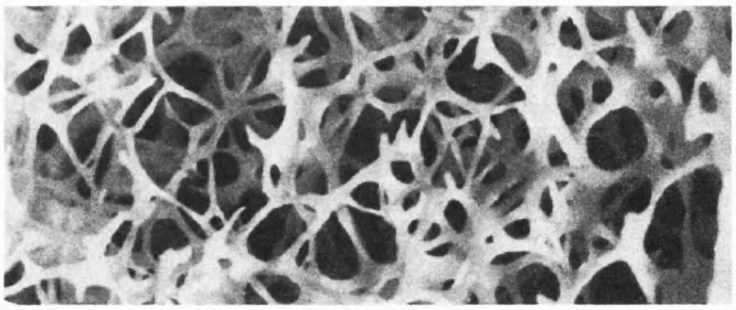

Figure 3.2 - Morphology of trabecular bone (Jee 1988)

3.3 Microscopic structures of bone types

Bone has a highly complex structure that is made predominately of extracellular matrix and living cells. The matrix constituent of bone consists of two phases. The first is organic and composed primarily of protein, glycoprotein and polysaccharide, which form collagenous fibres. The second is inorganic, consisting mainly of calcium phosphate crystals, making up the mineral phase.

The living component of bone consists of five main cell types; osteocytes, osteoclasts, osteoblasts, osteoprogenitor cells and bone-lining cells (Bouvier 1989, Vaughan, 1981, Jee 1988). The first three are considered the most important for the maintenance of bone. Osteoblasts are bone forming cells. They secrete osteoid or unmineralised bone matrix, which is the initial step in the bone creation process. Osteoclasts, on the other hand are bone removal cells. They are giant multinucleated cells that are responsible for the resorption or removal of bone matrix, ranging from 20 to over 100μm in diameter and containing from 2 to 50 nuclei. Osteocytes differ from the other bone cells as they appear to have no function, but are, in fact, osteoblasts which have become trapped in their own secretion of bone matrix. They are housed in lacunae and develop an extensive communication network via small capillary like tunnels called canaliculi. The schematic structure of a section through the shaft of a long bone is shown in Figure 3.3.

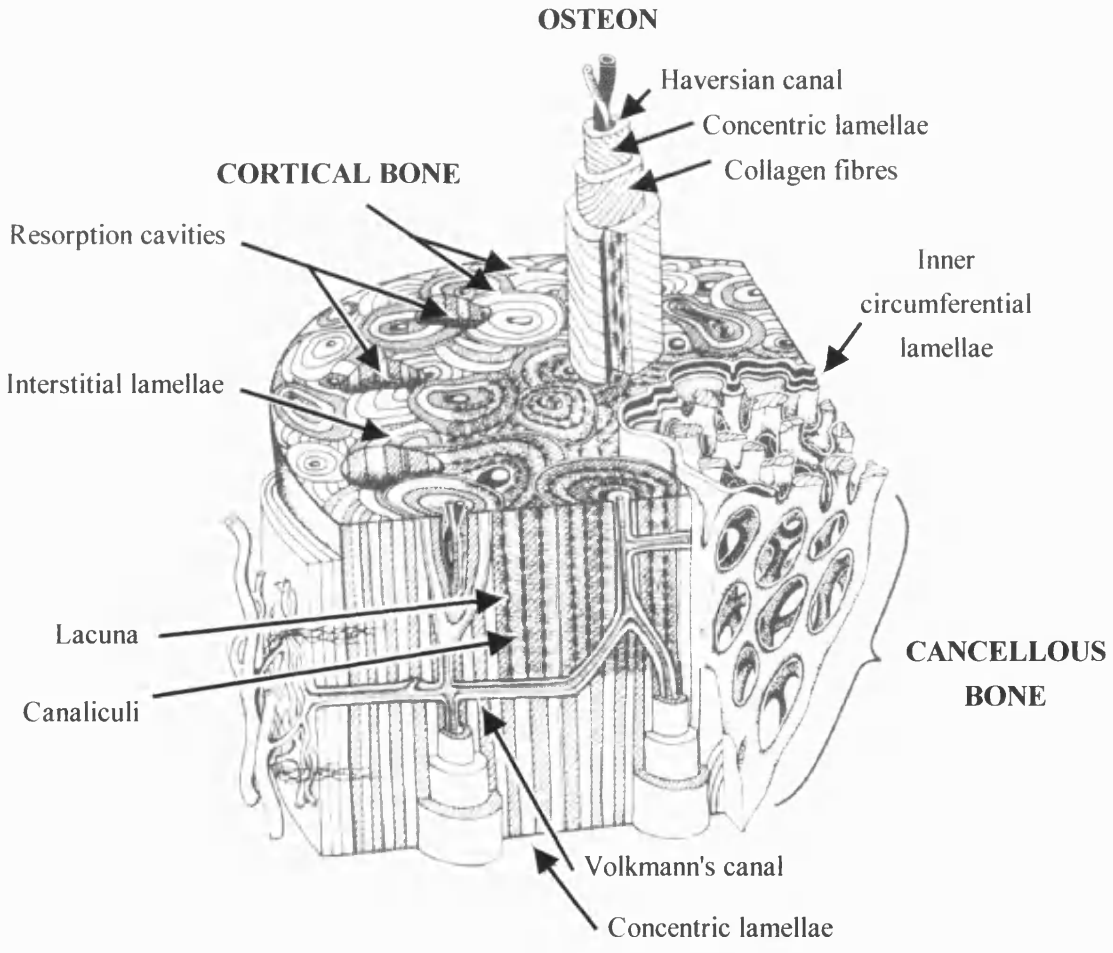

Figure 3.3 - Schematic section through the shaft of a long bone (Jee 1988)

Despite the variety of external forms in the skeleton, the morphology of bone at organ, tissue and cellular levels is relatively consistent. Each osteon consists of a central canal, which

contains nutrient vessels, nerves and other connective tissue. Surrounding this canal are layers of bone matrix called concentric lamellae, which are designated surface or circumferential lamellae when located on the external surface of the cortical bone or touching the periosteum. Channels oblique to these are called Volkmann's canals, which allow communication between the Haversian canals, and can be differentiated due to the lack of concentric lamellae.

Whilst all bone contains a similar structural makeup, it is laid down in stages before it is considered mature, or secondary bone. The stages of bone maturity are determined by different levels of structural organisation. The product of quick formation is called woven bone, which is often deposited in poorly organised, random orientations. As a result, the density of woven bone is low. It can be formed with no previous hard tissue or cartilage structure and so provides an ideal framework for the development of a boney structure. Periods of rapid bone growth, following fracture, for example, are hence often associated with woven bone formation, where repair is required under conditions where tension may remain.

Primary, or lamellar bone, is a highly organised, regularly layered tissue with a much greater mineral content than its woven counterpart. Unlike woven bone, primary bone requires the presence of pre-existing substrate before growth can commence. In general, it replaces the less mature woven bone, which is weaker but quicker in formation.

The product of previously existing tissue, or primary bone, that has undergone secondary reconstruction, is called Secondary bone (discussed in Bouvier 1989). This process of internal reconstruction enables the construction of extensive communication networks as seen in Figure 3.3. In cortical bone, the result is the creation of a secondary osteon. Once the secondary remodelling network is complete, the bone is considered mature (and receptive to mechanical remodelling).

3.4 Mechanical properties of bone

Bone provides the majority of the structural strength and stiffness of the human skeleton. There are several fundamental problems with quantifying the engineering properties of bone, however, since its composition differs with a great number of variants, including species, age, sex, health, and even the specific bone in question (McCalden *et al.* 1993, Currey 1984). Any measured property is thus subject to a great deal of variation from bone to bone.

When attempting to model any engineering material, knowing the elastic behaviour is of prime importance. The elastic constants give detailed information about how a material will deform under load. Problems arise, however, with linear elastic approximations to model the behaviour of bone, since bone has long-term growth patterns due to remodelling, age, health etc. that mean that the so called elastic constants are able to vary. Nevertheless, for the purposes of short term modelling, measurements of the elastic constants of bone are useful.

Bone has been shown to display biphasic properties, in which the interstitial fluids affect the compressive behaviour of the structure. The porous properties of bone have been studied by Carter and Hayes (1977), who examined both bovine and human bone. One hundred cylindrical specimens of trabecular bone were tested with and without the presence of bone marrow to determine the effect of the viscous flow. The study, which worked on the assumption that the solid phase of both trabecular and compact bone displayed the same properties, calculated a relationship for the compressive strength of bone relating the stiffness to both the apparent density and strain rate of the loading:

$$E = 3970\dot{\varepsilon}^{0.06}\rho^{3}$$

where E is the elastic modulus (MPa), $\dot{\varepsilon}$ is the strain rate (s^{-1}), and ρ is the apparent density (g cm^{-3}). For this relationship to be able to calculate the Young's Modulus, a value of strain rate must be assumed. The strain rate to which bone is normally subjected ranges from 0.001 s^{-1} for slow walking up to a value of 0.01 s^{-1} for vigorous activity, hence finding that the stiffness of bone can vary up to as much as 15% during normal activity. A strain rate of 0.01 s^{-1} is regularly used (Keyak *et al.* 1990, Skinner *et al.* 1994). This relationship is frequently used for modelling purposes where medical imaging data is available, since it is able to calculate the stiffness of bone as a function of its density.

Whilst this relationship provides a general relationship for human bone, a great deal of work has been done examining the properties of bone, localised to either the cortical or cancellous regions. These are detailed in the following sections.

3.4.1 Cortical bone

The mechanical properties of cortical bone have been measured is several studies, and it can be seen from Table 3.1 that the stiffness of cortical bone varies in the orthogonal directions. This indicates full anisotropy of the material, although properties in the radial and circumferential directions are similar in all studies, indicating that transversely isotropic material properties may be a useful approximation.

Group	Reilly and Burstein (1975)	Yoon and Katz (1976)	Ashman *et al.* (1984)
E_1 (GPa)	11.5	18.8	12.0
E_2 (GPa)	11.5	18.8	13.4
E_3 (GPa)	17.0	27.4	20.0
G_{12} (GPa)	3.6	7.17	4.53
G_{13} (GPa)	3.3	8.71	5.61
G_{23} (GPa)	3.3	8.71	6.23
ν_{12}	0.58	0.312	0.376
ν_{13}	-	0.193	0.222
ν_{23}	-	0.193	0.235
ν_{21}	0.58	0.312	0.422
ν_{31}	0.46	0.281	0.371
ν_{32}	0.46	0.281	0.350

The three direction was the long axis of the bone with one and two being the radial and circumferential directions respectively.

Table 3.1 - Elastic constants of cortical bone (As summarised by Cowin 1989)

In these studies, the properties of the bone specimens were calculated by ultrasonic techniques, apart from the experiments by Reilly and Burstein (1975), which were carried out using uniaxial compression tests. The values of Poisson's Ratios which exceeded 0.5 were accounted for by the kinematic nature of the material.

In addition, cortical bone stiffness can also vary with anatomical site. Ashman *et al.*(1984) demonstrated how the axial Young's Modulus varies around the circumference of the human femur (Figure 3.6).

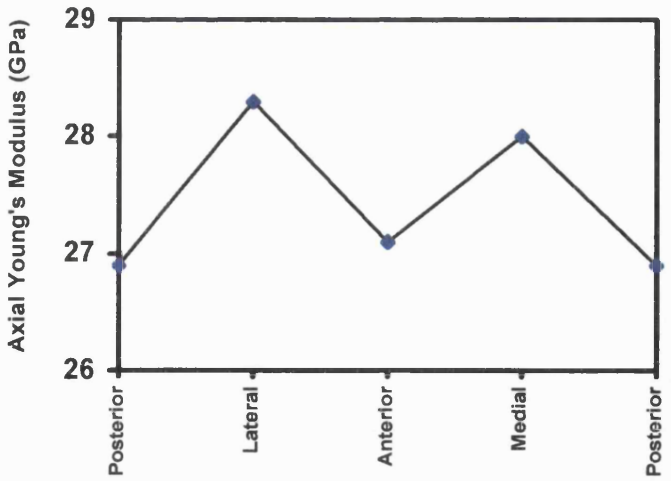

Figure 3.4 - Variation of the axial Young's Modulus around the circumference of a human femur (redrawn from Ashman et al. 1984)

It can be seen that the elastic constants of compact bone vary with position around the shaft of the bone. Similar results were gained regarding the location with respect to the length of the shaft, with the highest properties found at the mid-shaft sections. This demonstrates that the material properties are highly dependent upon a number of factors and that determination of the properties is difficult. The ranges of elastic constants between two studies (Reilly and Burstein, 1975 and Yoon and Katz, 1976) suggest that the material properties of the bone could be approximated to either homogenous or transversely isotropic.

3.5 Mechanical properties of cancellous bone

The fundamental difficulty with measuring the mechanical properties of trabecular bone is determining the size of specimen that is representative of the overall structure, which includes the spaces in between the trabeculae. The relationship between the mechanical properties of trabecular bone in tension and compression has been investigated by Rohl *et al.* (1991). Non-destructive testing of cancellous specimens from 11 human proximal tibiae (7 cadavers) was carried out in either tension or compression. Up to 0.6% strain was loaded for the duration of the tests and the 60 specimens were randomly allocated either a destructive tensile or destructive compressive test.

The mean values of Young's Modulus in compression were 485 MPa and 483 MPa in tension, suggesting that bone exhibits linear elasticity. Strength, ultimate strain and work to failure were all significantly higher in tensile rather than compressive testing (Table 3.2) indicating two independent failure mechanisms.

	Compression Mean	Tensile Mean
Young's Modulus (MPa)	485	483
Ultimate Strength (MPa)	1.90	2.42
Ultimate strain (%)	1.11	1.55
Work to failure (kJm^{-3})	20.09	35.10

Table 3.2 - Mechanical properties in tension and compression (Rohl et al. 1991)

It has been suggested by Wolff (1892 - reported by Treharne, 1981) that cancellous trabeculae have the same composition as cortical bone, exhibiting the same mechanical properties, but configured in a different structural arrangement. There is a problem of measuring the properties, however, due to the size of the specimens available.

Few investigators have modelled cancellous bone at the trabecular level; the majority of models are based on isotropic material properties. Interestingly, one of the best methods of determining the local properties of trabecular bone appears to be through the use of high resolution computer reconstructions (van Rietbergen 1998). The technique has given excellent results with comparisons against whale bone, but the accuracy of measuring human bone remains to be satisfactorily demonstrated.

3.6 Bone remodelling

Bone has the ability of self-adaptation to the mechanical demands placed upon it. It is able to both grow and resorb in order to maintain equilibrium between conflicting factors. Large bones are stronger with greater failure loads. Small bones, on the other hand, have a low maintenance cost and require little energy for locomotion and are hence lighter and allow faster movement (Currey 1984). Bone mass in vertebrates is thus maintained in an equilibrium state, according to the mechanical demands made upon it, by the continual growth and removal of bone matrix from the free surfaces of the bone. This process is called Bone Remodelling and is a direct result of the activity of the osteoclast and osteoblast cells, which

deposit and excavate the bone matrix on the surface of the bone in response to the changing mechanical stimulus. The response in trabecular and cortical bone is therefore slightly different. The honeycomb like structure of cancellous bone allows deposition of matrix on the surface of the individual trabeculae, hence inducing a change of the internal makeup of the bone. The result is a modification in localised density of the bone, hence altering the stiffness of the structure. Cortical bone, on the other hand, is compact in nature, so deposition of bone matrix occurs on the surface. The result, in this case, is a change in the thickness of the bone wall.

Under so-called "normal" physiological conditions, external forces acting on the body produce stresses and strains which may vary locally but which do not vary to such an extent that the equilibrium between osteoblastic and osteoclastic activity is disturbed. However, if there are significant changes in the local bone stress patterns, for example those produced as the result of the implantation of a prosthesis, then a mechanical stimulus is transduced into a biochemical stimulus which may preferentially activate osteoclasts or osteoblasts, leading to a change in bone mass. If the magnitude of the local remodelling potential is higher than that required to maintain balance in cellular activity, then bone mass would be increased locally. Conversely if the potential is too low then the local bone mass would be reduced. This process is demonstrated in Figure 3.5. Whilst the exact form of the biological remodelling stimulus remains the subject of investigation, it is thought to be some function of strain rather than stress (Carter 1984, Cowin 1993).

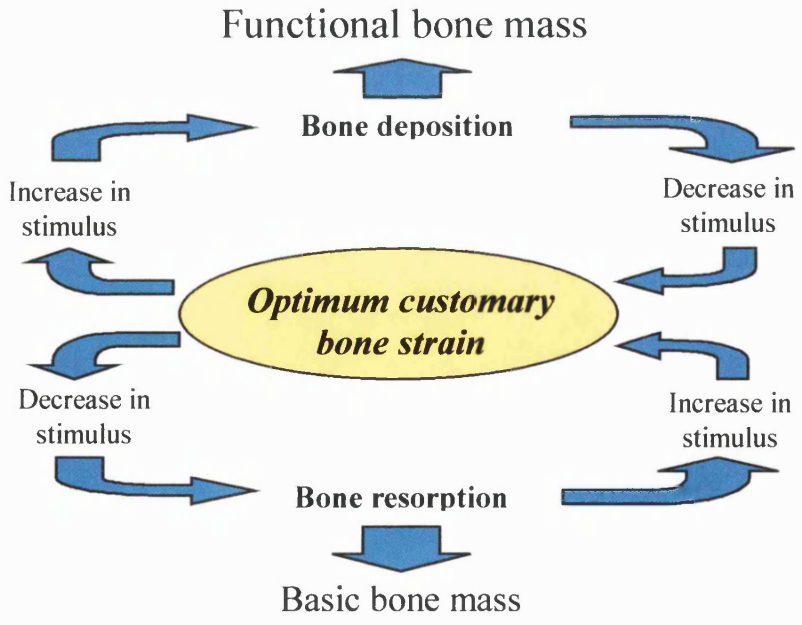

Figure 3.5 - Functional bone remodelling diagram (redrawn from Lanyon, 1980)

Under physiologically normal conditions, stresses and strains within the bone are at a customary level, maintaining an optimum constant bone mass. Should the level of activity increase, then a resulting increase in the bone strains and hence stimulus will occur. The relative activity of the remodelling cells is thus altered and bone deposition occurs. The resulting change in mass of the bone therefore alters the strain patterns within the bone, and remodelling continues until such time as the remodelling stimulus is altered to within the physiologically 'normal' range. The same process arises after a reduction in functional loading, whereby a decline in bone mass will cause normalisation of the local strains.

Bone remodelling is prominent in patients who have experienced THR, where the shaft of the implant hides or shields the surrounding bone from its functional loading, in an effect called stress shielding. This is caused by the introduction of a relatively stiff implant into the femur. As a result, the majority of the loading is taken by the prosthesis, causing alterations in the patterns of mechanical growth stimulus. This often leads to bone resorption around the implant stem (Cohen and Rushton, 1995), a contributing factor to long-term aseptic loosening of the prosthesis. Consequently, this process is a major predisposing factor to implant loosening. Modelling of this process is therefore of prime importance to allow theoretical testing of defined conditions representative of bone surrounding an implant

Chapter 4 Bone modelling review

4.1 Introduction

A large number of studies have been performed to simulate computationally the process of remodelling in the proximal femur (e.g. Weinans *et al.* 1992, Stülpner *et al.* 1997, Beaupré *et al.* 1990). There are a number of problems facing any researcher in the field of biomechanics, especially when studying human bone remodelling, due to the obvious restrictions on testing. It is therefore impossible to impose the specified conditions often required for the comparison of results with other techniques. The consequent lack of information makes it difficult to validate any results, and increasingly computer models are being compared to animal tests, where implants can be placed into healthy normal bone and the animal sacrificed at a later, specified time.

Even with the use of animal studies, one of the major difficulties facing researchers is the quantification of the conditions that are actually being used. Biological systems are highly variable, and reducing the number of unknown factors in a scheme as complicated as bone remodelling, is difficult. Magnitudes, positions and directions of loads are often part of a mathematically indeterminate system (Paul, 1967), and the exact remodelling stimulus is still the subject of investigation. Modern techniques attempt to reduce the number of unknown variables in order to gain reliable results, but unlike many engineering problems, biological problems rarely present an exact solution. The process therefore often attempts to define the reasons for the effect without fully knowing the cause. The result is that very little research in this field can give precise results and studies often serve to add to the probabilities by providing additional evidence.

In order for any study to provide a noteworthy contribution to the current understanding in biomechanics, it is first necessary to compile the literature in an attempt to determine the most reliable knowledge. The following sections review the current understanding of bone remodelling and the factors that are most likely to affect how and why bone responds to its surrounding mechanical environment.

4.2 Mechanical stimulus of bone remodelling

Bone remodelling was first examined in the late 19th century by both Roux and Wolff, who in 1892, published his major paper (reviewed by Treharne, 1981) describing his observations and ideas regarding the response of bone to mechanical loading. Although previous studies had noted both the ability of bone to remodel and that load had an effect on bone mass, Wolff was the first to connect these two ideas together. He suggested that the rules surrounding bone remodelling are in '*accordance with mathematical laws*' and offered an explanation in the form of a graph (Figure 4.1).

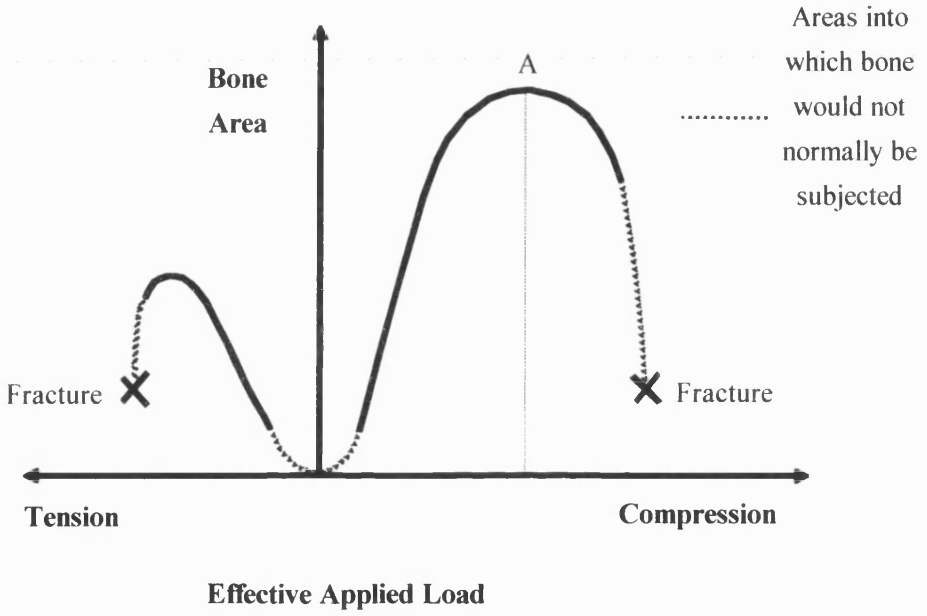

Figure 4.1 - The effect of load on bone area (Wolff's Law, reviewed by Treharne, 1981)

The dotted lines are regions of loading into which bone should not normally be subjected, but in the unlikely event, the crosses represent fracture or complete failure. The left-hand side of the graph shows the behaviour of bone in tension. Although little bone is subjected to tension in the human body, positive remodelling can occur as a response. If bone that is normally exposed to compressive loading is exposed to long periods of tension, however, resorption would occur. The centre of the graph shows regions of no applied stress, and is shown dotted.

The right hand side of the graph shows bone growing in response to compressive loading. More growth will occur due to higher magnitudes of applied load, until an optimum growth

rate is reached, shown as A. Thereafter, resorption will occur until fracture, since local bone death can result from excess loading. This phenomenon is often called pressure necrosis.

Neither Wolff, nor any researcher since, has been able to determine with any confidence the exact form of loading to which bone remodels. A great deal of work has since been done, however, to gain a better understanding of the remodelling processes that occur in bone.

It is believed that bone responds to a stimulus that must be dynamic in nature. Hert *et al.* (1969) examined the long term response of rabbit tibia to continuous but static bending applied by a pair of springs, one tensile and one compressive. The results showed that slight bending of the bones was induced during the growth period of the young animals but little or no remodelling occurred as a result. Once maturity had been reached, and the animals were no longer growing, very little further bending of the bones occurred. Several explanations of these results were discussed, including the possibility of remodelling, but most were discarded on the basis that the curving of the bones was developed exclusively during the growth period. However, they did conclude that the bending was caused as a result of growth whilst the static deformation was applied to the bones. Holding the bones in a curved manner during this period allowed the new growth to take up the deformed shape. Any internal reconstruction, surface remodelling or new bone formation due to growth that then did occur during this phase produced bone matrix layered down upon a strained configuration. Additional curving of the bone was then limited when growth of the animals halted due to maturity. Evidence was added to this hypothesis after observation that the majority of the curving of the loading pins occurred in the more peripheral of the sites. This bending was associated with the majority of growth of the young bones occurring in the endochondral bone. The relative thickening or thinning of the bones was commented on only briefly, but interestingly, nearly all the bone sites that had been in tension had resorbed. No adequate explanation was given for this reaction.

In further experiments (described in Hert *et al.* 1971), the effects of intermittent loading on the remodelling changes induced in the mid-diaphysis of rabbit tibia were examined (Hert *et al.* 1972). They demonstrated both periosteal and endosteal thickening over the loaded medial and lateral sides of the bone. Little or no new bone formation was seen over the neutral axis of the bone under the imposed loading conditions.

The finding that bone does not respond to continuous static loading but rather intermittent dynamic loading, was further examined by Rubin and Lanyon (1984), who conducted an important piece of research into the form of loading that induces bone formation. The aim of the study was to establish the effect of non-physiological loading conditions on bone remodelling. An avian ulna was functionally isolated, by surgical sectioning and capping, and the bone was artificially loaded *in vivo* using a double action pneumatic piston providing peak strain levels of 2000 x 10^{-6}. The loading, a known regime, was applied at 0.5 Hz over a number of consecutive cycles each day. It was found that the removal of load by complete functional isolation produced a steady decline in the bone mineral content over the six-week trial period. The cases of intermittent loading provided astonishing results, however. It was found that when a loading regime of 36 cycles per day was applied to the ulnae, extensive endosteal and periosteal new bone formation was seen. Increasing the number of daily cycles created no further increase in bone formation. In addition, only 4 loading cycles per day were required to prevent resorptive remodelling.

These results clearly support the work done on rabbit tibia by Hert *et al.* (1969) and provide considerable evidence to show the osteoregulatory signal must indeed be dynamic in nature. Further work by the same group (Lanyon, 1984) went on to examine the influence of peak strain magnitude on the remodelling in similar ulna sections. Using an identical preparation procedure to the previous study, the ulna was loaded at a constant rate (0.01 strain per second) for 100 cycles per day. Loading to 500 microstrain failed to prevent the reduction in cross sectional area seen in the functional isolation model. When the peak loading was increased to 1000 microstrain, however, there was complete maintenance of bone mass, and any further increase in load magnitude over and above this level produced a proportional increase in bone formation.

It was suggested that the specifications for bone are coded for genetically, but that structural 'normality' and load bearing competence is only achieved by the adaptive response to load bearing. The aim of remodelling is to adjust the structure's architecture to maintain the strain level at an acceptable or optimal level. This is achieved by changing both the geometry and the mass of the bone. The study concluded that since bone mass equilibrium is the resultant of both resorption and deposition of bone matrix, it is likely that, in the absence of all functional load-bearing, bone mass will decline towards a genetic minimum. The implications of this suggest that resorption of bone matrix is a continual process regardless of the loading

environment in which the bone is placed and that deposition of bone is dependent upon the functional stimulus.

O'Connor et al. (1982) studied the influence of the experimental rate of strain on the bone remodelling seen in sheep. An intermittent loading regime, applied at 0.5 Hz, was applied though implants that were inserted into the radius and ulna of the animals. They demonstrated that the ratio between the maximum strain rate of the artificial and the normal loading regimes accounted for the greatest variation in remodelling. Furthermore, the applied loads were well within the possible range of loading conditions that could be applied during normal locomotion, suggesting that remodelling is highly sensitive to strain redistribution. The experiments presented limitations that were seemingly overcome by the ulna osteotomies, however, since the sheep were allowed to wander freely during the non-experimental loading periods. This allowed non-regulated loading conditions to be applied to the test bones, and the imposed loading therefore became only a part of the total loading applied.

4.2.1 Sensitivity of loading to frequency

As described in the previous sections, it is generally accepted that static loads are essentially ignored as a regulatory stimulus and that loading must be of an intermittent nature in order to stimulate the formation of bone. Furthermore, both the magnitude of the load (Lanyon 1984, Rubin 1987) and the rate of strain (O'Connor *et al.* 1982) are important factors in the adaptation process. What connects these factors, but still remains of relatively unknown significance is the effect of the frequency of loading on remodelling.

Rubin *et al.* (1990) used spectral analysis techniques to record the strain frequencies present in the long bones of horses, dogs and turkeys resulting from standing and locomotion. It was found that whilst the majority of bone strains occurred in the 0 - 15 Hz bandwidth, there was a small but consistent strain peak, approximately 5 - 15 % of the magnitude, in the 15 - 30 Hz range. It was suggested that the force variations found at these frequencies, which could plausibly be created from muscle dynamics, could possibly be a significant factor in remodelling. If these higher frequency, low magnitude strains do hold some influence in remodelling, then they make an attractive alternative to the peak strain concepts, since these forces are present even during long duration activities like standing. It was observed that this component of the loading did not alter frequency despite changing speed and gait. Indeed, despite the low magnitude of these high frequency strains, the strain history information

received during a 24-hour loading period in the 10 - 100Hz range was larger by an order of magnitude than that seen in the 1 - 10 Hz range over the same period (Fritton *et al.* 1995).

This concept of frequency induced remodelling was taken further by the examination of bone mass under a variety of loading frequencies. It was shown that maintenance of bone mass required a lower level of peak strain magnitude with increasing loading frequency (reported in Rubin & McLeod 1995). This was demonstrated, again with the avian ulna model, that bone maintenance was preserved under a loading regime of 1800 cycles at a peak of 800 microstrain at 3Hz, but also under only 200 microstrain at an increased loading frequency of 30Hz. It was suggested that these results show that remodelling is dependent on several components of the loading mechanism, rather than a single component.

The significance of these frequencies was later disputed by Turner et al. (1995), who examined *in vivo* strain recordings taken from 11 skeletally mature foxhounds. Readings were taken from the long bones in the forelimbs of the animals during walking and standing still, followed by unweighted readings taken with the forelimbs raised from the ground, after tranquillisation and after sacrifice. This provided a negative control condition under which electronic noise could be calculated - a sequence that Rubin et al. (1990) had failed to conduct. What they found was that the components of strain within the 15 - 30 Hz band were significantly increased during activity, but remained lower than 4% of those seen at the lower end of the frequency spectrum. This contradicted the idea that these strains were present during long periods of low activity, as suggested by Rubin and co. workers.

4.2.2 Form of mechanical stimulus

Whilst it has become accepted that bone responds to some form of loading, the experimental work described in the previous section fails to uncover the form of the stimulus responsible for osteogenesis. The exact form remains open to speculation, but the knowledge gained from these experiments does point towards more probable parameters responsible for the activation of bone formation. Currey (1984) hypothesised that remodelling was the result of numerous factors, all significant to the survival of the bone, rather than a single continuum parameter. Amongst the many possible candidate parameters important to the adaptation response, it was suggested that static strength, impact resistance, architectural complexity, stiffness and fatigue resistance are all effective aims of the remodelling process. The growth response, it was implied, was simply the equilibrium balance of these goals.

Carter (1984) evolved a working hypothesis using the idea that strain remodelling is both specific and imprecise. The hypothesis was that evolutionary pressures genetically determine the basic structure and mass of each bone. Carter presented a growth curve for bone that required normal physiological activities to maintain remodelling equilibrium (Figure 4.2). Contrary to the 'dead zone' of Weinans *et al.* (1993) and Rietbergen *et al.* (1993), however, changes in bone mass were affected with increasing intensity as the bone strain history deviated further from the centre of the physiological band. The curve presented thus argued a non-linear remodelling response that assumed the change in bone mass was a function of the rate of change of a strain history function. This, in turn, was dependent upon cyclic strain range, the mean strain and the number of loading cycles. It was also considered that other characteristics could also be involved, such as strain rate and loading frequency.

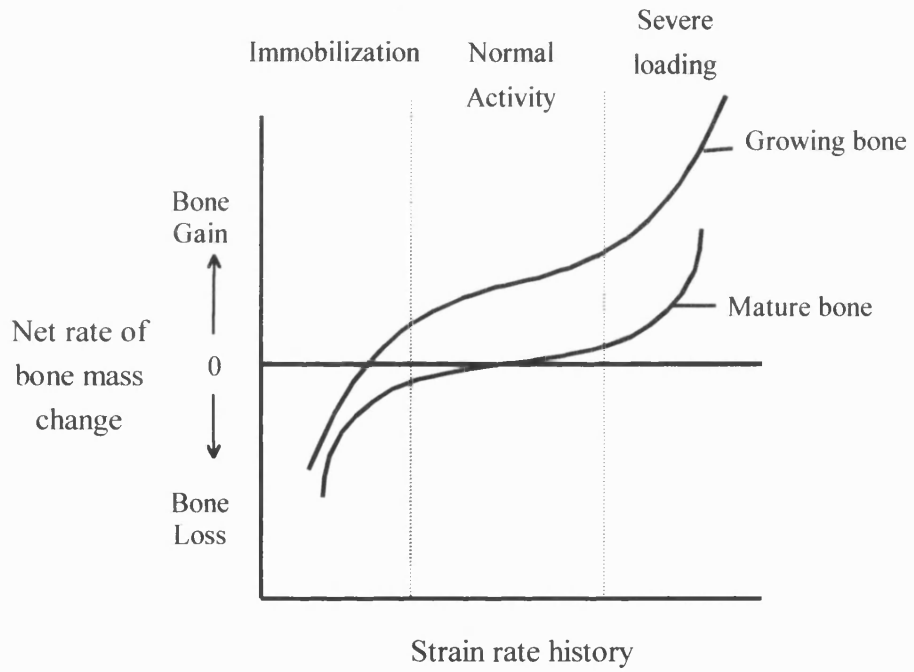

Figure 4.2 - Rate of bone mass change, dependent upon strain history (redrawn from Carter, 1984)

The ideas presented implied a whole series of curves changing gradient and translating in position which vary with age, also with a slightly different shape curve for each individual. It seems, however, that no exact mathematical relationship for the theorem has been proposed, making it impractical as a working model.

The use of Strain Energy Density (S.E.D) as a stimulus to initiate bone remodelling has been used to great effect by Weinans *et al.* (1993). The model, which is described in greater detail in Section 4.5, examined the remodelling that occurred around press-fit hip implants in canines. The same model was further developed by Rietbergen *et al.* (1993) whose model attempted to recreate the conditions imposed by a non-porous coated, full length press-fit stem. The use of strain energy density as a possible remodelling stimulus was refuted by Gross (1992), however, whose study involved placing rosette strain gauges on the third metacarpal bone of a horse. The value of strain energy density was quantitatively measured over a full gait cycle and plotted against position around the bone on a three dimensional image. The results showed a variation in S.E.D of up to two orders of magnitude around the bone. These results do not, however, invalidate the possibility of remodelling based on the difference in actual and physiological normal loading conditions. Other proposed stimuli include peak strain magnitude (Rubin and Layon 1985), rate of strain (Goldstein *et al.* 1991, Cowin 1996, Luo *et al.* 1995), and stress (Meade *et al.* 1984, Brown *et al.* 1990).

It has also been proposed that the purpose of remodelling is to delay and prevent microdamage by the excavation and rebuilding of damaged regions of bone (Martin and Burr 1982). The presented idea was based on the fact that crack lines tend to follow and enter osteonal cement lines or interlamella boundaries, and it was suggested that a crack is likely to become trapped within it. It is logical to suggest, therefore, that these cracks would change the stress field in the osteon or the wall of the canal. Any stress altered field due to cracking, therefore, would seemingly produce areas with reduced functional loading.

Whatever the complexity of the exact mechanism of changing the biochemical response into mechanical reception, the result is the production of a remodelling response. It would seem logical to assume that some form of the mechanical loading placed upon the structure induces the biochemical stimulus. This stimulus would therefore be the result of some function of the stresses and strains placed upon the bone, leaving a relatively simple function with which to represent remodelling. Computational modelling of the loading processes may begin to unravel the secrets of the remodelling stimulus.

4.3 Materials properties

Any attempt to accurately model bone material in three dimensions requires a method of quantifying stiffness throughout the structure. Finite Element models using uniformly homogenous material properties for both cortical and cancellous bone are frequently used in the literature (Spirakis *et al.* 1992, Weinans *et al.* 1993, Rietbergen *et al.* 1993). This approach is a generally accepted normal for the definition of cortical bone, since it is assumed to vary little in either density or stiffness across the material (as discussed in Chapter 3). This simplified definition for the material properties of cancellous bone seems inadequate, however, due to the large variation in structure within the proximal regions of the bone. Alternative attempts at modelling the non-uniform distribution of trabeculae throughout the structure have included micro-models of the trabecular morphology (van Rietbergen *et al.* 1995) and staged increases in the material stiffness throughout the cancellous regions (Taylor *et al.* 1995), ranging from 250 to 1250 MPa.

Perhaps the most physiological representative technique used for a macro model is one that relates the material stiffness directly back to the original structure. This technique has been achieved in a number of studies (Skinner *et al.* 1994, Keyak *et al.* 1990) all of which have taken the subject geometry from some form of scan. The approach was to calculate the position of the elements and relate back to the closest position on the original scans to calculate the density of that region. The stiffness was then calculated as some function of the density.

Rho et al. (1995) conducted a study examining the correlation between CT number, density and stiffness in a range of human bones. A number of independent variables were compared, finding the most significant determinant for the prediction of material properties in the proximal femur to be a power function of density. The results suggested that approximately 30% of the materials properties for cancellous bone were accounted for by the architecture of the structure i.e. the orientation of the trabecular struts altered the properties of the local material. The authors indicated that this was a major limitation of the Carter and Hayes' relationship (as described in Section 3.4) since their method gave no consideration of material orientation, hence ignoring anisotropy, the major reason for this structural stiffening. The paper went on to suggest two separate relationships between CT number (recorded in HU) and density for the human proximal femur; one for cancellous bone and one for cortical bone. The

equation representing the isotropic stiffness of cancellous bone in the proximal femur was given as

$$E = 5.05\ \rho^{1.269}$$

where E is the stiffness of the bone in GPa and ρ is the apparent density measured in kg/m^3. This equation is valid for bone with an apparent density of less than 1000 kg/m^3. The advantage of this method is that it is accurate over a small range of values and makes no attempt to represent all stiffnesses of bone.

4.4 Hip joint loading

Another issue that faces all models attempting to simulate bone remodelling is the highly variable loading conditions achieved in reality. Any representation that relies upon the level of loading in the bone (of which all strain values are a direct function), must approximate the loading in the joint, generally to a static value.

Perhaps the most comprehensive study into the femoral loading patterns was composed by Taylor *et al.* (1996) who discussed the distribution of stress and strain within the intact human femur. The aim of the research was to challenge previous simplistic loading regimes characterised by femoral head loading and abductor force producing a bending stress distribution pattern within the femur. The study was composed of two sections. The first considered the logical assumption that the femur is primarily loaded in axial compression, using growing evidence which suggests that there are mechanisms that act to reduce the external bending moment. A radiological study was performed to measure the *in vivo* deflections of the femur during one-legged stance, and a finite element analysis investigated the action of muscles and joint reaction forces in the reproduction of the experimental study.

The radiological procedure involved taking full length X-rays of two young male volunteers in the coronal plane during weight bearing and non-weight bearing. Three measurements were then taken for both the loaded and unloaded cases. Although the accuracy of the X-ray measurements were low (approximately ±1 mm) consistent displacements between the two subjects were found. In both cases, displacements in the coronal plane of less than 4 mm were measured in all areas of the femur, and less than 2 mm from the centre line at all points along the femoral shaft. The comparison finite element model resulted in displacements of as much

as 15 or 20 mm when under simple joint loading cases, evidently demonstrating over simplification of the loading situation. Further loading cases were examined including the addition of an iliopsoas and ilio-tibial tract force. The final loading conditions reduced the magnitude of the resulting stress and strain patterns to a virtually constant level.

A qualitative analysis into the effect of the ilio-tibial tract was performed by Rohlmann *et al.* (1982). Strain gauge measurements were taken of the femur during loading simulation of the stance phase of slow walking. Body weight, an abductor muscle force and a tension band force representing the ilio-tibial tract simulated the in-vivo forces in the loading rig. Several combinations of loading conditions were examined in the comparative finite element model, including differing relative magnitudes of the body weight vs. tension band force. Good qualitative results were gained from the study, although the stress and strain magnitudes varied up to 40%. The study demonstrated the contrast in the state of stress under different modes of loading including simulation of the abductor muscles and the ilio-tibial tract especially in the upper third of the femur. It was concluded that a single force on the femoral head parallel to the shaft axis may provide an adequate loading regime for a qualitative stress study of the femoral diaphysis. In order to fully establish the loading environment in the hip, however, the forces applied by the tract should be included.

4.5 Computational modelling of the bone remodelling process

Perhaps the most comprehensive modelling study of the bone adaptation process was carried out by Weinans *et al.* (1993). Eleven adult male dogs underwent total hip replacement surgery on the left side, and were sacrificed 6 months and 2 years later. The femora were harvested on both the operated and the contralateral sides, and the bones were sectioned at 1cm intervals. Simultaneously, three finite element models were created, one postoperative femur with prosthesis, one with additional partially fibrous membrane modelled, and the last of the contralateral femur of the dog.

The models were considered linear elastic and isotropic, with the Young's modulus of compact cortical bone considered a maximum of 22 GPa at a density of 1.73 g/cm^3. For the non-membranous implant, gap elements were introduced at the bone - implant interface which allowed slip and separation to occur. The adaptive bone remodelling theory involved a site specific formulation, whereby the operated femur attempted to normalise its stress-strain patterns locally to the same value as the untreated, contralateral femur, under the same loading

conditions. The bone mass was controlled by the elastic strain energy per unit mass. The bone attempted to remodel if the signal was outside the 'Dead Zone', the period in which no bone growth or apposition occurs. Internal, cancellous remodelling was defined by altering the bone mass. This was a function of the free surface area (which was itself a function of density), and the difference in remodelling potential between the operated and the contralateral femur.

External, or cortical bone remodelling was defined using a growth velocity of the surface nodes, expressed as a function of the remodelling stimulus, the density of the element and the time step. The determination of the direction of remodelling was not defined in the publication.

Since the models used a function of the difference in stress - strain pattern taken from the contralateral femur as the rate of remodelling, the iterative process was set up so the models could continually be compared against the non-operated situation. The model was run initially with an arbitrary time scale, which was later compared with the results of the bone slices taken from the dogs sacrificed at two years postoperatively. From this, a time constant was calculated which optimised the model geometrical similarities with the slices from the harvested bones. The results of the modelling suggested that the model with full contact bone - implant interface gave little agreement with the real life situation. The model using gap interface conditions, however, produced up to 95% conformity at the two year postoperative period.

It must be noted that the geometrical model was for one dog only, and the results were compared to the average of all eleven animals. This inhibited the accuracy achieved by the model, but there was a necessity to model in this manner due to the large amount of time required to create eleven working models, each with a different geometry. In addition, the FE mesh was less refined than the ideal situation, because of the limited computer resources available. Greater precision could have been obtained with a larger number of nodes and elements.

The dead zone in the model presented was set at a threshold value of ±35% of the reference signal to obtain greatest model - experiment similarity. It has been reported by Weinans *et al.* (1993) that Maloney *et al.* (1989) found values of closer to ±50%, whilst Frost (1990) suggested a variation in the value throughout the lifetime of the same person. The dead zone seems to be an unlikely proposition, however, as bone remodelling is such a diverse activity which does not occur discretely. Osteoclastic and osteoblastic activity occurs continuously,

forming a remodelling equilibrium, and so it would appear reasonable for the dead zone to be a polynomial function, rather than a ramp or step increase. This view was also endorsed by Carter (1984), whose paper is discussed in greater detail in Section 4.2.2. In addition, the size of the Dead Zone in this investigation is subject to the normal conditions and would vary across the bone. The Dead Zone is therefore a variable that appears to need further investigation.

A large number of other finite element models of the proximal femur have been created (e.g. Beaupre *et al.* (1990), Taylor *et al.* (1996), Keyak *et al.* (1990), Koeneman *et al.* (1995), Rohlmann *et al.* (1982), Skinner *et al.* (1994) Weinans *et al.* (1992)). The majority of models involved simple static analysis, with a few attempting to predict adaptive bone remodelling. Those that have endeavoured to include bone growth, have, in general, simplified the cortical - cancellous bone boundary, and used models averaging less nodes and elements than their static counterparts.

Beaupre *et al.* (1990) demonstrated bone atrophy under a reduction in loading history from normal physiological conditions. The results have limited scope, however, since the 2 dimensional nature of the model excludes the application of physiological loading and oversimplifies the complex shape of the natural bone. The model was also limited to internal, cancellous remodelling, allowing no external geometrical changes. Even in this simplified case, the boundaries between cortical and cancellous bone were well defined. Linear approximations were used to define the edges of the material boundaries.

One alternative method of structural remodelling was presented by Professor Claus Mattheck in the internal optimisation of tree structures (Mattheck 1994). His studies used the *axiom of constant stress* as a universal design rule for biological structures and simulate the adaptive growth using thermal expansion in FE analyses. The process involved the calculation of mechanical stresses from a plausible design proposal, derived from the loading conditions. A resultant temperature distribution map was equated to the mechanical stresses, with the highest temperatures corresponding to the most heavily loaded areas. Thermal expansion was then applied to the model, producing growth, manifested as "tree rings". The optimisation procedure was completed using mesh correction to smooth the resulting geometry. In certain cases, the cambium of trees, for example, growth was limited to the outer layers to exclude internal entanglements by using a coefficient of thermal expansion equal to zero.

4.6 Cancellous remodelling

Cancellous remodelling has been achieved by a number of researchers. Notably, Beaupré and co-workers have developed a system which was capable of two-dimensional internal and external remodelling [Beaupré, Orr & Carter, 1990a, Beaupré, Orr & Carter, 1990b]. Their theory worked on the premises that bone needs a certain level of mechanical stimulation to maintain itself.

The majority of attempts to model the long term adaptation process of cancellous bone have been homogeneous, consequently approximating effects of the porous properties that the material exhibits.

Huiskes and co. workers have carried out notable research in their attempt to model the inhomogeneous nature of the material by examining the microstructure using FE analysis (van Rietbergen *et al.* 1995). The study examined the micro-structural properties and loading of the individual trabeculae by reconstructing small cubes of cancellous bone taken from the human tibial plateau.

4.7 Summary

A number of studies relevant to the modelling of bone have been reviewed here. The functions of mechanical loading that are currently thought to govern bone remodelling have been discussed, showing that the localised strain in the bone is believed to play an important role. Modelling of the femoral loading environment has been examined, showing both a comprehensive and representative model of the loading conditions (Taylor *et al.* 1996). In addition, the most comprehensive FE models to date have been discussed, including the methods that have been used to represent the remodelling that occurs in bone.

Chapter 5 Finite Element modelling

5.1 Introduction to the Finite Element Method.

Until the mid 20th century, engineering structural analysis was based upon solving a large number of simultaneous equations by hand, creating tedious and time-consuming calculations. The natural consequence was to simplify any problems, reducing the number of unknowns. Where complex geometries were involved, structures tended to be approximated into a collection of basic geometrical shapes e.g. cylinders, cubes, beams and plates, making the problem a practical size, but potentially giving highly inaccurate results.

With the advancement of aircraft technology, structural engineers looked towards a more robust, accurate method of analysis. Simultaneously, the digital computer was evolving giving much more powerful analysis capability. The implementation of the Finite Element Method (FEM) for structural analysis began in the 1950s (Turner *et al.* 1956). The rapid development that ensued quickly provided relatively solvable numerical formulations to what were previously considered complex problems. Modern day Finite Element programmes now have applications in a diverse range of engineering fields, from automotive industries (Morin, 1995), aquatic applications (Andreau, 1995), to biomechanics (Huiskes and Chao 1983, Rohlmann *et al.* 1988).

In its most basic form the FEM can be described as a technique for obtaining the solution to a complex problem by subdividing it into a collection of smaller and simpler problems, each of which can be solved using numerical techniques (Zienkiewicz 1967, Hart 1989). Any elastic solid structure or continuum essentially consists of an infinite number of degrees of freedom. The complete analytical construction of this problem is thus too large to consider.

The FEM enables simplification of the structure by subdividing it into a number of regions, called elements. Discretisation of the structure into these elements reduces the number of interconnecting points into a finite number of nodes. Each element becomes an ideal representation of the material volume. In this manner, the real continuum is reduced into a discrete number of finite elements, and hence a finite number of equations, and the structure becomes more readily solvable.

When a structure is analysed, each element is considered a free body with a unique set of displacement conditions, based upon the imposed constraints and the surrounding material. It is assumed that the idealised characteristics of the material are precisely known. The basic behaviour of the element will then be of the form :

$$\{\mathrm{F}\}^n = [\mathrm{k}]^n \{\delta\}^n$$

where $\{\mathrm{F}\}^n$ represents the force vector of element n, $[\mathrm{k}]^n$ is the stiffness matrix and $\{\delta\}^n$ is the corresponding nodal displacement matrix. The complexity of the mathematics of the structure advances with the addition of initial conditions, non-linearities and temperature strains. A full account of the FE method is described in detail by Zienkiewicz (1967). FE analysis is now capable of solving problems involving complex geometries, loading patterns including stresses, strains, pressures, temperatures, and electric currents, and varying material properties. The method thus provides an excellent complement to experimental and analytical models, and with simple analytical verification of modelling accuracy, can prove invaluable as a tool for meaningful predictions.

It must be clearly noted that this method provides an approximation rather than an exact solution. In general the larger the number of elements, the more accurate the analysis becomes, as the number of degrees of freedom approaches that of the continuum. This can be confirmed with a convergence test on the number of elements, or using error analysis examination. Different types of elements will also affect the solution. The complexity of the analysis increases at a high rate with numbers of elements, however, leading to a compromise between accuracy of results and computation times. There are also a number of inaccuracies that must be taken into account when an analysis is performed using this technique. No real material can be exactly expressed in terms of its mathematical properties due to imperfections such as surface flaws and inhomogenaities. Any material definition, therefore, uses approximations in mathematical equations to represent the material characteristics. A model will also inevitably have simplifications to the exact geometry. In addition, any loading or boundary conditions may contain imprecisions. It is therefore important to be aware of both inaccuracies and approximations that may occur in a model and assess the order of achievable accuracy in the problem. An error comparison or convergence study can give clear indications.

5.2 Finite element modelling

The process of model creation through to solution and results has a number of discrete stages. In general, FE software packages operate in three stages to complete this process. Pre-processing involves the initial creation of the model, then the full computational analysis of the problem occurs separately in the processor solution phase. Post-processing subsequently evaluates the results gained from the analysis. Whilst the entire process is normally possible within a single package, the stages may often be individual software components with a common file format to allow interaction and compatibility between various pieces of software within the suite.

5.2.1 Pre-processing

Whilst the analysis of computational problems often uses a text format input to define the problem, a variety of front-end packages are available for their creation. In general, a finite element model must include geometrical data and information regarding interaction and interconnection of elements, definition of material properties, and a loading history for the structure, including boundary conditions. Additional material behavioural characteristics such as temperature and porosity may be defined if necessary. The definition of these properties occurs during the pre-processing phase.

The definition of geometry typically occurs in several stages, using a solid model assembly structure. Points, which are considered the lowest level in the structure, are defined using co-ordinate position. Lines or curves are created from the interconnection of these points, and are the next structural level. Surfaces or patches can then be defined from a variety of techniques that involve sweeping the curves into areas. Two-dimensional meshing can then be performed at this stage. Solids are the top level of the geometry structure, and are primarily created using surfaces, although may also use a combination of points and curves.

Once the geometry is completed, finite element meshing of the structure can occur. Nodes are located at the intersections between elements and are positionally determined within the solid model according to the mesh density required. Elements are defined in terms of the order in which the nodes are connected. The majority of packages have auto-meshing functions, although complex geometries will require a great deal of intervention to ensure good element shape and connectivity. The properties of the materials are then assigned directly to those

elements representing that volume of the structure. Likewise, loads and boundary conditions are typically applied directly to the elements and nodes.

The output from pre-processing is in the form of an analysis *deck*, or command file. It contains all information necessary for the processor to perform the analysis.

5.2.2 Processing

The full computational analysis or 'number crunching' occurs during processing. The input deck is submitted to the computer, often as a queued or background job, and the analysis is performed. The output is often incomprehensible, and stored in non-decimal characters, and hence the results require some form of viewer before they can be understood.

5.2.3 Post Processing

This section of the package allows viewing of the results taken from the processor. It provides a number of abilities, including producing contour plots and viewing output graphs.

5.3 The ABAQUS software

The ABAQUS finite element package (Hibbitt, Karlsson and Sorensen, Inc. 1998) has been chosen for the modelling of bone and its remodelling theories since it has powerful algorithms for user definition of material properties. The main processing package requires an input file, which is essentially all the information required from pre-processing, which can be written as a text file (with a .inp file extension) or created in the pre-processing stage. The computational analysis is then performed by submitting the input file to a queuing system (examples of these input programs can be seen in Appendices A & B).

The ABAQUS pre-processing software is supplied as a separate package called ABAQUS PRE (which is a subset of the PATRAN pre-processing package), and runs in an X window display environment. It is one of the few pre-processors with the ability to automatically mesh with 3 dimensional cubic shaped elements and creates an output file for storage identical to the ABAQUS input file. All ABAQUS post-processing is again done in an independent package called ABAQUS POST. Analysis of all defined parameters is possible, with printing abilities using the ABAQUS PLOT command.

Chapter 6 Cortical bone remodelling

6.1 Introduction

After consideration of the current techniques used to predict the remodelling associated with the implantation of a prosthesis, it was decided to investigate an entirely different approach to remodelling. Previous models have included the use thermal expansions and nodal velocities, as described in Section 4.5. The alternative approach, to be used in this study, was to use swelling strains. Swelling is a phenomenon associated with the change in volume of a solid through the absorption of moisture or surrounding fluid. Mathematically, swelling is a measured physical change in volume in response to any physical quantity or parameter. In its simplest form, the *SWELLING card applies a volumetric strain rate to the elements of a magnitude defined by predefined user fields (Hibbitt, Karlsson & Sorensen, 1998). It was proposed that the long term remodelling of cortical bone could be represented using the Finite Element Method by imposing swelling strains to create changes in the size of the elements.

Both the thermal expansion and swelling techniques were examined and compared for flexibility and the ability to develop the code under different demands. It was found that the two processes were mathematically similar, but having different options within the code associated with them. The use of a thermal map required a reference value for the coefficient of thermal expansion and needed continual knowledge of the current temperature and any heat applied to the model. The application of thermal strains also had limited options for controlling the direction of expansion and contraction. The use of swelling, on the other hand, applied strains directly to the element using the *SWELLING card. In addition, it allowed access to the *RATIOS sub-option which enabled definition of the element orientation, and hence the ability to strain the elements in specific directions. As a result it was decided to use swelling strains to expand the elements to represent long-term growth.

A preliminary overview of bone remodelling using the ABAQUS swelling code is shown in Figure 6.1. Each element could calculate a remodelling orientation in a direction defined as perpendicular to the surface using the *ORIENTATION card. The remodelling stimulus could be calculated in the USDFLD subroutine using values of stress and strain from the applied loading. Proportional swelling of the elements would then represent the bone

remodelling resulting from the change in the local loading environment. Cyclic application of the loading and remodelling would provide an iterative solution to the problem.

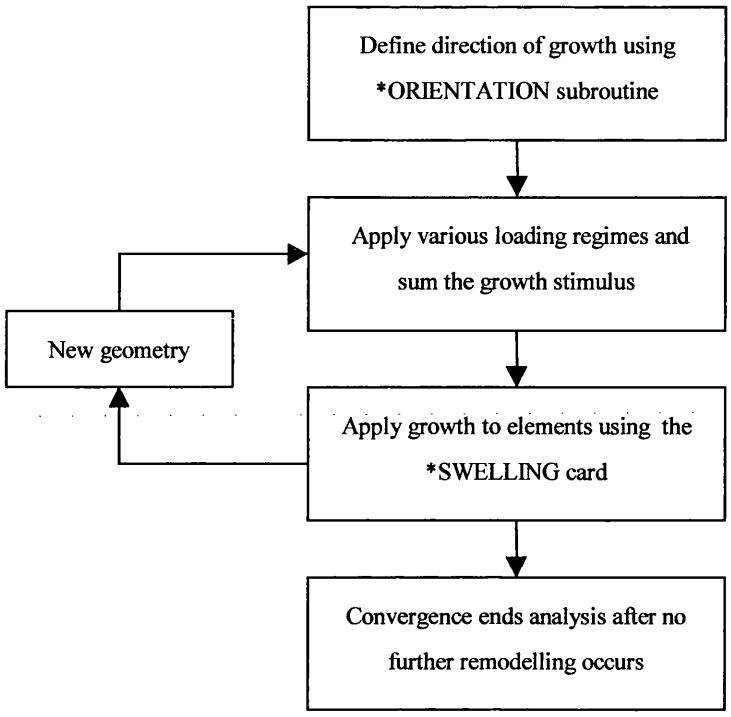

Figure 6.1 - Overview of bone remodelling using ABAQUS swelling code

6.2 Basic developmental model

6.2.1 Swelling of elements

Elemental swelling is achieved in the ABAQUS code using the *SWELLING card. Under normal conditions, this card produces a specified value of strain in the current element, based upon the original size of the element in that direction. In order for the elements to swell in response to the loading conditions, it was necessary to make the magnitude of the swelling strain dependent upon the mechanical stimulus (described further in Section 6.2.3). The sub-option of the *SWELLING card, DEPENDENICES, allowed the swelling magnitude of each element to vary with the values of *Field Variables*. These variables, which could be calculated within the User Subroutine USDFLD, were able to pass an independent value of growth requirement to each element. The *SWELLING card then applied a volumetric swelling strain rate to each element of a magnitude equal to the value of the field variable.

The User Subroutine USDFLD provided additional capabilities in that it was able to recall model stress and strain data throughout the loading history. This allowed continuous updating of the growth requirements, hence making an iterative process possible.

The user was able to modify whether the element length was updated or not during the analysis by specifying a geometrically linear or non-linear analysis (Engineering or Cauchy strain). Under these conditions, it was necessary to define a geometrically non-linear analysis (by using the NLGEOM command) so that the element lengths were updated in each increment. The magnitude of the elemental swelling therefore remained accurate throughout the analysis since any applied strain was a function of the current rather than the original element size.

6.2.2 Loading history

Any progressive growth pattern in a structure will continually alter the localised geometry and hence subsequently alter the mechanical loading environment. As a result, an iterative solution was needed in order to ensure modelling accuracy in the cortical bone, since any calculation using finite strains required progressive updates of the value of original length. Each element must therefore recalculate its growth requirement at every loading step. In addition, the loading patterns placed upon bone under normal physiological loading conditions are highly complex. Different loading regimes can be seen for every action and position of the skeleton (Adams and Swanson, 1985). The model therefore required a form of loading that allowed a variety of loading environments in a repeated manner to permit progressive growth with varying geometry.

A method of allowing progressive loading cases was devised, in which each step consisted of a number of loading increments (Figure 6.2). Each of these incremental loads represented a set of conditions seen in the 'normal' physiological environment - running, walking or climbing stairs, for example. In this manner, a strain pattern for each loading regime was produced in which the remodelling response of the bone could be calculated. Each set or group of these individual conditions could then represent an 'average' day or week in which normal physiological loads were applied. These loads could then be repeated after the growth response of the elements had occurred or a new set of conditions could be imposed upon the model.

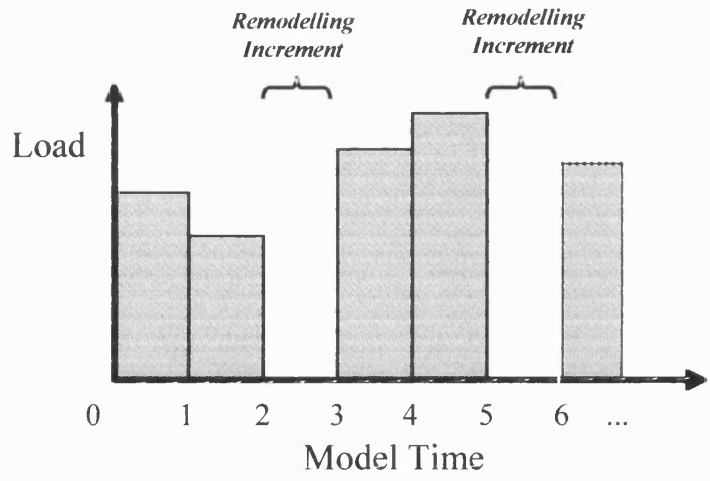

Figure 6.2 : Model loading history

This method of loading involved a number of time increments, N, per step, (shown as three per step in Figure 6.2 - two with load and one without) in which each of the increments imposed the boundary conditions associated with a different set of physiological loading conditions. These loading conditions could vary over each stage, but are only applied over N increments. The final increment in each step was a 'Remodelling Increment' in which no load was applied, but the growth requirements from the previous increments were calculated and the remodelling routine implemented by making the *SWELLING card active. The elements were thus 'grown' or 'resorbed' accordingly. In this manner, the final increment became equivalent to sleeping and rest periods, dependent upon the modelling timescale.

It must be noted that the growth periods on the loading history were all applied over a single time unit, since the *SWELLING routine imposed a volumetric swelling strain *rate* - a timescale which may not be appropriate to the cyclic nature of the loading regime. Normalisation of the time scale, to a loading period of a single unit of time, removed the 'rate' from the swelling expansion. As a result, it was necessary to multiply the response of the bone by a time constant in order to return the time scale to the physiological correct loading period.

6.2.3 Remodelling stimulus

There is continued discussion in the literature concerning the nature of the mechanical remodelling stimulus that relates the biological bone growth to the functional loading conditions (see Chapter 4). It may be that the remodelling stimulus is a function of a great

number of mechanical signals that all interact in an intricate manner (Carter 1984) rather than a single sensory response.

In order for the elements to calculate their local growth requirement, the remodelling stimulus was determined during the loading increments using the User Subroutine USDFLD. This mechanical parameter gave a quantitative measure of the mechanical remodelling requirement produced biologically within the bone. It was decided that *strain rate* would be used as the mechanical remodelling stimulus over the initial development models (O'Connor *et al.* 1982, Luo *et al.* 1995), although the code was constructed in such a manner that different mechanical stimuli could easily be introduced.

Interestingly, evaluation of the strain rate as a remodelling stimulus must examine micro time scales since the loading and unloading of bone tissue occurs at rates consistent with physiological normal loading conditions i.e. walking, running etc. As a result, the remodelling stimulus is calculated in response to loads that are applied at a frequency of approximately 1-2Hz. However, the remodelling response of the bone occurs over a much greater period of time (Lanyon, 1992). The resultant remodelling stimulus was therefore the summation of the individual stimuli over several thousand loading cycles. It was assumed that these cycles were typical of the average human physiological response.

In order to quantify the remodelling stimulus, the six components of strain, which include the three shear components, were required. The magnitudes of these strains were evaluated by calling the subroutine GETVRM from within the USDFLD code. This standard ABAQUS subroutine returns the values of various variables requested by the user (in this case the six components of total elastic strain) at the beginning of each increment. The GETVRM routine may be called from a number of places within ABAQUS, but when called from the USDFLD subroutine, the arrays returned hold the value calculated at the end of the previous increment. As a result, allowance was made for the discontinuity in timescale by storing these values as *State Variables* that could be recalled in any subsequent increment. Once returned, the strain arrays were converted into principal strain values for evaluation of the remodelling potential using another standard ABAQUS subroutine, SPRIND. This routine simply returned an array of three principal strains (PS(n), n = 1,2,3) given an array of six components of strain (S(n), n = 1 to 6). Since the timescale on the loading history was normalised, simple strains could be read, giving direct calculation of strain rates without the necessity for timescale redistribution.

6.2.4 Calculation of remodelling potential

The remodelling potential, equivalent to the biological growth potential, was calculated using the standard tri-linear remodelling curve (Figure 6.3) (Huiskes *et al.* 1987, Beaupré *et al.* 1990, van Rietbergen *et al.* 1993, Orr *et al.* 1990). The Dead Zone represented the period in which the loading conditions were at physiological equilibrium and no preferential remodelling occurred. If the functional loading on the local bone area increased from this normal dead zone position, (towards point D), then a positive growth stimulus would be obtained. Likewise, after a reduction in load, during periods of bed rest, for example (towards point A), a resorbing stimulus would be obtained.

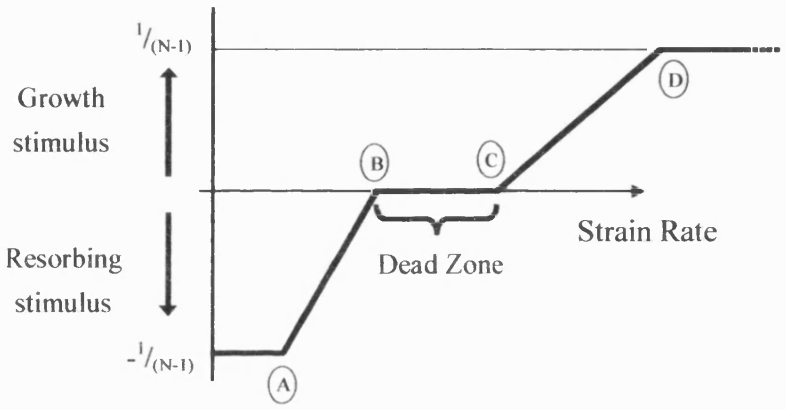

Figure 6.3 - Tri-linear remodelling curve

Each increment was subjected to a maximum allowable remodelling value of $\pm^{1}/_{(N-1)}$ where N is the number of different loading conditions applied to the model (as described in Section 6.2.2). Therefore a remodelling potential for every loading environment could be calculated. The final increment in each step was a 'remodelling increment' in which no load was applied but the remodelling requirements for the whole step were summed to create a total remodelling stimulus. In this manner, the greatest possible potential to grow or resorb over the whole step was ± 1 (since addition of stimulus during the remodelling increment was excluded). A strain rate constant allowed this to be converted into a percentage growth, and hence the rate of remodelling could be controlled for both accuracy and convergence criteria. Points A to D were defined in the code, to allow alteration of the remodelling scale.

6.2.5 Element swelling

The growth potential values for each loading increment were retained as *State Variables* for storage from one increment to the next, but the final total stimulus in the 'growth increment' was saved as a Field Variable and passed into the *SWELLING option. Since the Strain Rate Constant multiplied by the remodelling stimulus correctly defined the percentage growth required, the swelling parameters were derived from linear correlation (Figure 6.4). For the remainder of the step (during the loading increments), a *Field Variable* of zero magnitude was passed to the *SWELLING card to ensure no expansion occurred until the final *'remodelling increment'*.

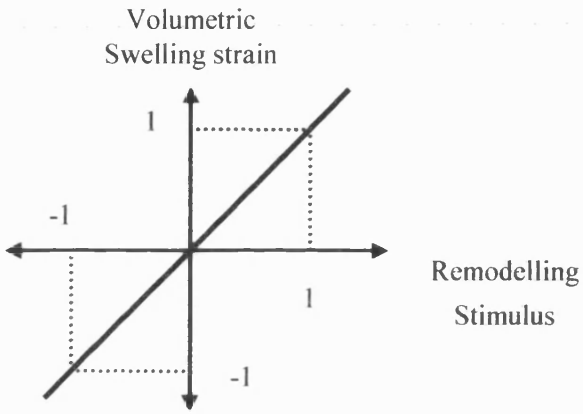

Figure 6.4 - Stimulus correlation for the *SWELLING card

6.2.6 Direction of remodelling

The default direction of action for material properties for any standard element was along global axes (usually rectangular). For it to be possible to allow swelling perpendicular to the free surface, the *ORIENTATION card was used to define a local axis system for each element. The OFFSET TO NODES option of the card was used to define two of the element directions. Figure 6.5 shows a 2 dimensional representation of both an eight and twenty noded element brick element. The orientation of the primary direction of growth for each element was determined as a vector passing through two user-selected nodes, shown as ① and ②. Direction 2 passed perpendicular to this vector, through another user-defined node, ③. The third direction was automatically calculated by ABAQUS as perpendicular to directions 1 and 2. Swelling strains were then applied in these three orientations, calculated differently for each element, and stored for the duration of the analysis.

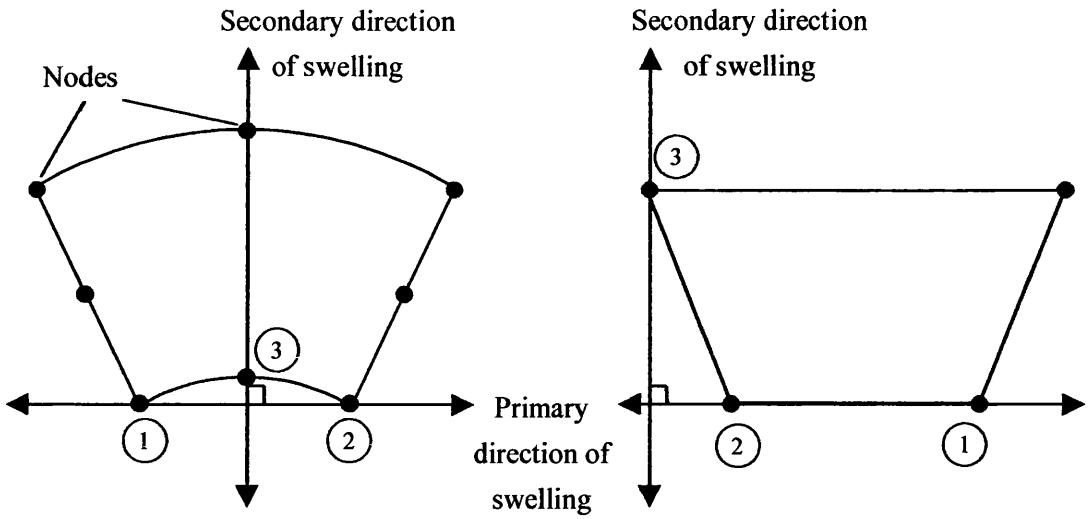

Figure 6.5 - Growth direction for 20 and 8 noded brick elements

Under normal default conditions, the swelling subroutine equally strained elements in all three dimensions. Application of this to the cortical bone model induced an increase in height and width of the bone in addition to wall thickening. The obvious outcome of this would be a global expansion of the structure, and in terms of biological models, would induce an incorrect increase in height of the body under positive remodelling.

To resolve this and allow growth perpendicular to the free surface only, the *RATIOS parameter was used. This card, which is part of the standard ABAQUS input deck, allowed modelling control of the swelling direction given in terms of the local element orientation. In this manner, unidirectional expansion of the elements was ensured, and growth normal to the free surface could be defined. Growth of the elements under these conditions was constrained to direction 2 only (Figure 6.4). The numbering of the element directions was dependent upon the order of the nodes, however, so some user intervention was required during their creation to ensure the correct elemental surfaces are outward facing. Obviously, in larger models there is no guarantee that all elements would be orientated in the same direction, producing remodelling in a variety of directions within the model. In general, however, pre-processing packages define matching directions to element sets, so only low levels of user intervention to ensure all elements remodel perpendicular to the free surface should be required on larger models.

6.2.7 Development model

The basic model for the development of the cortical remodelling algorithm consisted of four 20 noded cubic elements in a quarter circle construction, using symmetry on the boundary conditions to represent the effect of a full circle. The loading was applied as a pressure on the upper surface of the model, with solid surface support on the lower, allowing for sliding and growth of elements (Figure 6.6). The geometry was chosen in order to enable the possibility of simultaneous endosteal and periosteal bone growth or resorption.

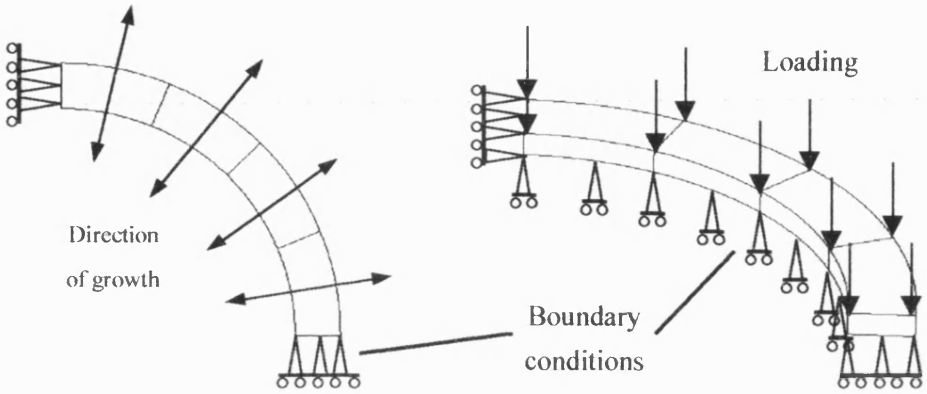

Figure 6.6 : Basic model for development of the swelling code

The bone adaptation process was being explored in this development model and hence the magnitudes of the resultant growths were not significant. In addition, the material properties and loading forces were arbitrary. For consistency, however, material properties of cortical bone were used (Cowin, 1989). The Young's Modulus was set to 17 GPa with a Poisson's Ratio of 0.33. The model was both homogenous and isotropic. For the purposes of simple loading for the development model, a pressure of $10N/mm^2$ was applied.

6.2.8 Removal of swelling strain from stimulus

Problems arose in the remodelling process since enlargement of the elements through the *SWELLING parameter was induced by applying swelling strains to the elements. The strain determined in any of the increments following the first step included strains due to both the imposed load and the previous swelling growth (Figure 6.7). In addition there were slight effects from remodelling elements on their surrounding neighbours, producing small, unwanted strains. Since the calculated value of stimulus was a function of the element strain,

under growth conditions, each element remodelled to a continually increasing total strain. The result was the production of self-perpetuating growth that increased exponentially, leading to an ever-enlarging model. Similarly, any resorbing stimulus lead to a continual reduction in material.

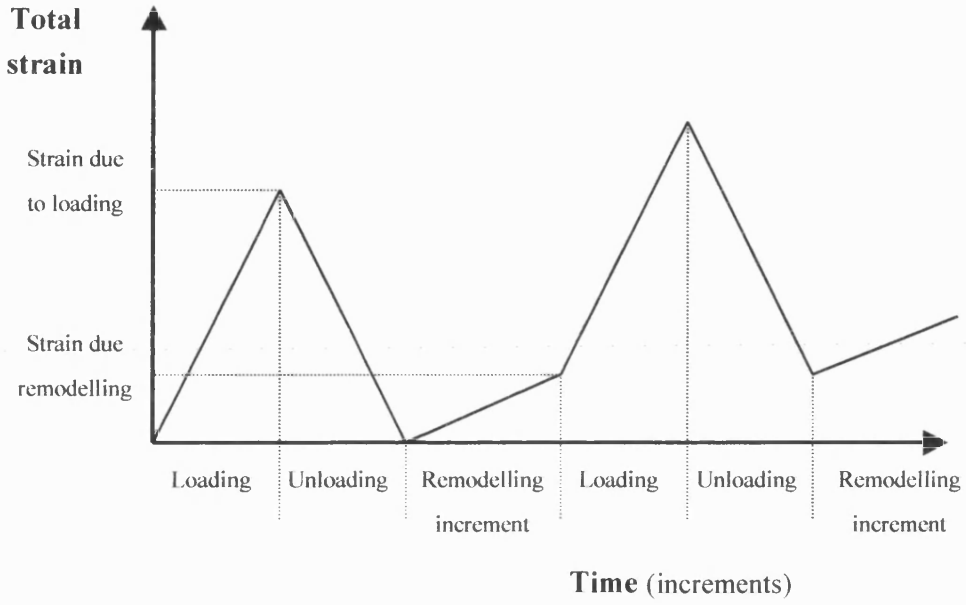

Figure 6.7 - Summation of total strain with loading increments

It was obviously necessary to remove this addition of the swelling strains from the calculation of stimulus in order for the remodelling to move towards equilibrium. The remodelling stimulus due to the applied loading was subsequently calculated from the difference between the swelling induced strain and the total induced strain (Figure 6.8). As a result, differentiation was required between the first and the remaining increments in each step due to the method of loading. The values of strain carried forward into the first increment of each step were purely a result of the swelling growth from the previous step and as such were recorded temporarily as *State Variables*. The magnitudes of strain read in the remaining increments of the step could then discard the previous growth from the actual mechanical remodelling stimulus by simple subtraction.

The resultant values of strains were identical to the elastic strains at the end of the first remodelling increment. It was not possible to simply use these elastic strains to determine the stimulus, however, due to the effect of remodelling of an element upon the surrounding elements. When remodelling growth or resorption occurred, the change in volume of that element produced a small force on the neighbouring elements, resulting in small inaccuracies in the calculation of the stimulus. It was noted that these forces had little or no influence on

the geometry of the structure, but it was necessary to calculate the stimulus from the original six components of strain. Once accounted for, this had only a second order effect on the remodelling, since the values were removed before calculation of the stimulus. It was recognised that this effect could indirectly influence the remodelling by slightly altering the elastic loading environment.

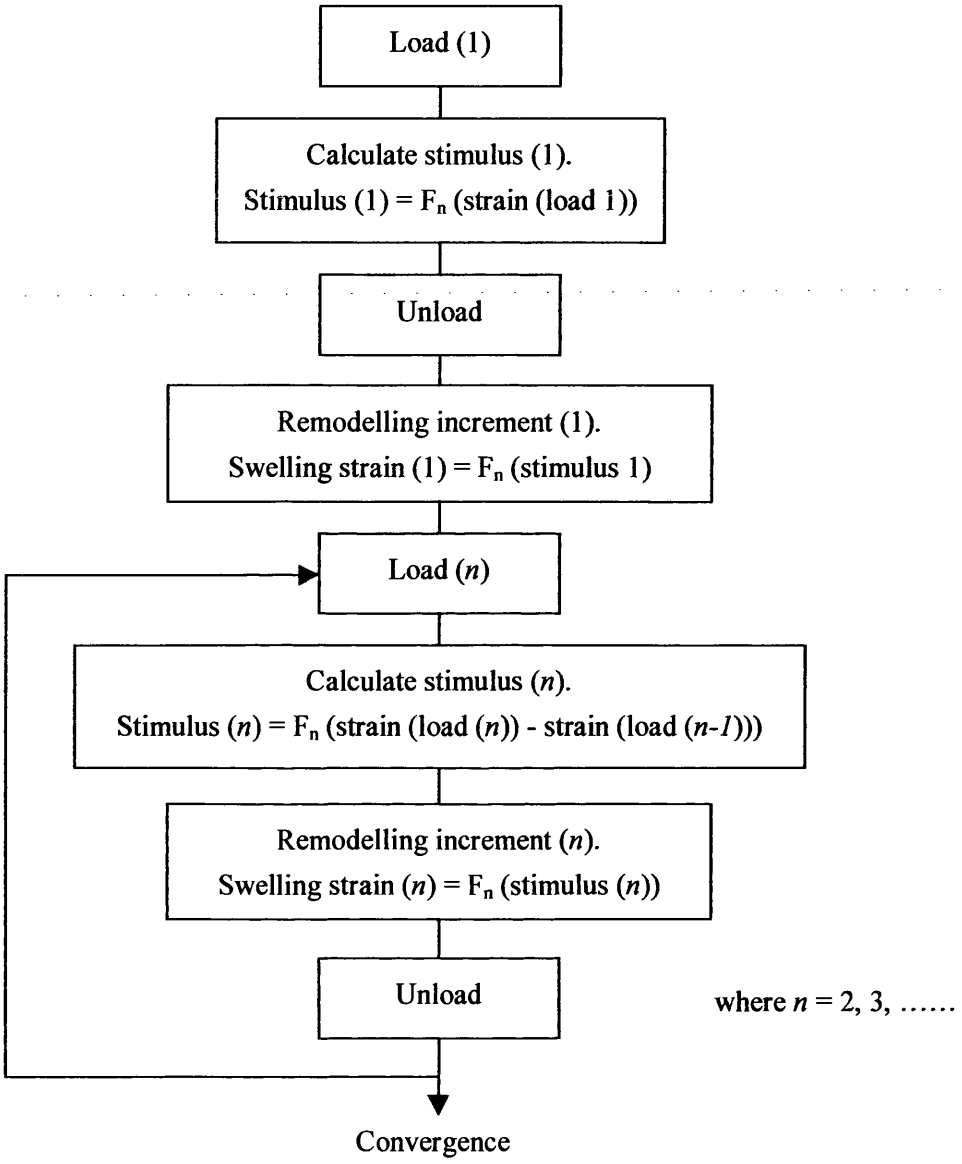

Figure 6.8 - Strain removal from stimulus

The determination of remodelling stimulus as a function of stress was calculated in the same manner as discussed above, with the removal of any swelling effects from the stress environment before the calculation of stimulus occurred.

6.3 Initial results

Growth of the elements was achieved in response to the applied loading. The growth occurred in the third increment of each step and continued in progressively decreasing amounts until the Remodelling Stimulus in the elements had entered the Dead Zone region of the curve (Figure 6.3) and no further expansion occurred.

The initial growth patterns displayed a rippling effect on the surface of the elements (Figure 6.9). It became clear that the swelling of the model did not represent the desired remodelling since smooth expansion of the surfaces should have been achieved as a constant distributed load was applied. Interestingly, lifting of the inner surface of the elements occurred with increasing growth. Equally, the outer edge of the elements appeared to thin slightly, leaving a gentle pitch to the upper surface of the mesh. Although perhaps trivial when viewed at the elemental level, this aspect of the growth rapidly deteriorated into a significant problem when the code was applied to a multi-layered analysis. This was demonstrated when both leaning and tipping of the entire stack of elements occurred.

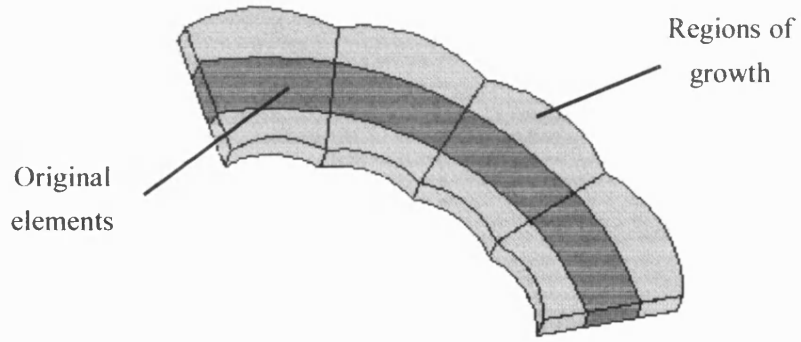

Figure 6.9 - Initial growth pattern

Examination of the results showed that the definition of the direction of growth was inadequate. Each element had a number of material integration points at which the magnitude and direction of the required swelling growth is calculated. The OFFSET TO NODES option of the *ORIENTATION card gave an identical growth direction for every point of the element (Figure 6.10). As the progressive expansion of the mesh occurred, the outer surface of each element effectively grew away from one another leaving an inward curve to the neighbouring edges. At the inner or periosteal surface, the directions of growth of the adjoining elements intersected, causing the opposite effect. The resultant growth, which degenerated progressively with increasing expansion, caused the 'rippling' effect.

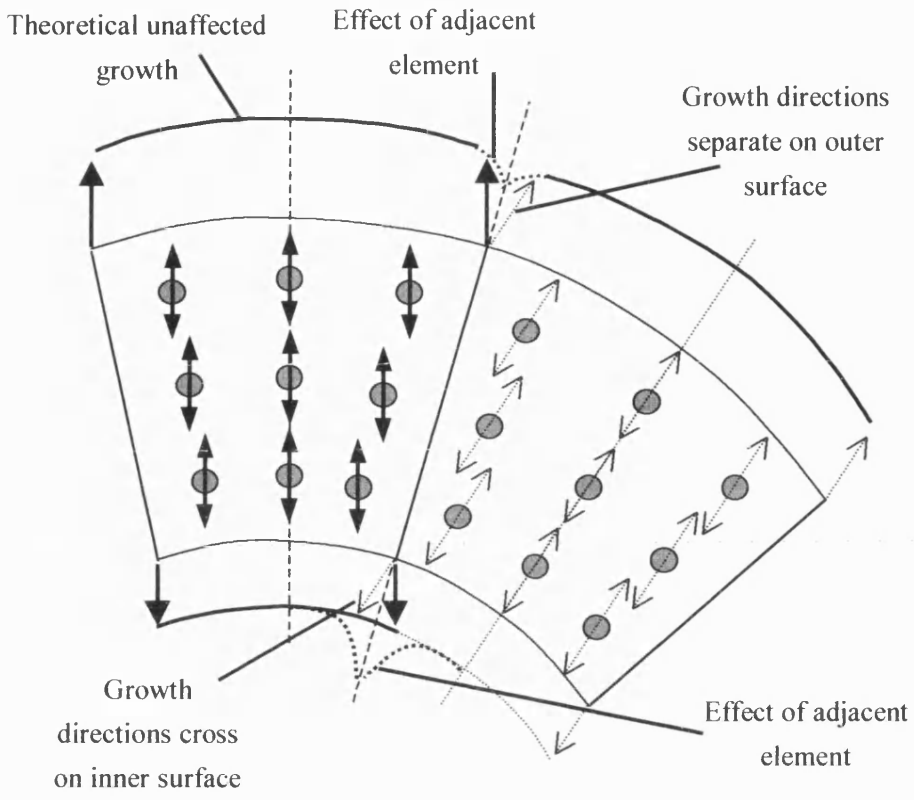

Figure 6.10 - Material integration point growth direction

To improve the definition of the surface expansion, the ORIENTATION subroutine was used to determine an individual growth direction for each material point. Two methods of definition were developed.

6.4 Integration point remodelling directions

6.4.1 Edge vector technique

The first technique to define the orientation of each material point involved the determination of vectors outlining the four edges of the element. These were calculated using the co-ordinates of the element corner nodes in the desired direction of growth, normal to the free surface (c.f. Figure 6.5). The co-ordinate position of each node in space is available within the ORIENTATION subroutine and could be read from the CNODES array. Each pair of nodal positions was expressed as a vector through simple subtraction of individual co-ordinate components (Figure 6.11). The perpendicular distance from the material integration point to each of these four vectors was then calculated (Bowyer 1990). The final direction of growth for each integration point was then determined as a component of each of the edge vectors, dependent upon the distance to each one.

$$\text{Material Point Direction Vector} = \sum_{N=1}^{4} \frac{\text{Edge Vector, N}}{\text{Distance to Vector N}}$$

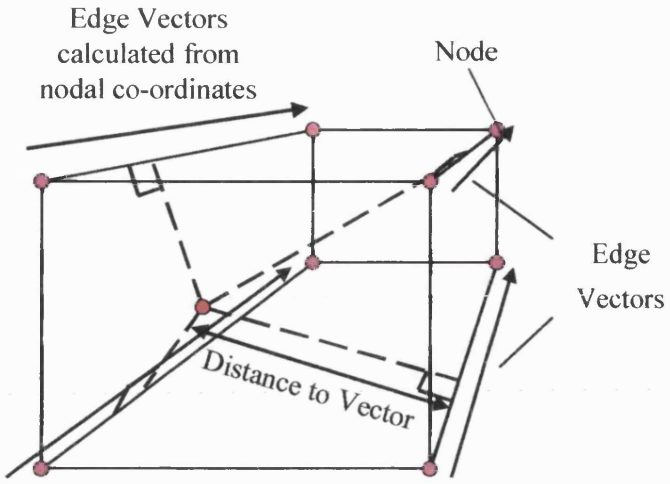

Figure 6.11 - Calculation of material point orientation

Since only the corner nodes of each element contributed to the calculation of the material point growth direction, the code was valid not only for twenty noded elements, but also for eight noded brick elements, where mid-side nodes are not present. This implied, however, that no account could be taken of the effect of the mid-side nodes in the case of the twenty noded elements.

6.4.2 Edge vector growth results

The growth results for the analysis using the edge vector technique are shown in Figure 6.12. Expansion of the elements perpendicular to the free surface occurred giving good circular growth until approximately 250% expansion when slight rippling started. Once again tilting of the upper surface appeared after the rippling effect began. Interestingly the tipping of the elements was only initiated once the rippling became apparent. It was concluded from this that the incline of the elements was a result of the Poisson's Ratio effect. Stretching and compression of the outer and inner surfaces would have occurred, causing the perpendicular thinning and thickening of the wall. This was deemed to be the same effect as that seen earlier in section Figure 6.8, where the remodelling affected the neighbouring elements.

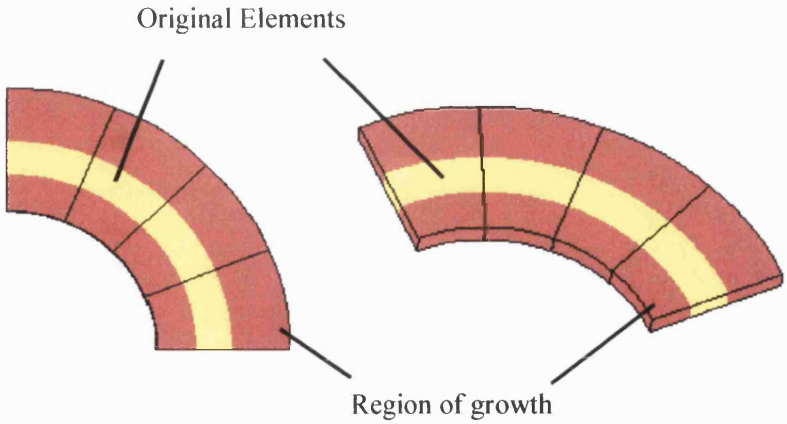

Figure 6.12 : Model growth after swelling

Despite the slight rippling and tilting of the elements, the method gave a good representation of the required growth. In general, normal physiological growth would vary the wall thickness by only a small percentage, and the technique presented gave visually correct results until several orders of magnitude of expansion were achieved.

The progressive growth of the elements is displayed in Figure 6.13. The magnitudes of the peaks show the percentage expansion of one material point of one element in the model, and appear only during the *'growth increment'* of the loading cycle. An expansion of approximately 120% was modelled, retaining the capability of the elements within their functional limitations, so that no rippling occurred.

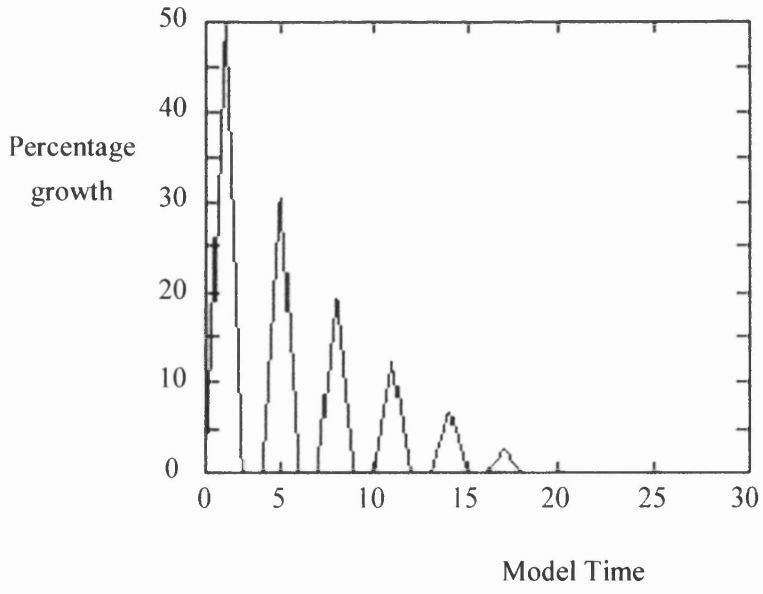

Figure 6.13 : Graph of Progressive Growth

The exponential decay in the model growth was due to the progressively reducing stress and strain patterns and hence remodelling potential, caused by the increasing size of the elements. The final steady state was a result of sufficient reduction in stimulus to have entered the dead zone of the tri-linear remodelling curve.

6.5 Discussion

It must be noted that it is the process being elucidated here. The magnitudes of the results gained from this model were not significant, since the determination of the remodelling parameters such as physiological normal stimulus would vary according to the location within the bone. In a remodelling simulation, these values would be defined by the previous modelling of the natural situation, under normal conditions. Bone remodelling would then occur when the remodelling stimulus differed from these predefined normal values.

The code has been constructed in such a way that the calculation of the stimulus may be easily altered, and hence various predictions using stress or strain based stimuli may be examined against animal experimental data. The header of the subroutine USDFLD contained all the variables that needed to be defined before the analysis. Minimal subsequent alteration to the code was required.

Interestingly, remodelling growth that was produced within the model presented also caused an increase to the applied pressure on the upper surface due to the enlargement of the loading area. Whilst this was essentially a second order effect and deemed insignificant compared to the change caused by growth of the model, this aspect was considered for any non-linearities which occurred during the analysis.

The determination of material orientation was considered limited in the case of quadratic elements, since the definition was based only upon the eight corner nodes. In an attempt to modify this process to be more responsive to the whole element situation in the case of quadratic elements, a second technique was considered.

6.5.1 Pre-analysis technique

The second method of analysis involved the examination of the material point co-ordinate position, since it was established that the growth orientation of an element was calculated at its material points. In order to gain the necessary data, a 'pre-analysis' was required so that

the three co-ordinates of each material calculation point could be written to a temporary file. This pre-analysis involved running one increment of the full analysis in which simple elastic material properties were used. Model node and element definition was identical, although no boundary constraints or loading conditions were initially required. A script of separate FORTRAN code was developed using the ORIENTATION subroutine, which was included in the pre-analysis input deck for completeness. The subroutine, which was automatically called for every material point in the analysis, specifically wrote the three co-ordinates to a user named file in a fixed format.

The ORIENTATION subroutine for the full analysis then included code that read the values of co-ordinate position of every material point from the user file into an array. Definition of growth direction was then calculated according to the type of element. The 20 noded brick element was initially examined and a demonstration of the material point orientation is shown in Figure 6.14. Since co-ordinate positions for all material points within the same element were recorded in the same array, each material orientation could be defined using vectors involving the surrounding material points.

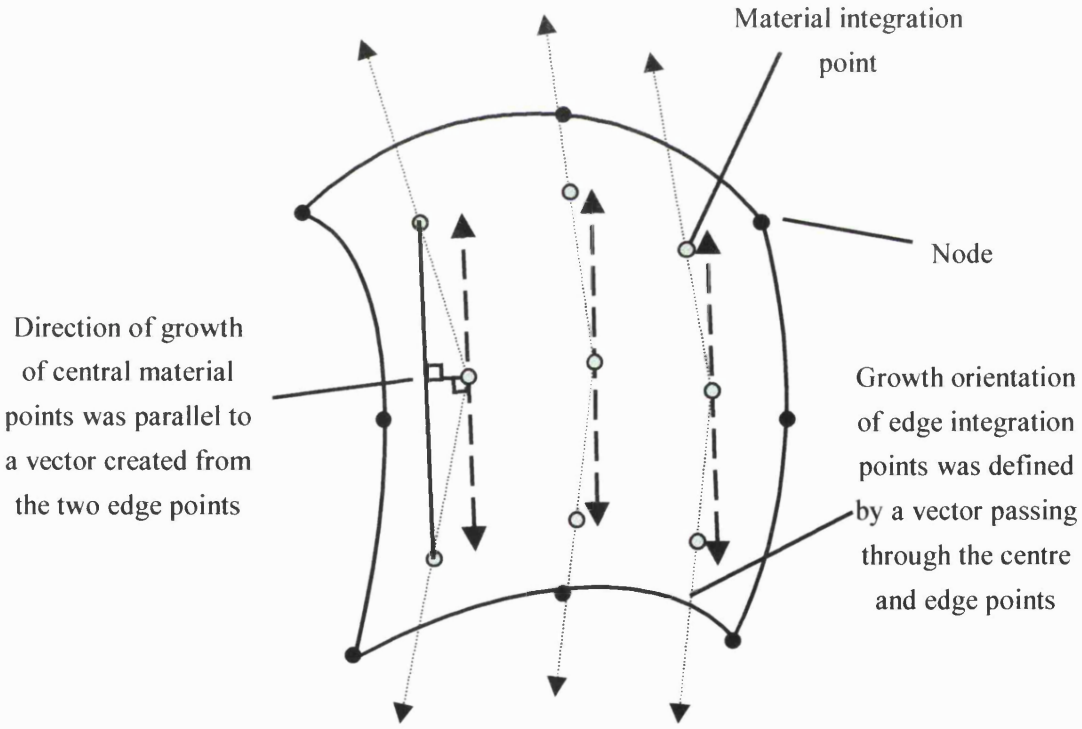

Figure 6.14 - Definition of material point orientation for a 20 noded brick element

Direction one for surface material points was defined as a vector passing through both itself and its corresponding central material point in a straight line. The orientation of the material

points at the centre of the elements was determined from the co-ordinates of the two corresponding surface points. The vector defining material direction 1 travelled through these surface points, passing through the central material in question. The orientations assigned to directions two and three for the material were not important, since swelling remodelling was limited to direction one only.

Definition of the growth orientation for eight node brick elements occurred in a similar manner, although the reduction in numbers of material points meant that all points were considered surface material points since no central points exist. The ability to expand prism elements was also developed although natural limitations occurred due to their topology. Growth could only occur in one direction relative to the element (Figure 6.15).

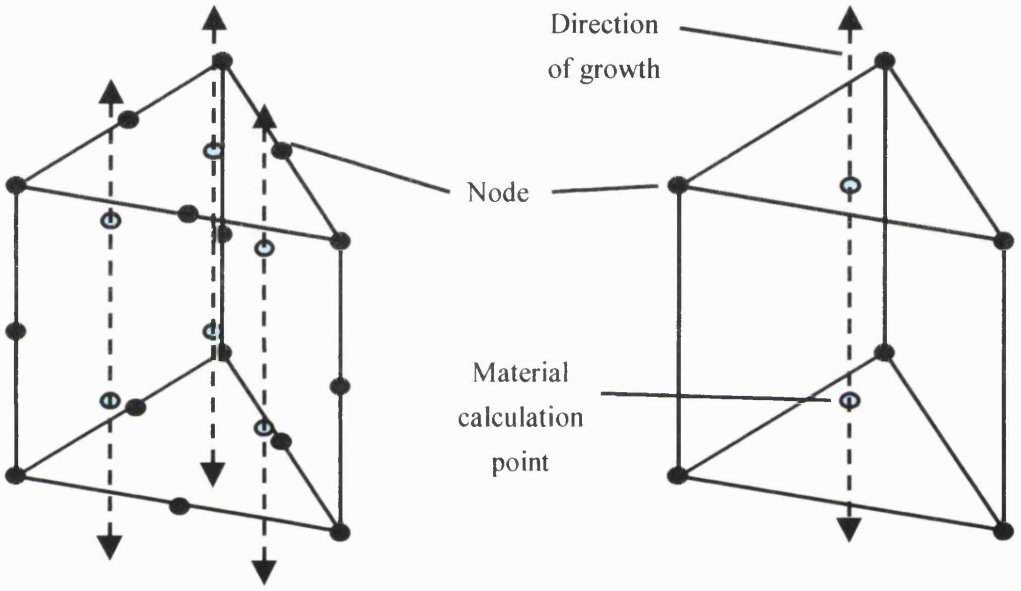

Figure 6.15 - Definition of material point orientation for prism elements

The limitation of these elements to grow in one direction only, implied that it was necessary to design any element mesh in an arrangement so that remodelling occurred only along their length.

6.6 Mesh independent growth

The growth regime presented here had the obvious drawback that the magnitude of all elemental growth was subject to a percentage change in dimension, and was hence dependent upon the initial size of the element. The magnitude of the cortical bone remodelling was thus a function of the mesh with which it was modelled.

To remove this mesh dependence, the cortical remodelling had to have the ability to grow on an absolute, global scale. The application of swelling growth to each material calculation point was achieved by relaying the value of FIELD(1) back to the ABAQUS code. This value became the swelling strain rate for that point. Since the applied timescale over the growth period of the loading history was unity, the "rate" in the equation may be ignored, resulting in the field variable equating to the strain at that point. Assuming that the length of each element in the direction of growth was updated after each swelling step then it was possible to apply growth as a function of the current size of the element. The value of swelling strain relayed in the field variable was:

$$\text{Swelling Strain} = \frac{\text{Growth Extension (in mm)}}{\text{Current Length of Element}}$$

In order to achieve swelling growth on an absolute scale, the code had to be aware of the present size or length of the element in the direction in which the swelling growth was applied. To gain this information, the pre-analysis routine was used, since the co-ordinate positions of all nodes were already known. The magnitude of the vector adjoining two nodes could be calculated;

$$\text{Distance} = \sqrt{\left(c_{i1} - c_{j1}\right)^2 + \left(c_{i2} - c_{j2}\right)^2 + \left(c_{i3} - c_{j3}\right)^2}$$

where c was the co-ordinate position and i and j were the two node numbers. Only two nodal positions for each element were taken for this procedure, taking this distance as an approximation of size for the entire element. This assumed low variation in thickness across the face of the element. Accuracy of this calculation could be improved by taking the element size across each edge in the direction of growth, and relating these values to the local integration points. Like most FE analyses, the precision of this procedure would increase with mesh density. This pre analysis calculation of the elemental size was stored in a local file named 'elsize'.

After being read into the User Subroutine (USDFLD) from file, the initial magnitude of element size was stored as a local state variable. During growth or swelling increments, the value of the Field Variable (FV1) passed back into the code was the strain divided by the size of the element. This was equivalent to passing the absolute growth in mm divided by the size of the element. The absolute swelling applied to the element was the maximum

extension in mm, multiplied by the stimulated growth or resorption (calculated from the tri-linear remodelling curve, expressed as a percentage of the maximum growth):

$$\text{Swelling Strain} = \frac{\text{Growth Requirement (\%)} * \text{Maximum Allowable Growth (mm)}}{\text{Current Length of Element}}$$

In this way, the user was able to define the maximum and minimum allowable growth in mm, and the resultant swelling gave an absolute growth, regardless of mesh size. It was then necessary to update the state variable (STATEV(5)) containing the length of the element in line with the resulting growth after every swelling increment. This ensured that the correct current length of element was used for future calculations of growth. This was achieved by summing the current length of element and the change in length (in mm) after each growth increment had occurred. The execution the procedure is detailed below, in Figure 6.16.

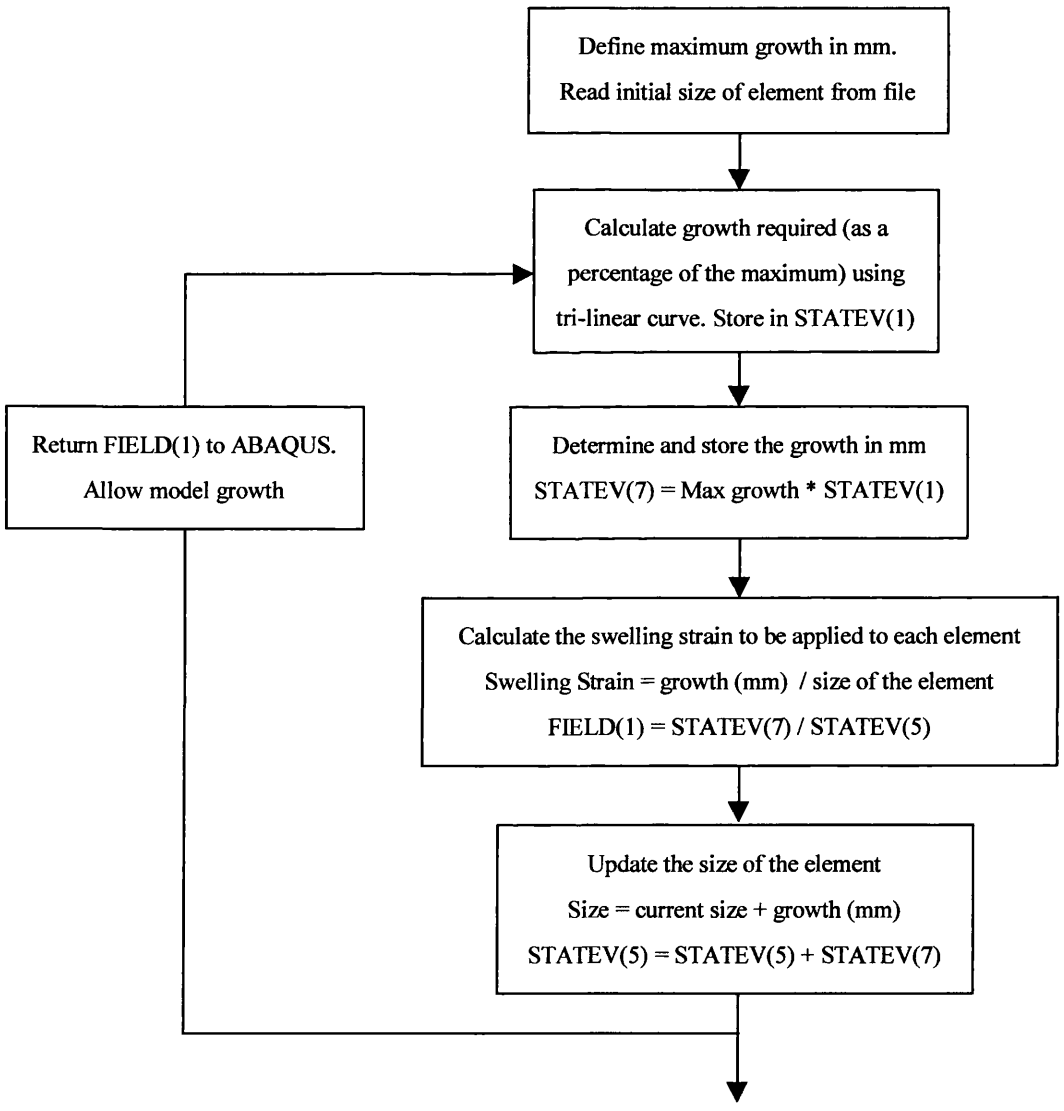

Figure 6.16 - Procedure to grow independently of mesh size

The procedure was tested using a single element model with an initial length in the growth direction of 10mm. The element was subjected to an imposed maximum growth of 2mm per swelling step, regardless of the calculated stimulus. The element growth correlated with predicted results, displaying progressive expansion in only the designated growth direction. Results for the size of the element are shown in Figure 6.17. Here, it can be seen that the length of the element was initially read into the analysis during the first growth step where an additional 2mm swelling was imposed upon it. Thereafter, uniform extensions of 2mm occurred during every remodelling step, consistent with the imposed swelling history.

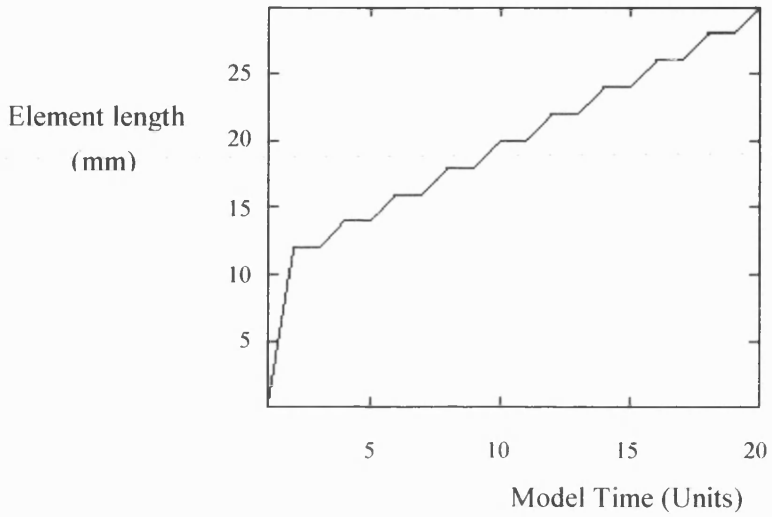

Figure 6.17 - Variation of element length with model time

Validation of the mesh independent coding was gained from the examination of the values of swelling strain returned from the subroutine (Figure 6.18). The progressive exponential decay in magnitude of the values of the field variable (FV(1)) peaks was due to the decreasing fraction of swelling strain required to produce a uniform growth of 2mm.

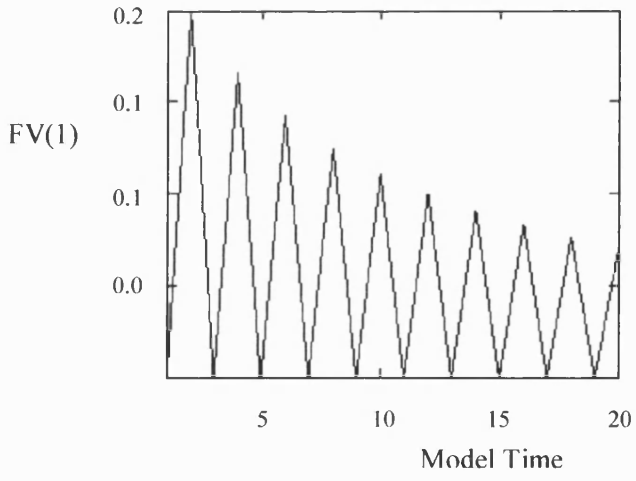

Figure 6.18 - Reduction of Swelling stimulus to allow constant growth

Confirmation of the correct growth magnitude on an absolute scale was gained by testing a similar element but of different original dimensions. Again, expansion of the correct and constant value occurred independently of the existing size of the element. In addition, the coding was confirmed against remodelling in a variety of directions.

6.7 Code modifications

Inaccuracies became apparent in the values of strain under the present loading regime, resulting in the appearance of warnings in the ABAQUS message (.msg) file. The model appeared to be unable to maintain remodelling equilibrium under so called physiological loading conditions using a one-percent dead zone band. Errors in the calculation of the remodelling stimulus appeared to become additive and within four or five growth steps, the model would commence with small amounts of growth. This process initiated an unrecoverable growth response, and once the first growth had occurred, and the model appeared to swell uncontrollably until errors terminated the analysis. Examination of the state of strain revealed only a small increase in the strains after each loading increment. It must be considered, however, that models, in general, will only be strained to within two or three percent. Added to this is the accuracy of the dead zone region that covers, in this case, only one percent of the remodelling strain values. An error in strain of 10^{-4} (the accuracy to which ABAQUS calculates strain) would therefore become substantial relative to the magnitude of the dead zone region and would rapidly lead to the introduction of growth when summed over several growth increments.

In order to reduce the relative magnitude of the strain error to the dead zone, experiments using the *CONTROLS parameter were performed, in which it was possible to control the level of accuracy to which ABAQUS calculated the values of strain during each iteration. Similar models were run each with an increased level of accuracy relative to the last. Surprisingly, only a small difference in the level of the calculated strain was found, insignificant to the magnitude of error that was being summed over the growth increments. Interestingly the error was constantly positive and hence one in which growth to the model, rather than resorption, was always introduced.

Examination of this increasing growth showed that the deformation resulting from a single loading increment introduced an overload situation, in which no convergence of the strain solution appeared to occur. Test modelling was carried out which considered the loading environment of the remodelling elements. It was found that a reduction in the applied loads

gave a more accurate strain analysis. The application of minute loads, in the order of one percent of those desired, gave accurate solution convergence, resulting in growth stability. Under these conditions, and a proportionate reduction in the imposed physiological strain environment, the model was able to actively maintain its geometry indefinitely. The resulting diagnosis was that the elements had been overloaded beyond their material capability for a single increment. The modelling solution was either to accept the convergence limitations of the elements and under-load the model or provide a mechanism to ramp the applied loads over a period of time, whereby decreasing the incremental load magnitude. Since any reduction in the overall structural loads would produce an entire change in the strain environment, and hence a variation in the long-term growth patterns, this option was clearly not plausible. As a result, the code was modified to include a ramp loading profile.

This profile meant that the loading was still applied over a cycle of loading, unloading and remodelling, but the unloading took on an active step before remodelling occurred. The cycle therefore contained three steps, loading, unloading and then remodelling.

At the same time, an attempt was made to reduce the effect of remodelling on the surrounding elements. The Poisson's Ratio was altered for each of the remodelling increments and assigned a value of zero, so that the pressure created on the neighbouring elements during growth or resorption was reduced. Whilst the technique produced only a small difference in the values, the results were satisfactory, and the method was retained in the model.

6.8 Stability of swelling code

Under extreme loading and growth conditions, slight instabilities have been observed in the long-term growth patterns in the simple four-element model. They manifested themselves as oscillations in the swelling magnitudes, resulting in inconsistent growth convergence. Initial growth patterns show a stable reduction in element extension (Figure 6.19). After apparent convergence has been reached, however, the model visibly displayed fluctuations along the length of the elements, first growing, then shrinking, and alternating from end to end of the four-element model.

Examination of the process has revealed a number of attributes relevant to the understanding of the element growth. Firstly, and most importantly, it has been observed that each material integration point has an individual set of remodelling goals, each with it's own tri-linear

remodelling curve. After a change in the loading conditions of the element, therefore, it is possible for a single element to have a variety of growth aims, signifying conflicts in the remodelling goals of the integration points within each element. On a global scale the effect appears insignificant, as each element retains enough stability for the ABAQUS code to continue the analysis. When viewed on a local scale, however, any instability may cause a loss of accuracy in the predictive capabilities of the code.

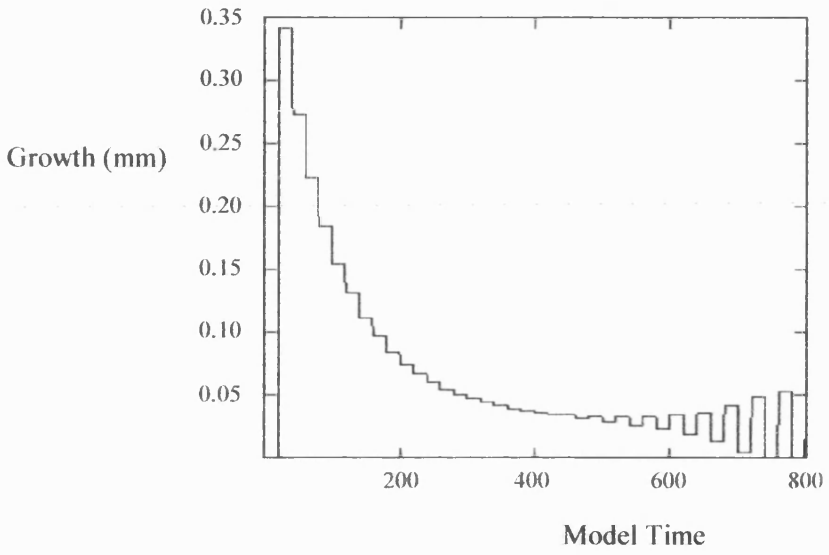

Figure 6.19 - Instabilities in the model growth

Figure 6.20 shows the growth patterns of three different integration points within the same element of a stable analysis. It demonstrates that the same element was able to produce different growth results according to the position within the element. This contributes towards the ability of quadratic growth patterns to occur, but various problems arise as a direct result.

The innermost point of the element rapidly reached growth convergence within approximately 13 loading steps, shortly followed by the central point. The outermost point, however, continued its attempt to grow by a minute amount each step. This would seemingly be pushing the inner points further towards the centre of the Dead Zone region of the graph, but the magnitude of growth is remarkably low (<0.15%, since it was the only point of three remaining growing), contributing little towards instability.

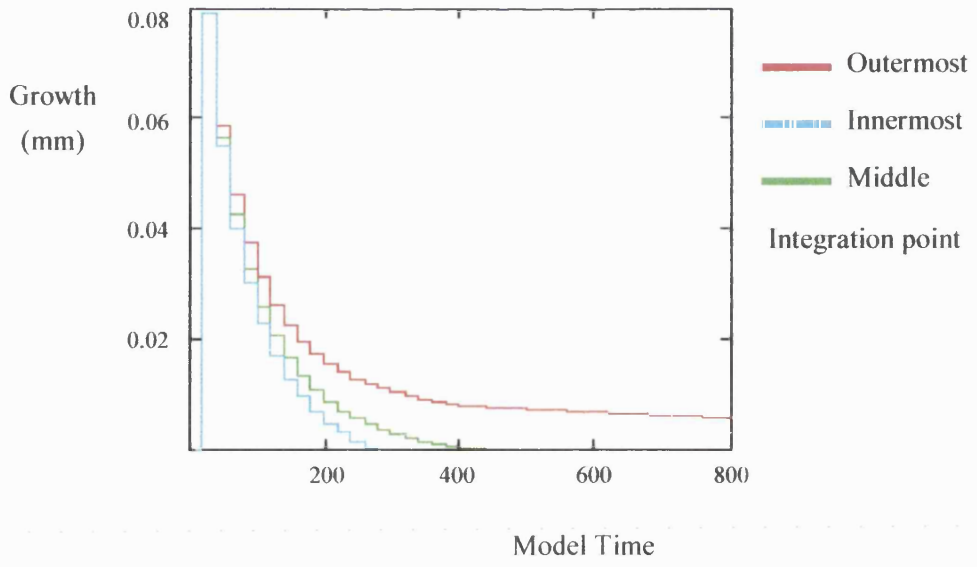

Figure 6.20 - Growth history of three different material calculation points within the same element

The corresponding stimulus history of the outermost material calculation points shows a reducing stimulus towards the dead zone, tailing off towards convergence above the dead zone (Figure 6.21). It is this remaining stimulus that provides the impetus for the outermost integration points to continue growth despite the halt in swelling of the other points in the element.

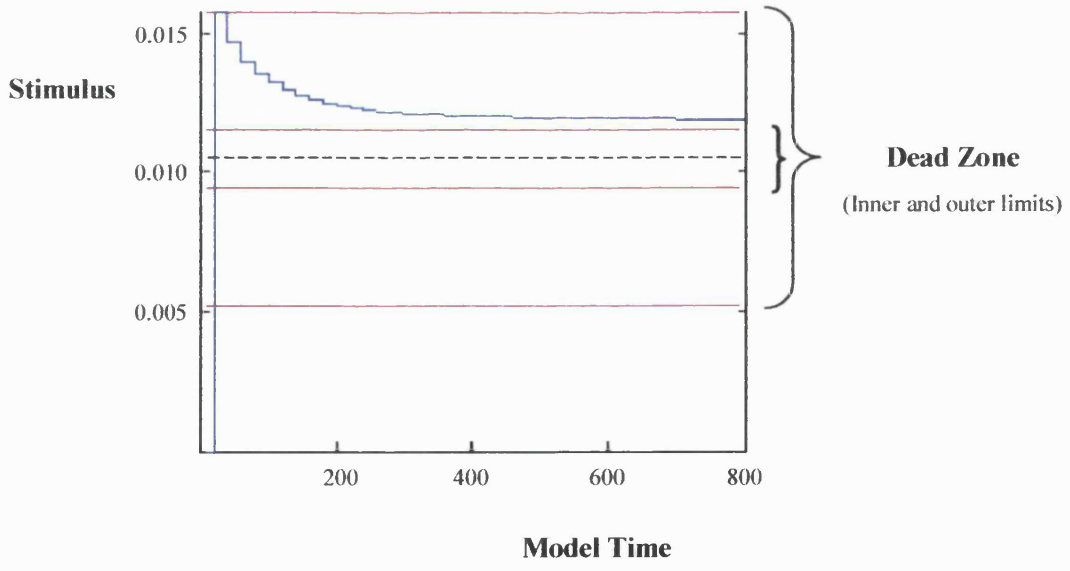

Figure 6.21 - Stimulus history of the outermost integration point

It should be noticed that the remodelling potential for this outermost material integration point never reached a position of complete convergence. It was surmised that the reason was

been a result of the conflicting interests of the local remodelling aims. The effect of various modelling parameters was studied in order to assess the stability of the swelling code and determine the causes of the oscillatory instabilities seen in Figure 6.19. Since many of the models studied displayed complete long-term growth stability, it was rational to assume that combinations of a number of parameters must have influenced the stability of the code - these were identified as:

- Initial size of the element
- Variation in remodelling stimulus across the element
- Growth imposed
- Boundary conditions
- Size of the Dead Zone

The variation in remodelling stimulus across the element was itself a function of the loading conditions. Since this, the initial size of the element and the imposed boundary conditions could not be defined within the code, the only parameters which could be varied were the growth magnitude and the size of the Dead Zone. The effect of these two parameters was studied and is shown in Figure 6.23. Each analysis was run with a specific combination of the Dead Zone period and the maximum allowable remodelling growth. The resultant stability was assessed by visual examination of the long-term growth graph, with instabilities being defined when oscillations in growth rate occurred (as seen in Figure 6.19).

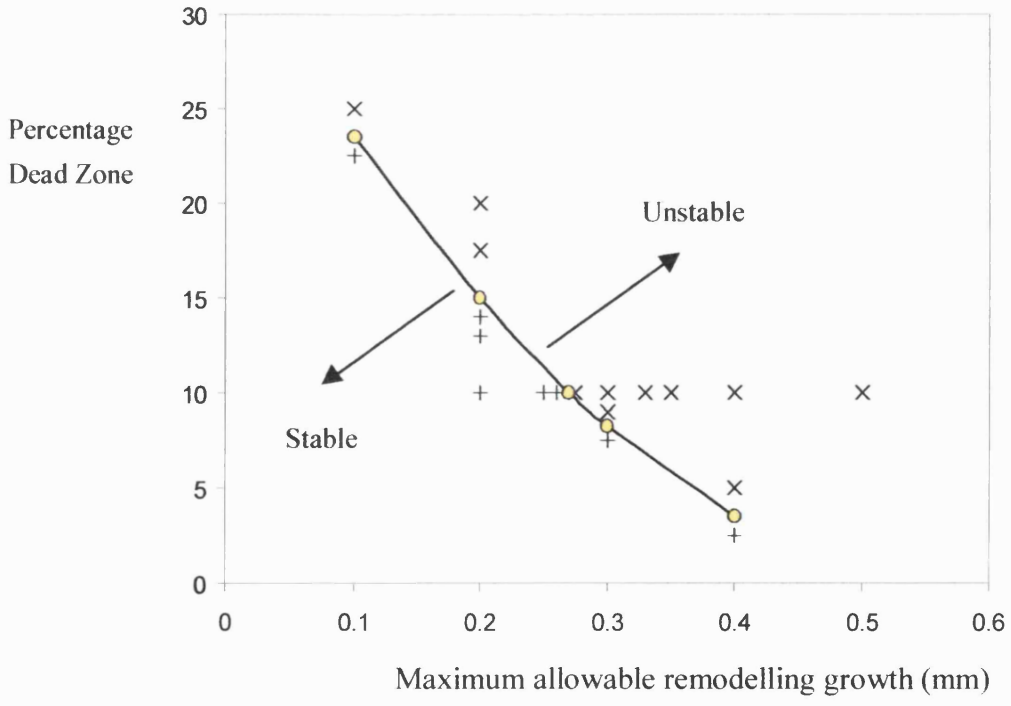

Figure 6.23 - Dependence of the code instabilities

It can be seen that the model produced a long-term stable solution for smaller values of both growth and remodelling Dead Zone. It must be noted that the instabilities seen in these models was only seen as small remodelling fluctuations at a very late stage of the remodelling process. In real terms, they are of little concern to the modelling of bone, in which the maximum growth allowed would be minute compared to the values discussed, and well within the stable regions of the graphs shown here. In addition, the boundary conditions and geometry of the four-element quarter circle model were not particularly steady, since all the elements could move towards and away from the centre of the circle. Additional stability would be provided in the boundary conditions of a model with central elements.

Many of the instabilities seen in the code were completely avoidable with the application of sensible parameters. The application of more stable boundary conditions than seen in this model may well result in a code that that is not susceptible to any instabilities.

6.9 Discussion

A method of modelling the long-term growth or resorption associated with bone remodelling has been presented here. Validation of the approach is discussed in Chapter 7, where the study of a variety of modelling applications is considered.

The method of using swelling to physically enlarge or reduce the size of the elements is affected by a number of limitations. Most notably, the technique is unable to apply remodelling growth or resorption to elements other than brick elements or prism elements that posses the correct orientation. The method is also functionally less efficient than the previous models (discussed in Chapter 4) since the calculation of the remodelling potential requires loading and unloading of the model for each remodelling step.

Chapter 7 Validation of swelling code

7.1 Introduction

Validation of any modelling code is an essential part of the development process. The following sections show a few of the more important models used during the study to examine the response of the swelling code. A range of models also enables the discovery of both behavioural properties and limitations of the code. These are described and discussed in order to provide a realistic assessment of what the technique is and is not able to achieve.

7.2 Remodelling of simple beam model

The swelling code was applied to a simple beam model (Figure 7.1) in order to assess the response of the elements under a variety of remodelling conditions. The static stress and strain distribution of a built in cantilever beam under simple loading is well established. It is known that the neutral axis travels the length of the beam, and hence each element is subjected to a variance in remodelling potential across its span.

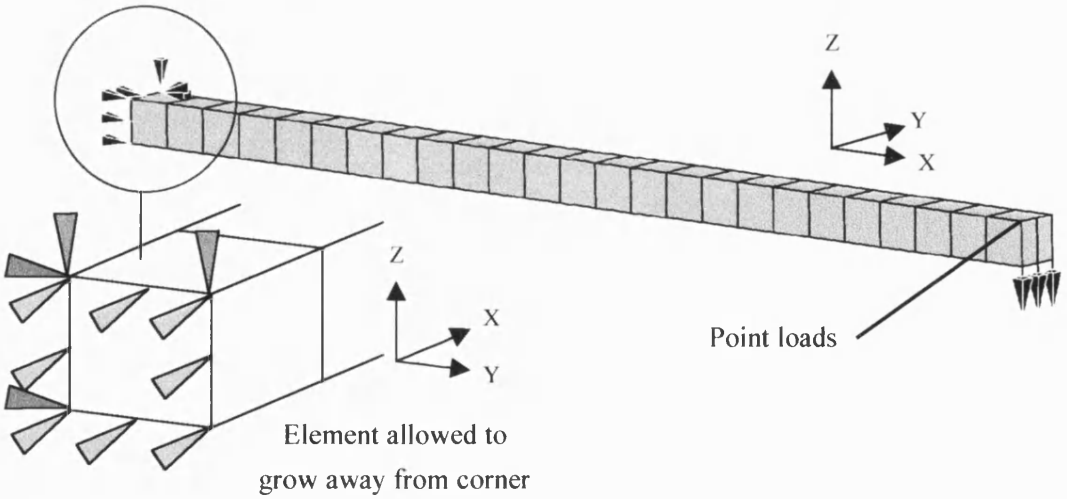

Figure 7.1 - Beam model showing both boundary and loading conditions

The beam was constrained in a manner that allowed both deformation under loading and remodelling of the end elements. The material properties were assigned values associated with cortical bone ($E=17000N/mm^2$ and $\nu = 0.3$). The most compressive principal strain was taken as the stimulus to which the beam material remodelled, and the resulting 'normal'

loading conditions of the beam were established (Figure 7.2) by applying three point loads, each of 0.3N to the end of the beam.

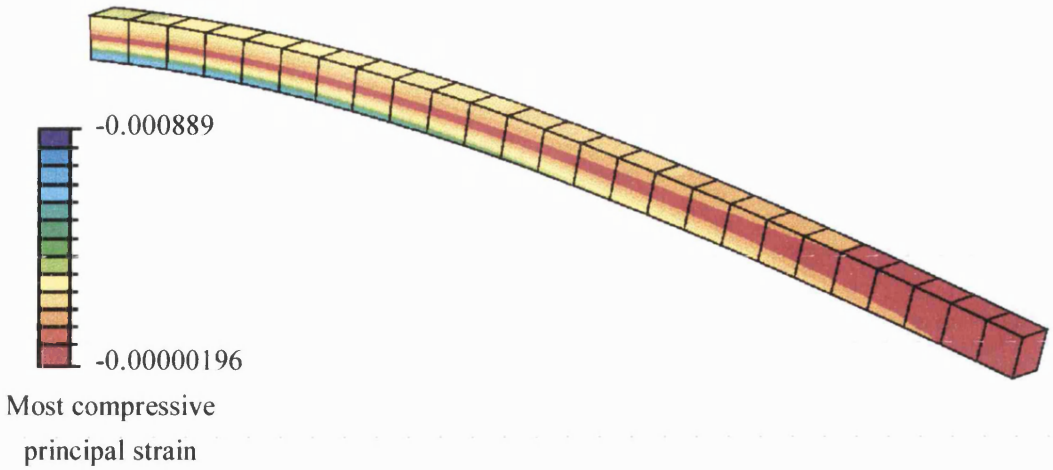

Figure 7.2 - Normal loading conditions of the beam

The loading on the beam was then increased in magnitude to 0.5N and the material was subjected to comparative remodelling i.e. a remodelling potential calculated from a comparison of the stimulus with the 'physiological normal' conditions rather than remodelling to an absolute stimulus scale. Although remodelling was not continued to a convergent solution, the resulting morphology of the elements allowed a good insight of the process that occurred. The results are displayed in Figure 7.3

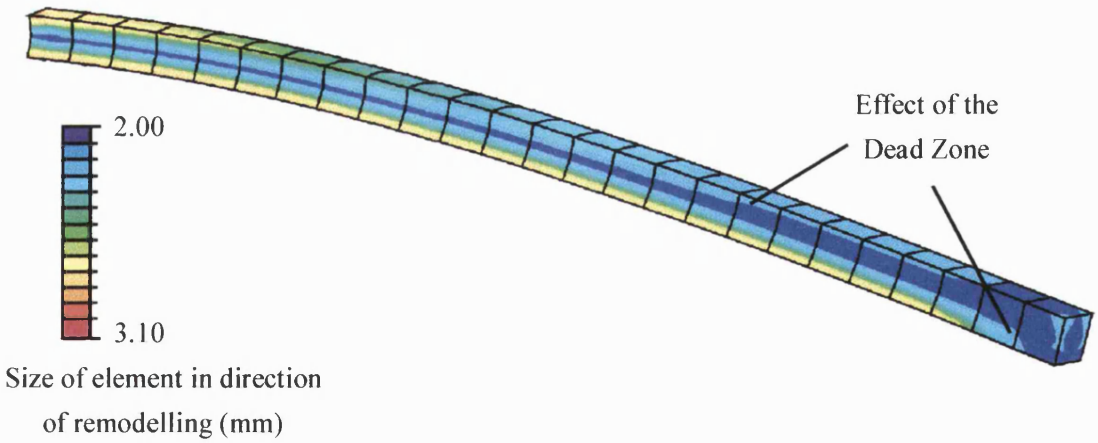

Figure 7.3 - Beam after remodelling

The remodelling of the elements produced growth on the upper and lower surfaces of the beam in accordance with the remodelling potential. The relative magnitudes of the growth decreased with increasing distance from the boundary constraints. The neutral axis of the

beam showed no remodelling, producing a beam shape comparable to the engineering I-section. This is shown in more detail for the third element away from the constraints in Figure 7.4. This element was chosen as it displayed the remodelling attempting to move material away from the neutral axis, whilst it was sufficiently distant from any of the localised effects of the boundary conditions.

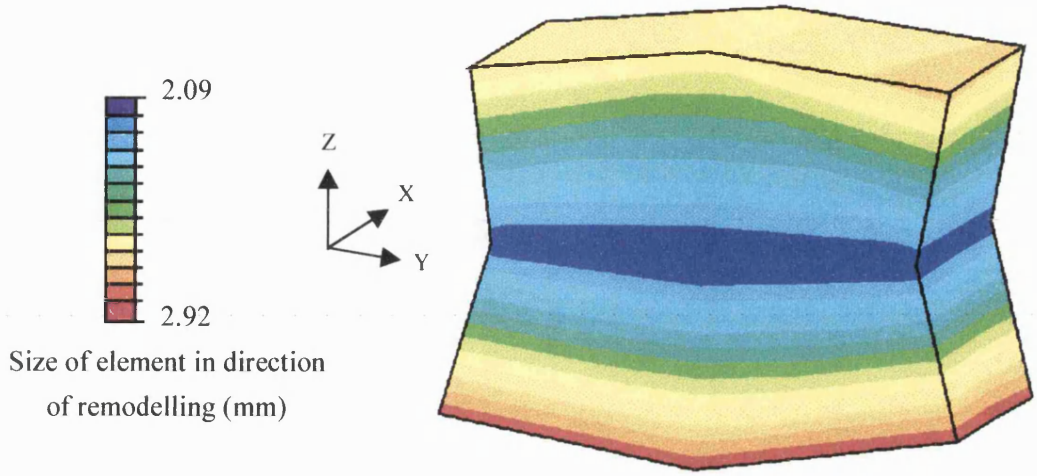

Figure 7.4 - Remodelling of a single element

The structure displayed varying remodelling patterns across each element, indicating that the code was able to cope with contrasting conditions over short distances. Interestingly, the orientation of remodelling was progressively changed as the growth of the element continued. This was displayed on the upper and lower surfaces that were deformed rather than remaining flat. The curvature of the element increased with distance from the neutral axis, and the effect was deemed to be a result of the elastic properties of the material. Whilst this appeared problematic over the distance displayed here, the effect is highly localised and caused as a result of the range of remodelling requirements over a single element. This effect is highly unlikely in the application of the code to a real remodelling situation, and would normally be resolved by an increase in the mesh density.

The remodelling of the beam showed progressive convergence towards the physiological normal solution. The result of this can be seen in the reduction of the deflection of the beam under the same loading conditions after remodelling had occurred (Table 7.1).

Deflection conditions	Maximum deflection (mm)
Before any remodelling occurred	5.05
After remodelling with a Dead Zone of 10 %	4.03

Table 7.1 - Maximum deflection of simple beam model

The deflection of the beam was significantly reduced after the remodelling of the beam, reenforcing the comparison with the engineering I-section causing an increase of stiffness in bending.

7.3 Cylindrical remodelling experiments

A further set of numerical experiments was carried out in order to test the operation of the code under circumstances more comparable with the required use. In addition, it was necessary to examine two basic features of the remodelling response; what, if any, are the remodelling differences between the 8 and 20 noded brick elements and should the cortical bone be composed of a one or two element thick layer. A cylindrical model was used (Figure 7.5). The model was bisected along a plane of axial symmetry, with translation constrains applied to all the faces of the elements shown in darker shading. The entire base of the model was constrained in the z-direction with a single node preventing movement in the x-direction, so as not to constrain or predetermine the growth of the base elements.

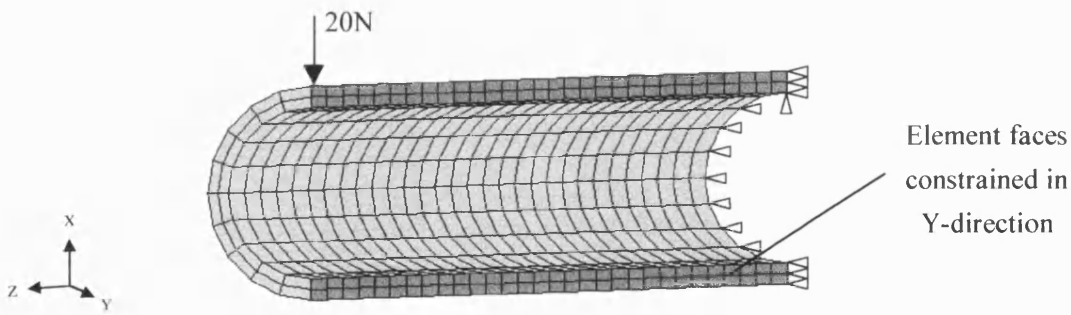

Figure 7.5 - Mesh of cylindrical test model (8 noded brick elements)

The material properties of the model were defined using approximate properties of cortical bone, with a Young's Modulus of 18 GPa and a Poisson's Ratio of 0.3. The 20N load was applied as a nodal force on a single central point of the model in the x-direction. The remodelling was initially specified using equivalent strain (ε_{eqv}) to a global remodelling scale, where

$$\varepsilon_{eqv} = \frac{2}{9}\sqrt{\left(\varepsilon_{P1} - \varepsilon_{P2}\right)^2 + \left(\varepsilon_{P2} - \varepsilon_{P3}\right)^2 + \left(\varepsilon_{P1} - \varepsilon_{P3}\right)^2}$$

Where ε_{p1} , ε_{p2} and ε_{p3} are the three principal strains.

The dead zone was effectively removed by defining the two mid points of the tri-linear curve as coincident. Whilst the load and the remodelling curve magnitudes seem somewhat arbitrary, it was the relative change in morphology of the structure that was being explored here. The remodelling patterns produced are shown in Figure 7.6

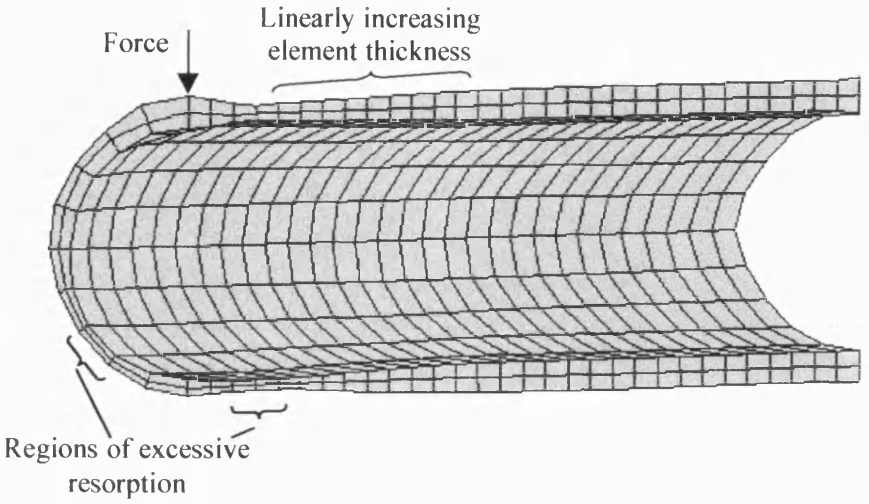

Figure 7.6 - Remodelling of cylinder model

Since the remodelling potential of this system was determined from the absolute values of the stimulus, with no comparison against a 'normal' condition, growth occurred in the regions of high loading. Progressive linear thickening of the elements was seen for elements situated on the line of bisection. Errors were caused in the analysis by excessive resorption of the elements in two regions of the model, resulting in the material integration points attempting to pass through each other. This gave the impression that the elements were turning inside out. These problems were curtailed by limitation of the maximum allowable resorption.

The model consisting of twenty noded brick elements displayed similar remodelling patterns to its eight noded counterpart (Figure 7.2). Less extreme growth patterns were seen after remodelling in this model, caused by earlier termination of the analysis, but the remodelling displayed similar features. The principle regions of growth were around the boundary constraints and the loading locations, and resorption occurred on the opposite side from the load.

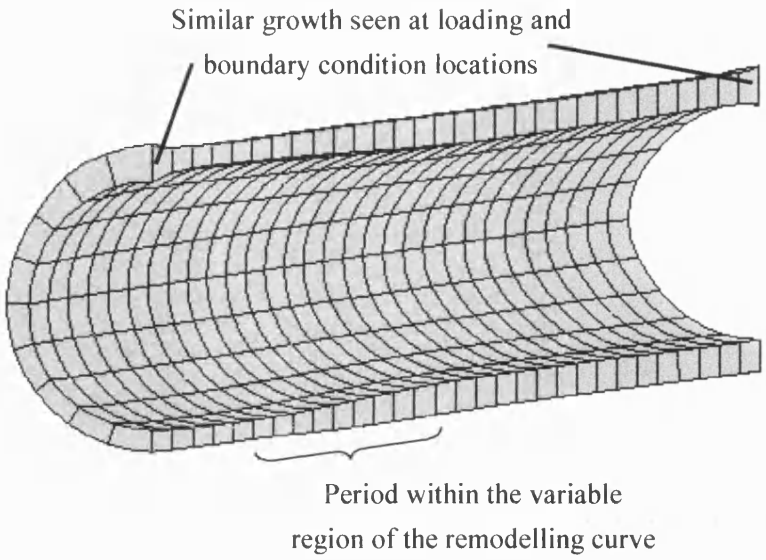

Figure 7.7 - Remodelling of cylinder model comprised of twenty noded elements

The comparative remodelling patterns of the two meshes provided confidence in the different sections of code used between the twenty and the eight noded elements. The stability of the twenty noded element model was of concern, but the analysis was similar to the four-element model described in the previous Chapter (Section 6.2.7) where the instabilities were discussed. As a result, should any analysis using quadratic elements appear unstable, reduction to a linear model should provide a more stable solution. Assuming a stable result could be gained, however, the twenty noded element model produced a smoother, more continuous remodelling pattern and would be used in preference to the eight noded element model.

The differences between one and two layers of elements was minimal, although in certain regions of the two-layered model it was noticeable that the two elements differed in the amount of remodelling. This was obviously not possible in the single layered model, although the quadratic elements were able to account for the movement better than a single layer of linear elements due to the mid-side node. Over a small range of remodelling values, however, the differences were indistinguishable.

7.4 Validation against turkey ulna model

Final validation of the swelling code was gained from comparison with the study undertaken by Brown *et al.* (1990) who examined the remodelling response of a functionally isolated

turkey ulna under the application of a well-controlled mechanical environment. The ulnae of two turkeys, which were initially considered to be in a state of remodelling equilibrium under a normal physiological loading environment, were isolated from further physiological loading by surgical sectioning. Both ends of each ulna were pinned and capped and subjected to a known cyclic Instron loading regime. The animals were sacrificed after a four and eight-week loading period. The ulnae were then sectioned and the resulting new bone formation observed (Figure 7.8). The resulting radiographs illustrated periosteal remodelling with preferential thickening on the ventral surfaces. The eight-week bird also displayed growth along the caudal surface.

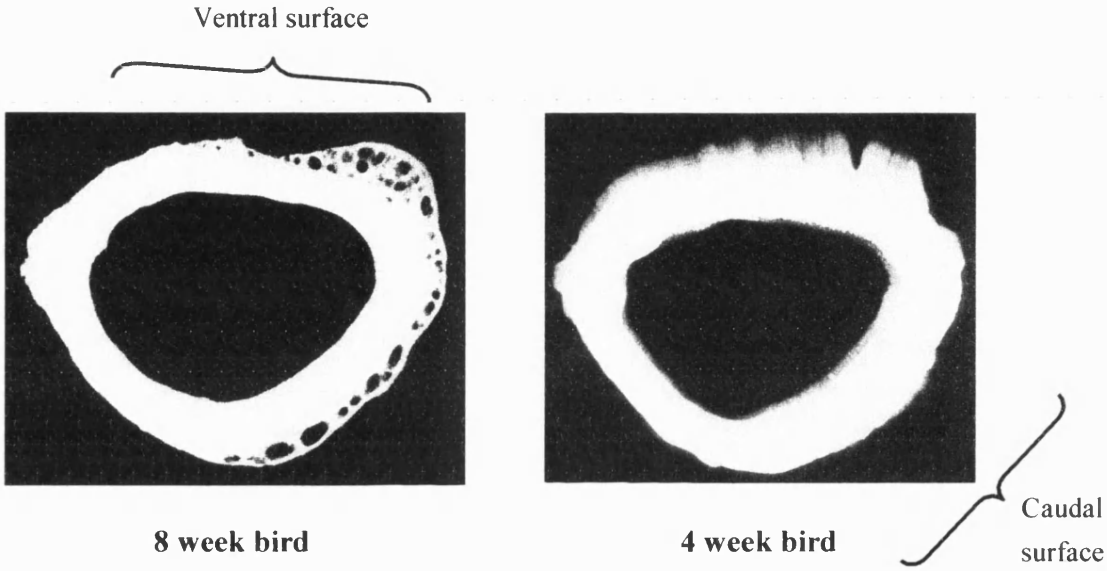

Figure 7.8 - Radiographs of the ulnae mid-section geometry after rem odelling (Brown et al. 1990)

A finite element model of the ulna section of a similar turkey, which had undergone in vitro strain gauge testing, was constructed from a series of projected photographic images. The model was loaded in accordance with the experimental studies, and a static analysis performed for analytical evaluation of candidate stimuli. The signal was defined as the change in the absolute value between the normal physiological loading case (Wingflap case) and the Instron loading conditions (so called Instron case). The study then examined and compared the remodelling associated with new bone formation on the periosteal surface of both the 4 and 8 week ulnae with a number of possible remodelling stimuli calculated from the FE model.

The study used the single best degree of linear correlation as a measure to determine the most probable objective stimulus to represent biological periosteal remodelling. As little change was observed on the endosteal surface of the bones, this remodelling was ignored.

Twenty-four different candidate parameters were compared, with the conclusion that the most tensile principal stress correlated most closely with the remodelling seen in the 4-week bird, having a Pearson coefficient of 0.823. Interestingly, the paper reported that the most tensile principal stress and the most tensile principal strain gave different values of correlation with the 4-week bird (0.464 for the most tensile principal strain) despite the linear homogenous isotropic material properties used for the analysis. These parameters gave lower correlation with the remodelling seen in the 8-week bird (0.63).

7.4.1 Ulna model creation

Rubin and Qin (personal communication) generously contributed the ulna geometry for use in this study. The data, which was received as a series of point co-ordinate positions, was read into ABAQUS PRE to create a mesh corresponding to the Brown *et al.* (1990) study (Figure 7.9). A series of curves were defined through the points with closed loop interpolated splines. The curves were then split in half about two diametrically opposite points on the periosteal surface, aligned with the corresponding endosteal points. Six pairs of surfaces (each pair consisting of one periosteal and one endosteal surface) were created along the length of the shaft by 'sweeping' the relevant curves.

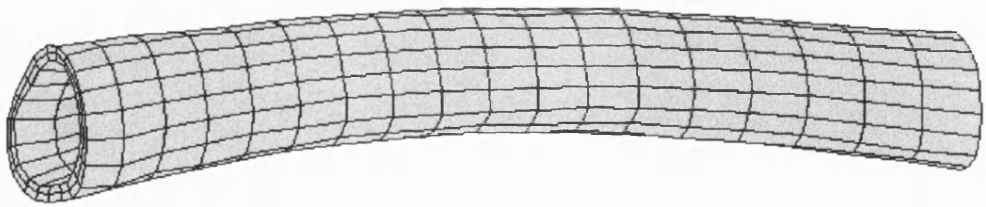

Figure 7.9 - Finite element mesh of the turkey ulna

Six solid entities were produced from the surfaces giving three equal length sections. 720 three-dimensional 8 noded brick elements were produced using the ABAQUS PRE automatic mesh generator in a configuration as close to the original mesh used in the Brown study as possible (Figure 7.9). The Young's Modulus of the cortical bone was 11 GPa and the Poisson's Ratio was set as 0.3, corresponding to the Brown publication. Whilst the mesh attempted to duplicate the original study, small variations in the element arrangement mesh were inevitable, since different packages containing a variety of parameter definitions were used for its creation.

7.4.2 Wingflap case

Brown assumed the physiologically normal conditions for the turkey to be the situation immediately before sacrifice, since the turkeys had been allowed to move freely. As mentioned earlier, the strain environment under these circumstances had been previously determined during an *in vivo* study (Rubin and Lanyon, 1985). It was surmised that the load during free movement would have originated from a linear contact over the condyles, even though the finite element model didn't extend to the ends of the bone. The result was the assumption that the bone loading conditions could be approximated to a pin load bisecting the bone. They then adopted an iterative approach to calculate the position and orientation of these pin loads that gave midsection strains consistent with those seen during vigorous wingflapping. These conditions, which corresponded to a resultant force of 239N, were applied to the finite element model and deemed to be the physiologically normal loading case (Figure 7.10).

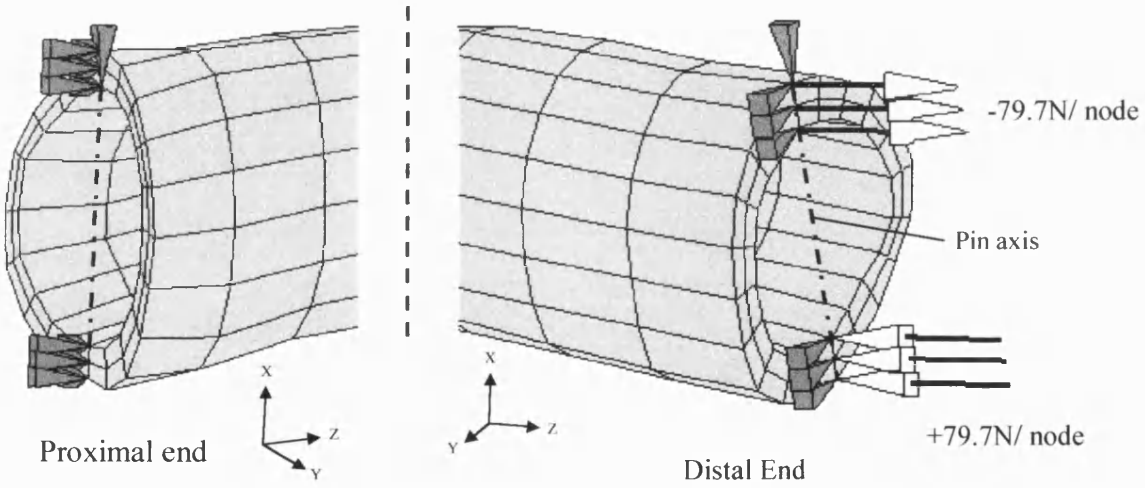

Figure 7.10 - Boundary and loading conditions for the wingflap loading case

It was necessary to alter the boundary conditions at the proximal end from those imposed on the Brown model, since no remodelling occurred on the original mesh. The fixed pin constrains were replaced by conditions preventing movement along the z and y axes, but only a single node was constrained along the X-axis in order to allow movement and growth in a direction perpendicular to the surface (Figure 7.10). Similar conditions were applied to the distal end of the bone with movement restricted according to a set of local axes, aligned with the loading pin. Whilst the wingflap model was examined only to determine the physiological normal stress and strain environment, with no remodelling occurring, it was considered that these alterations should be made in both models for consistency between the two cases.

Since the boundary conditions surrounding the loading pin were altered, it was deemed necessary to validate the resulting loading environment against the original model. This was achieved most easily by comparison of the position of the mid section neutral axis, since these results were detailed in the Brown publication. Figure 7.11 shows the resulting correlation of the Brown study against our FE model loaded as Figure 7.10.

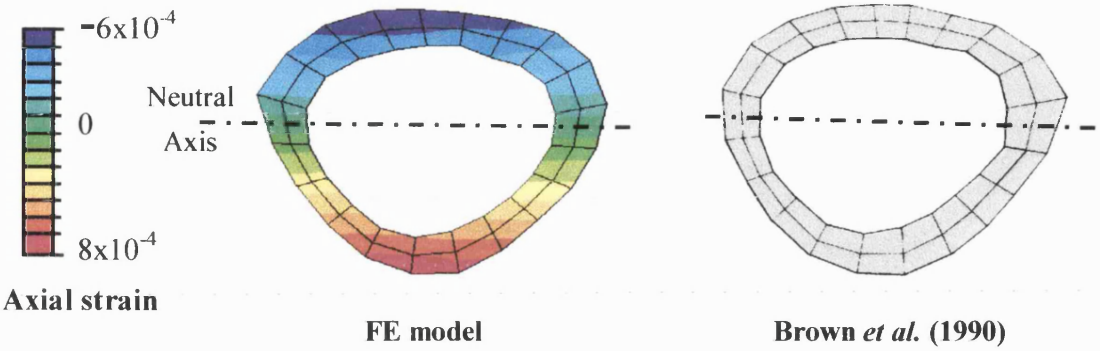

Figure 7.11 - Correlation of midsection neutral axis with experimental data under wingflap loading conditions

The predictions clearly demonstrated excellent comparison of the position of the mid-section neutral axis with the Brown study. This provided confidence in both the loading and boundary conditions used. Since the wingflap case was able to determine the physiological normal environment for the objective remodelling stimulus, the analysis under these conditions became the Model Pre-Analysis (see Chapter 6).

7.4.3 Instron loading case

Subsequent to sectioning and capping, the surgically isolated ulnae of the two test animals in the Brown study were attached to pairs of steel forks that gripped the fixation pins. The load, which was transmitted via forks, was imposed by the Instron machine in controlled uniaxial displacements, creating a controlled loading environment. The resulting experimental loading conditions were assigned to the finite element model (Figure 7.12). Similar to those placed upon the Wingflap Loading Case, the boundary conditions again allowed the constrained nodes translation perpendicular to the surface of the bone.

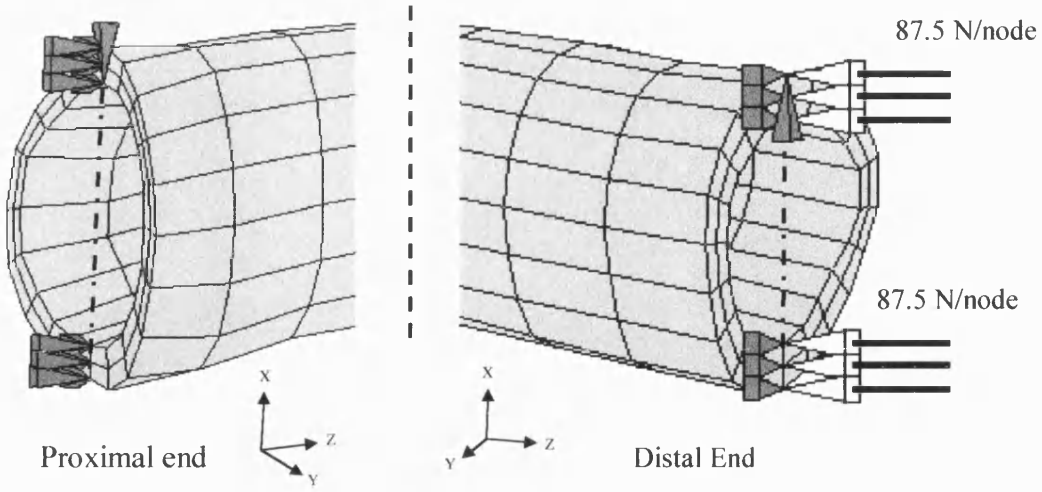

Figure 7.12 - Boundary and loading conditions applied to the Instron case

The correlation of the mid-section neutral axis position between the strain tested ulna and the FE model was again examined (Figure 7.13). Good correlation was gained in both position of the neutral axis and magnitude of axial strain, which is shown in Table 7.2. The number of the strain gauge relates to the position shown in Figure 7.13, and the result is given as strain rate per Newton of applied load.

Strain Gauge	Brown *et al.* (1990) Strain / N ($x10^{-6}$)	This FE study Strain / N ($x10^{-6}$)
1	-3.26	-3.38 (-3.12 to -3.64)
2	0.34	0.28 (0.16 to 0.54)
3	-2.05	-2.08 (-1.82 to -2.34)

Table 7.2 - Correlation of mid-shaft strains with experimental data

The position of the axis demonstrates that almost complete uniaxial bending was produced during the Instron loading despite the compressive loading conditions. Questions were raised on the application of the loading and boundary conditions applied to the model, since controlled boundary displacements would cause a higher degree of compression within the bone than the application of forces would. This was caused by the controlled movement of the nodal positions imposing predetermined deformation of the entire shaft of the bone. The application of the load using forces, on the other hand, allowed the nodes to move in a manner determined by the shape and properties of the bone. As a result, the displacement of

the nodes at the points of loading may have been unequal at the medial and lateral sides of the bone. Comparison between the two types of loading was performed, resulting in the decision to continue with the application of point force loading, since closer correlation of the mid-section neutral axis with the Brown study was achieved.

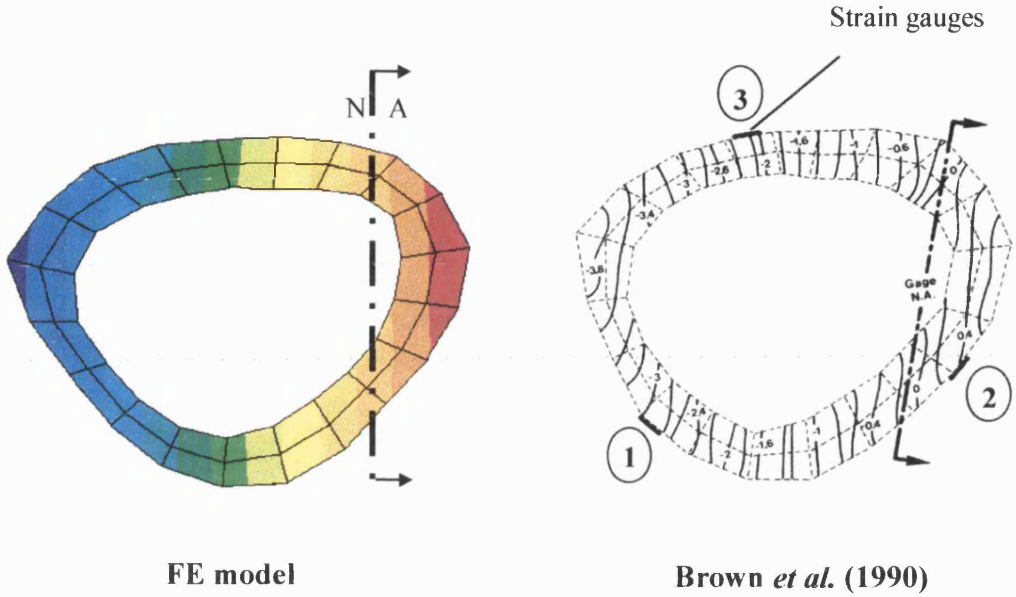

FE model **Brown *et al.* (1990)**

Figure 7.13 - Correlation of midsection neutral axis with experimental data under Instron loading conditions

The good comparison of neutral axis positions, both in the physiological normal wingflap and the Instron loading case, together with the agreement of the strain gauge results provided good validation of the Finite Element model of the turkey ulna.

7.4.4 Extension of Brown's study: Predictions of remodelling using the swelling code

After the application of the boundary and loading conditions was sufficiently validated, the Wingflap Loading Case was run as a Pre-Analysis in order to determine the magnitude of the physiological normal loading condition and hence the centre of the dead-zone for each element of the model. The analysis was run using two values of dead zone threshold; 40% as in the original study, and at 10% in an attempt to establish the sensitivity of the code to the input parameters. The remodelling stimulus was initially defined as the most tensile principal stress, as recommended by the original study, and the remodelling algorithm was applied to all elements, using the loading environment produced by the Instron loading case.

The loading for the remodelling bone was applied as a ramp increase over a period with two increments per step. Unloading was ramped in a similar manner, and every third step was designated as a remodelling period.

7.4.5 Remodelling results

The preliminary remodelling predicted after the initial loading but before any remodelling increments occurred, is displayed in Figure 7.14. The predicted remodelling was based on the signal difference between the normal wingflap stimulus and that calculated under the Instron loading case, and is shown as a percentage of the maximum possible growth in millimetres. A comparison is given with the new periosteal bone formation seen in both the 4 and 8 week birds.

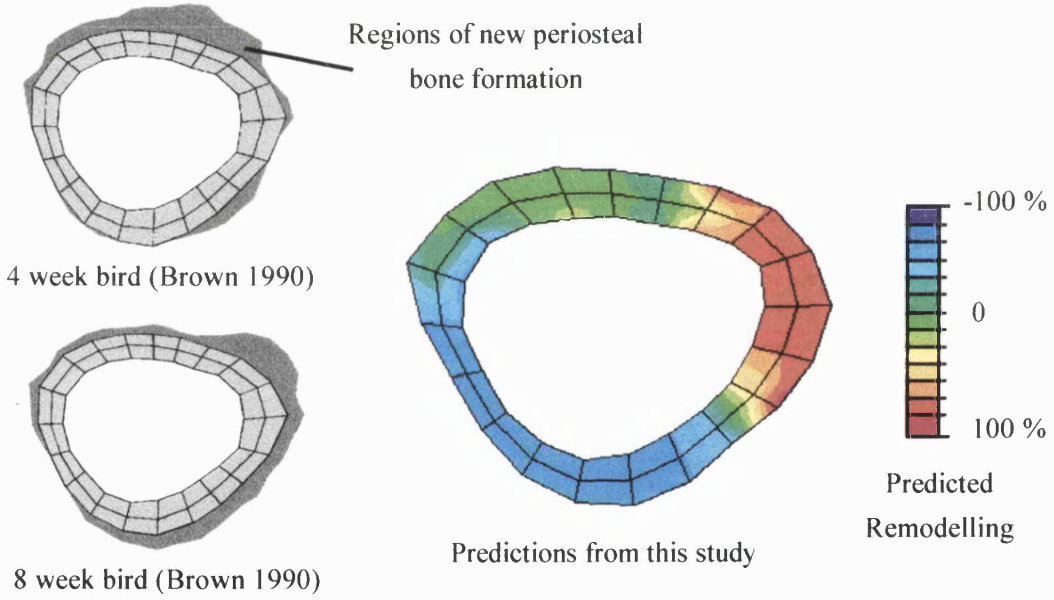

Figure 7.14 - Predicted remodelling of ulna mid-section before remodelling occurred

Interestingly, the regions of projected new bone formation (regions shown as light green through to red) are qualitatively different from those presented as the 4-week experimental remodelling study and closer to the longer term remodelling results seen in the 8-week bird. Of all the predicted remodelling results, however, this stimulus did give the best visual comparison to both of the bird sections. This supports the Brown study in the correlation of the most tensile principal stress with the remodelling seen in the turkey ulnae, but suggests that the stimulus may provide a better comparison with the 8-week, rather than the 4-week bird.

The mid-section remodelling resulting from the principal tensile stress stimulus is displayed in Figure 7.15. Three results are shown, providing a comparison between the rate of remodelling and the size of the Dead Zone. Remodelling was halted after a maximum allowable 0.42 mm growth because this was the first point at which the stability routine became active: a point after which the remodelling would be affected by imposed conditions. Beyond this point, it was necessary to actively prevent the elements from excessive resorption by precluding any remodelling from occurring under certain conditions. These circumstances were specified as periods when the remodelling was negative (identified as resorption) and of a magnitude greater than or equal to one third of the current size of the element in the direction of growth. This is due to the fact that the majority of resorption may occur at a single integration point.

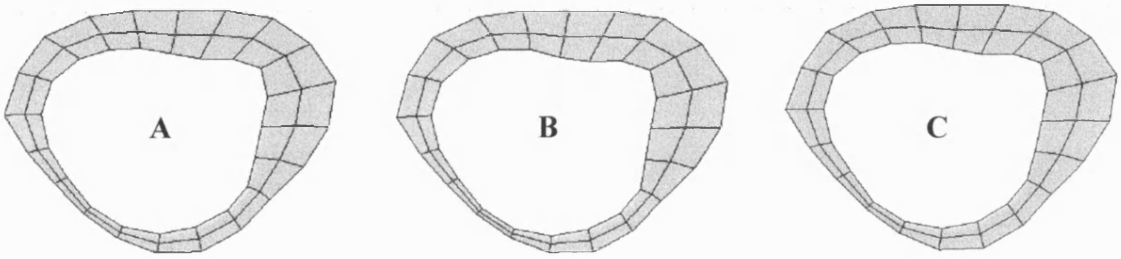

Principal stress stimulus. 7 Remodelling steps at a maximum of 0.06 mm/step. 10% dead zone.	Principal stress stimulus. 14 Remodelling steps at a maximum of 0.03 mm/step. 10% dead zone.	Principal stress stimulus. 14 Remodelling steps at a maximum of 0.03 mm/step. 40% dead zone.

Figure 7.15 - Remodelling of ulna mid-section under various stimuli and growth rates

Whilst the remodelling of the mid-section of the ulna broadly followed the new bone growth seen in the experimental studies, the stimulus used for the remodelling was brought into question. Each analysis using the most tensile principal stress exhibited severe resorption in regions of the bone wall (Figure 7.16). This resorption continued until the elements simply collapsed in upon themselves causing instabilities and eventually errors in the analysis.

It must be noted that confidence in any continued remodelling is reduced after the growth patterns of the elements are curtailed. This is due the effect of the artificial changes on the surrounding material. In addition, precision of the stress / strain environment is often reduced by the time of intervention, since the elements were likely to have altered their Jacobian ratio sufficiently to have introduced inaccuracies into the analysis. Had the stability routine been disabled, then the remodelling of the bone would continue into the shape shown in Figure 7.16.

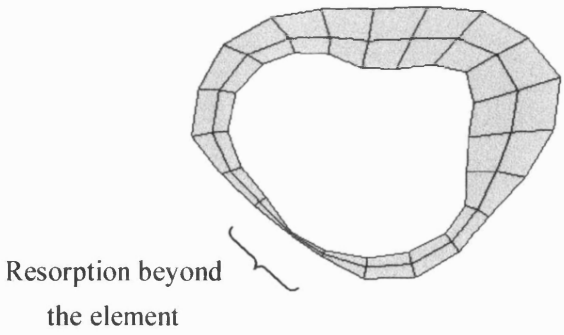

Figure 7.16 - Final morphology of mid-section under most tensile principal stress stimulus

As a result of this excessive resorption behaviour, all of the following analyses of the ulna are shown until a maximum remodelling growth or resorption of 0.42 mm. The final mid-section of the ulna FE model under these conditions is shown in Figure 7.17 for a number of different remodelling stimuli used in the original Brown study.

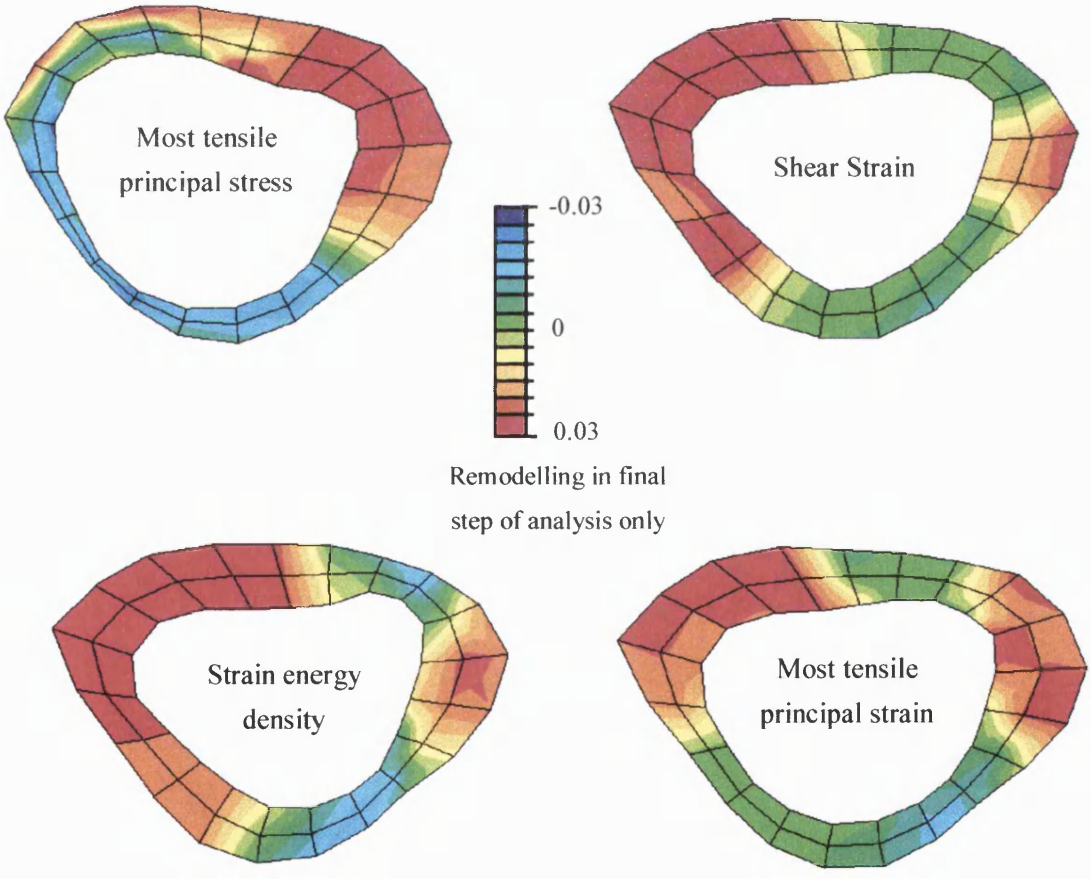

Figure 7.17 - Remodelling under different stimuli

The majority of the remodelled sections tended to be dominated by the two different positions of the neutral axes since the stimuli were based on stress and strain. Element

growth was generally seen around the wingflap neutral axis since the remodelling attempted to restore the low magnitude of the physiological normal levels of stimulus. In a similar manner, resorption was seen across the Instron neutral axis. The notable exception to this was the most tensile principal stress, which produced remodelling growth in the regions of the Instron Loading Case neutral axis. This result provided excellent agreement with the original Brown paper.

The stimuli examined were calculated using the definitions applied in Brown *et al.* (1990), and were all a function of the principal stresses and principal strains except for the longitudinal shear stress. The problem with this stimulus, of course, was that the orientation of each element integration point had been redefined in order to establish the direction of remodelling. Whilst this provides no complication for any function of the principal values (the orientations of these values are determined independently), the orientations determined for the longitudinal shear were approximate, rendering the results for this stimulus alone, unreliable.

7.4.5.2 End sections of the Ulna

The stress and strain environment at the end sites, near the surgical sectioning, were highly complex, and were dominated by the presence of local loading variations. The original experimental studies showed prolific new bone formation in a seemingly chaotic pattern (Figure 7.18). Predictions of the remodelling in these areas was deemed virtually impossible, and any similarities in the morphology of the remodelled elements and the end section of the animal were considered coincidental.

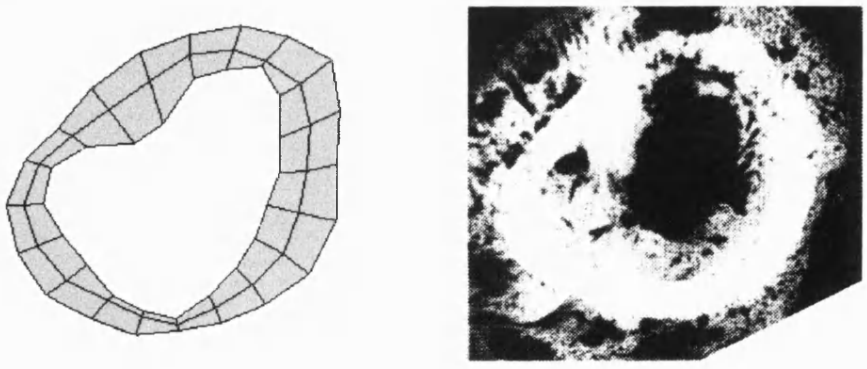

This study | Brown *et al.* (1990)

Figure 7.18 - Irregular remodelling at the end sites

7.4.6 Dead Zone modification

The remodelling of the ulna models displayed a high degree of sensitivity to changes in the magnitude of the stimulus around the neutral axes. This was, in part, due to the width of the Dead Zone of the tri-linear remodelling curve. Normally, the centre of the Dead Zone was equal to the physiological normal value of the stimulus, and the size of the Dead Zone was then determined as a percentage of that value. Any material calculation point that was positioned on the neutral axis under the physiological normal loading, therefore, would have had an initial stimulus value of zero. Since the tri-linear curve for each element was generated based upon a percentage of its own physiological normal value of stimulus, the Dead Zone would also have a zero magnitude, regardless of the percentage value allocated to it. Consequently, any change to the neutral axis resulting from a change in loading (after the functional isolation by surgical sectioning, in this case) would produce localised maximum growth, no matter how small the change in magnitude of the stimulus. In other regions of the same bone, however, a difference of the same magnitude from the normal physiological stimulus would induce a far smaller remodelling response.

This was especially prevalent in the examination of the remodelling seen in these turkey ulnae since the imposed loading conditions severely altered the position of the neutral axis from the physiological normal wingflap case. The result was that highly localised regions of bone deposition and resorption were found around the positions of both the wingflap and Instron neutral axis. Perhaps more importantly, however, was that these regions were found under high bone remodelling gradients (shown in Figure 7.17), demonstrating the problem with the tri-linear curve.

To improve these localised problems, a new method of defining the Dead Zone was devised. Instead of calculating the dead zone as a percentage of the local stimulus, a standard value of the dead zone was given to all elements. This allowed every element the same sensitivity to the surrounding environment, regardless of the initial physiological normal. The position of the centre of the Dead Zone was still determined in the same manner, based on the normal value of stimulus. The magnitude of the dead zone was based on the initial remodelling potential of the elements, i.e. the difference in stimulus between the normal Wingflap Loading and the imposed Instron Loading conditions. This gave a predicted range of values for which the stimulus varied, with the zero position defining zero remodelling.

The dead zone was then defined as a fraction of the range of stimulus values. In this manner, any change in stimulus due to the loading conditions would be proportional to the predicted

remodelling values in that region. Should a section then have generally high values of stimulus over a small range, then the remodelling would be sensitive to smaller changes in loading conditions.

This technique was applied to the ulna model, for which the remodelling potential under a most tensile principal stress stimulus was displayed in Figure 7.14. Since the values of remodelling potential were only calculated for the region of remodelling interest, the calculation could be based upon the actual values of most tensile principal stress (not shown) rather than the percentages displayed. In this case, the Dead Zone for the entire model would take on a standard magnitude, based on the actual value at, say, 20% of this scale.

An additional advantage of this method is that it is possible to define the dead zone based upon a specific region of remodelling interest, and disregard any unwanted or incorrect areas such as localised boundary conditions: the size of the dead zone would simply be a function of the values seen in the regions of interest. When used for the turkey ulnae, this method allowed the dead zone to be tailored to the mid-section region of the bone, ignoring the end sites, which are known to be problematic.

7.4.7 Application of the modified Dead Zone to the ulna models

The calculation of the modified Dead Zone was applied to the ulna models and the resulting remodelling reassessed. A value for the magnitude of the Dead Zone was calculated independently for each stimulus based upon the initial remodelling potential, and the analysis was run for an identical period as the previous models, with the same range of allowable remodelling growth and resorption. The final shapes are displayed in Figure 7.19, in which only the remodelling potential for the final step is shown. The remodelling of the ulna under a hydrostatic stress stimulus is also shown since it gave good visual correlation with the remodelling seen in the Brown experimental studies. Interestingly the shape resorbed to a point where the stability code is required, but the stimulus gave a good qualitative representation of the remodelling that occurred in the 8-week bird. This again, like the most tensile principal stress stimulus, was in disagreement with the Brown study, who stated a better correlation with the 4-week bird.

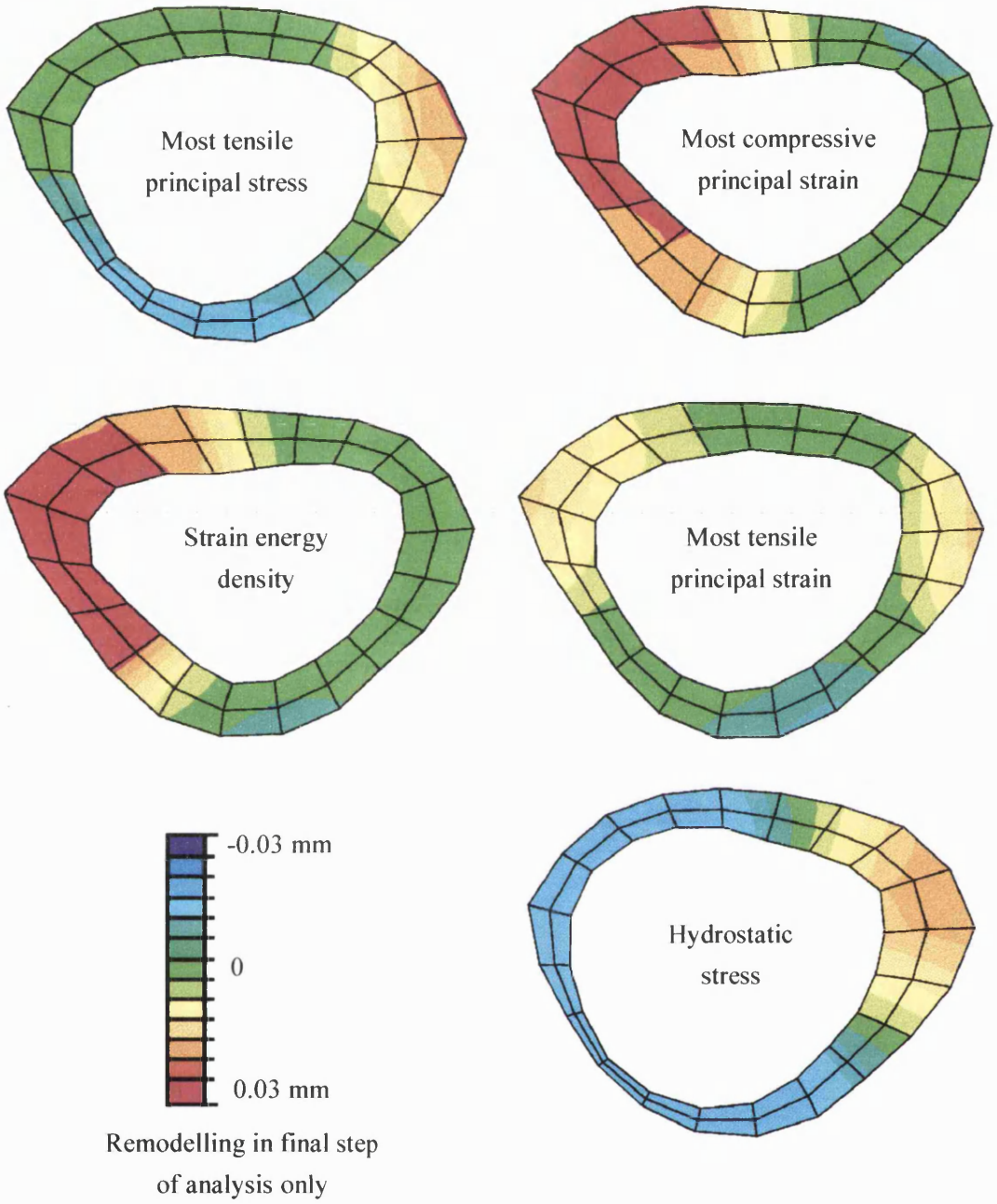

Figure 7.19 - Ulna mid-section remodelling using new dead zone definition

The modification of the Dead Zone obviously made a significant difference on the remodelling of the ulnae. Much smoother regions of bone deposition and resorption were seen, with far less erratic remodelling patterns. An additional benefit of the modified Dead Zone was the apparent remodelling stability inherent in the models. This is clearly

demonstrated by comparison of the ulna under the strain energy stimulus (cf. Figure 7.17 and Figure 7.19). The shape before modification of the Dead Zone showed significant regions of bone deposition around the neutral axis of the Wingflap Loading Case, with regions of resorption in between. The remodelling after the modification of the Dead Zone showed over half the section of the bone with no potential to remodel. In addition, the remodelling growth on the opposite surface is significantly reduced, with less change in the remodelling gradient.

It can clearly be seen that the final morphology of the bone is highly dependent upon the remodelling stimulus used. This is a particularly positive result, which demonstrates the sensitivity of the remodelled morphology to the mechanical parameters used in the analysis. It demonstrated that the code does not produce similar results regardless of any changes made.

The code has been unable to define the detail of remodelling seen in the ulna experimental studies, although this is likely to be a function of the remodelling stimuli. Remodelling using the swelling code has, in general, shown more change due to remodelling on the endosteal rather than the periosteal surface. Again, this may be a function of the stimulus used, and in no way invalidates the results. Deposition and resorption of bone material has been shown in the correct regions, according to the stimulus.

7.5 Conclusions

A finite element model has been constructed to reproduce the geometry, materials properties and loading conditions of the ulna experiments reported by Brown *et al.* (1990). The model predictions have shown good agreement with the static analytical results regarding the position of the neutral axis for both the Wingflap and Instron Loading Cases. In addition, considerable agreement was found between the static strain gauge readings from the turkey ulna under loading and our FE predictions.

Remodelling predictions for the mid-section of the ulna based on the most tensile principal stress stimulus correlate well with the published data for the 8-week bird. However, subsequent progressive remodelling predictions indicate some difficulties with the stimulus in the longer term, since the elements tend to resorb beyond their topological limits. Remodelling predictions based upon the majority of the remaining stimuli tested correlated poorly with the changes seen in the experimental studies. Finally, the solution was relatively

Chapter 8 Cancellous bone remodelling

8.1 Introduction

The mechanism of trabecular remodelling is the deposition and resorption of bone matrix from the free surfaces of the trabeculae that form the internal material cavities, as discussed in Chapter 3. The highly inhomogeneous nature of the material presents obvious difficulties in even the simplest static analysis of such a structure, before the process of remodelling is even considered. In order to model the density and architecture of cancellous bone accurately, it would be necessary to examine the properties of the bone at tissue or trabecular level. The study of bone at these micro-structural levels using FE analysis would require elements of a size consistent with the trabeculae - a size far too small to be practical in the examination of a macro model of bone. One such study (van Rietbergen *et al.* 1995) used 296,679 elements in the analysis of a 5 mm cube of trabecular bone. Whilst useful as a micro analysis of the trabecular architecture, this study contributes more in terms of material information than as an investigation regime - their work compared the relationship between the localised trabecular properties and the more global properties of the cancellous bone.

To produce an FE model with a manageable number of elements capable of representing the properties of the material, approximation of the inhomogeneous nature of trabecular bone to a continuum became essential. When using elastic theory, applied to continuum mechanics, it is implied that the model of the material is continuous, even though the actual material may contain holes. It is therefore essential to represent the material over a length that is appropriate to the size of both the material and the holes. Cowin (1993) suggested that when trabecular bone is modelled as a continuum, it is necessary to consider the properties of the material over a minimum of several trabecular widths - a distance approximated as 5mm in the publication. Interestingly, a length scale over which the properties of cortical bone could be considered continuous was also established as about 50 μm. This allowed elastic theory to be applied at different structural levels.

The benefits of modelling trabecular bone as a continuum were considered to be numerous: representation of the cancellous bone in this manner ensured compliance with the external model of the cortical shell, both in mesh and remodelling coding. To create a FE functionally

remodelling proximal femur, limitation of numbers of elements is essential to minimise CPU time. Using larger homogeneous elements assists this analysis time optimisation process. Also, any non-continuum model would require a more complicated remodelling technique, since all of the internal cavities of the trabecular structure would become free surfaces capable of remodelling.

Two distinct options became available in the modelling of the cancellous bone. The first used the user material interface (UMAT), a subroutine option of ABAQUS in which the user can mathematically define the constitutive behaviour of a material. The development of this technique is shown in Appendix A, but the method was not chosen to model the cancellous bone adaptation due to the complexity of the algorithm.

As a result, a second method of modelling the cancellous bone adaptation process was considered. This is described in the following section.

8.2 Elastic card option

The second analysis technique examined for modelling the process of cancellous bone remodelling was developed as a continuation of the swelling code study. The method represented the variable properties of trabecular bone as an homogenous material model in a manner similar to that used in the previous method. The remodelling of the material then involved a variation of the elastic stiffness and was enabled by an upgrade in the ABAQUS software.

8.2.1 Development of method

Determination of the elastic properties of homogenous materials uses the *ELASTIC card within the ABAQUS software. This option was used, along with the DEPENDENCIES option, which made it is possible to directly relate the stiffness of the element integration point to the value of a field variable. In this manner, a value of stiffness was directly assigned to the cancellous bone material according to the relevant variable. The value of these field variables was determined during the subroutine USDFLD, the same routine in which the cortical swelling was calculated. Consequently, a value for the growth stimulus could be assigned to the cancellous bone in an identical manner to that used in the cortical bone remodelling

algorithms. The same routines developed for the tri-linear remodelling curve were then utilised for this routine.

The current value for the material stiffness was stored in the state variable, STATEV(2), similar to that described in Section 6.2.3. Once the calculated remodelling stimulus was assigned to the local element, a multiplication factor was used to magnify the values to a maximum and minimum variation in stiffness. This value of remodelling was then added to the current value of the element stiffness. Convergent remodelling was then achieved over progressive loading steps by continual addition to the element stiffness.

8.2.2 Verification of remodelling method

The method was tested for remodelling response using the beam model (Figure 8.1) used for verification of the cortical remodelling algorithm as described in Section 7.3. The geometry of the model remained identical, although the boundary conditions were altered slightly as a simplification: rather than the complicated constraints seen in the cortical model to allow remodelling growth and resorption, this beam was simply built in. Once again, the beam was constructed of twenty-five 20 noded brick elements each with an initial stiffness of 1000N/mm^2.

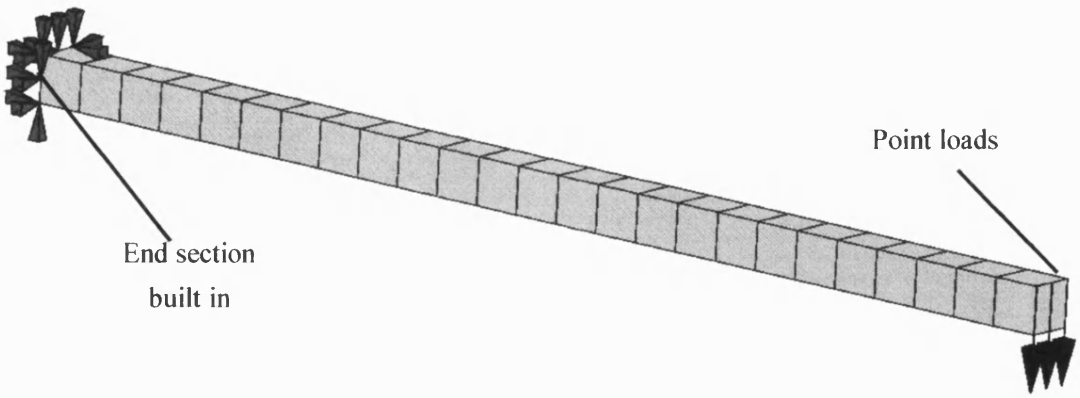

Figure 8.1 – Simple beam model with built in constraints

To determine the 'normal' loading environment, a single loading step was applied to the model with three point loads of 0.03N. During the remodelling analysis, the load was applied in the same manner as the cortical model, with progressive loading, unloading and remodelling steps. Here, the load was simply increased from 0.03 to 0.05N over the same loading positions.

8.2.3 Results

The model was initially loaded to provide information regarding the normal stress / strain environment. Compressive strain was taken as the remodelling stimulus for the analysis and the deformed plot is shown in Figure 8.2. The peak values relating to the contour colours are shown

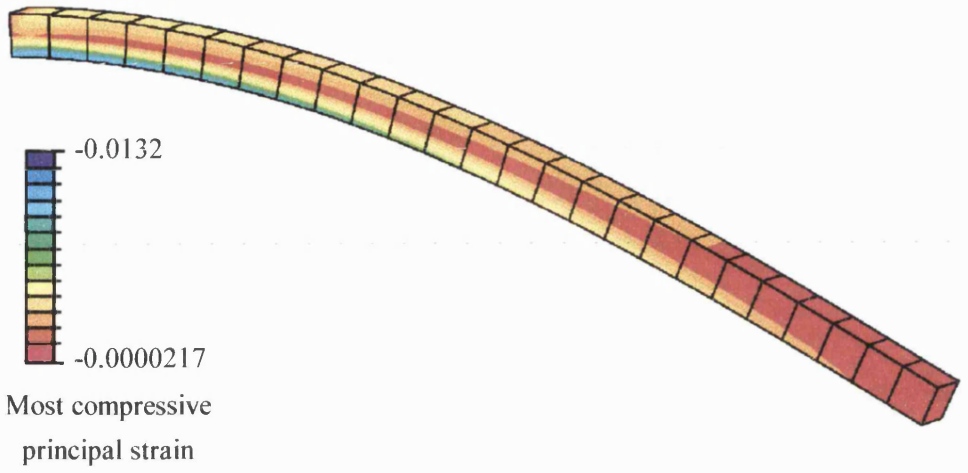

Figure 8.2 – Normal compressive strain environment

The beam displayed the predicted static response to the simple loading applied. The neutral axis of the beam produced values of strain approximating to zero, and the influence of the load increased with distance from the loading sites.

Remodelling using the *ELASTIC card method was then applied to the beam to determine the stiffness response of the system over ten loading steps, each with a maximum stiffening rate of 100 N/mm^2 per remodelling step. The tri-linear curve was assigned a dead zone period of 0.02, and the final stiffness of the model is shown in Figure 8.3.

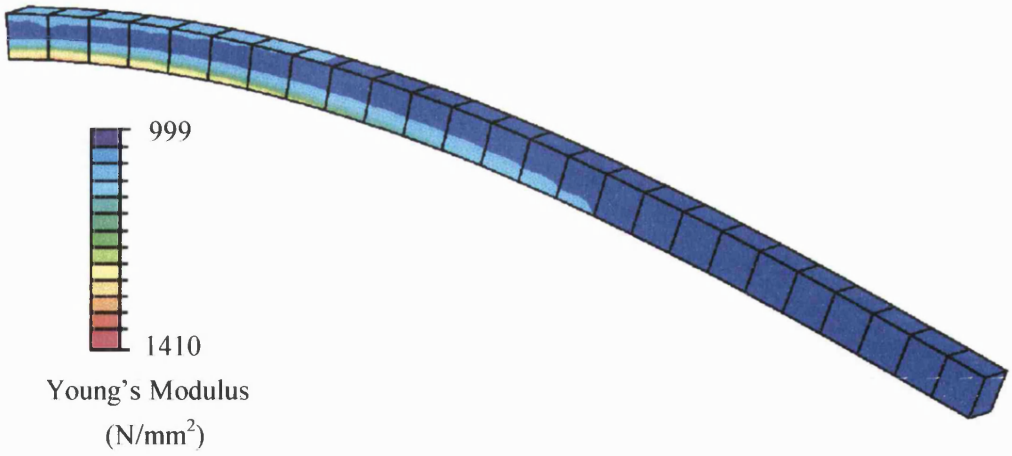

Figure 8.3 - Stiffness after 10 remodelling steps

It can be seen that stiffening of the beam was produced both above and below the neutral axis, with a large region unaffected by the remodelling. This was attributed to the Dead Zone region of the tri-linear remodelling curve, in which the low magnitudes of stimulus around the neutral axis remained below the value of 0.02 (the value assigned to the Dead Zone period).

To demonstrate that the stiffening response of the beam indicated a progression towards convergence, a graph of the change in Young's Modulus was constructed for the integration point with the most remodelling potential (Figure 8.4).

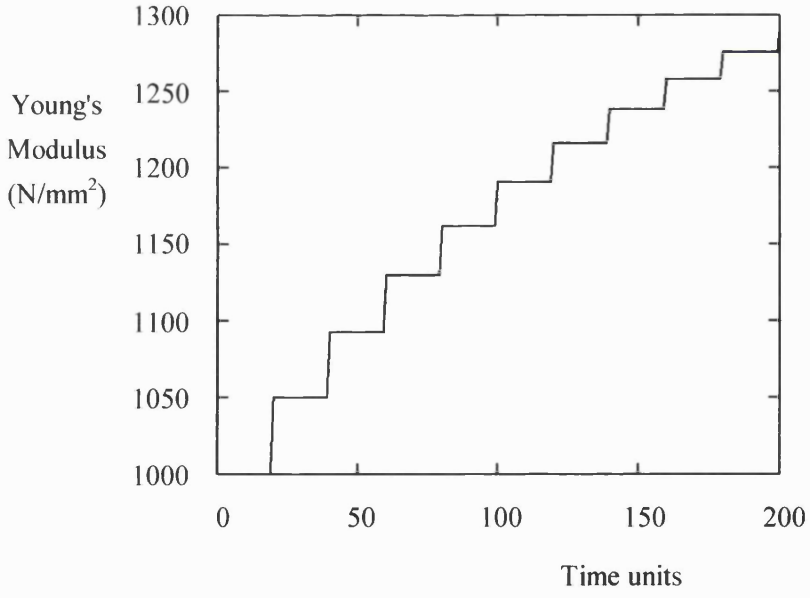

Figure 8.4 – Variation of integration point stiffness with time

The progressive decline in the amount of increase in stiffness shows the action of the remodelling reducing the most compressive principal strain. With more remodelling cycles, the beam would eventually reach a convergent solution when the stimulus was reduced to zero – the point at which the compressive strain throughout the beam entered the Dead Zone region of the tri-linear remodelling curve.

It can also be seen that the Young's Modulus varied across each element after the remodelling occurred, showing that the stiffness of the elements was calculated locally at the integration points. The upper surface of the beam was subjected to a far smaller change in most compressive principal strain than the lower, and this was reflected in the reduced levels of remodelling (Figure 8.5). Again, this graph was constructed from the values at a single integration point on the upper surface near the built in end of the beam.

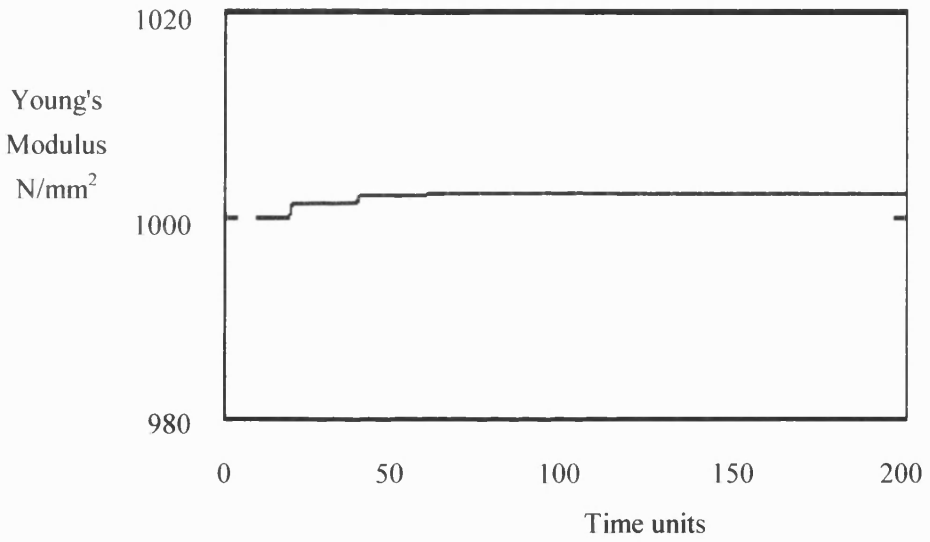

Figure 8.5 – Remodelling of upper surface of the beam

The graph shows that the change in Young's Modulus was small compared to the lower surface of the beam, demonstrating the small increase in stimulus after the higher levels of loading. The curve levelled out very rapidly, indicating convergence of this region of the beam to within the Dead Zone. Notice that the upper surface was stable with no remodelling occurring despite the continued remodelling response from regions of the lower surface.

A comparison model was analysed which possessed no Dead Zone i.e. one that used a bi-linear remodelling curve. The identical loading and boundary conditions were applied, resulting in the contours shown in Figure 8.6.

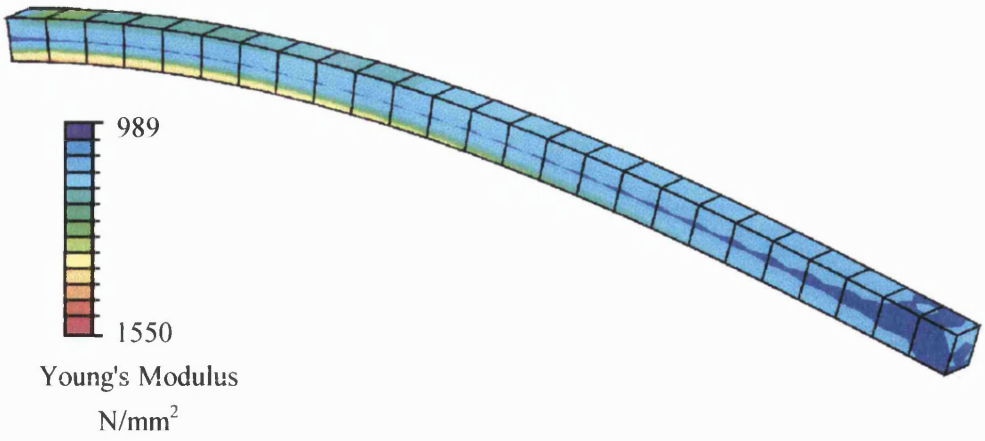

Figure 8.6 – Remodelling of beam with no Dead Zone

Over the same remodelling period, the analysis with no Dead Zone produced more extreme peak values of Young's Modulus. The region of little or no stiffening at the neutral axis of the beam was greatly decreased due to the model possessing no period over which zero remodelling was imposed. This resulted in the regions with a small negative stimulus being allowed to remodel, accounting for the areas of reduced stiffness. In addition, the removal of the Dead Zone allowed the positions of high remodelling potential to stiffen to a greater degree, since the periods of maximum remodelling encompassed a greater range of the remodelling stimulus. This was shown in the increased values of Young's Modulus compared with the previous model.

To reach convergence, this model had to continue remodelling until the most compressive principal strain environment in the beam completely matched the environment during the 'normal' analysis. This would obviously take a significantly longer period of time than the previous analysis, which possessed a Dead Zone.

The remodelling of the beam produced a section that was more resilient to bending. This was proved in the difference of the maximum values of deflection seen in the models, under the same loading conditions (Table 8.1). It can be seen that the remodelled versions of the beam bend significantly less than before remodelling occurred. The relatively large difference in the deformation between the remodelled beams demonstrated the sensitivity of the model to the remodelling parameters such as the tri-linear remodelling curve.

Deflection conditions	Maximum deflection (mm)
Before any remodelling occurred	7.72
After remodelling with a Dead Zone of 0.02	7.18
After remodelling with a Dead Zone of 0.0	6.74

Table 8.1 - Maximum deflection of simple beam model

8.3 Discussion

Two different approaches to modelling the process of cancellous bone adaptation have been examined. Both methods model the material as homogenous and isotropic. In addition, both techniques essentially produce the same end point in providing a stiffness of the material that is capable of altering in response to the loading environment.

For simplicity, the *ELASTIC card method was chosen over the UMAT technique (Appendix A). A great reduction in coding time was required, with the additional benefit of validation of the routine mathematics from ABAQUS. Whilst the UMAT routine could be adapted to be compatible with the swelling code for the cortical bone remodelling, the *ELASTIC method was also instantly complaint with this modelling technique, using a minimum amount of code.

Chapter 9 Construction of the FE Femoral Model

9.1 Overview

Before it was possible to run any predictive analysis, it was first necessary to create a static model of the natural femur to predict the physiological normal conditions to which the bone was subjected. An overview of the process used to create the finite element model input deck is shown in Figure 9.1.

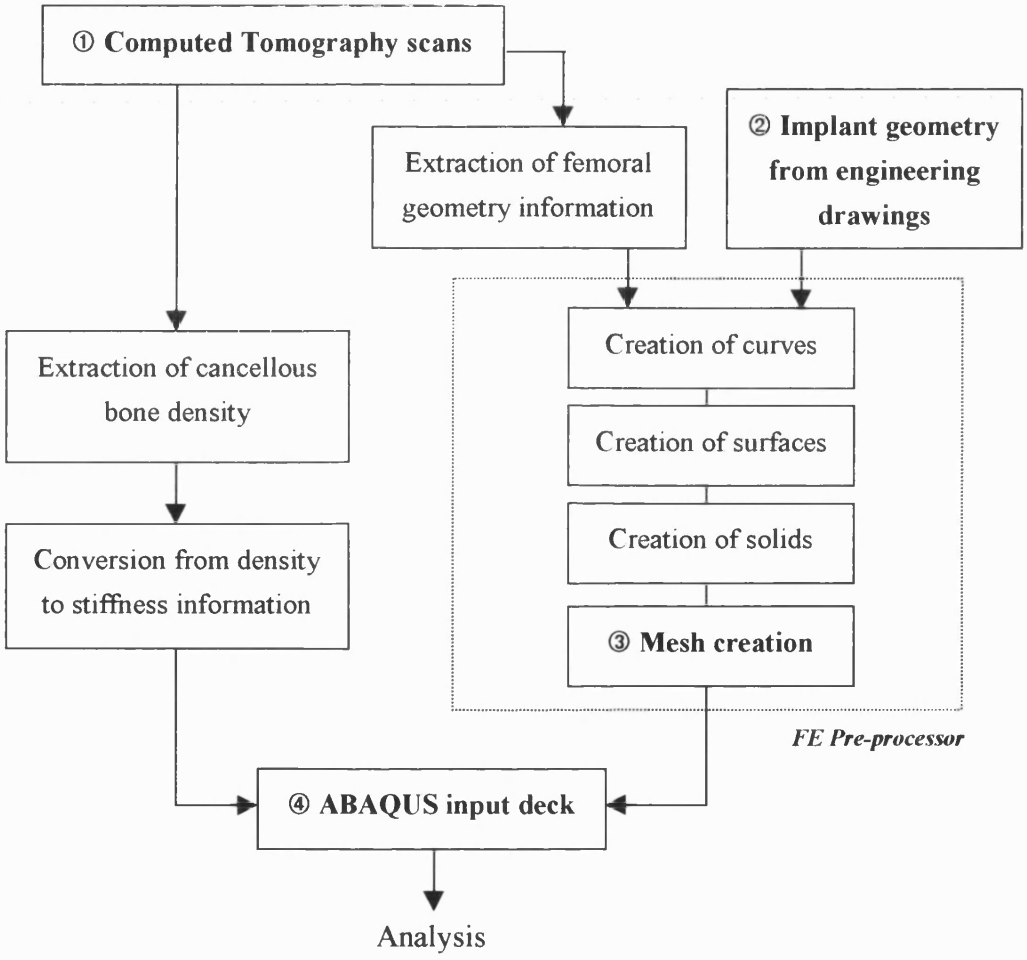

Figure 9.1 - Overview of the model creation process

Data from Computed Tomography scan images (shown as ① in Figure 9.1, and discussed further in section 9.2) provided both the geometry of the natural bone and information regarding the stiffness of the cancellous bone material. The geometrical information, together with the shape of the implant (②, and discussed in section 9.5), was utilised within

the pre-processor to create the finite element mesh of the structure (③). The combined sections of the model were sufficient to create an ABAQUS input deck (④) from which the natural hip model could be analysed (described in full detail in section 9.10).

9.2 Computed Tomography scan data

A representative model of the femur requires both the materials properties and the architecture of the structure. Computed Tomography (CT) is a technique which can give both geometrical and material density data about an object in three dimensions without the requirement for slicing or destroying the subject (Rohl *et al.* 1991, Parker 1980). It is predominantly used in medical applications where there is a need to visualise human internal organs without destroying or entering the body, and has been used here to supply the required data.

By the use of precisely aimed X-rays, the method produces images in the form of slices through the object. These slice images vary in greyscale, creating a full black and white picture as though the object had been sectioned and photographed, hence giving a relative measure of density and geometry. The pixel brightness seen in CT film is proportional to the CT number; lighter shades correspond to large CT numbers and dark shades corresponding to low CT numbers. A typical example is given in Figure 9.2, showing a section through the mid-shaft of a femur. The slices can then be built up, one on top of another, to give a complete three-dimensional representation of the subject.

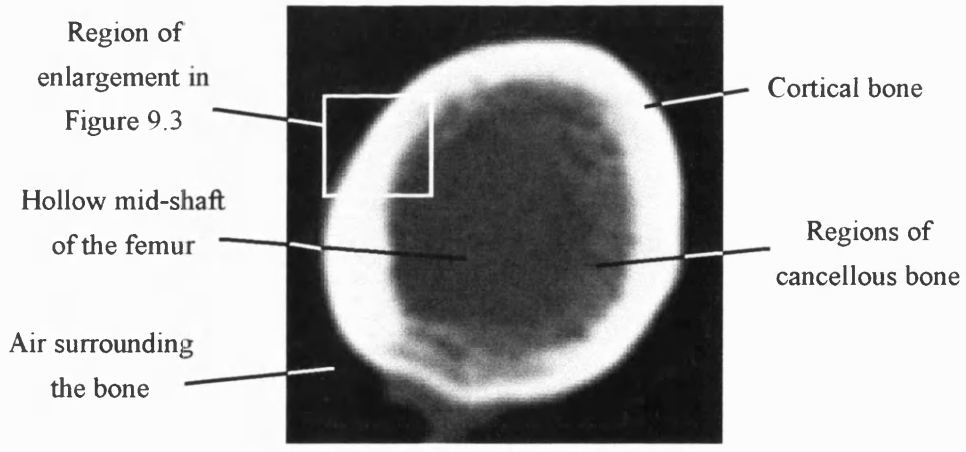

Figure 9.2 - CT Scan image through the mid-shaft of a human femur

Since it is 'impossible' for the computer to see and store continuous data, the processor breaks the information into discrete blocks, called voxels. A voxel is a volume element, similar to pixels on a monitor in three dimensions rather than two, typically about 1mm by 1mm by the slice thickness (usually 2, 5 or 10 mm), although these values are dependent upon the type of machine in use. The process uses volume averaging over each voxel, thus working out the average density in a volume, and assigning that value to the voxel. Figure 9.3 shows an enlarged view of a small region of Figure 9.2. Close examination reveals the voxels averaging the density of each volume of bone to become small cubes each with a single colour.

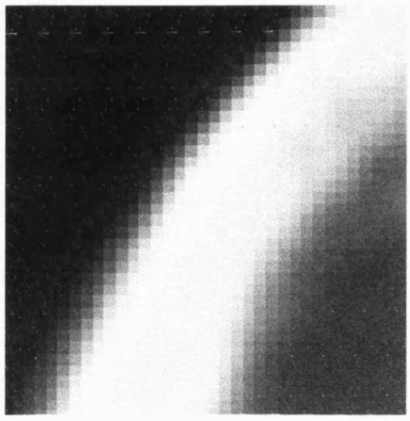

Figure 9.3 : Enlarged View of CT Scan Image

Once the processor has stored the full image for that slice, the X-ray heads then translate their position down the subject and begin their rotation once again for the next slice. In so doing, multiple sections down the length of a solid object can be examined. The most recently developed machines are able to scan in a continuous, helical manner, saving both time and exposure to radiation. The data from these machines is more detailed, and the slice position can be defined after the scanning has taken place, according to requirement.

The numerical greyscale data for each slice taken from a CT scan can be stored in Hounsfield Units (HU), a measure of density. In practice, however, values of density are initially taken as a measure of raw CT number, with each different scanning machine having a slightly different calibration process into HU. The variation in the constant is caused by parameters such as power rating and beam concentration.

The CT number is basically a representation of the relative attenuation of the tissue (μ_t) with respect to the attenuation of water (μ_w) (Parker 1981). The Attenuation Coefficient, K, is dependent upon the beam energy of the scanning device and the scale into which the data is being converted. When the Hounsfield scale is used, this constant has the value of 1000.

$$\text{CT number} = \frac{\mu_t - \mu_w}{\mu_w} \times K$$

The conversion process from raw CT values to HU will then be of the form: -

$$HU_{Subject} = 1000 \frac{CT_{Subject} - CT_{Water}}{CT_{Water} - CT_{Air}}$$

where CT is the recorded CT number, HU is the value in Hounsfield Units, and the subscripts water, air and subject relate to the CT values of water, air and the material being examined respectively (Rho *et al.* 1995). The scaling constant of 1000 (which used to be 500, in older CT machines) is an accepted convention since the CT values of air and water are close to -1000 and 0. CT numbers, when expressed in the above form, are termed as Hounsfield Units, considered a universal scale. A CT number of zero (when measured in HU) corresponds to the attenuation of water. Materials with values above zero HU have greater attenuation, and below, less. Typical values of various materials are shown in Table 9.1.

Material	Range (HU)
Air	-1000
Lung	-800 to -200
Fat	-100 to -20
Water	0
Muscle	+20 to +140
Cortical Bone	+140 to +1200

Table 9.1 - Typical HU values of various materials (Parker 1981)

Once calculated, the Hounsfield distribution is generally stored in large matrix format, typically 512 x 512 or 1024 x 1024. In order for CT scans to give more information than geometry alone in modelling situations, the values of HU must be converted into a density or stiffness. In practice, bone phantoms (objects of known density) are used to precisely determine the relationship between HU and bone density. This process involves placing the phantoms, (usually fluids containing 50, 100 and 200 mg/cc of calcium hydroxyapatite) in the field of view and recording the CT numbers for each object. A linear regression is then

performed on the data to calculate the mathematical relationship. The calibration shows that the attenuation of the x-ray beam is proportional to the density of the tissue.

Rho *et al.* (1995) studied a number of site specific relationships between CT number and the density of human bone, including the proximal femur. The resulting correlation for this region was given as

$$\rho = 131 + 1.067\mathrm{CT}$$

where ρ is the density of the bone measured in g/cm^3, and CT is the CT value of the bone measured in HU.

The scan data used in this study (discussed further in section 9.3) was supplied in Hounsfield Units, where the process of transforming the data from raw CT numbers into HU was done on the original scanning machine. Since no information regarding any phantoms was given, the relationship above was used for the conversion process.

With the use of these mathematical relationships, it was possible to build up a complete density map of the subject using CT scanning. This information therefore provides the basic materials properties and morphological data to commence construction of the femoral FE model.

9.2.1 Bone modelling applications of CT scanning

CT scan data has been used in a number of applications for modelling of the proximal femur (e.g. Weinans *et al.* 1993, Skinner *et al.* 1994, Keyak *et al.* 1995, Keyak *et al.* 1990, Huiskes *et al.* 1991). The slice data has been used to provide information such as external geometry, position of the cortical - cancellous bone interface and density. Each slice was capable of portraying local information, with the model surface being built up by concatenation of the connecting layers.

An apparent problem with the use of CT Scan data for modelling is geometrical deterioration at the edge of a structure. Since the scanning procedure averages density volumes over a defined area, the surface of the structure tends to become distorted, giving a stepped effect. This problem was evident in Keyak *et al.* (1995) where two femurs were scanned into 320 by 320 matrix images. In their study, a three-dimensional FE model of each femur was

automatically generated from the bone scans using 3mm linear cubic elements. The bones were then tested to destruction. The corresponding finite element model predicted failure of the bone matrix based on a distortion energy theory with material failure occurring at locations with four continuous elements having low factors of safety. The results are given below in Table 9.2.

Parameter	Femur	Predicted	Measured
Onset of Failure	A	3000 N	6400 N
Onset of Failure	B	8000 N	9600 N
Ultimate Strength	A	7000 N	7293 N
Ultimate Strength	B	11,000 N	13,055 N

Table 9.2 - Predicted and measured failure loads (Keyak et al. 1995)

Although seemingly good results were obtained, it should be noted that all predicted values underestimated the experimental results. The model disregarded data for elements on the surface of the model, however, because of partial volume effects. The problem relates to the method of scanning, in which the cubic area scanned may contain both bone and the surrounding air. The effect can be reduced by increasing the number of voxels scanned and hence decrease the element size. The limits of this procedure are provided by the computing power available. Also, the meshing technique used allowed corners to produce stress concentrations that are predominant in areas of rapidly changing geometry (Figure 9.4). The effect of this was a reduction in the required loading for each mode of failure.

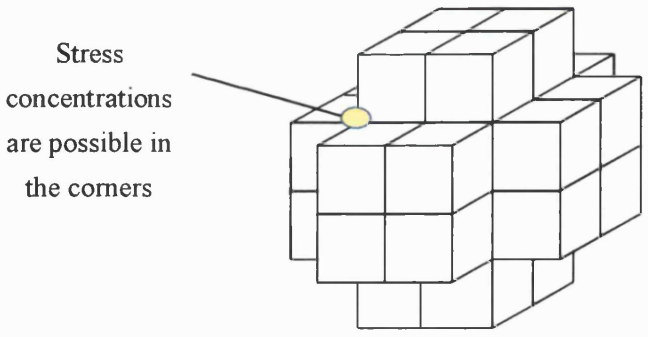

Figure 9.4 - Mesh redundancy and stress concentrations

This method of automatic meshing was not appropriate for the present study due to the technique developed for the swelling growth of cortical bone (Chapter 6), which requires a smooth periosteal surface mesh.

9.3 CT Scans of human proximal femur

9.3.1 CT scan data

Thirty-eight files, each containing a single slice of CT scan data, were generously provided by Andersen (1995), for use in this study. The scan data came from the femur of a 48-year-old male cadaver, with no documented evidence of degenerative bone disease. One file consisted of an X-ray image of the human femur (Figure 9.5), and thirty-seven files contained slice images taken across the transverse plane.

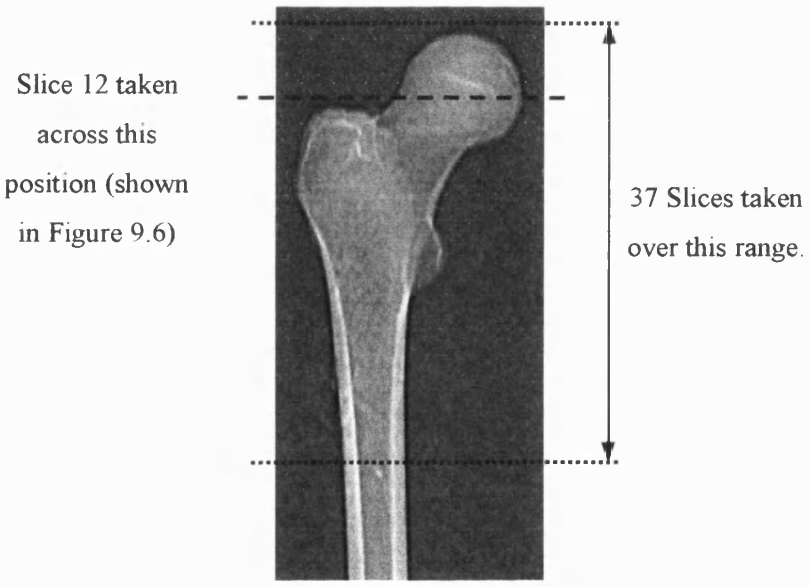

Figure 9.5 - Proximal femur from which scan data was taken

Figure 9.6 shows a selected area of slice number 12. This provides an example of the type of images acquired, and shows the section through the base of the femoral head, as demonstrated in the X-ray image, Figure 9.5.

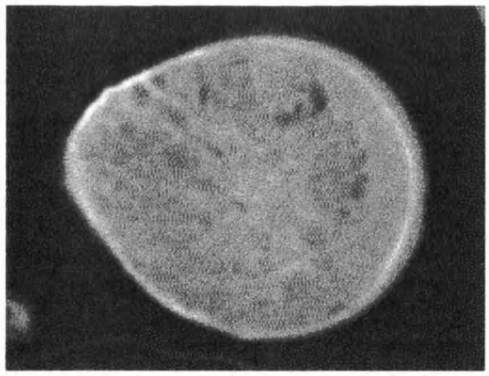

Figure 9.6 - Slice 12 - A section through the base of the femoral head

The files were received in CART (Computer Assisted Radio Tomography) format, which stores the density data in a series of two bit hexadecimal numbers. The files were sectioned into a 512-byte header, which contained scanning equipment and patient information, and the remaining scan image data. As a result, the CART format of the files could not be visualised without modification. A conversion program, written in C, allowed the data to be transformed from the CART format into PPM format. This is a recognised standard format of graphics files, and allowed computer visualisation of the images through numerous graphics packages. The conversion process firstly involved reading the values from the CART files in hexadecimal and ignoring the first 512 Bytes of data. The remaining values from the CART file were then rewritten into a new file with a .PPM extension, in ASCII columns.

Unfortunately the PPM format created large files (circa 3.5 MB), and limited computer resources required that disk space be kept to a minimum. The files were therefore converted once again into the more compressed JPG format, reducing the average file size to approximately 80 Kbytes.

9.3.2 Scan header information

Information regarding the slice attributes was contained within the initial 512 bytes of each scan file, and varies according to the type of scanner used. The most significant information with relevance to the model creation was stored in the first 38 bytes of the header and is shown below (Table 9.3).

Byte Contents	File Position (Byte No.)	Description
File Identification	0	–
Number Of File Slice	2	Slice number
Number Of Blocks	4	–
Distance Adm Blk	6	–
File Creation Date	8	Date of scan
Equipment Code	10	–
Relative Slice Position	12	Z-position of slice in mm from datum
Matrix Size X	14	Image size in voxels, X and Y equal values
Matrix Size Z	16	–
Pixel Size X	18	Size in mm of 1000 voxels in X-direction
Pixel Size Y	20	Size in mm of 1000 voxels in Y-direction
Index First Line X	22	–
Index First Line Z	24	–
Index Region Of Interest	26	–
Reconstruction Area X	28	–
Reconstruction Area Z	30	–
Magnification	32	–
Number Of Bits	34	–
Number Of Slices	36	–
Thickness of Slice	38	Thickness of current scan slice (mm)

Table 9.3 - CT scan header information

Each byte of data contained in the header is a pair of hexadecimal numbers, with the first pair numbered zero. The header data block for slice 12 is shown below in Table 9.4, where three numbers of importance have been highlighted - byte position 12/13, 18/19, and 38/39. These represent the values for depth position of the slice relative to the top slice, the pixel size (x 1000 mm) in the X direction, and the thickness of the slice scanned (mm) respectively.

Byte position	Hexadecimal data
Bytes 0 - 15	0006 0001 0200 0001 2cc5 044a ***ffde*** 0200
Bytes 16 - 31	0200 ***0138*** 0138 0000 0000 0000 0000 0000
Bytes 32 - 47	03e8 000c 0001 ***0002*** 0000 0000 0000 0000

Table 9.4 - Scan file header data

Once the correct information byte was located, the value of the relative position of the slice was extracted. The datum position for the scan images in the Z-axis was slice 2, at a position of FFFF (hexadecimal). Consequently, the correct relative positions of the remaining slices

in mm was the value of the header byte 12 subtracted from FFFF (hexadecimal). Hence, the position of slice 12 is 33 mm down the Z axis, since:

$$\text{FFFF - FFDE} = 21 \text{ Hex} = 33 \text{ mm}$$

The remainder of the values were direct measurements, hence the size of the pixel in the X-direction was 0.312 mm / pixel, and the slice thickness was 2 mm. The result of the information gained from the individual headers of each slice related to the relative slice positions of all the scans. Concatenation of the slices gave a complete 3D representation of the femur.

9.3.3 Contour extraction

After visualisation of the scan data, it was necessary to extract the geometry of the femur from the images. The technique described by Sumner *et al.* (1989) was used. The study analysed digital images of bone cross-sections, obtained using CT techniques, and developed guidelines for outlining the periosteal and endosteal boundaries of human bone. In their study, thirteen femora had been scanned and then sectioned for quantitative measurement of the boundary and interface locations. It was found that the best evaluation of cortical thickness using CT scanning techniques was best established by defining the two boundaries at separate threshold values. The results showed that for human bone scanned in air, which is the same scanning technique as the cadaver used in this study, the optimum threshold value for the periosteal contour location was -50 HU (with a range from -550 to 950 HU). The endosteal contour location was identified at 550 HU (range -50 to 550 HU).

The femoral images were previewed using these recommended optimum thresholds by modifying the greyscale range of the images. All pixel values greater than the threshold value were altered to 255, and seen as white, with all other values becoming 0, shown as black. This technique showed defined regions of black and white, and hence strongly contrasting boundary outlines (Figure 9.7).

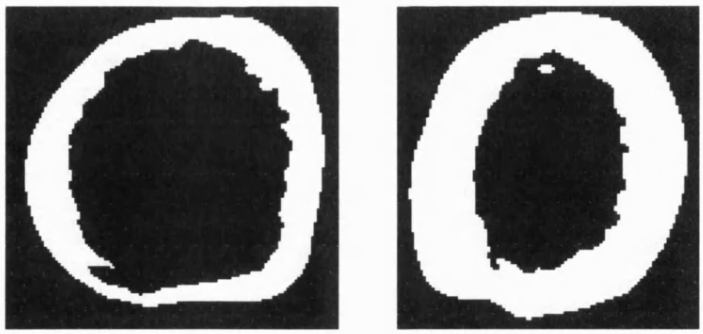

Figure 9.7 - Contour based approach to edge definition

With the threshold value defined as -50 HU, the periosteal surface definition gave a clear definition of the boundary, using the original scan images as visual confirmation. Nevertheless, deviation from the femoral architecture became apparent on the modified image in the more proximal regions of the bone. Upon examination, it was found that some of the original scans had regions with poorly defined grey areas that became better delineated as cortical bone when the image was modified. It was assumed that this problem arose because of the partial volume effects, where the scanning machine averages the material density over the cubic volume of the voxel. Large variations in the geometry of the object being scanned often caused rapid changes in the gradient of the surface of the object, relative to the axis of the scanning machine. As a result, the real surface cuts through a voxel, and the material property measured by the scanner represents neither the bone nor the air around it, but rather an average over that volume. These regions of the image thus appeared as grey areas with low definition, and are particularly prominent in the scans taken around the greater trochanter and femoral head.

To resolve this problem, the periosteal boundaries were examined under a number of threshold values, and it was found that the most physiologically representative surface contour was defined when the value of the threshold was increased from -50 HU to 150 HU. The result of this action was to greatly reduce the quantity of vague, indistinct grey area. The physical effect of increasing the periosteal surface threshold value was to contract the external surface of the bone. The volume of cortical bone was thus reduced. The significance of this change is small, however, since the variation chosen for this bone is well within the range of values recommended by the Sumner study. In addition, the physical distance moved by the contour is small, often less than a single pixel (0.312 mm), except for the targeted areas.

To confirm that the scanning of the femur had been performed in air, the greyscale of an image was examined across a mid-shaft section of the femur where there was no evidence of any cancellous material (Figure 9.8). The graph shows only the central region of the image, centralised over the femoral shaft, with the remainder of the image excluded. The two large peaks show the walls of the femoral shaft, with the shaft interior in the central region. The phenomenon of 'beam hardening' was apparent at the edges of the areas with rapidly changing gradients, which accounted for the presence of peaks and troughs in the values of HU at the edges of the bone. These areas should ideally display a smooth variation in HU, but the effect gave localised regions of unreliable data. This problem was inconsequential, however, when viewed over the global cross sectional variation.

The graph revealed that the femur was scanned in air, since the area surrounding the bone showed values of approximately -1000 HU. The element of interest here, however, was that the central region of the shaft exhibited values of approximately 0 HU, showing that this region was still filled with some form of fluid during scanning. Since it is both very difficult and of no interest to refill the hollow regions of a bone, it was deduced that the femur was freshly removed from the cadaver when it was scanned. The liquid remaining inside the shaft of the femur would have been metabolic fluid such as blood and bone marrow. This finding would also account for some of the less dense grey areas seen on the periosteal surface of the bone, had the bone not been sufficiently cleaned, and lumps of fat and muscle remained.

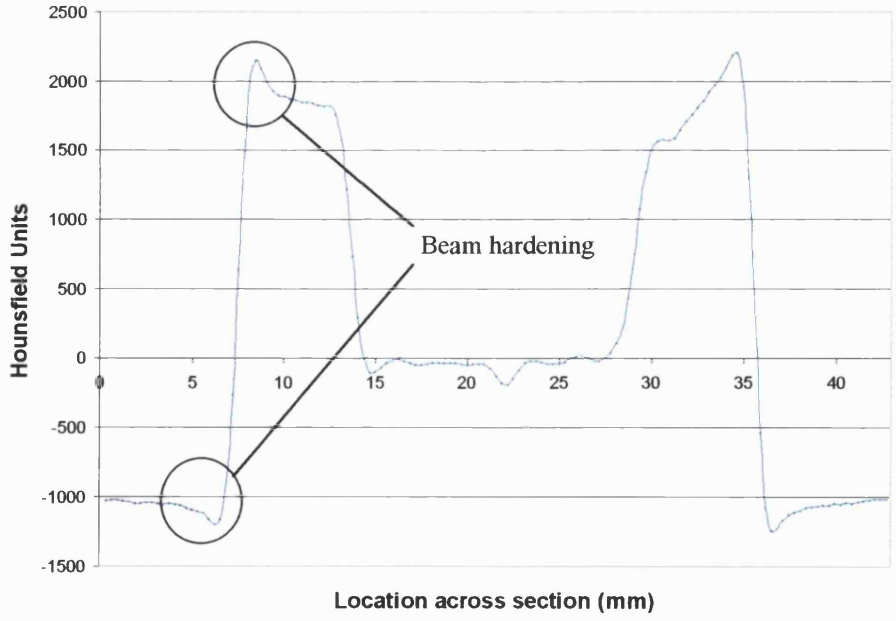

Figure 9.8 - Variation of Hounsfield Units across section 36 (shaft of the femur)

The result of this finding was that the geometrical edge contours of the periosteal and endosteal surfaces had to be examined under two different thresholds; the periosteal surface in conditions scanned in air, and the endosteal surface in conditions scanned in water. According to the Sumner study, therefore, the resulting threshold values for the endosteal surface were increased to 850 HU.

The endosteal surface definition was examined using the revised threshold value of 850 HU. The interface between the cortical and cancellous bone often displayed low levels of contrast, resulting in several geometrically complex finger like protrusions (seen in Figure 9.7). Unfortunately, geometrical simplifications to this interface became necessary, since the cortical bone remodelling technique required clearly defined boundaries. In addition, the geometrical complexity of modelling this interface accurately would have had serious implications on the meshing of the structure.

As a result of these underlying problems, it was decided that the surface definitions would not be taken directly from the contour extraction algorithm. Rather, a simple co-ordinate point method was chosen in preference. This method involved converting each scan into a pair of greyscale boundary images, one showing the external cortical surface, and the other using the higher threshold value, defining the cortical - cancellous boundary. A series of points around the edge of the bone was then determined from cursor co-ordinate position on the image. A higher density of points was taken for areas of complex geometry, and the values were stored. All of the images, however, were still the size of the original scans, and a scaling process had to occur to allow modelling of the real physiological magnitude. To calculate the scaling factors, information regarding pixel size and relative slice position was taken from the data contained in the header of each slice. Each point was scaled according to the pixel size of 0.312mm (identical for both the X and Y directions). A FORTRAN script was written which converted these points into a file format ('neutral file format') recognisable by the pre-processor, ABAQUS PRE.

9.4 Creation of femoral geometry

9.4.1 Edge contour creation

The co-ordinates that were taken from the density contour maps were read into the pre-processor as geometrical points, and were stored in different groups for housekeeping

purposes. Closed loop interpolated splines were fitted to the points to create a series of curves both for the periosteal and the endosteal surfaces (Figure 9.9).

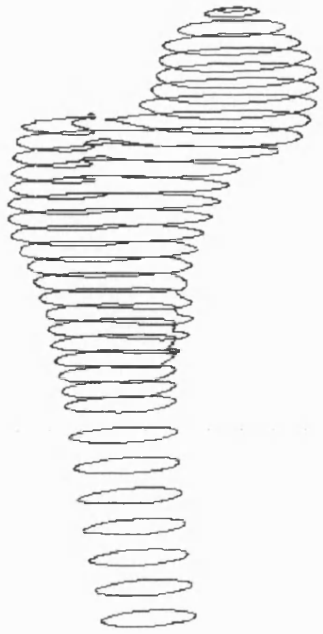

Figure 9.9 - Splined curves created through the geometrical points (endosteal curves shown only)

9.4.2 Division of the femoral geometry

In order to create solids and finally an element mesh from the curve information (shown in Figure 9.9), it was necessary to break the curves into a number of sections. This enabled discretisation of the femoral volume into more simple shapes that could be meshed by the ABAQUS pre-processor.

The sectioning of the femoral curves was carefully designed to be compatible with the remodelling methods developed in the previous chapters. It was intended that a single mesh should be used for both the physiological normal analysis, with the natural femoral head, and the postoperative THA analysis, with the implanted prosthesis. To achieve this, the natural femoral model had to include the elements of the implant geometry defined within it. Since the prosthesis should sit entirely within the regions of cancellous bone, the entire group of elements in the implant set could be analysed using the material properties of cancellous bone in the natural hip situation. When the implanted model was to be analysed, the elements of the femoral head would simply be removed, leaving the elements of the top section of the

prosthesis exposed above the femoral neck resection. The material properties of the prosthesis elements would also be converted into those of the implant material, resulting in a separate analysis using the same basic model mesh.

The advantages of this technique were numerous. It was possible to include remodelling based on comparison with the physiological 'normal' condition, without having to locate the same position on a different mesh. Since this method essentially used the same elements for the two different analyses, the physiological normal stimulus could be stored by each element, and was exactly correct in position. The method also meant that only one mesh need be created for the entire analysis. In addition, comparison of the loading and boundary conditions between the natural and the implanted femoral model was minimal, since the majority of these constraints remain unchanged. Also, if the entire model was bisected down the line of the centre of the implant shaft, it was possible to present remodelling results using a central section of the model. This sectioning of the FE model, however, depended upon the position of the implant.

There were, however, several disadvantages inherent in using this method. Since the morphology of the bone was taken from a natural, unimplanted, cadaveric femur, it was impossible to evaluate the *in vivo* remodelling produced in the long term after the insertion of a prosthesis for this individual case. Comparison of new bone formation and resorption had to be compared against generalised results published in the literature. In addition, the exact position of the implant within the femur was unknown and 'best' possible or ideal positioning of the prosthesis became an assumption.

It was noted that any possible features of the remodelling code were ideally incorporated at the design stage of the mesh. It was proposed that the mesh should eventually be able to include both creep of the cement mantle and slip interface conditions between the prosthesis and the cement. Regardless of any user code that may have been required for this analysis to occur, the mesh should be designed to cope with these conditions. For any form of interface slip conditions in ABAQUS, contact surfaces must be used. These surfaces (which are described in more detail in section 9.6.5) do not require the two opposing element faces to have identical meshes. It was therefore possible to have an entirely discontinuous mesh between the implant and the cement. The option to 'tie' these surfaces together was available in ABAQUS. This is a technique to constrain one surface onto another, without allowing relative movement, and was to be used during the natural static model to alleviate the problems of the mismatch in meshes across the implant - cement boundary.

With these conditions in mind, the model was designed subject to the following constraints:

1. The implant was to be meshed with the best possible shaped elements, regardless of the surrounding elements, since the mesh was to be discontinuous across the implant – cement boundary.
2. This implant mesh was to sit within the natural femoral model mesh (see Figure 9.10).
3. The cement mantle / cancellous bone was to continue down the length of the implant shaft until it reached at least the end of the prosthesis.
4. The model was to be designed in two halves, corresponding to the bisection line down the length of the implant.
5. Tied surfaces were to bind the elements of the implant and the cancellous bone for the natural femur analysis (section 9.6.5).
6. Both the cement and the implant regions of the mesh were to be assigned the material properties of cancellous bone for the initial static analysis.
7. Cement and implant material properties were to be applied to the respective elements for the implant and remodelling investigation.
8. Slip conditions could be easily introduced to the implant - cement interface by altering the type of contact surfaces used.
9. Creep conditions could be introduced to the elements surrounding the implant

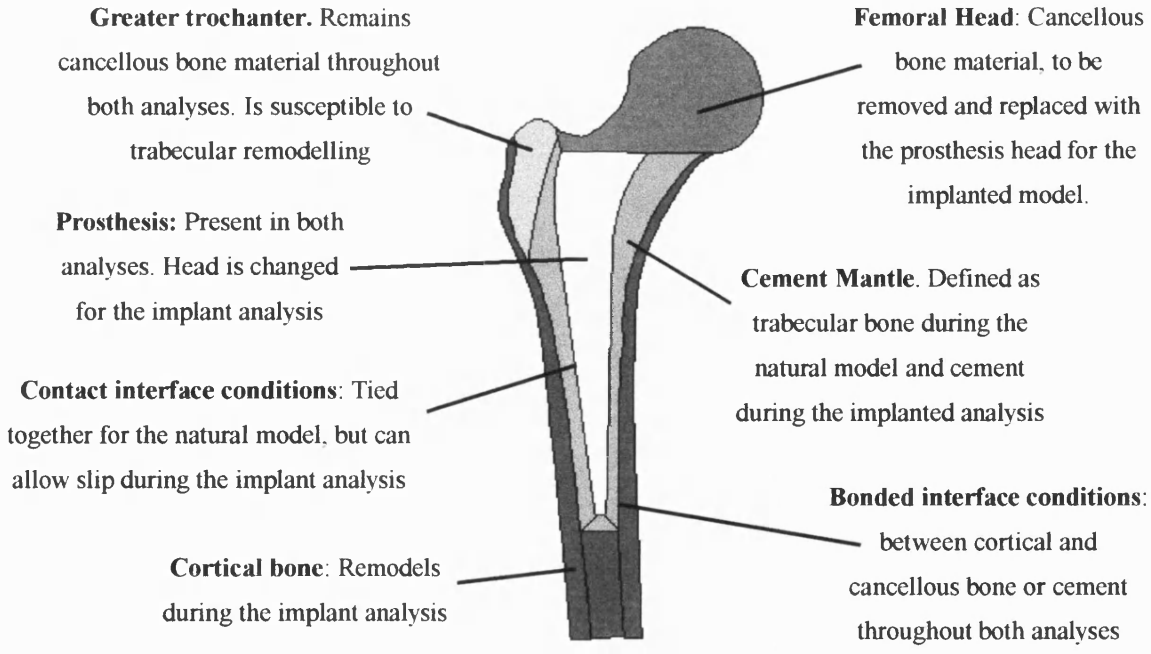

Figure 9.10 - Schematic section of natural femur with internal implant geometry

In order to make this technique possible, it was necessary to section the curves relative to the position of the implant. It was therefore essential to perform 'virtual surgery' and insert the geometry of the implant into the femoral model before any division of the surfaces could occur.

9.5 Selection of implant

9.5.1 Selection from implant templates

Howmedica generously supplied the geometry and details of the Exeter Hip System for use in the study and standard clinical procedures were used to select the size of the implant. This involved placing transparent templates of the standard stems (Figure 9.11) on a 20% oversized X-ray (taken in the frontal plane) of the proximal femur. The centre of the implant head was located over the centre of the femoral head and the long axis of the stem was positioned such that it was parallel with the shaft of the femur. The implant size that most closely aligned these two axes was selected, giving consideration to the space available for the cement mantle: - indicators are drawn on the templates at various positions around the implant.

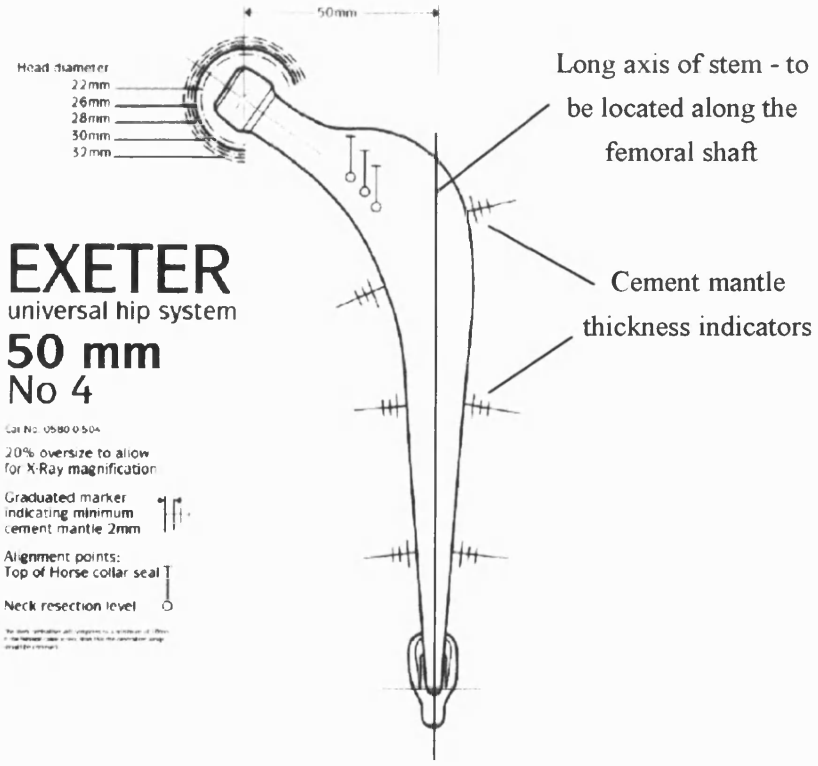

Figure 9.11 - Standard Exeter stem selection template (Howmedica 1995)

Figure 9.11 shows the selected implant size - the Exeter stem, number 4. It was noted that the implant was larger than the more commonly used stems. This was attributed to the use of a Scandinavian bone (it is generally accepted that Scandinavian skeletons are larger than their mid-European counterparts).

9.5.2 Creation of the implant FE model

Engineering drawings of the Exeter stem enabled construction of the prosthesis as a geometrical model in ABAQUS PRE. The process involved constructing a centre section of the implant and then projecting the contours onto two angled planes either side of vertical. These new curves formed the basis of the double taper of the shaft of the implant. Surfaces, solids and ultimately the finite element mesh were built up (Figure 9.12). The mesh of the structure was completely smooth, using 20 noded brick and 15 noded wedge elements throughout (although the diagram portrays slight line roughness, this is due to the format of the picture file).

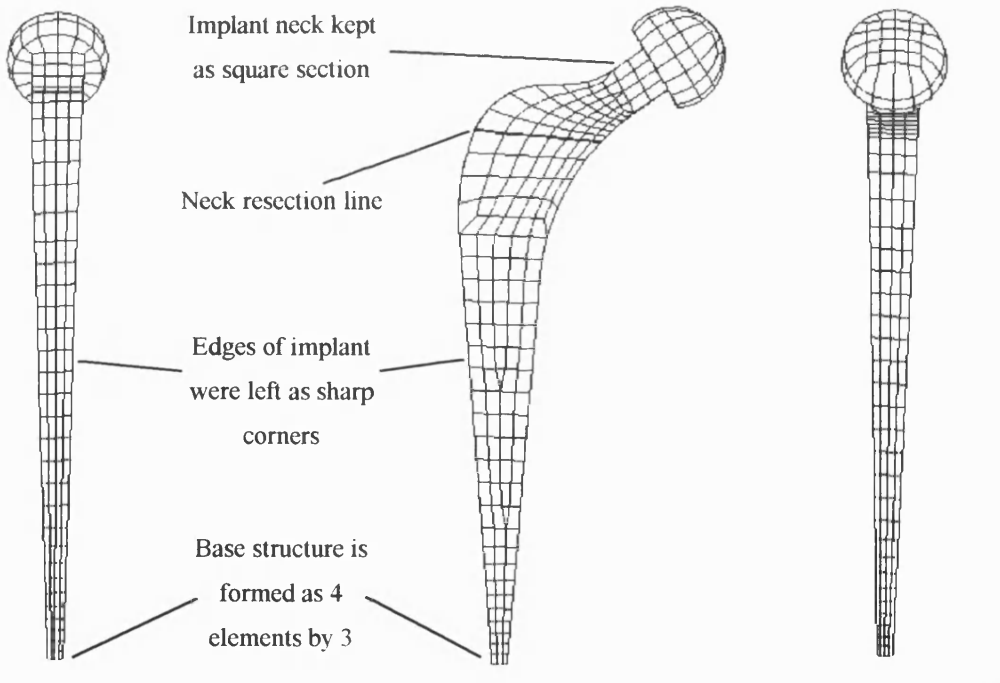

Figure 9.12 - Mesh of the Exeter implant

In order to allow modelling of both the natural and the implanted femur using the same basic finite element mesh, it was necessary to split the neck of the implant in the same place as the femoral neck resection (described further in Section 9.6.2). The lower half of the model was then retained in both the natural and the implanted analysis, and the materials properties

changed from cancellous bone to steel. The elements of the natural femoral head would be removed and replaced by the head of the implant for the remodelling analysis.

The neck of the finite element model differed from the engineering drawings since it maintained the rectangular cross section of the shaft rather than tapering to a cylindrical section. This provided a much simpler method of meshing the structure, ultimately providing better element topology. It was considered that the shape of the neck contributed little to the transfer of the load to the femur, especially as the material strength was completely dominant over that of the bone and cement.

Whilst the construction of the spherical head could be seen as purely aesthetic, and models in the literature frequently omit them (Spirakis *et al.* 1992, van Rietbergen *et al.* 1993), several advantages were gained by its inclusion. Firstly, the head provided a more physiological location for loading the model (discussed further in Section 9.8) - by moving the position of the loads, it is possible to create unwanted and incorrect moment arms in addition to the hip joint load. Secondly, the head allowed easy positioning of the implant with the femur, as discussed in 9.5.3.

An additional alteration of the implant geometry from the original design was that no fillet radii were included on the edges of the implant shaft. Their incorporation would have significantly increased the complexity of the mesh structure of the entire bone model, despite the contact surface interface, since the continuous geometry of the fillets would have been required within the cancellous bone. For the natural femoral analysis, the shape of the shaft edges was not important, as long as congruous morphology was maintained across the contact surfaces, since the material properties were constant throughout this interface. The effect of the fillet geometry was far more significant during the implant analysis where there was a variation in the properties of the materials. The presence of the corner radii was accounted for in the use of the SMOOTH parameter of the *CONTACT PAIR card, and is described further in Section 9.6.5. The option approximates any sharp corners in a contact surface to a smoothed edge in order to remove any instability in the code. The effect of this option is to mathematically smooth the edges of the implant, providing a good modelling approximation, but also greater convergence stability. The Engineering design of the implant used corner fillets of 2 and 4 mm, resulting in the use of a smoothing parameter of 0.4 of the average element length. This converted to a value of approximately 2mm.

The distal end of the stem reduced to a small cross sectional area forcing a significant reduction in the size of the elements. Wedge elements were introduced down the length of

the shaft in order to reduce the number of elements and hence maintain their average size. Due to the importance of the structure, and in an attempt to preserve accuracy, it was decided to retain at least a minimum number of three elements across the section in each direction. One of the original design criteria was that the model was to be split in the medial - lateral plane. This required an even number of elements, resulting in the distal tip of the stem being split into a 4 by 3 element cross section.

9.5.3 Location of the implant

During the surgical procedure, the surgeon is able to asses the situation and guide the implant into a position of best fit. Due to the limitations of the mathematical model, however, it was impractical to manipulate the implant due the difficulty of visualisation of a three-dimensional model on a flat screen. An alternative method of positioning the prosthesis was used, which assumed that the implant was positioned in its 'ideal' location. The centre of the head of the implant was located in a position coincident with the centre of the natural femoral head, and the shaft positioned so that the stem tip sat centrally within the femoral shaft. These two points were then maintained as fixed positions whilst the mid-section of the shaft was rotated to release the implant neck from the calcar region of the femur. This allowed the maintenance of a sufficient amount of local cement mantle to seat the implant correctly. The final location of the implant within the femur is shown in Figure 9.13.

Interestingly, the base of the femoral neck intruded into the space required for the implant (Figure 9.13). The surgical occurrence of this problem is low, since rotation of the implant is provided until the stem is seated correctly. In this case, however, special consideration and continual checking of the relative positioning of the implant and cortical shell had to occur to ensure that the two entities did not violate each others physical space. Final location of the stem was confirmed when these checks had taken place.

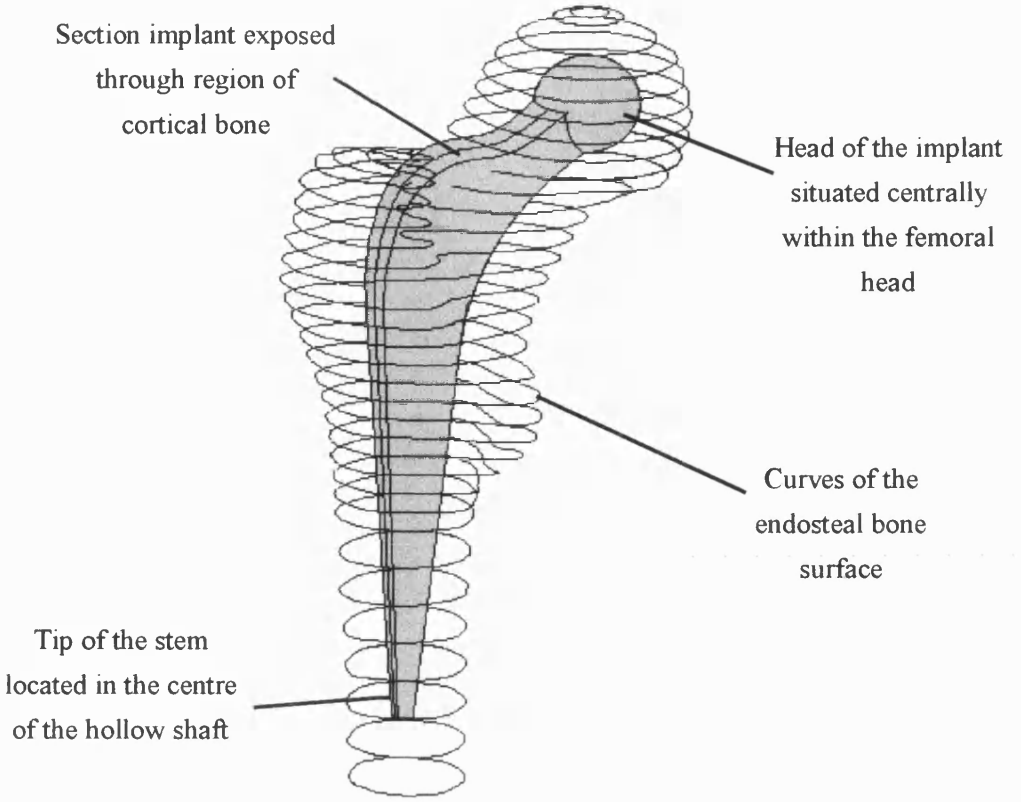

Figure 9.13 - Location of the implant within the proximal femur

9.6 Construction of the natural femur FE mesh

9.6.1 Regions of cortical bone

The endosteal and periosteal surfaces of the femur were created by 'sweeping' the curves translated from the CT scan data into three dimensions. The pre-processor, ABAQUS Pre Version 5.6, created surfaces by fitting a linear mathematical relationship though the curves. As a result, a more approximate reproduction of the physiological geometry was created when more curves were swept. Consequently, the surfaces were created in a number of smaller sections of approximately 5 or 6 curves. The volumes between these two sets of surfaces represented the region to become cortical bone.

It became clear from examination of both the endosteal and periosteal surfaces that certain sections would give minute volumes to the cortical bone regions created. These regions were particularly prevalent in the femoral neck and head where the cortical bone is a thin shell. It

was decided that any elements created in this region would be too poorly shaped to give accurate results. The decision was therefore taken to extend the cortical bone regions up to the femoral neck but no further. The femoral head consisted entirely of cancellous bone with no cortical surround.

The effective removal of the cortical shell from the femoral head would have obvious implications; The alteration in stiffness of the structure would produce changes in the stress and strain patterns seen throughout the bone, but this method was considered both a better and a more simple solution than the alternative of including the cortical material. In order to incorporate the cortical surface, the size of the elements required for processor accuracy would artificially alter the stiffness of the bone by a far greater amount than its removal. Examination of the cross section of a human femur revealed that the regions of cortical bone thinned remarkably quickly towards the femoral neck - providing an ideal location to end the cortical bone material - and thicker, more dense bone was seen in the trabecular struts passing through the femoral head. It was considered that macro modelling of the changes in the cancellous structure without the cortical shell would provide a sufficiently accurate model of the changes in stiffness across the femoral head. In addition, the femoral head was not included in the remodelling analysis, and was therefore not a region of interest with respect to prosthesis loosening.

9.6.2 Femoral neck resection

The position of the resection line in the finite element model was located to reproduce the modern surgical goals of preserving the calcar (Bannister 1993) by raising the cut up the femoral neck. The resection position was also dependent upon the shape of the implant within the bone, since a section of the implant neck protruded into the region of cortical bone (Figure 9.13). In surgical practice, a section of bone can be removed from the medial aspect of the greater trochanter using a v-shaped tool in order to fit the neck of the prosthesis. The dual resection line (Figure 9.14) presented in this model represented a compromise between the physiological reality, the ideal section and the modelling simplicity.

Elements above this cut could then be assigned various material properties in the natural model and the implanted analyses, but both sets of elements retained a continuous, smooth interface.

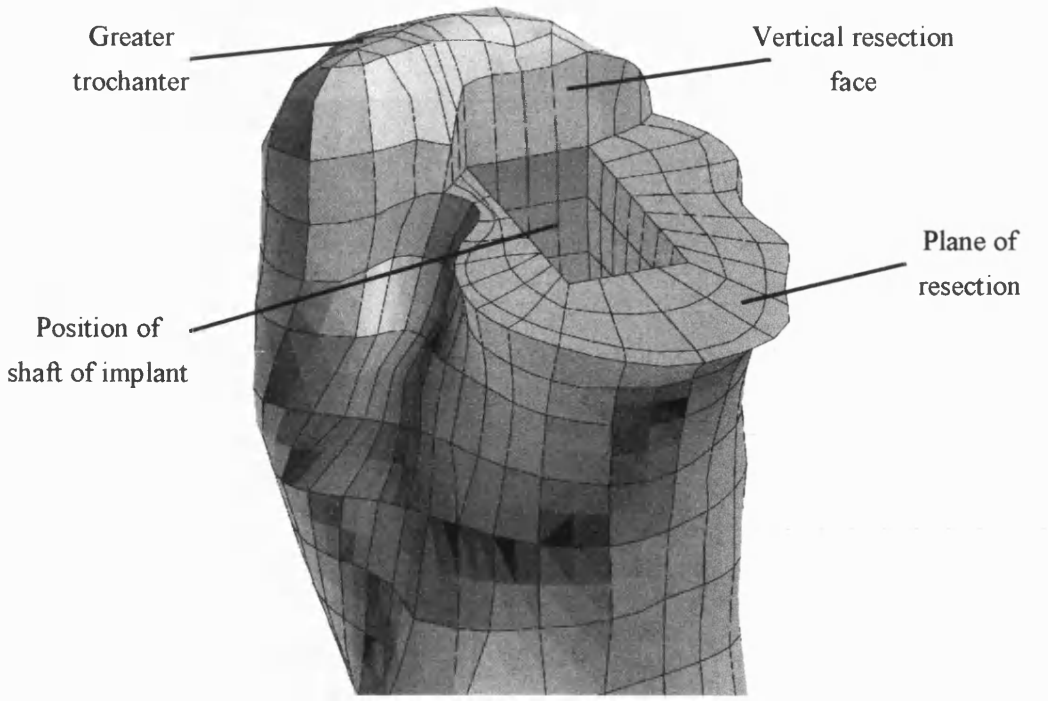

Figure 9.14 - Location of the femoral neck resection

9.6.3 Extension of the femoral shaft

The CT scan slices used to create the model geometry gave information up to a point of approximately 200mm distal from the tip of the femoral head. The position of the final slice was roughly coincident with the location of the tip of the implant, once inserted. One of the regions of remodelling interest, however, was around the stem tip, giving rise to concerns of localised interference from the boundary conditions in this area.

Extension of the bone was achieved by translating the cross section of the final slice down the length of the bone by 30mm. Construction lines were extended down the bone in the direction of the localised surface gradient taken over the final few slices of CT scan images. The position of this replica slice was determined from the bisection of these construction lines and the slice plane. The contours were scaled in accordance with the relative position of the projected construction lines, resulting in a 4% reduction in distance across the section. The mesh of the extended zone is shown in Figure 9.15.

9.6.4 Finite element mesh

The majority of the elements in the natural hip model were created using the automatic mesh generating facility of ABAQUS PRE. A small number of elements in the neck and greater trochanter region of the bone were meshed manually due to the complexity of the structure geometry. The final mesh of the natural hip model is shown in Figure 9.15. Tied contact of internal elements was required for the completion of the mesh, and is shown in the figure, and detailed further in section 9.6.5.

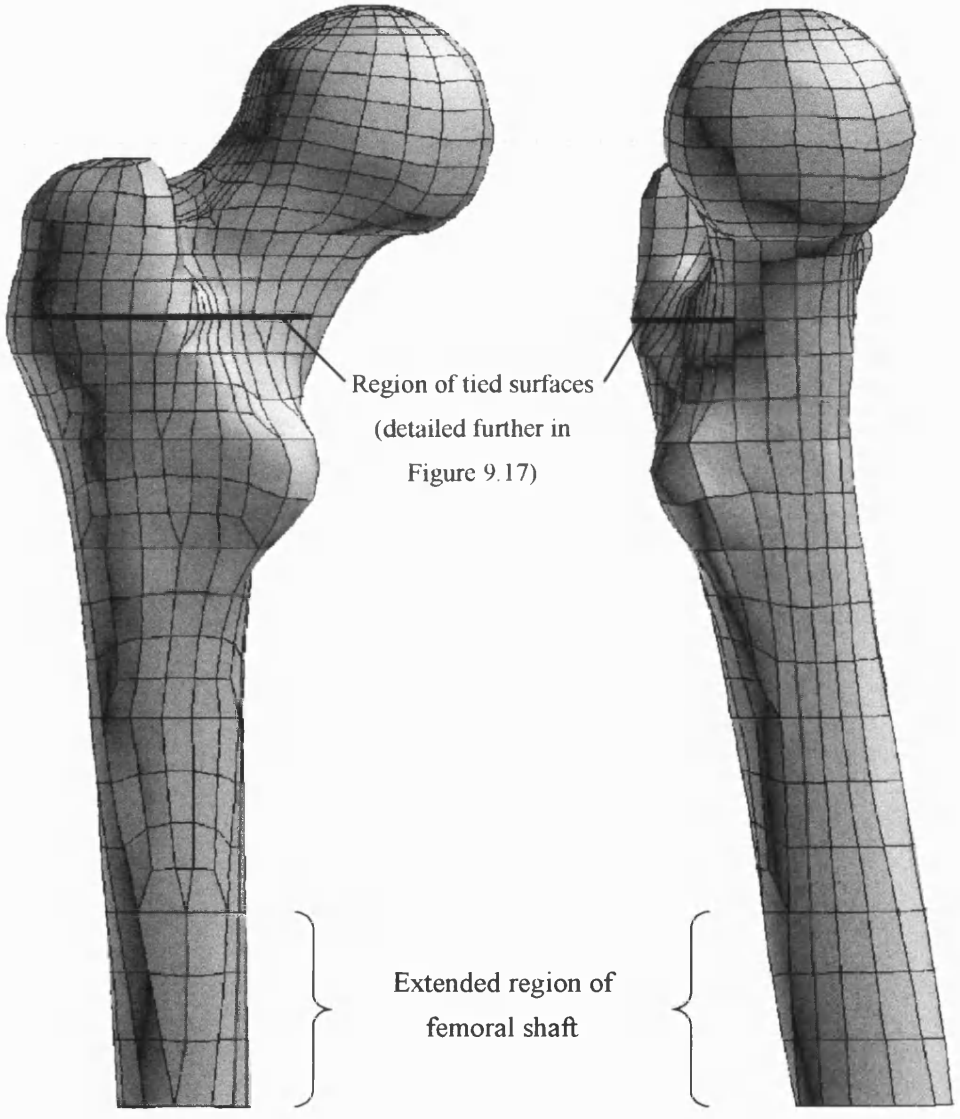

Figure 9.15 - Finite element mesh of natural femur

In an attempt to economise on the efficiency of the analysis, the minimal number of elements for definition of the problem was desired. To this end, reduced numbers of larger elements

were used progressively down the length of the femoral shaft, towards the regions of geometrical simplicity. This was achieved using both wedge elements and a complex mesh arrangement, where both mesh structures were consistent into the cancellous regions of the bone. The element arrangement ceased at the implant interface since mesh discontinuities were allowed across the contact surfaces.

A total number of 2324 elements were used in the model of the natural femur, of which 2154 were twenty noded bricks, 168 were fifteen noded wedges and 2 were ten noded tetrahedrons. Of the wedges, 25 were cortical bone, and 143 were cancellous bone (63 in the 'removable' head region). There were a total number of 14188 nodes.

The cancellous bone interface with the mesh of the prosthesis (also of cancellous bone material during the natural hip analysis) was created using automatic element surfaces, generated from within ABAQUS using the *SURFACE DEFINITION and the *CONTACT PAIR card options. The two surfaces were 'tied' together for the duration of the analysis of the natural hip (Figure 9.16).

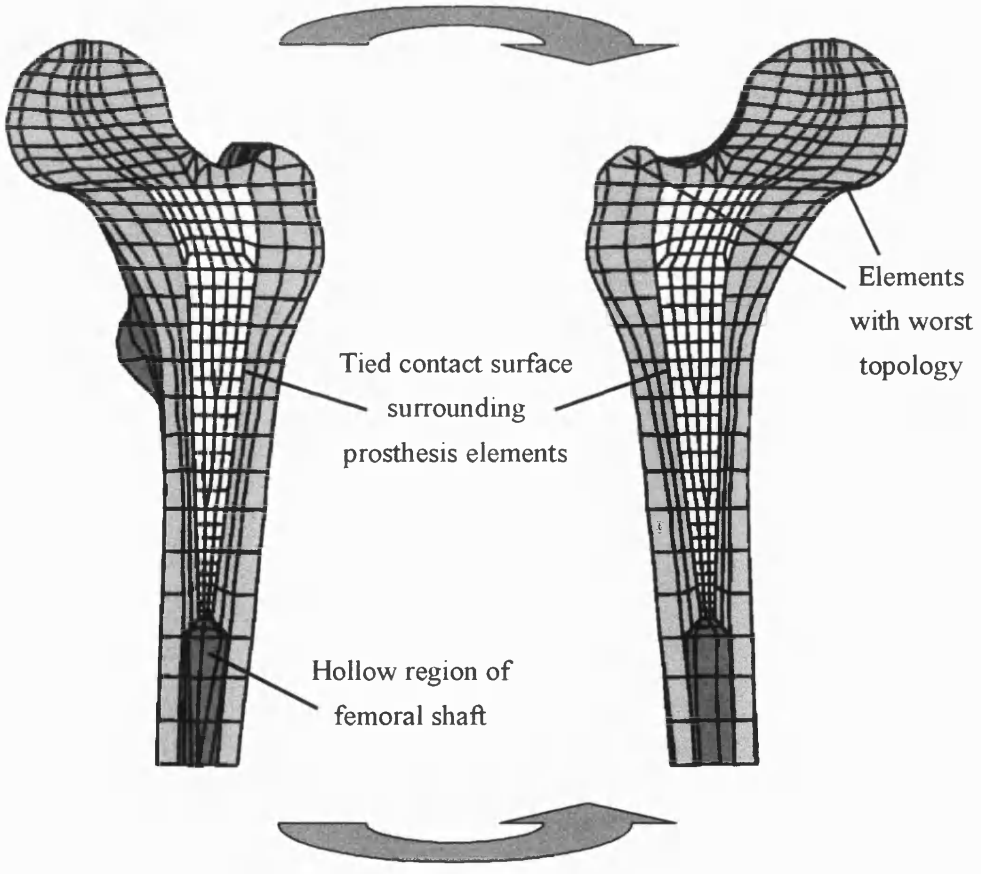

Figure 9.16 - Bisected view of natural femur model

The regions of light shading show sections of the bone split exactly down the plane of the implant bisection, whereas the darker regions are set back from the cut.

A number of elements were later highlighted during the analysis for their poor topology, generally indicated by an edge angle of either greater than 135° or less than 45° in tetrahedral brick elements. These elements were most often situated down the edges of the implant in the cancellous / cement material regions, where the mesh transformed from a square to a cylindrical section arrangement. The angles of the corner elements were therefore often degenerated beyond the normal limits of accuracy but mostly by no more than a couple of degrees. The elements with the worst topology in the model were situated in the tip of the greater trochanter where tetrahedral elements were forced to degenerate into a smooth surface and in the femoral neck, at the tip of the medial calcar region. These elements, however, were considered less important since they were not present in the remodelling implant analysis.

9.6.5 Perpendicular contact surface

The use of a tied contact surface became necessary across a perpendicular section of the femoral shaft in order to compensate for a rapid change in the localised geometry. Without the use of this technique, the elements would have been created with severe morphological distortions since the endosteal surface became convoluted in this region. The result was to create two independent mesh structures, each arranged in the best configuration for the local geometry, and discontinuous across the connecting boundary (Figure 9.17). The two surfaces were then tied for the duration of the analysis.

Since no single node may be associated with both surfaces of any tied contact, it was necessary to completely disassociate the two node sets even if some were close enough to be equivalenced. The two contact surfaces were then defined using the automatic surface generating methods within ABAQUS, and the tied contact interaction applied.

Significant problems were later found during the model processing, resulting in early termination of the analysis, reported with a number of negative eigenvalue problems. It was found that these were caused as a result of having nodes associated with both the perpendicular and the implant / cement contact interfaces. In general, it is necessary to define both a master and a slave surface for each contact interaction that occurs in ABAQUS. The nodes of the slave surface are then considered individual entities that interact with the master

surface according to the type of contact defined. Since a number of the nodes were included in two independent tied slave surfaces, separate conditions imposed by each contact interaction caused over-constraint of the nodes.

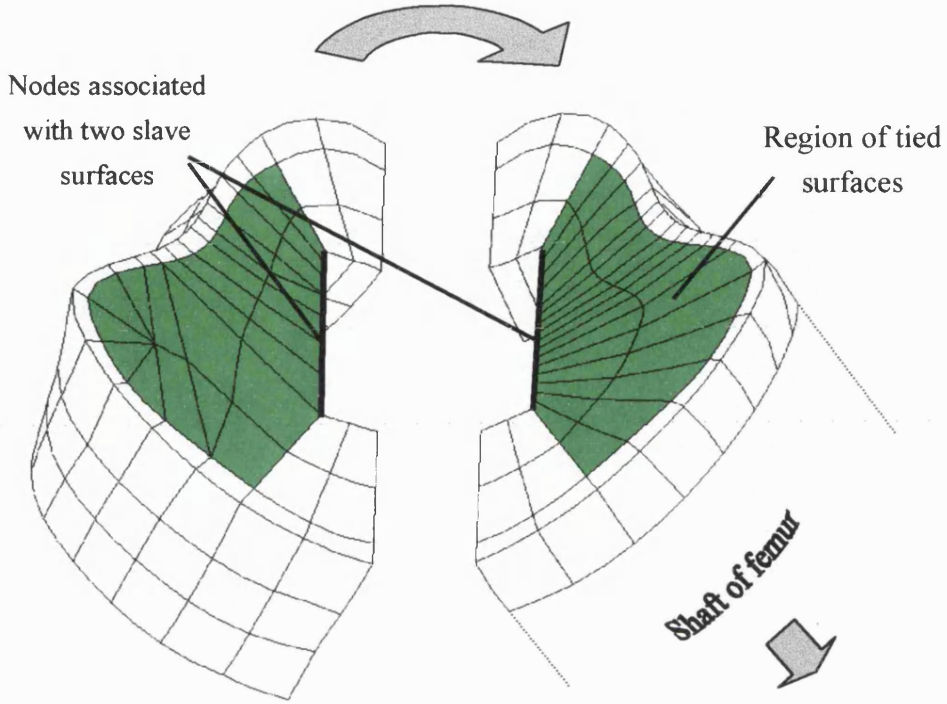

Figure 9.17 - Tied surfaces across discontinuous mesh

This was corrected by manually generating the slave surface of the implant / cement interface by using the *CONTACT NODE SET card and excluding the mutual nodes present in both groups. In this manner, all of the nodes of the lower perpendicular surface were continuously tied to the upper master surface, and those nodes on the master surface acted as slave nodes to the implant master surface. The analysis was then able to run without eigenvalue problems.

9.7 Materials properties

9.7.1 Cortical bone

The materials properties of cortical bone were considered homogenous and isotropic, using values for Young's Modulus of 17GPa and a Poisson's ratio of 0.33 (Cowin 1989). No remodelling coding was used for the natural femur model.

9.7.2 Cancellous bone

The mesh of the natural femur included elements geometrically derived from the implanted model in order to be consistent across the two analyses. Obviously, sections of the natural model would normally have excluded certain regions of elements, especially in the hollow femoral shaft. The method chosen to determine the materials properties for the trabecular bone was to extract the density and hence stiffness information from the CT scan data. Defining varying properties for each element throughout the structure in this manner enabled the model to both establish a more accurate density map of the material, and exclude the unnecessary elements in the femoral shaft by effectively providing a zero stiffness.

In order to extract the density information from the CT scan data, it was first necessary to calculate the centroid position of all the cancellous bone elements. This was achieved using the pre-analysis and recording the position of integration point number 14 (for 20 noded brick elements) to file. Prism and tetrahedral elements posed a slight discrepancy as they posses no central integration point, but rather have equally distributed points. For these, integration point number 4 was chosen, which involved a slight variation from the centre of the element due to the offset of the integration point.

A FORTRAN script was written to relate the position of the integration points to the nearest area of scan data from which an approximate density could be calculated. Initial attempts simply determined the greyscale of the closest point on the nearest slice by examining the Z-axis co-ordinate position followed by the X and Y-axis position within the slice. The density of the local structure was then determined using the process described in section 9.2, followed by the calculation of a single representative density using the Rho *et al.* (1995) relationship,

$$E = 5.05\rho^{1.269}$$

where E is the Young's modulus and ρ is the density of the cancellous bone measured in kg/m^3.

One of the obvious drawbacks of this method is that no account was given to the geometry of the element, and the process assigned a value of stiffness based upon a 0.312 mm^3 volume averaged cube from the CT scan voxels. Due to their small size, each voxel could easily have penetrated a cancellous cavity or equally a trabecular strut, giving rise to extreme values of stiffness. To account for this, the density of the bone was averaged over five voxels - the

approximate width of the smallest element in the cancellous bone regions of the model. The stiffness was then calculated and assigned to each element based on that volume.

Problems to the process were caused by the distribution of the scan slices, since the vertical projection of points onto the closest scan layer occasionally allowed the points to protrude into free air. This generally occurred on surface elements in positions of severe gradient, on the femoral neck or greater trochanter, for example. The result was that certain elements could be assigned negative values of density, based on the negative values of HU for air, hence terminating the analysis due to errors. To resolve this, a number of measures were taken to ensure that these elements were attributed sensible values for stiffness.

The first measure taken was to alter the method with which the representative CT scan slice was chosen. Rather than simply taking the closest scan to the centre of the element, regions of the bone were allocated various slices, based upon the local gradient of the bone surface. The uppermost volumes of the femoral head were all projected downwards (more distal) onto the nearest slice, as were the positions on the greater trochanter, whilst sections of the femoral neck were projected upwards. This ensured that the density values of the elements related to the nearest slice with an inward position of the bone surface, rather than being projected outward into mid-air.

In addition to this slice selection procedure, a secondary measure was taken to ensure that no element was assigned a zero or negative stiffness value. Values of HU were measured across separate cross sections of the femoral shaft to determine the difference in values between the hollow shaft and the regions with dense trabecular bone. This would highlight the magnitudes of the regions that should be ignored as regions of fluid.

The first section, shown in Figure 9.18, was taken across CT scan slice 20, a region in which trabecular bone was first considered to be present from the base of the shaft. It clearly details the walls of the femur at the edges, centred by the mid-shaft of the femur, filled with both biological fluids and cancellous bone, providing a range of approximately 200 to -100 HU.

This was compared against the section previously examined in Figure 9.8, where the hollow shaft of the femur was filled only with fluids, and the values of HU remained negative throughout the mid-shaft regions. The values here (Figure 9.18) were not only higher, but also displayed fluctuations, probably where there were small regions of trabecular bone. It was therefore decided that the boundary between the trabecular bone and the fluids was at approximately 0 HU, giving a calculated value of 383 g/cm^3.

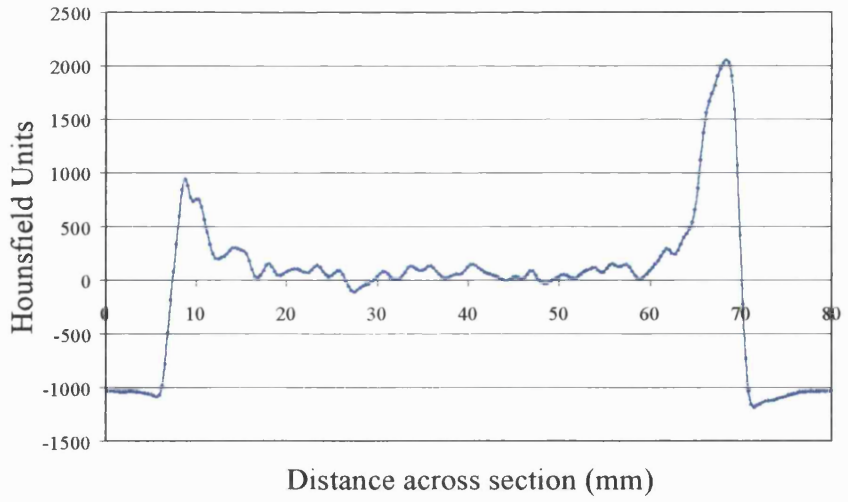

Figure 9.18 - Variation of HU across the femoral shaft

This was confirmed by the section taken across the femoral head, Figure 9.19, which displayed values mostly of 300HU upwards for the dense trabecular regions of the bone. Notice also that the values for cortical bone peak only just above 800HU indicating only the thinnest cortical shell.

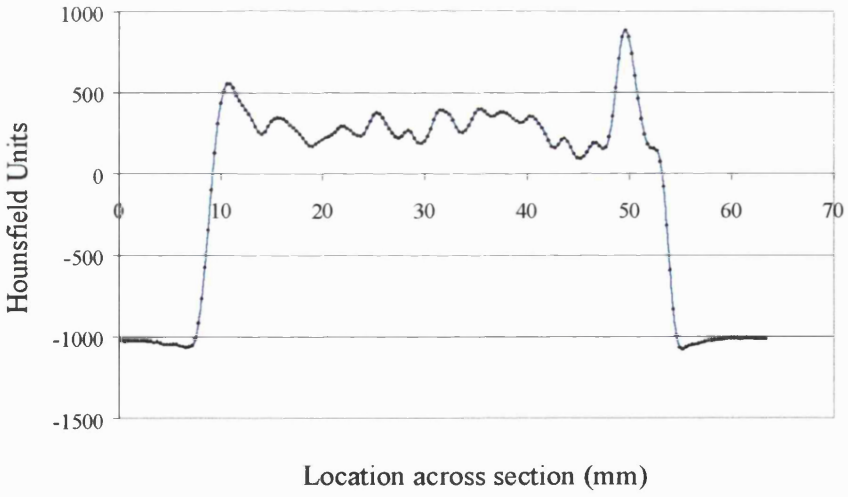

Figure 9.19 - Variation of HU across a femoral head section

From these values, it was decided to limit the stiffness of all the cancellous bone above slice 20 to a value greater than 383 g/cm^3. This ensured that any element in the dense trabecular area maintained a sufficient Young's Modulus for the analysis. Elements below slice 20 were deemed to be in a region where the structure was composed primarily of biological fluids. A calculated stiffness of below 383 g/cm^3 (and corresponding value of HU below zero) would

therefore mean that the volume consisted purely of fluid and could therefore contribute little to the stiffness of the structure. Under these conditions, the element was assigned a stiffness value of 0.001 MPa, a value that is low enough not to influence the stress or strain environment of the bone. The remainder of the elements, whose stiffnesses are higher than 383 g/cm^3 retained their values, which were calculated directly from the scan data. The final stiffness contour map is presented in Figure 9.20, in which only the elements above the most distal cancellous bone element are shown.

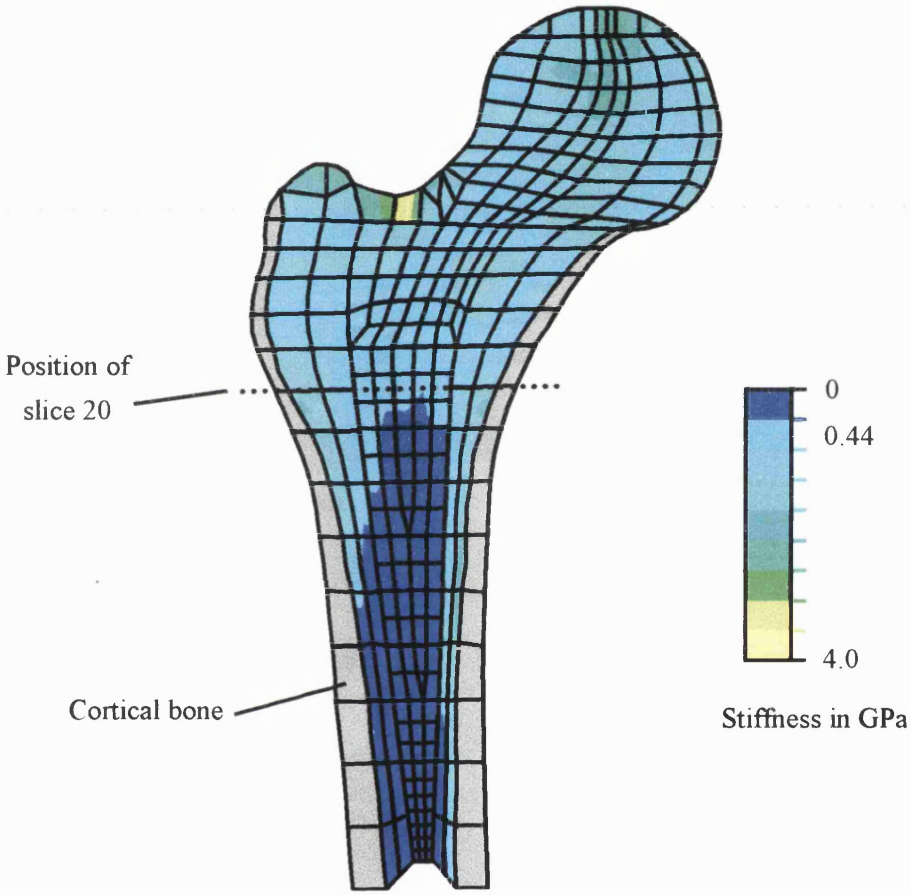

Figure 9.20 Variation in HU across the femoral head

The stiffnesses of the model elements were calculated after the first analysis of the natural hip model. The values of stiffness attained from this method were then used during the second analysis, in which the physiological normal stimuli were calculated.

9.8 Loading and boundary conditions

9.8.1 Hip joint loading

The mode of loading for the hip was taken from Taylor *et al.* (1996). Their study, described previously in Chapter 3, examined the effect of a number of loading cases on a finite element model, including the use of the joint reaction force, abductors, ilio-tibial tract and iliopsoas, on the bending produced in the femur during loading. The results were compared against radiographs of *in vivo* deflections of the femur during one-legged stance. Comparison of the two gave magnitudes of the loads and reactions that most closely duplicated the *in-vivo* femoral deformations.

These conditions were applied to the model by use of nodal forces on an axis system consistent with that used in the original study. The position of the loads is shown in Figure 9.21 with the corresponding component magnitudes detailed in Table 9.5.

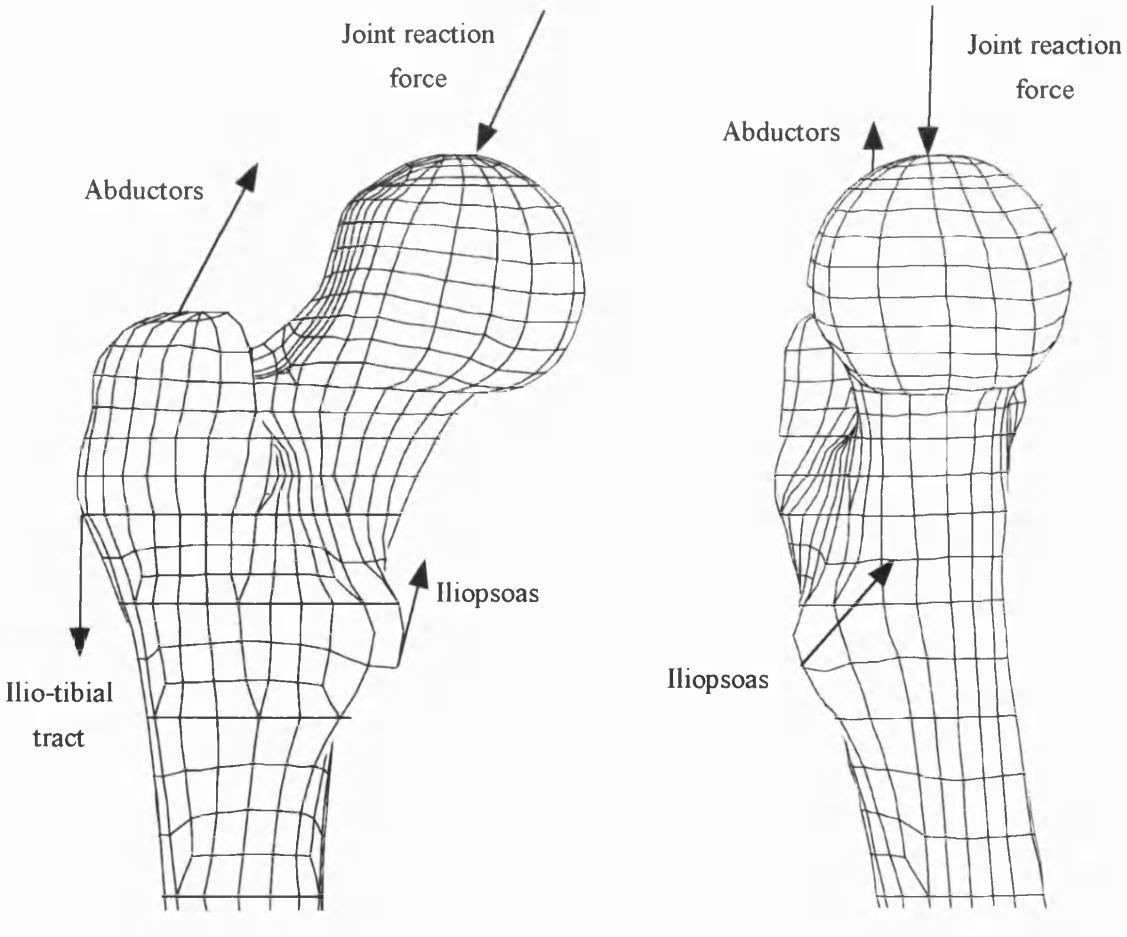

Figure 9.21 - Hip joint loading

Load	Force components / kN			Resultant force
	X	Y	Z	kN
Joint Reaction force	1.062	-2.800	0.130	2.997
Abductors	-0.430	1.160	-	1.237
Ilio-tibial tract	-	-1.200	-	1.200
Iliopsoas	-0.078	0.525	-0.560	0.771

Table 9.5 - Muscle and joint reaction forces for femoral loading

For the implant model, the joint reaction force was simply relocated from the head of the natural femur to the centre of the head of the implant. This assumed that the joint would have been used in an identical manner after the replacement of the hip joint. The static analysis of the natural model was simply loaded and held whilst the calculation of the physiological normal stimuli occurred. After the model was inserted with the implant, the loading was cycled between loading, unloading and remodelling, in a manner described in Chapter 6.

9.8.2 Boundary conditions

Identical problems were encountered with the boundary conditions as those seen in the turkey ulna model (described in Section 7.4.3), where the cortical bone remodelling technique required free perpendicular movement across the constraints. As with the turkey ulna model, the boundary constraints were arranged in a straight line or 'pin' configuration across the centre of the femoral shaft (Figure 9.22) to restrict movement along the remodelling plane. A local co-ordinate system was created in line with the femoral cut (down the length of the implant shaft) and the six nodes of the cortical bone were constrained perpendicular to its length. A single additional node was constrained along the length of the X-axis to stop any sliding of the base of the femoral shaft along this axis. The entire base of the shaft was then constrained onto a plane at Z=0 to restrain any lifting of the shaft in bending.

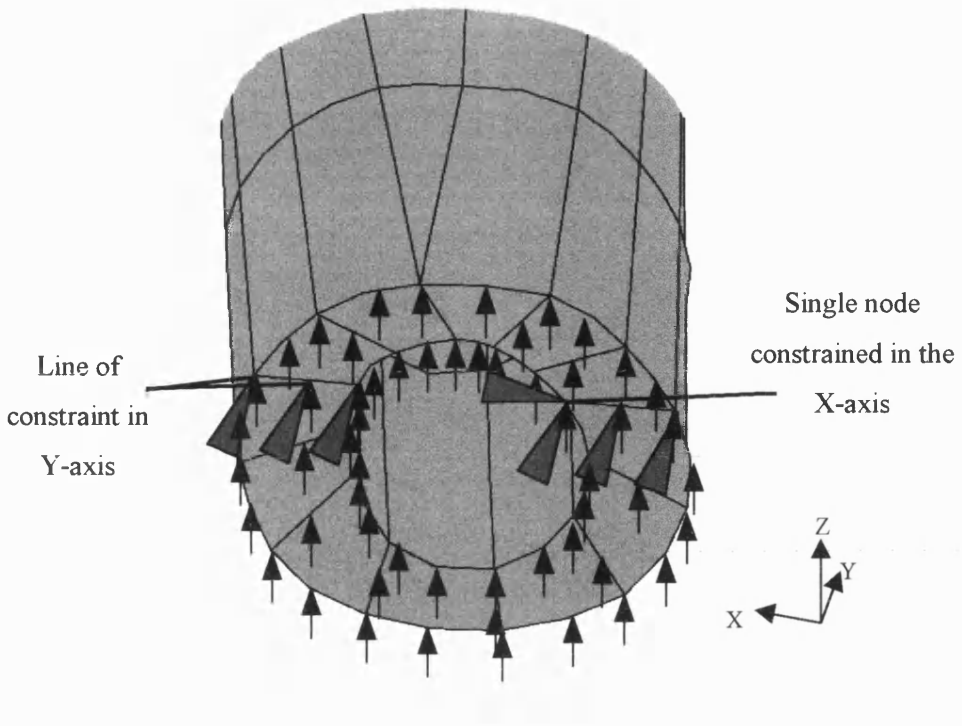

Figure 9.22 - Boundary conditions at the base of the femoral shaft

9.9 Implanted hip model

9.9.1 Mesh of the implanted hip model

The mesh of the implanted femoral model was identical to the natural femur model below the line of the neck resection since the geometry of the structure below the cut remained the same (Figure 9.23). The natural femoral head was replaced by the elements of the head of the implant and the contact surfaces adjusted accordingly: the tied interface on the neck resection line was removed and the common nodes of the implant head and stem were equivalenced. In addition, the stem surface, which made up the master surface of the cement - implant interface, was extended to include more elements of the implant neck. This allowed the surfaces to remain in contact under loaded conditions when the slip interface became operational, rather than the nodes falling off the edges of the companion surface.

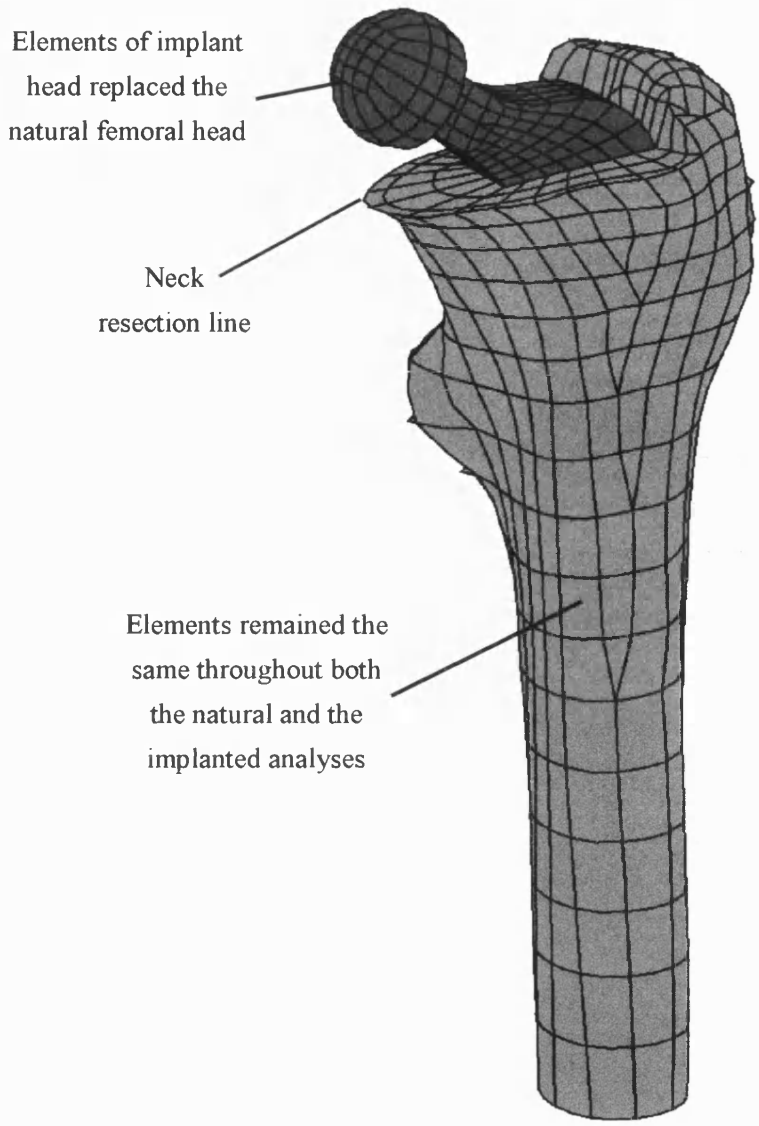

Figure 9.23 - Implanted femur model

During total replacement of a hip, the trabecular bone is reamed out from the femoral shaft and replaced. Likewise, in the finite element model, the majority of the cancellous bone was replaced by the cement mantle and the implant itself. There were also regions of cancellous bone in the greater trochanter that remained intact throughout both the natural and the implanted analyses. These regions, shown in Figure 9.24, were susceptible to cancellous remodelling

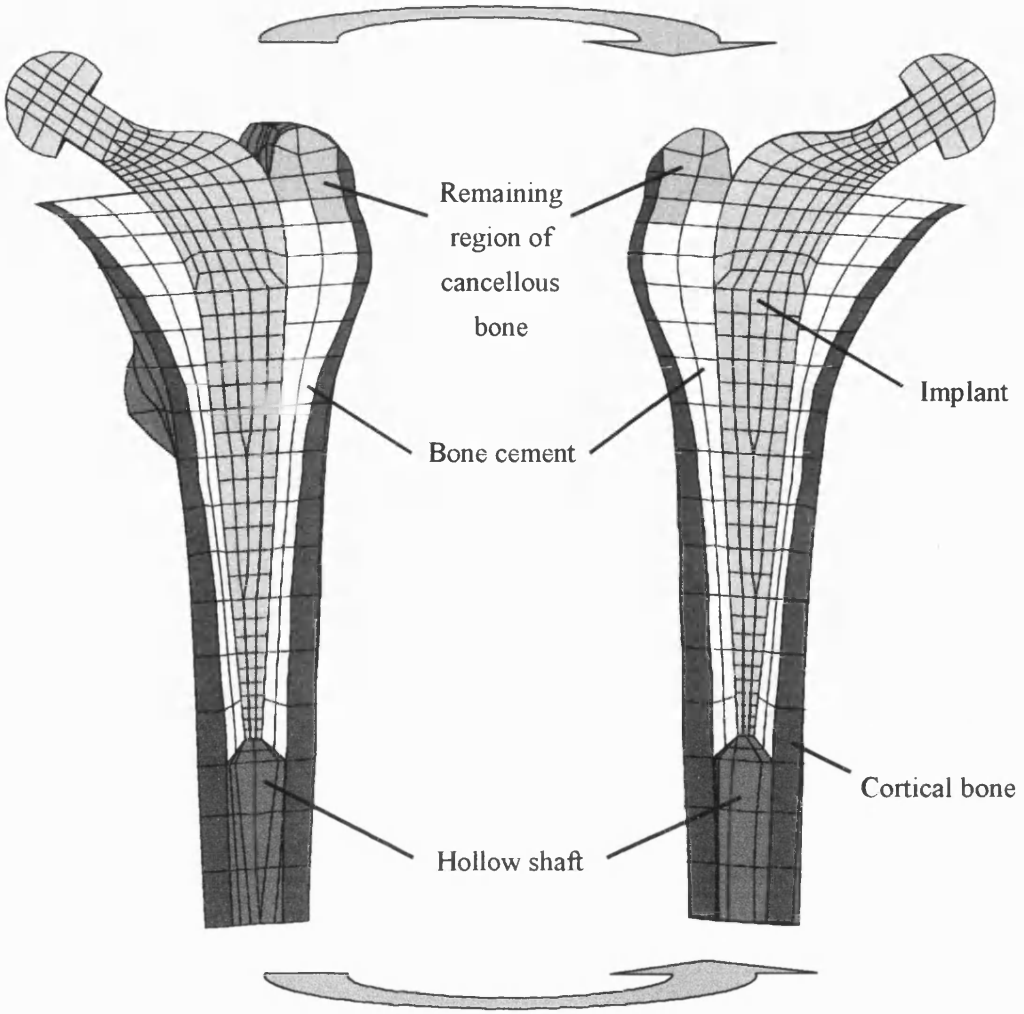

Figure 9.24 - Section of implanted model

The implanted model comprised of 1952 elements and 12619 nodes. 804 elements were associated with the implant and 667 with the cement mantle. 72 cancellous bone elements were still present from the natural model and the remainder were cortical bone. A value of 0.2 was used as the friction coefficient between the implant and the cement.

9.9.2 Materials properties

The material properties applied to the femoral model, other than those associated with the regions of cancellous bone (which are discussed in Section 9.7.2) are displayed in Table 9.6. The implant and cement regions of the bone were simply the same elements as in the natural hip model, with altered material properties according to the sections that were surgically replaced. The values of the final properties used for the remodelling analysis are

Regions of model	Young's Modulus / GPa	Poisson's Ratio	Reference
Cortical bone	17	0.33	Cowin (1989)
Cancellous bone	Various (from scan)	0.30	---
Stainless steel	210	0.30	Jones (1980)
Cement mantle	2	0.30	Wheeler *et al.* (1995)

Table 9.6 - Materials properties for remodelling analysis

9.10 Overview of analysis procedure

An overview of the complete analysis procedure from the first pre-analysis until the long-term remodelling predictions around the implant stem is shown in Figure 9.25. Before any remodelling results could be gained, it was necessary to complete the second pre-analysis (shown as 2) in order to gain the results of the physiological normal conditions for each of the stimuli examined (marked 3). These values were each written to an independent external file during the second pre-analysis for storage. Any remodelling analysis then simply picked the required objective stimulus and recovered the values from the relative file.

The largest modification between the two models was the replacement of the femoral head with the neck and head of the implant (marked 5). The small remaining regions of trabecular bone retained their original materials properties and were subjected to cancellous bone remodelling. The materials properties of the elements in the centre of the femoral shaft were altered to model the implant and the cement mantle (marked 6), whilst the sections of cortical bone were subjected to remodelling. The hip joint reaction loading was changed from femoral head to the head of the prosthesis (shown as 7), although the boundary conditions remained identical to the natural hip model. The model was then ready to be subjected to the cyclic loading associated with remodelling.

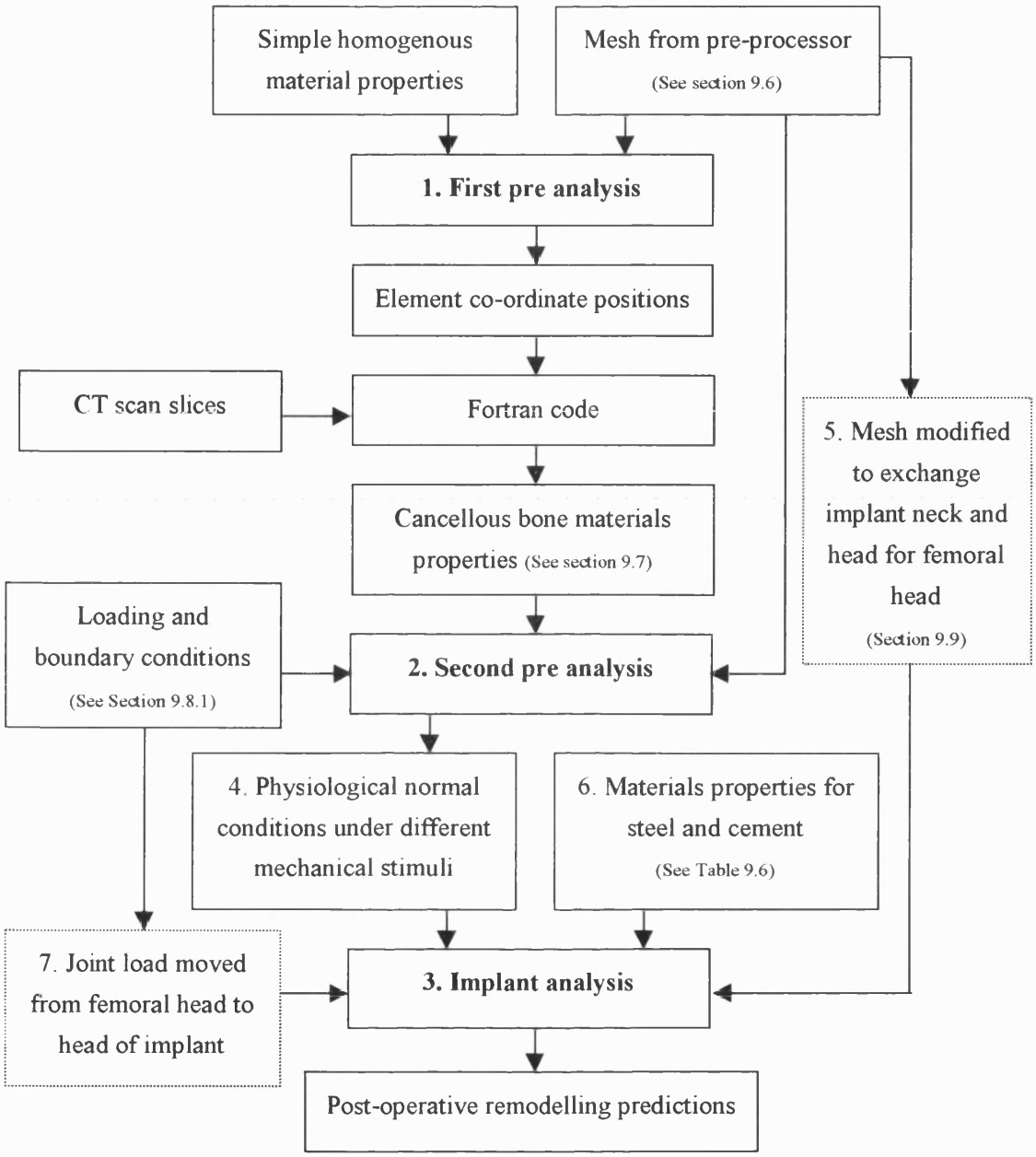

Figure 9.25 - Overview of remodelling analysis

9.11 Remodelling parameters

The analysis of the implanted model was subjected to a variety of parameters that effected the resulting remodelling. Most important of these was the mechanical signal to which the cortical and cancellous bone remodelled. It was considered that whilst all the stimuli would be considered for the analysis, final judgement would be reserved until after the pre-analysis predictions had been viewed.

Rate of remodelling for the cortical bone was taken from Beaupré *et al.* (1990) who based their remodelling upon a maximum rate of bone deposition of 1.0 μm / day. This resulted in the long-term value of 0.365 μm/year. Cancellous bone remodelling, on the other hand, was not assigned the same level of importance within the remodelling bone. Previous studies in the literature have based trabecular remodelling on the density of bone (Stülpner *et al.* 1997, Beaupré *et al.* 1990). This study has not extended the code to include this. As a result a stiffening value of 50 N/mm^2 per year has been taken.

The Dead Zone values for each remodelling situation would be determined directly from the pre-analysis predictions, according to each stimulus.

9.12 Discussion

The modelling of the cortical and the cancellous bone geometry may appear slightly irregular due to the abrupt termination of the cortical bone at the femoral neck. The remodelling of cortical bone elements that neighbour cancellous elements did not provide problematic distortions, however, because the natural model did not include any form of remodelling. The combination of these elements only existed during the natural hip pre-analysis since the adjoining cancellous elements were removed after the insertion of the implant. The removal of the femoral head, preceding the analysis of the implanted model, also removed the most poorly shaped elements (in the femoral neck) from the analysis.

It should be noted that no four noded tetrahedral or six noded prism elements (which are all considered too stiff in bending) were used in the analysis, as the model was primarily based upon twenty noded brick elements. Degeneration of the topology of these elements created ten and fifteen noded elements.

The geometry of the prosthesis was simplified, especially around the neck, where a square section replaced the cylindrical neck of the actual implant. This was not considered of special importance, since the stiffness of the structure was significantly higher than any other part of the model. As a result, relatively little compression or bending would have been associated with the implant, and the altered neck section would contribute little. Also, the neck was not in contact with the bone, so no localised variation to the loading patterns could be transferred.

More significant than the changes to the implant neck, however, were the alterations made to the edges of the implant, since these were in contact with the bone. To model the fillet radii on the corners of the shaft would have been a significantly large amount of extra modelling time. The transfer of the load through filleted edges would improve the stress and strain environment, but the presence of the cement mantle provided a load-mediating layer. Had creep properties been included in the cement material, then the addition of the fillet radii would have been a valuable addition.

9.12.1 Recommendations for future modelling

Several limitations to the modelling technique have become apparent over the course of developing the femoral model. A number of recommendations for creation of a second-generation model have been made as a result: -

1. CT scan slice data should be taken both at more frequent intervals down the length of the bone (perhaps at 2 or 3mm intervals over the proximal section of the femur, increasing to 10mm over the more distal regions of the shaft)
2. The scanned slices should continue further down the shaft of the femur to a location where the strain environment would remain unaffected by the localised effect of the tip of an implanted prosthesis.
3. Scans would be taken in two planes; one set correlating to the shaft of the femur, and the other correlating to the neck and the femoral head. This would allow any areas of complex or convolute geometry to be cross-referenced to the opposing set of scans.
4. The angle between the femoral condyles and the head/neck would be recorded to provide information pertaining to the relative position of the bone with respect to corresponding studies in the literature. This would also allow the calculation of the position of the bone relative to the plane of scanning.
5. The model should include fillet radii to model the implant as accurately as possible. This would allow the addition of creep within the cement mantle at any time without the loss of any accuracy due to the geometry of the structure, or high stress concentrations within the cement mantle.
6. Density of the cancellous bone should be calculated as a function of density.

Chapter 10 Results and discussion

10.1 Natural hip analysis

The natural femoral model was analysed under the conditions described in the previous chapter. The output of this initial analysis was 13 different files, each containing the values of stimulus under normal physiological loading conditions of the natural bone. The different stimuli calculated are shown in Table 10.1.

Stimulus	Formula used
Most tensile principal stress	EP_1
Most compressive principal stress	EP_2
Intermediate principal stress	EP_3
Most tensile principal strain	SP_1
Most compressive principal strain	SP_2
Intermediate principal strain	SP_3
Shear strain	$(EP_1 - EP_2)2$
Shear stress	$(SP_1 - SP_2)/2$
Strain energy density	$(EP_1*SP_1+EP_2*SP_2+EP_3*SP_3)*27$ / Volume of Element
Von Mises stress	$SQRT(0.5*((SP_1-SP_2)^2+(SP_2-SP_3)^2+(SP_3-SP_1)^2))$
Hydrostatic stress	$(SP_1+SP_2+SP_3)/3$
Deviatoric stress	$SQRT((SP_1-SP_2)^2+(SP_2-SP_3)^2+(SP_3-SP_1)^2)/3$
Osteogenic index	Deviatoric stress + Hydrostatic stress / 2

Where EP are principal strains, SP are principal stresses, and the subscripts $_{1,2,3}$ relate to the principal directions

Table 10.1 - Formula for stimuli

The initial results of the physiological normal conditions under the most tensile principal strain are shown in Figure 10.1. Only the cortical regions of the bone are presented, and the image shows isochrome contours between the colours to enhance the contrast. It was found that throughout the study the majority of the stimuli exhibited peak values close to the positions where the boundary conditions were present. It can be seen that the removal of the most distal layer of elements of the femoral shaft produced a significant difference in the contour maps,

which was additionally enhanced by the lower values of peak stimulus. Reduction of these peaks improved the sensitivity of the contour map over the remaining regions of the bone.

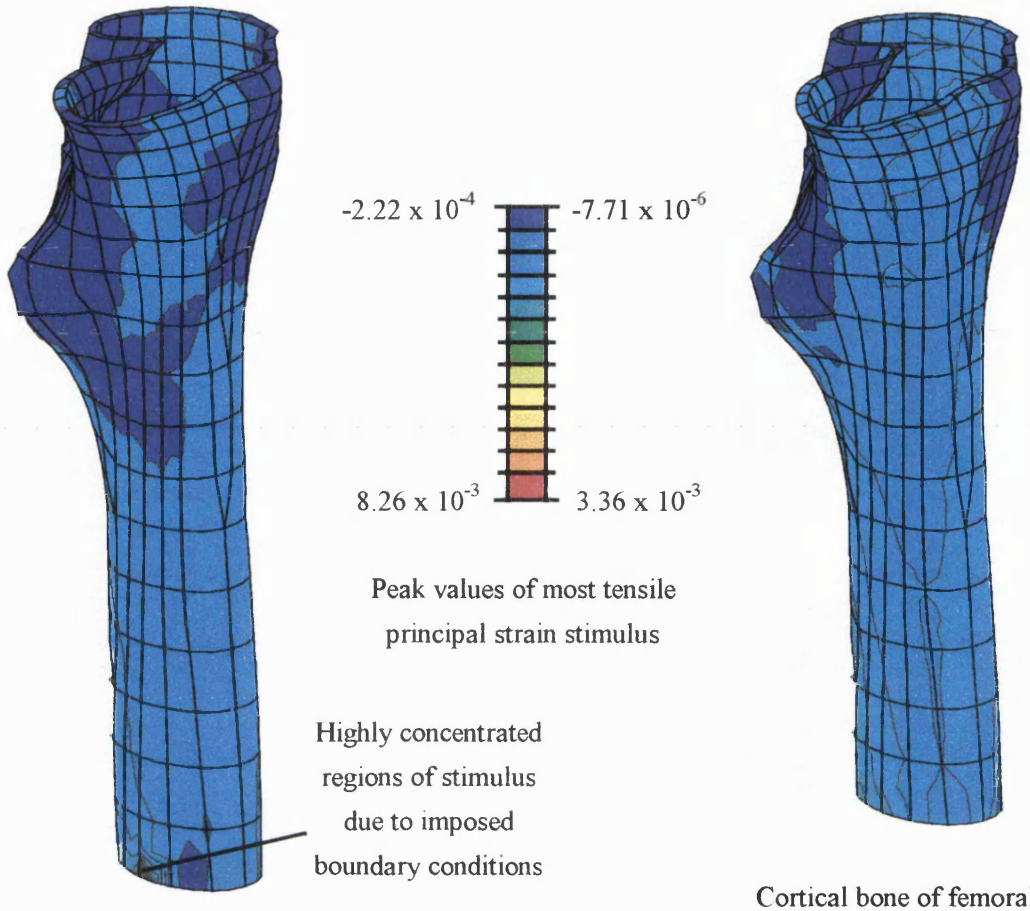

Figure 10.1 - Natural femoral model under physiological normal conditions (Static analysis)

The values for the basic principal stresses and strains are detailed in Table 10.2. It demonstrates for nearly all values of stress and strain that the most extreme or peak values were present in the most distal elements of the femoral shaft. The most positive tensile and most negative compression values are highlighted in bold text. As the peak stresses and strains within the cortical bone region, these were deemed to be some of the most significant values for remodelling. Removal of the lower layer of elements reduced the range over each stimuli by as much as 80%.

Stimulus	Peak values	
	With base elements	Without base elements
Most tensile principal strain	-0.000222 **0.00826**	-0.00000771 **0.00366**
Intermediate principal strain	-0.00123 0.000913	-0.000612 0.000913
Most compressive principal strain	**-0.00683** 0.000107	**-0.00246** 0.0000121
Most tensile principal stress N / mm^2	-53.7 **192**	-2.89 **61.8**
Intermediate principal stress N / mm^2	-80.4 96.3	-12.7 15.1
Most compressive principal stress N / mm^2	**-160** 60.9	**-36.8** 3.04

Table 10.2 - Effect of removal of most distal elements on peak stimuli

It was decided that this lower layer of elements was to be removed for the calculation of all the normal physiological stimuli for the natural femoral model since this increased the sensitivity of the remodelling values to the local regions. In this manner, the remodelling of the majority of the femoral shaft was not dependent upon values determined by elements that were heavily affected by the localised boundary conditions. This effectively targeted the remodelling values to the regions of bone affected.

After the removal of these elements, the normal environment for the natural bone was determined for all of the relevant stimuli. Four of these are shown in Figure 10.2.

It can be seen that under these conditions, the anterior surface of the femur tended to be under the most compression (using the convention of positive tensile and negative compressive stresses and strains). This was confirmed by the presence of tensile stresses on the posterior aspect of the femoral shaft. The strain energy density showed a highly localised contour map, concentrated around in the anterior aspect of the calcar region.

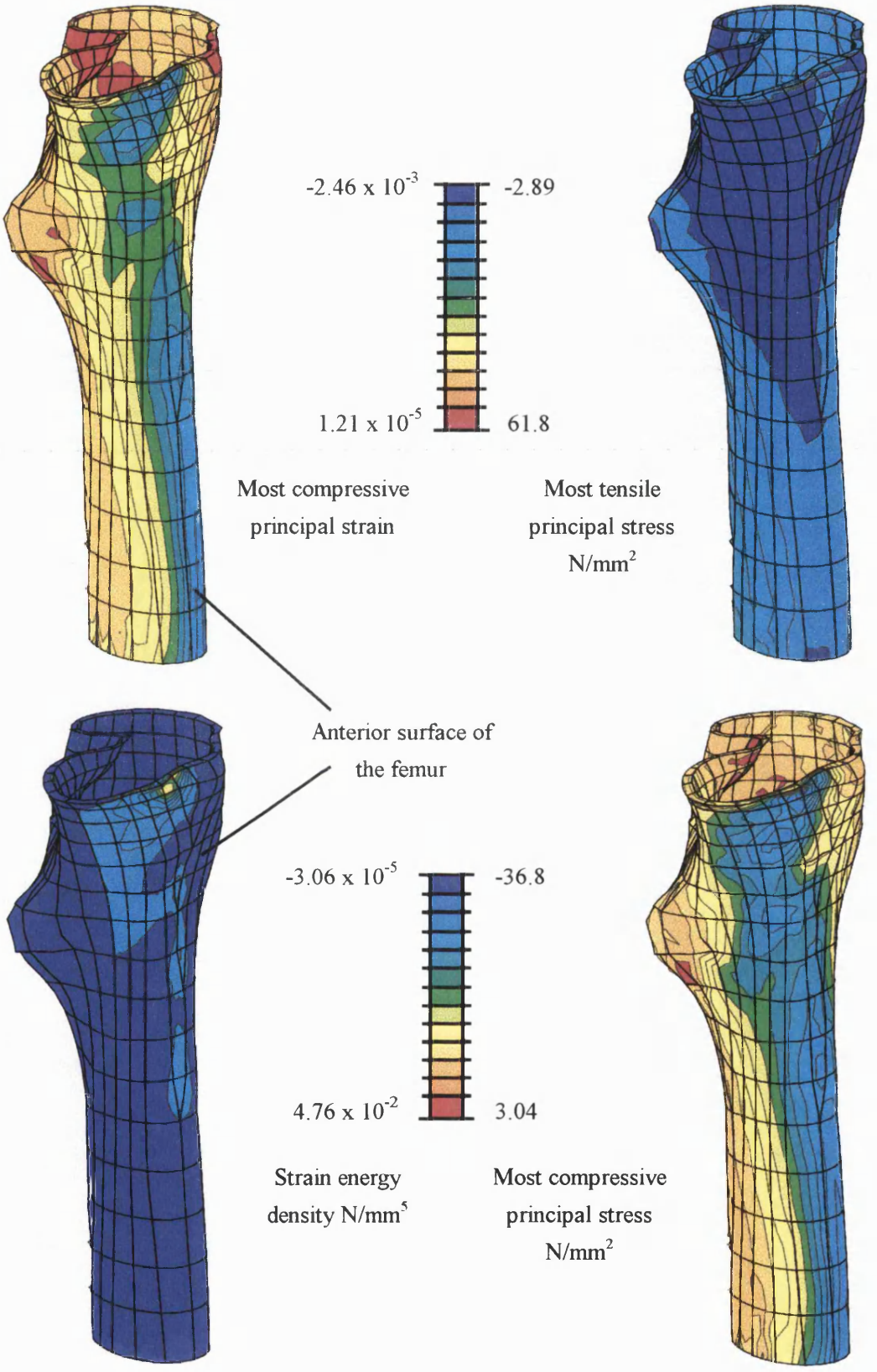

Figure 10.2 - Normal environment for the natural femur (static analysis, no remodelling)

Observation of the opposite surface of the femoral shaft showed a localised increase in stimulus around the contact position of the ilio-tibial tract for the majority of stimuli. The increase in values was small in comparison to those produced around the regions of the boundary conditions, however, due to its relatively small magnitude.

10.2 Implanted femur

The implanted femur was loaded in the manner described in Chapter 9, and was run under two sets of conditions. The first included slip interface conditions at the stem - cement interface to model the effect of the smooth, polished stem. The second method demonstrated the effect of the rough matt stem by considering the case in which no relative movement between the stem and the cement mantle occurred, by 'tying' the surfaces together. This allowed comparative predictions under the two different loading environments.

The static stress strain environment for the two cases was compared and comparisons of the peak values are shown in Table 10.3. In addition, the contour maps for both cases are shown in Figure 10.3

Stimulus	Peak values	
	Slip interface	Tied interface
Most tensile principal strain	-0.00326 0.000148	-0.00326 0.0000312
Most compressive principal strain	-0.00217 0.0000799	-0.00218 0.0000247
Most tensile principal stress (N/mm^2)	-2.42 37.9	-2.47 37.3
Most compressive principal stress (N/mm^2)	-0.404 3.06	-0.28 3.08

Table 10.3 - Comparison of slip and non-slip interface conditions on implanted femur

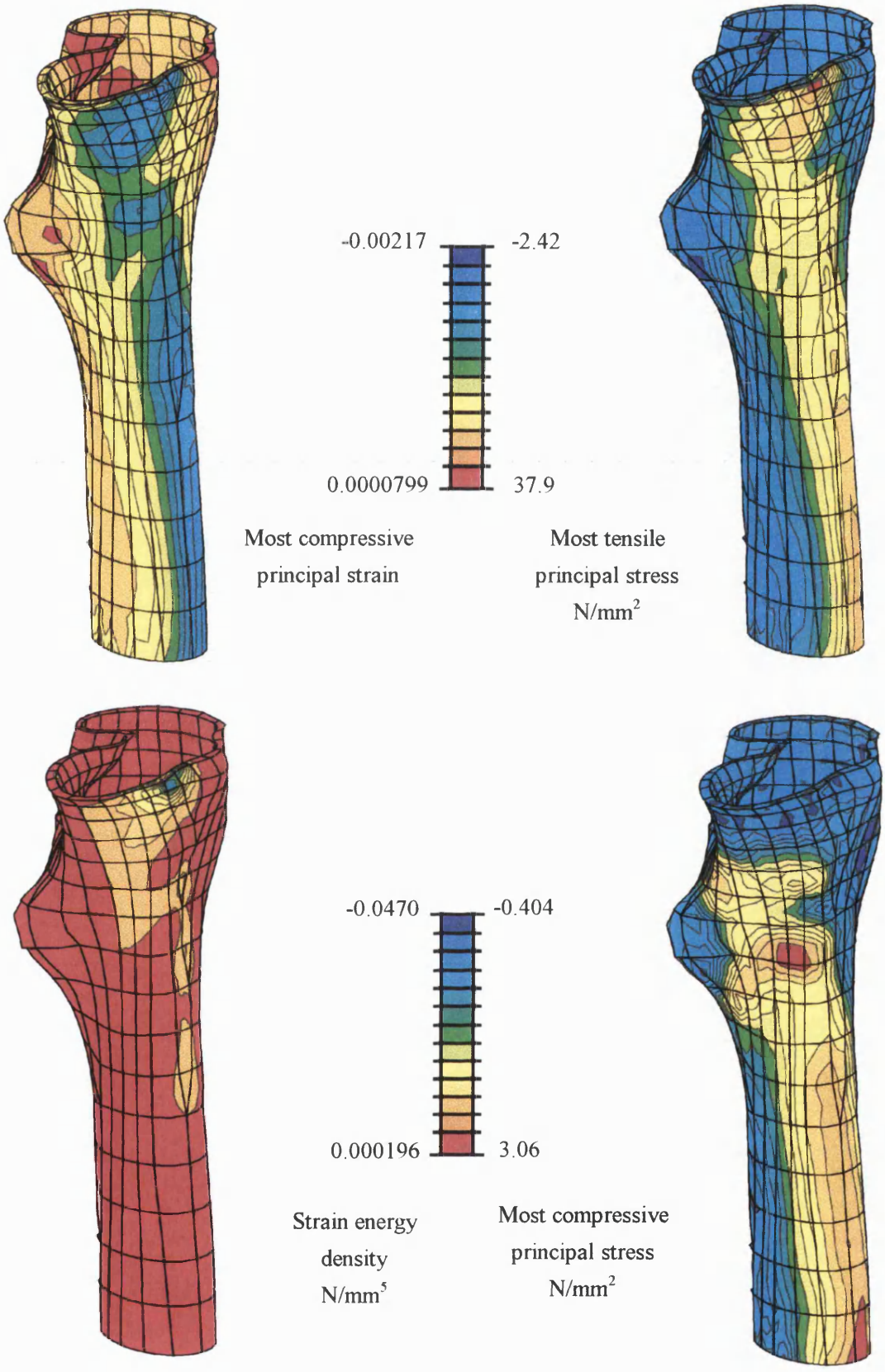

Figure 10.3 - Stress and strain environment for the implanted femur with slip interface conditions (Static analysis, no remodelling)

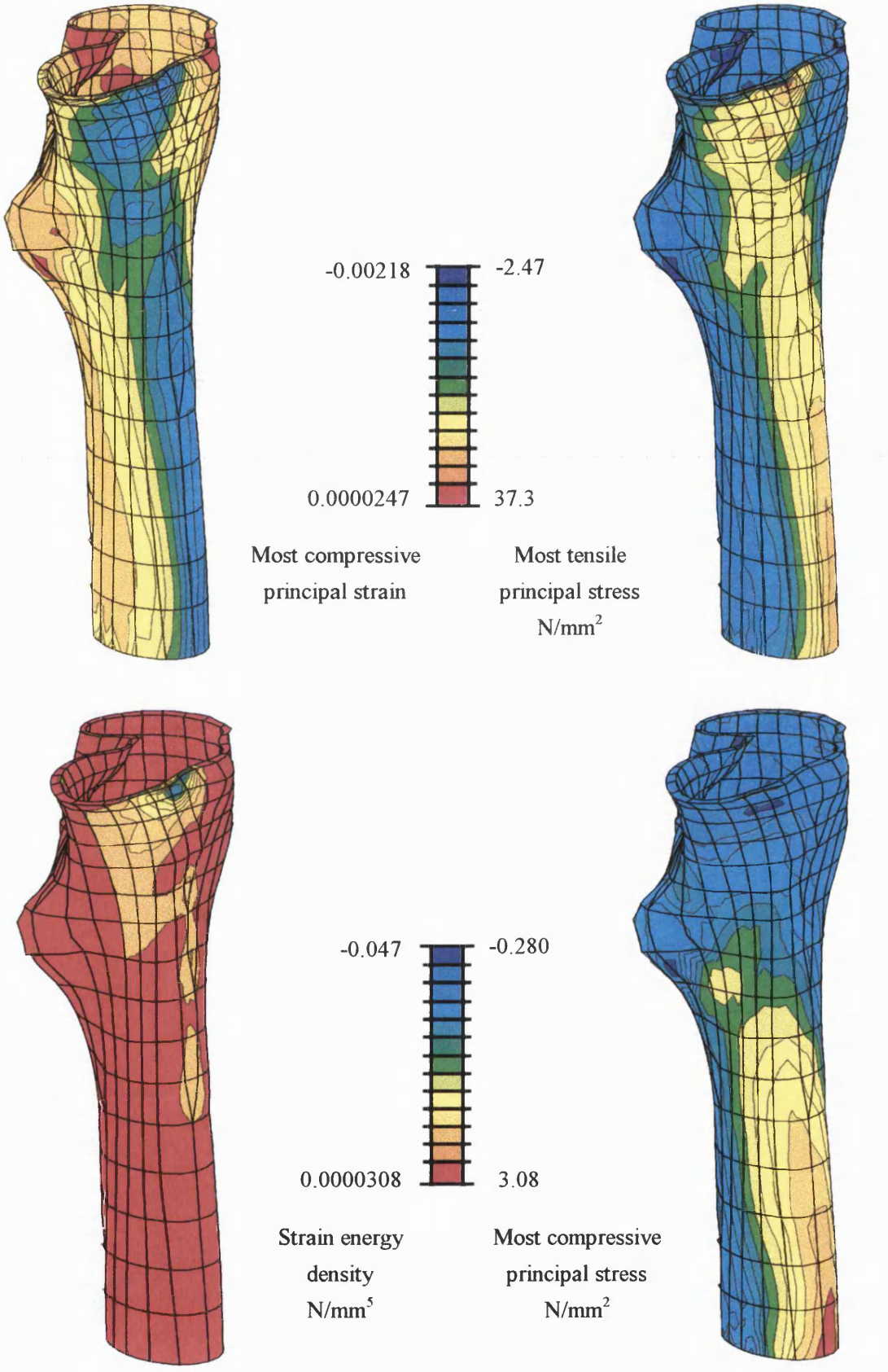

Figure 10.4 - Stress and strain environment for the implanted femur with tied interface conditions (Static analysis, no remodelling)

In each of the above cases, the values of stimulus from the implanted femur with the tied interface conditions were imposed upon the slip interface model in order to equalise the contour maps. The contours on each map therefore represent the same values for both the polished and matt stem models. The peak values were stated on each model.

From a comparison of the two cases (slip and non-slip interface conditions), it can be seen that all models give remarkably similar results, although a significant difference was noticeable under the calcar region when examining the compressive stress environment. Here, the localised region displayed a decrease in stress (more positive) in the polished stem model. This would be associated with relative resorption compared with the tied interface conditions, if this were the remodelling stimulus. The global magnitudes of the stimulus, however, were much larger throughout the remainder of the shaft.

Perhaps the most significant result, however, was the reduction in peak values between the natural and the implanted femoral models. The values of both tensile and compressive stress and strain were all reduced, demonstrating the effect of stress shielding caused by the presence of the implant. This effect is seen in the potential for the bone to remodel, as described in the following sections.

10.3 Pre-remodelling predictions

The pre-remodelling predictions were determined with a static model by calculating the difference in stimulus between the natural femur model and the implanted model. This allowed an initial view of the remodelling that was to occur in the first step of the analysis and gave an indication of the remodelling that would occur during the entire analysis.

After initial bone remodelling predictions were gained from calculating the difference in stimuli between the natural and the implanted femur, it was noted that incorrect results were seen when strain energy density was used. Small diamond shaped areas of lower remodelling potential were present in the centre of each element suggesting a problem with the calculation of the element volume.

It was found that the volumes of the integration points varied throughout each element, with the largest volume associated with the central point, followed by the mid-face points and finally the corner integration points had the smallest volume. When the strain energy density

was calculated, division by the local integration point volume caused variation within the element and hence the diamond pattern effect. This problem was resolved by calculating the total volume of the element by summing the individual integration point volumes, and dividing the total by the number of integration points in each element (according to type) to give an average integration point volume. This volume was assigned to the element and the strain energy density calculated accordingly.

This resulted in a reduction in accuracy when remodelling according to this stimulus, and one that was dependent upon mesh density. It was confirmed that this problem had not arisen during the turkey ulna modelling (Chapter 7) since the models had all consisted of eight noded brick elements rather than their twenty noded counterparts. These elements contain only eight material integration points, each of an identical volume, and so the problem had simply not arisen.

The difference in predictor stimulus between the natural and the smoothly polished implant femoral models is presented for both strain energy density and most compressive principal strain (Figure 10.5). As the calcar region of the femur is currently the area of greatest clinical remodelling interest, this region has been presented. From this angle, the extreme values of remodelling potential show the peak magnitudes throughout the whole cortical region of the bone.

Since the values shown for each stimulus are differences between the natural and the implanted femoral model, the zero contour defines the position at which the value of the stimulus is the same in the two models. These were therefore regions associated with no remodelling. The contours have been adjusted for the case of the most compressive principal strain stimulus to account for association of resorptive remodelling with a more positive stimulus. Notice that both of these models predicted little or no bone deposition or regions of severe resorption especially in the anterior calcar region.

From the examination of the initial results, a number of stimuli could be immediately eliminated as viable predictors of remodelling. The remodelling associated with the majority of the remaining stimuli tested produced growth in the calcar region and resorption throughout the remainder of the bone, in contrast to that generally seen *in vivo*.

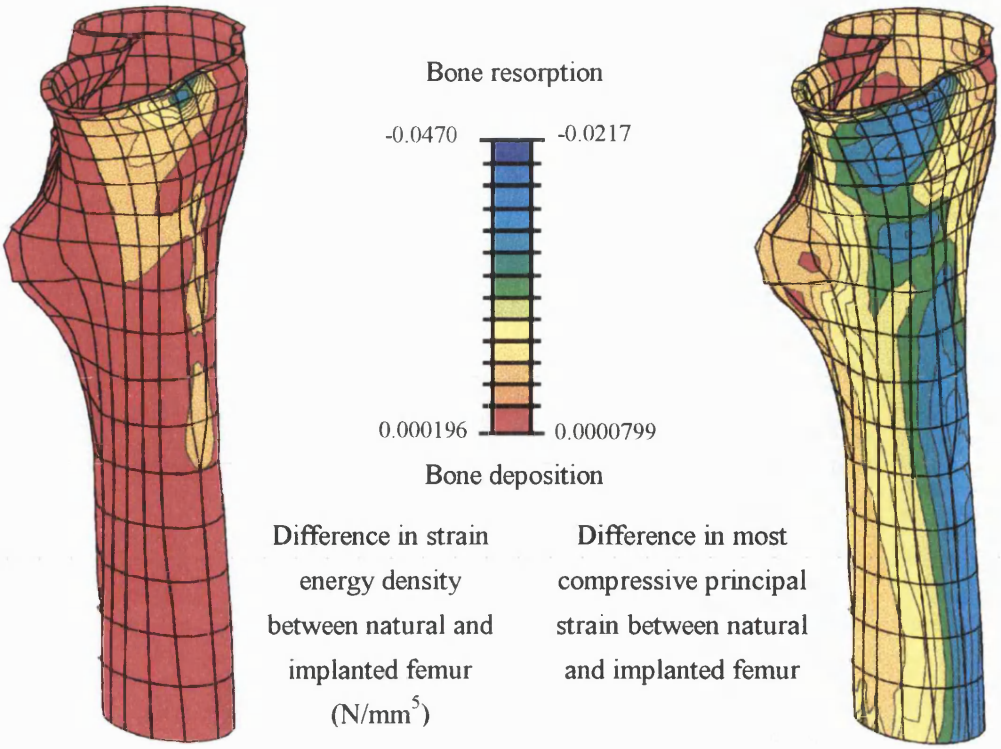

Figure 10.5 - Pre-remodelling predictions (slip conditions, static analysis, no remodelling)

The resulting values of static remodelling potential were compared for the polished and the matt stem. The graphical results showed remarkably similar contour locations, although the extreme values differed (Table 10.4).

Stimulus	Peak predictive remodelling potential	
	Slip interface	Tied interface
Strain energy density (N/mm^5)	-0.0470 0.000196	-0.0470 0.0000308
Most compressive principal strain	-0.00217 0.0000799	-0.00218 0.0000247

Table 10.4 - Comparison of slip and non-slip interface conditions on remodelling potential

Although the magnitudes were small in each case, the predictions of remodelling for the slip interface conditions showed comparatively more bone deposition. This indicated a remodelling environment in which an overall reduction in bone resorption was seen.

The predictions of remodelling using strain energy density as a stimulus produced a highly stable remodelling environment, with large areas of bone seeing low levels of difference in stimulus. Only small areas of the proximal femur were associated with the potential to remodel, although steep remodelling gradients were seen in the calcar regions predicting extensive resorption. In order to predict a wider range of remodelling behaviour to this stimulus, the sensitivity of the tri-linear curve was altered to exhibit a response to much smaller changes in stimulus values. This was achieved by decreasing the size of the Dead Zone in the tri-linear remodelling curve. The additional sensitivity produced the remodelling predictions seen in Figure 10.6.

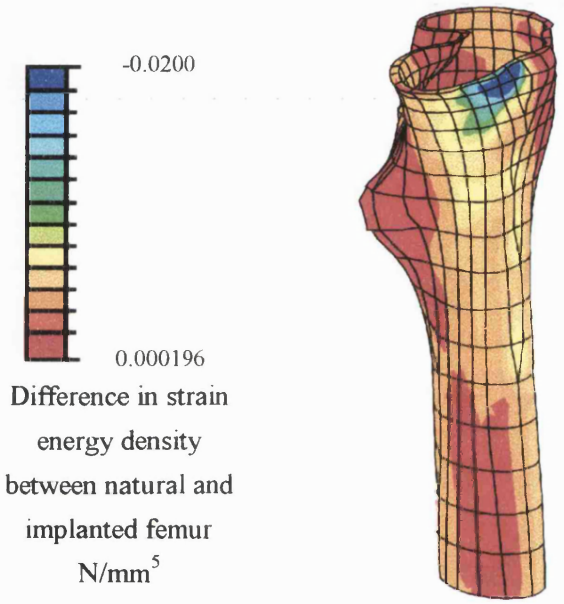

Figure 10.6 - Static pre-remodelling predictions of strain energy density with increased remodelling sensitivity

This remodelling contour map was obtained by adjusting the minimum (or most negative) value of the stimulus. The image presents the same differences in stimulus as Figure 10.5, but with an effective shift in the colour scale. The peak value of -0.02 is therefore not representative of the actual value, but merely represents a value beyond which all regions of dark blue are equal to or more negative than -0.02. Under these conditions the predictions showed higher values of remodelling over a much greater region of the bone.

10.4 Cancellous bone remodelling predictions

The same process performed on the cortical bone was undertaken for the regions of cancellous bone that remained in the implanted analysis. The stress and strain environment was established for the natural bone followed by a calculation of the differences in the stimuli after the implantation of the prosthesis.

Since the majority of the remodelling stimuli had been rejected based on the cortical bone predictions, only most compressive principal strain and strain energy density are presented (Figure 10.7).

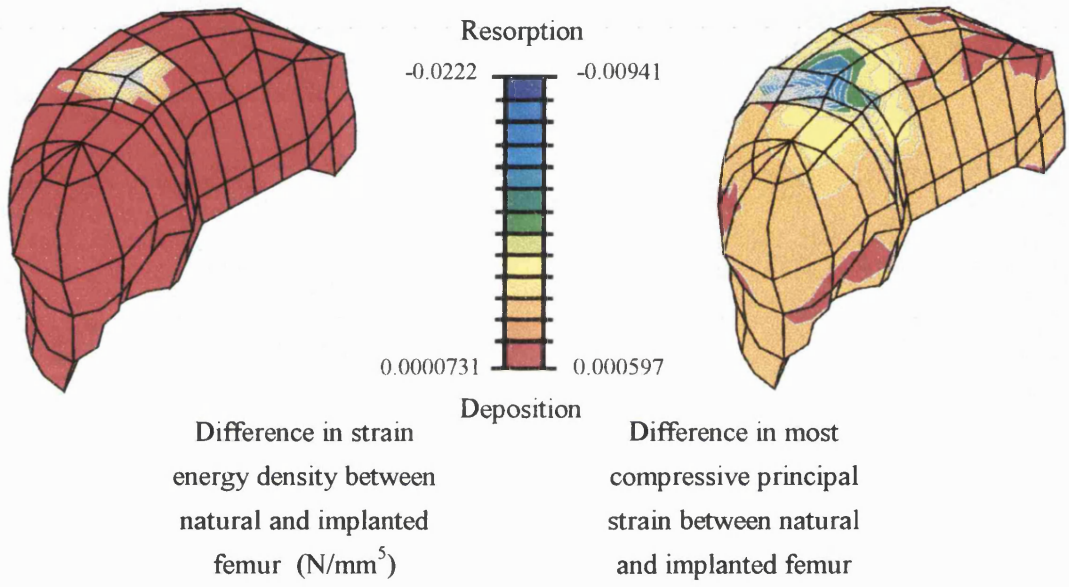

Figure 10.7 - Static pre-remodelling predictions of cancellous bone

Again, the predicted regions of resorption under a strain energy density stimulus were highly localised and concentrated around the location of the abductor force. Similar results were seen using the most compressive principal strain, with resorption concentrated around the site of the abductor muscles. These results are in general agreement with *in vivo* studies. The magnitudes of the predictions, however, show a much lower level of remodelling activity compared with the cortical bone, probably as a result of relatively little change in the area as a result of introducing the implant.

10.5 Discussion of pre-remodelling predictions

From the selection of stimuli, both strain energy density and most compressive principal strain proved to be the most reliable predictors of remodelling. This promotes these stimuli good predictors of bone remodelling, as they support the clinical evidence of resorption in the calcar region. Use of these stimuli is also supported by the remodelling predictions of both Lanyon and Huiskes and co. workers (as described in Chapter 4).

In general, the predicted resorption associated with the calcar region was also present in the anterior regions of the bone. In fact, nearly all the stimuli, regardless of the quality of the predictions had proximal anterior values closely resembling those seen in the calcar region. The posterior regions, meanwhile, seemed closer to the remodelling equilibrium, with little potential to grow or resorb. This consistency in behaviour between the calcar and anterior regions of bone is undoubtedly a function of the loading regime applied to the bone, and could be further informed by the application of a number of different loading regimes.

10.6 Remodelling results

The remodelling code was run for the femoral model under a strain energy density stimulus. Tied interface conditions were used (the slip interface significantly increased the computation power required, and was therefore limited in availability) with a maximum cortical growth rate of 0.365 mm / year (taken from the value of 1μm / day used by Beaupré *et al.* 1990). Three models, each using most compressive principal strain as the stimulus, were run for a period of one year. The first used 6 time steps of 2 months, the second 2 time steps of 6 months and the final model remodelled in a single step for the whole year period. It was found that both the final values and the distribution of remodelling were almost identical. Based on these, it was decided to allow the long term remodelling of the proximal femur to occur in time steps of one year.

The model was then subjected to long-term remodelling under a strain energy density stimulus. The tri-linear curve was specified as described in the previous section (10.3) and the resulting remodelling is shown in Figure 10.8.

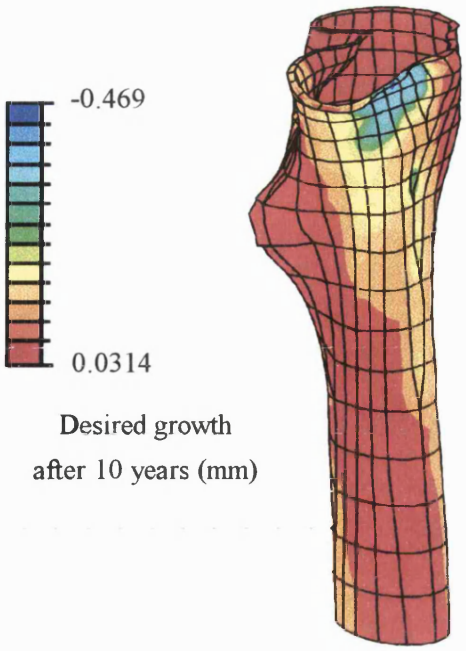

Figure 10.8 - Remodelling after 10 years under a strain energy density stimulus (tied interface conditions)

It can be seen that the potential to remodel has decreased over the ten-year time period. The region of most remodelling potential in the calcar region remained the most active area, and continued to resorb at a maximum rate of 0.469mm / year. This value was higher than the specified value of 0.365mm / year and the difference was directly attributable to the fact that the size of the element was calculated across a single edge: If a difference in thickness was present across an element, it is possible to remodel at a rate slightly greater the than the value specified since the calculation of growth rate was based upon the single length for the whole element (This was discussed in detail in Section 6.6). This inconsistency was a function of the mesh density, and would decrease with a finer mesh.

The remodelling of the proximal femur under a most compressive principal strain stimulus displayed similar final remodelling patterns to those seen in the strain energy density case (Figure 10.9). The results for the polished stem are shown, although the tied interface conditions, representing the matt stem, displayed almost identical remodelling patterns.

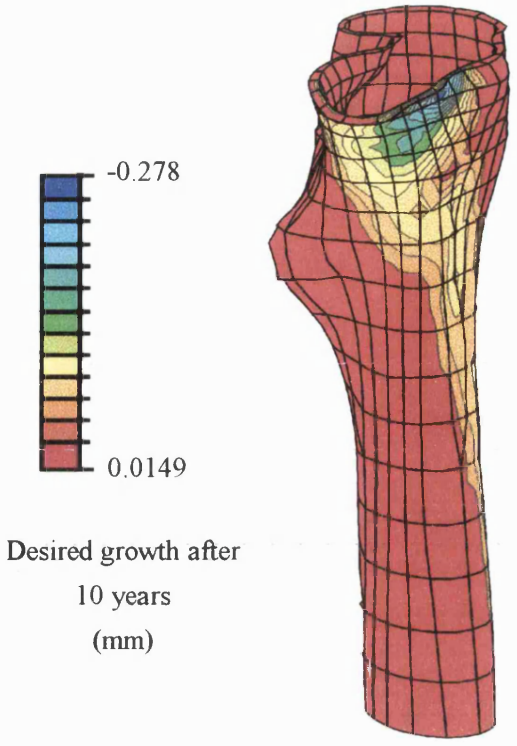

Figure 10.9 - Remodelling potential after 10 years under the most compressive principal strain stimulus

The value of maximum remodelling potential has been significantly reduced from the maximum of 0.365mm / year, demonstrating that the entire region of cortical bone was within the normal extent of the tri-linear curve. This showed the stability of the stimulus under these conditions, compared to that calculated using strain energy density (Table 10.5). In addition, the patterns of remodelling potential had significantly altered from the original predictions (cf. Figure 10.5), effectively reducing the fringe areas of lower remodelling potential into the Dead Zone of the tri-linear curve. Interestingly, the final remodelling patterns of both strain energy density and most compressive principal strain appear remarkably similar, with resorption under the calcar and in the anterior shaft of the bone.

Stimulus	Remodelling potential after 10 years (mm)	
	Slip interface	Tied interface
Most compressive principal strain	-0.278	-0.280
(Max and min)	0.0149	0.0110
Strain energy density (N/mm^5)	-0.469	-
(Max and min)	0.0314	

Table 10.5 - Remodelling potential after 10 years

Once again the slip interface conditions gave a more stable remodelling solution than the tied conditions. Remodelling of the bone using slip interface conditions and a strain energy density stimulus was not available due to the limitations of the computer resources.

10.7 Discussion

The remodelling results shown in this chapter have demonstrated resorption in the areas that are clinically relevant, under stimuli that agree with the current understanding in the literature. Indications have been given throughout that the slip interface conditions of the polished stem provide a better remodelling environment for the proximal femur than those of the matt stem. Although the differences in predictor values were small, the evidence was consistent across more than one stimulus. Whilst this alone is not proof of the proficiency of the polished stem, the results do correlate with the experiences of the Exeter stem (Fowler *et al.* 1988, Howie *et al.* 1998). Modelling the creep of the cement mantle would also be advantageous in order to gain confirmation of these results and to quantify the effect of the slip of the stem within the cement at the stem-cement interface.

The contrast between the tensile and the compressive stimuli provided an interesting comparison with the turkey ulna model. The femur was predominantly loaded in compression, making the compressive stress and strain the peak stimulus values. The main load on the turkey ulna (Chapter 7), on the other hand, was in bending, despite the compressive regime applied to it. Under these conditions, either the tensile or the compressive loads may have been the main forces in the model. This could account for the differences found in the remodelling

stimulus, and the fact that the most tensile principal stress correlated most closely with turkey experimental model.

The modelling of the cancellous bone proved to be an interesting concept. Each element was modelled as both homogenous and isotropic. The application of different mechanical properties to each element, however, altered the structural properties to create a global inhomogeneous model for the cancellous bone.

The model highlighted a number of questions concerning the ease of the technique with respect to the current remodelling methods, particularly the method of translation of nodal position as used by Huiskes, Weinans and co. workers. Movement of the nodes in their model implied that the method is capable of remodelling any element type, but perhaps more importantly, it would not be necessary to define which elements were cortical bone and which were cancellous. In addition, one of the limitations which was inherent in the swelling technique was that the orientation of the entire remodelling element had to be defined, rather than just the surface nodes. This limited the calculation of any remodelling stimulus to the principal values of stress and strain, including any combination thereof, since the material calculation points were re-orientated by the swelling routines. This, however, was not a significant problem, as nearly all of the stimuli were based upon principal values.

The swelling technique had the advantage of running alongside a very powerful commercial Finite Element package. This allowed access to other sophisticated modelling strategies such as biphasic cartilage algorithms which can be integrated into future studies of, for example, bone and cartilage interaction in osteoarthritis.

Chapter 11 Conclusions and further work

11.1 Conclusions

This study has developed a new technique capable of modelling the long-term adaptation process of bone. It has used standard swelling routines to represent the remodelling of cortical bone and additionally incorporated cancellous bone remodelling by altering the stiffness of the material in response to the applied stimulus. The work has reached the following conclusions.

- A method of altering the size of elements in response to a mechanical loading stimulus has been examined (Chapter 6)
- It is possible to represent the long-term remodelling associated with cortical bone using swelling to physically enlarge and decrease the size of the elements (see Chapter 7). This has been validated against experimental remodelling studies
- The static Finite Element model of the turkey ulna has been validated against the strain gauge data published in Brown *et al.* (1990) (see Section 7.4). Good comparisons of both the physiological normal wingflap conditions and the applied Instron loading regime were achieved
- The remodelling seen in the avian ulna experiments most closely matched the remodelling patterns created under a most tensile principal stress stimulus. This correlated with the conclusions of the original study.
- Few other mechanical remodelling stimuli produced remodelling comparable to that seen in the turkey ulna (see section 7.4.7)
- Some stimuli appeared not to approach remodelling equilibrium, although the extreme variation from physiological loading was acknowledged. This suggests that these stimuli need a loading environment close to the physiological normal loading environment.
- A different approach to modelling the Dead Zone of the tri-linear remodelling curve has been developed in which the sensitivity of the material to remodelling remains constant throughout the structure (Section 7.4.6). This has demonstrated a significant improvement on the stability of the remodelling patterns seen at the ulna mid-section (Section 7.4.7)
- Cancellous bone remodelling has been modelled by altering the stiffness of the elements in response to the applied loading (Chapter 8)

- Models using homogenous elements can display structural inhomogeneity by allowing the mechanical properties of the elements to vary throughout the structure. This was achieved in the human proximal femur using the information from CT scan data (Section 9.2.1)
- Of the stimuli examined, remodelling in the proximal femur was most closely correlated with that seen under a strain energy density and a most compressive principal strain stimulus (Chapter 10)
- Under the applied conditions, remodelling in calcar regions was associated with the anterior regions of the shaft.

11.2 Further work

This study has investigated a number of responses of the swelling code under varying remodelling circumstances. The experimental models have uncovered some limitations of the technique, which need to be further examined before the method can gain wider use. These have initially been identified as follows:

- To further examine the swelling response in order to allow more global use of the swelling code across element types. This could remove the limitations of meshing with only brick and prism elements.
- To investigate a different approach to the orientation of remodelling. The method presented in this study essentially based the swelling direction upon the local element mesh, whereas remodelling relative to the bone surface would allow less sensitivity to the local mesh structure.
- To develop the variation due to remodelling in cancellous bone as a function of density rather than Young's modulus, incorporating the relationship developed by Carter and Hayes (1969) between the two variables.
- To include the use of anisotropy in the bone material definition. This would allow a quantitative evaluation of the changes involved in modelling this feature, both in terms of a static and remodelling model.
- To include the remodelling algorithms in the cartilage models currently being developed to evaluate the effect of crystal aggregates on the remodelling seen in bone.

References

AAOS (American Academy of Orthopaedic Surgeons) (1999) web site reference: http://www.aaos.org/wordhtml/press/hip_knee.htm

Andreau C (1995), Analysis of a floating launching device for submarines, 1995 *ABAQUS Users' Conference Proceedings*, Paris, pp 69 - 84

Adams D and Swanson SAV (1985), Direct measurement of local pressures in the cadaveric human hip during simulated level walking, *Annals of the Rheumatic Diseases*, Volume 44, pp 658 - 666

Ashman RB, Cowin SC, van Buskirk WC, and Rice JC (1984), A continuous wave technique for the measurement of the elastic properties of bone, *Journal of Biomechanics*, Volume 17, pp 349 - 361

Andersen E (1995), Scandinavian Customised Prosthesis AS, Personal communication.

Bannister G (1997), Personal communication.

Bannister GC (1993), The fixation of the femoral component in total hip replacement, MD Thesis, Department of Orthopaedic Surgery, Faculty of Medicine, University of Bristol

Bannister G (1988), Mechanical failure in the femoral component in total hip replacement. *Orthopaedic clinics of North America,* Volume 19, Number 3, pp 567-573

Beaupré GS, Orr TE and Carter DR (1990), An approach for time-dependent modelling and remodelling – Theoretical development, *Journal of Orthopaedic Research*, Volume 8, pp 651-661

Beaupré GS, Orr TE and Carter DR (1990), An approach for time-dependent modelling and remodelling – Application: A preliminary remodelling simulation, *Journal of Orthopaedic Research*, Volume 8, pp 662 - 670

Bereiter H, Huggler AH, Jacob HAC, Seemann P (1991), The Thrust Plate Prosthesis. A new concept in hip prosthesis design. Eight years of clinical experience, *Orthopaedic Related Science*, Volume 2, pp 191 – 202.

Bouvier M (1989), The biology and composition of bone, *Bone Mechanics*, CRC Press Inc, Chapter 1, pp 1 – 13.

Bowyer A and Woodwark J (1990) A programmer's geometry, Butterworths, England

Brown TD, Pedersen DR, Gray ML, Brand RA and Rubin CT (1990), Toward an identification of mechanical parameters initiating periosteal remodelling: a combined experimental and analytic approach, *Journal of Biomechanics*, Volume 23, Number 9, pp 893 – 905

Bundy TJ (1989) The mechanical properties of composite materials. In: *Bone Mechanics,* CRC Press Inc, Chapter 8

Carter DR (1984), Mechanical loading histories and cortical bone remodelling. *Calcified Tissue International*, Volume 36, pp S19 - S24

Carter DR and Hayes WC (1977), The compressive behaviour of bone as a two phase porous structure, *Journal of Bone and Joint Surgery*, Volume 59A, pp 954 - 962

Cheal EJ, Spector M and Hayes WC (1992), Role of loads and prosthesis material properties on the mechanics of the proximal femur after total hip arthroplasty, *Journal of Orthopaedic Research*, Volume 10, pp 405 – 422

Cohen B and Rushton N (1995), Bone remodelling in the proximal femur after Charnley total hip arthroplasty. *Journal of Bone and Joint Surgery*, Volume 77-B, Number 5, pp 815 – 819

Corel Corporation (1992), CorelDRAW - Version 3.0, Ottawa, Ontario, Canada.

Cowin SC (1996) Strain or deformation rate dependent finite growth in soft tissues, *Journal of Biomechanics*, Volume 29, Number 5, pp 647 - 649

Cowin SC (1993), Bone stress adaptation models *Journal of Biomech Eng*, Volume 115, pp 528 – 533.

Cowin SC (1989a), The mechanical properties of cancellous bone. In: *Bone Mechanics*, CRC Press Inc, Chapter 7, pp 129 - 157

Cowin SC (1989b), The mechanical properties of cortical bone tissue. In: *Bone Mechanics*, CRC Press Inc, Chapter. 6, pp 97 - 127

Currey JD (1984) What should bones be designed to do? *Calcified Tissue International*, Volume 36, pp S7 - S10

Davy DT and Hart RT (1983), A theoretical model for mechanically induced bone remodelling, *American Society of Biomechanics*, Number 10, pp 10

Dieter GE (1988) Mechanical Metallurgy SI Metric Edition, McGraw - Hill Book Company (UK) Limited, pp 72 - 75

Eftekhar NS (1987), Long-term results of cemented total hip arthroplasty, *Clinical Orthopaedics*, Volume 225, pp 207 - 217

Fagan MJ (1992), Finite Element Analysis: Theory and Practice, Longman Scientific and Technical

Fowler JL, Gie GA, Lee AJC, Ling RSM (1988), Experience with the Exeter total hip replacement since 1970, *Orthopedic Clinics of North America*, Volume 19, Number 3, pp 447 - 489

Ford H and Alexander JM (1977), Advanced Mechanics of Materials *2nd Edition*, Ellis Horwood Limited

Fritton SP, McLeod KJ, Fritton JC, Brand RA and Rubin CT (1995) Persistent, low magnitude strains as the dominant source of mechanical information in a bone's 24 hour strain history, *41st Annual Meeting, Orthopaedic Research Society*, pp 547

Gere JM and Timoshenko SP (1984) Mechanics of Materials 3rd Edition, PWS-Kent Publishing Company

Goldstein SA, Matthews LS, Kuhn JL and Hollister SJ (1991) Trabecular bone remodelling: An experimental model, *Journal of Biomechanics*, Volume 24, pp 135 - 150

Green JH and Silver PHS (1981), An introduction to human anatomy, Oxford University Press, Oxford

Gross TS, McLeod KJ and Rubin CT (1992), Characterising bone strain distributions *in vivo* using three triple rosette strain gauges, *Journal of Biomechanics*, Volume 25, pp 1081 - 1087

Hart RT and Davy DT (1989), Theories of bone modelling and remodelling. In: *Bone Mechanics*, CRC Press Inc, Chapter 11, pp 253 - 277

Hart RT, Davy DT and Heiple KG (1984), Mathematical modelling and numerical solutions for functionally dependent bone remodelling. *Calcified Tissue International*, Volume 36, S104 - S109

Hart RT (1989), The finite element method. In: *Bone Mechanics,* CRC Press Inc, Chapter 4, pp 53 - 74

Hert J, Liskova M and Landrgot B (1969) Influence of the long term continuous bending on the bone, *Folia Morphologica*, Volume 17, Number 4, pp 389 - 399

Hert J, Liskova M and Landa J (1971) Reaction of bone to mechanical stimuli. Part 1. Continuous and intermittent loading of Tibia in rabbits, *Folia Morphologica*, Volume 19, Number 3, pp 290 - 300

Hert J, Pribylova E and Liskova M (1972) Reaction of bone to mechanical stimuli. Part 3. Microstructure of compact bone of rabbit tibia after intermittent loading. *Acta Anatomica*, Volume 82, pp 218 - 230

Hibbitt, Karlsson and Sorensen (1998), ABAQUS (standard) version 5.6, User Manuals I, II & III, Pawtucket, RI, USA

Howie DW, Middleton RG and Costi K (1998) Loosening of matt and polished cemented femoral stems. *Journal of Bone and Joint Surgery*, Volume 80-B, Number 4, pp 573 - 576

Howmedica (1992) Exeter Total Hip System. Surgical technique, Howmedica International. AEX01/0192/SE

Huiskes R and Chao EYS (1983) A survey of finite element analysis in orthopaedic biomechanics: The first decade, *Journal of Biomechanics*, Volume 16, Number 6, pp 385 - 409

Huiskes R, Weinans H, and van Rietbergen B (1992), The relationship between stress shielding and bone resorption around total hip stems and the effects of flexible materials. *Clinical Orthopaedics and related research*, Number 274, pp 124 - 134

Huiskes R, Weinans H, Grootenboer HJ, Dalstra M, Fudala B and Slooff TJ (1987) Adaptive bone-remodelling theory applied to prosthetic-design analysis, *Journal of Biomechanics*, Volume 20, No. 11/12, pp 1135 - 1150

Huiskes R, Weinans H, van Rietbergen B (1992) The relationship between stress shielding and bone resorption around total hip stems and the effect of materials, *Clinical Orthopaedics and Related research*, Number 274, pp 125 - 134

Jee WSS (1986) The skeletal tissues. In: *Cell and Tissue Biology,* 6th Edition, Chapter 7, pp 213 - 254, Urban & Schwartzenberg

Jones RM (1975) Mechanics of composite materials, Hemisphere Publishing Corporation, pp 31 - 42

Kapandji IA (1970), The physiology of the joints Volume 2: lower limb. Churchill Livingston books, Longman Group Ltd, Edinburgh

Kearns McCarthy C, Steinberg GG, Agren M, Leahey D, Wyman E and Baran DT (1991) Quantifying bone loss from the proximal femur after total hip arthroplasty. *Journal of Bone and Joint Surgery*, Volume 73-B, pp 774 - 778

Keyak JH, Lee IY, Rossi SA and Skinner HB (1995) Prediction of femoral fracture load and location using CT scan-derived finite element models, *41st Annual Meeting, Orthopaedic Research Society*, Orlando, Florida, pp 457

Keyak JH, Meagher JM, Skinner HB and Mote CD (1990), Automated three-dimensional finite element modelling of bone: A new method, *Journal of Biomedical Engineering,* Volume 12, pp 389 - 397

Klien-Nulend J, van der Plas A, Semeins CM, Ajubi NE, Frangos JA, Nijweide PJ and Burger EH (1995), Sensitivity of osteocytes to biomechanical stress in vitro, *The FASEB Journal*, Volume 9, pp 441 - 445

Koeneman JB and Hansen TM (1995) A metabolic model of bone adaptation to mechanical stimulus, *41st Annual Meeting, Orthopaedic Research Society*, pp 180

Lanyon LE (1984) Functional strain as a determinant for bone remodelling, *Calcified Tissue International*, Volume 36, pp S56 - S61

Lanyon LE (1992), Control of bone architecture by functional load bearing, *Journal of bone and mineral research*, Volume 7, supplement 2, S369 - S375

Lanyon LE (1981), Adaptive mechanics – the skeleton's response to mechanical stress. *Mechanical Factors and the Skeleton*, pp 72 - 82, John Libbey & Company Ltd

Lanyon LE, Hampson WCJ, Goodship AE and Shah JS (1975) Bone deformation recorded in-vivo from strain gauges attached to the human tibial shaft, *Acta Orthop Scand*, Number 46, pp 256 - 268

Lu TW, Taylor SJG, O'Connor JJ and Walker PS (1997) Influence of muscle activity on the forces in the femur: An *in vivo* study, *Journal of Biomechanics*, Volume 30, Number 11-12, pp 1101 - 1106

Luo G, Cowin SC, Sadegh AM and Arramon YP (1995) Implementation of strain rate as a bone remodelling stimulus, *Journal of Biomechanical Engineering*, Volume 117, pp 329 - 338

Martin RB and Burr DB (1982), A hypothetical mechanism for the stimulation of osteonal remodelling by fatigue damage, *Journal of Biomechanics*, Volume 15, pp 137 - 139

Marston RA, Cobb AG and Bentley G (1996) Stanmore compared with Charnley total hip replacement, Journal of Bone and Joint Surgery, Volume 78B, pp 178 -184

Mathiesen EB, Lindgren JU, Reinholt FP and Sudmann E (1987) Tissue reactions to wear products from polyacetal and UHMW polyethylene in total hip replacement, *Journal of Biomedical Materials Research*, Volume 21, pp 459 - 466

Mattheck C (1994), Design in Nature, *Interdisciplinary Science Reviews*, Volume 19, Number 4, pp 298 - 314

McCalden RW, McGeough JA, Barker MB and Court-Brown CM (1993), Age-related changes in the tensile properties of cortical bone, *Journal of Bone and Joint Surgery*, Volume 75A, Number 8

Meade JB, Cowin SC, Klawitter JJ, van Buskirk WC and Skinner HB (1984), Bone remodelling due to continuously applied loads, *Calcified tissue international*, Volume26, S25-S30

Morin G (1995), Thermo-mechanical fatigue analysis of engine collector rings. *1995 ABAQUS Users' Conference Proceedings*, Paris, pp 619 - 632

Nordin M and Frankel VH (1989), Biomechanics of the hip. In: *Basic Biomechanics of the Musculoskeletal System* 2nd Edition, Lea and Febiger, Chapter 7, pp 135 - 151

O'Connor JA and Lanyon LE (1982), The influence of strain rate on adaptive bone remodelling, *Journal of Biomechanics*, Volume 15, Number 10, pp 767 - 781

Orr TE, Beaupré GS, Carter DR and Schurman DJ (1990), Computer predictions of bone remodelling around porous-coated implants, *Journal of Arthroplasty*, Volume 5, pp 191 - 200

Paul JP (1967) Forces transmitted by the joints in the human body, *Proceedings of the Institution of Mechanical Engineers*, Volume 181, Part 37, pp 8 - 15

Parker RP (1981), Measurement of basic CT data. In: *Physical aspects of Medical Imaging*, pp 291 - 301

Qin Y, Rubin CT and McLeod KJ (1995), Correlation of *in vivo* bone adaptation and mechanical parameters using low magnitude, high frequency loading. *41st Annual Meeting, Orthopaedic Research Society*, Orlando, Florida, pp 176 - 30

Reilly DT and Burstein AH (1975), The elastic and ultimate properties of compact bone tissue, *Journal of Biomechanics*, Volume 8, pp 393 - 405

van Rietbergen B, Huiskes R, Weinans H, Sumner DR, Turner TM and Galante JO (1993), The mechanism of bone remodelling and resorption around press-fitted THA stems. *Journal of Biomechanics*, Volume 26, Number 4/5, 369 - 382

van Rietbergen B, Huiskes R, Weinans H and Odgaard A (1995), A new method to determine trabecular bone elastic properties and loading using micromechanical finite element models, *Journal of Biomechanics*, Volume 28, Number 1, pp 69 - 81

van Rietbergen B, Odgaard A, Kabel J and Huiskes R (1998), Relationships between bone morphology and bone elastic constants can be accurately quantified using high-resolution computer reconstructions, *Journal of Orthopaedic research*, Volume 16, pp 23 - 28

Rho JY, Hobatho MC and Ashman RB (1995), Relations of mechanical properties to density and CT numbers in human bone, *Medical Engineering and Physics*, Volume 17, Number 5, pp 347 - 355

Rohl L, Larsen E, Linde F, Odgaard A and Jorgensen J (1991), Tensile and compressive properties of cancellous bone, *Journal of Biomechanics*, Volume 24, Number 12, pp 1143 - 1149

Rohlmann A, Cheal EJ, Hayes WC and Bergmann G (1988), A non-linear finite element analysis of interface conditions in porous coated hip endoprostheses. *Journal of Biomechanics*, Volume 21, Number 7, pp 605 - 611

Rohlmann A, Mössner U, Bergmann G and Kölbel C (1982), Finite-element analysis and experimental investigation of stresses in a femur, *Journal of Biomedical Engineering*, Volume 4, pp 241 - 246

Rubin CT, Li C, Sun Y, Fritton C and McLeod K (1995), Non-invasive stimulation of trabecular bone formation via low magnitude, high frequency strain. *41st Annual Meeting Orthopaedic Research Society*, Orlando, Florida, pp 548

Rubin CT, McLeod KJ and Bain SD (1990), Functional strains and cortical bone adaptation: Epigenetic assurance of skeletal integrity, *Journal of Biomechanics*, Volume 23, pp 43 - 54

Rubin CT and Lanyon LE (1987), Osteoregulatory nature of mechanical stimuli: Function as a determinant for adaptive remodelling in bone, *Journal of Orthopaedic Research*, Volume 5, pp 300 - 310

Rubin CT and Lanyon LE (1984), Regulation of bone formation by applied dynamic loads, *Journal of Bone and Joint Surgery*, Volume 66A, Number 3, pp 397 - 402

Rubin CT and Lanyon LE (1985), Regulation of bone mass by applied mechanical strain magnitude, *Calcified Tissue International*, Volume 37, pp 411 - 417

Rubin CT and McLeod KJ (1995), Endogenous control of bone morphology via frequency specific, low magnitude functional strain, In '*Bone structure and remodelling*', World Scientific Publishing Co., London, pp 79 - 89

Semlitsh M (1989), Twenty years of Sulzer experience with artificial hip joint materials *Proceedings of the Institution of Mechanical Engineers: Engineering in Medicine*, Volume 203, pp 159 - 165

Skinner HB, Kilgus DJ, Keyak JH, Shimaoka EE, Kim AS and Tipton JS (1994), Correlation of computed finite element stresses to bone density after remodelling around cementless femoral implants, *Clinical Orthopaedics and Related Research*, Volume 305, pp 178 - 189

Sochart DH and Porter MLP (1998), Long-term results of cemented Charnley low-friction arthroplasty in patients aged less than 30 years, *Journal of Arthroplasty*, Volume 13, Number 2, pp123 - 131

Spirakis A, Starke G and Learmonth ID (1992), A three dimensional finite element analysis study of the effect of straight and anatomic cemented stem on stresses in the proximal femur and cement mantle, *Computer methods in Biomechanics and Biomedical Engineering*, pp 66 - 75

Stülpner MA, Reddy BD, Starke GR and Spirakis A (1997), A three dimensional finite analysis of adaptive remodelling in the proximal femur, *Journal of Biomechanics*, Volume 30, pp 1063 - 1066

Sumner DR, Olson CL, Freeman PM, Lobick JJ and Andriacchi TP (1989), Computed tomographic measurement of cortical bone geometry, *Journal of Biomechanics*, Volume 22, pp 649 - 653

Sulzer Medical Technology Ltd, PO Box, CH-8401 Winterthur, Switzerland.

Taylor M, Tanner KE, Freeman MAR and Yettram AL (1995) Cancellous bone stresses surrounding the femoral component of a hip prosthesis: An elastic-plastic finite element analysis. *Medical Engineering & Physics*. Volume 17(7), pp 544 - 550

Taylor ME, Tanner KE, Freeman MAR, and Yettram AL (1996) Stress and strain distribution within the intact femur: compression or bending? *Medical Engineering and Physics,* Volume 18, Number 2, pp 122 - 131

Tanabe Y and Kobayashi K (1994), Anisotropy in the dynamic non-linear viscoelastic properties of bovine compact bone, *Journal of Material Science: Materials in Medicine*, Volume 5, pp 397 - 401

Treharne RW (1981), Review of Wolff's Law and its proposed means of operation *Orthopaedic Review,* Volume X, Number 1, pp 35 - 47

Turner MJ, Clough RW, Martin HC and Topp LJ (1956), Stiffness and deflection analysis of complex structures, *Journal of Aero. Sci.* pp 805 - 823

Turner CH, Yoshikawa T, Forwood MR, Sun TC and Burr DB (1995) *Journal of Biomechanics*, Volume 28, Number 1, pp 39 - 44

Vaughan J (1981), The Physiology of bone, Oxford Scientific Publications, 3rd Edition, pp 1 - 26

Verdonschot N and Huiskes R (1997) Acrylic cement creeps but does not allow much subsidence of femoral stems. *Journal of bone and joint surgery*, Volume 79B, Number 4, pp 665 - 669

Weinans H, Huiskes R, van Rietbergen B, Sumner DR, Turner TM and Galante JO (1993), Adaptive bone remodelling around bonded non-cemented total hip arthroplasty: A comparison between animal experiments and computer simulation, *Journal of Orthopaedic Research*, Volume 11, Number 4, pp 500 - 513

Wheeler JPG, Miles AW and Clift SE (1997), The influence of the stem-cement interface in total hip replacement - a comparison of experimental and finite element approaches. *Journal of Engineering in Medicine,* Volume 211, pp 181 - 186

Wilson KJW (1990), Anatomy and physiology in health and illness, Churchill Livingston books, Medical division of Longman Group UK Ltd. New York

Yoon HS and Katz JL (1976), Ultrasonic wave propagation in human cortical bone II Measurements of elastic properties and micro-hardness, *Journal of Biomechanics*, Volume 9, pp 459 - 464

Zienkiewicz OC (1967), The finite element method in structural and continuum mechanics , McGraw-Hill Publishing Company Ltd, Maidenhead, England

Appendices

A. Use of User Material

B. Taylor WR and Cliff SE (1997) *A simple three dimensional technique for iteratively modelling the cortical and cancellous bone adaptation process.* Twelfth UK ABAQUS user group conference, 10-11Th September 1997, Telford Shropshire.

C. Taylor WR and Cliff SE (1998) Swelling as an approach to the simulation of cortical bone remodelling, in *Computer Methods in Biomechanics and Biomedical Engineering-2,* Ed. Middleton J, Jones ML and Pande GN, Gordon and Breach Science Publishers (Amsterdam), pp 263-269.

Initial Investigations of Cancellous Bone Remodelling

A.1 The User Material interface

A User Material (UMAT) is a subroutine option of ABAQUS in which the user can mathematically define the constitutive behaviour of a material. It is most often required for the modelling of a material that is not included in the standard ABAQUS material library, and so allows the analysis of both unusual and complicated materials.

A UMAT consists of FORTRAN code that forms a subroutine to be called by ABAQUS every time the material definition or constitutive behaviour is required. The routine is run at every material calculation point for which the material is used, but is capable of using both initial conditions and boundary conditions placed upon the individual elements and storing progressive iterative values for every element. It is therefore an extremely powerful and flexible tool for analysis. In its simplest form, the UMAT coding follows a basic procedure that is demonstrated in Figure A.1. Each time ABAQUS requires information regarding the material response of a particular element, it calls the UMAT subroutine. The final output of the routine is the Jacobian, which is the full constitutive relationship of the material in matrix form. This is returned to ABAQUS for the calculation of a convergent solution.

The UMAT facility has been used in these circumstances to define the constitutive relationship of cancellous bone. The initial specification for the routine was that each element was to be able to respond to the remodelling stimulus by altering its stiffness according to basic strain magnitude placed upon it. The cancellous bone material was to be created as both isotropic and homogeneous, but subsequent remodelling would allow localised alterations in stiffness at an elemental level according to the remodelling information received.

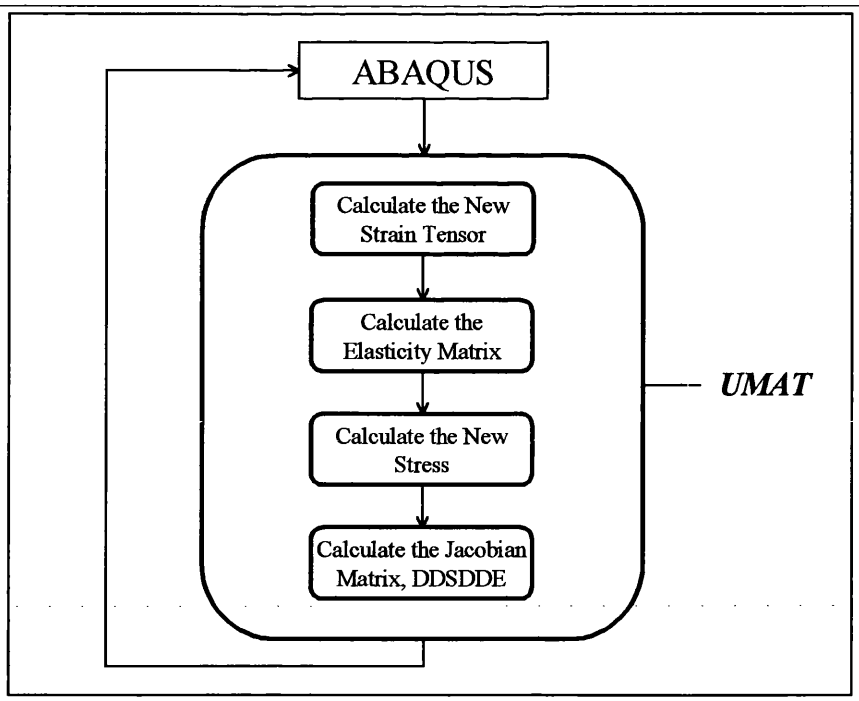

Figure A.1 - Simplest form of UMAT coding

A.1.1 Development of a UMAT

The following section describes the general process whereby a UMAT is developed. Each step for the general development of the stress - strain relationship of a material is described. In addition, a method of altering the properties of the material in a manner representative of bone remodelling is outlined. This process is described for the bone material stiffening in response to compressive strain (ε_3) only. For the purposes of the description, it is assumed that the cancellous bone material was to be isotropic, allowing calculation of a single value of Young's modulus. In addition, variation in the cancellous bone stiffness was used to represent the change in density of the material during remodelling.

In linear elastic materials with no time dependence, the stress - strain relationship of a material can be considered constant. This allows the definition of a Young's modulus for the material, a constant value, to be the gradient of the stress - strain curve. In reality, however, any material stress-strain (stiffness) relationship is described in terms of an elasticity matrix, or Jacobian, which includes any anisotropy or inhomogeneity the material possesses. Young's modulus is merely a simplified version of this matrix, useful for linear materials. Should the stress-strain relationship become a time dependent property (for example, one that includes yield or creep properties) then there will be a whole series of elasticity matrices, calculated

according to position in time. For the purposes of the bone material modelled here, however, time dependence is ignored, since no age related properties of the bone are to be contemplated.

Consider it possible for the Young's modulus of the material to be an arbitrary mathematical function of stress and strain. Once this mathematical relationship has been established, an instantaneous Jacobian can be calculated for any value of strain. Now, since for any instant in time Hooke's Law holds true, it is possible to construct a graph showing the relationship between stress and strain. An example of this is shown below in Figure A.2 (note the values of E represent the stiffness matrix rather than Young's modulus). Since the Jacobian describes only the instantaneous stiffness of each element, this graph must be used to define a dual-purpose relationship. Firstly the long term, remodelling curve specifies the evolutionary path of the material, and has been labelled the evolutionary curve. The instantaneous values of the stress - strain relationship vary up and down this curve changing with each increment, forming the second purpose of this graph being the tangent modulus, the actual stiffness at any point in time. It must be noted that this graph is never actually produced or calculated by ABAQUS, but is rather utilised purely as a sequence of single points calculated at that instant in time during each increment.

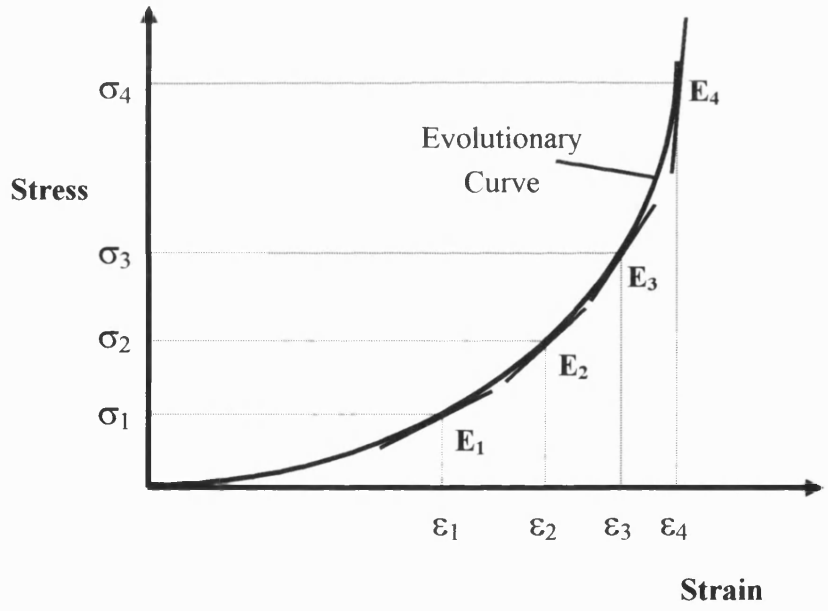

Figure A.2 - Evolutionary Stiffness Curve

Once this curve has been established, ABAQUS must be able to differentiate between long term evolutionary and short-term instantaneous stiffnesses. For this to be possible, ABAQUS uses an incremental sequence for which there are a number of runs, or passes, through the

UMAT coding for each increment. This provides a basis upon which convergence of solutions can rely. Each increment represents a snapshot of time, an immediate, current situation. Within each increment there are a number of passes, each attempting to converge to an increment solution. The UMAT coding must therefore equate to a pass within an increment, with the ability to allow the solution to converge. The following diagram (Figure A.3) is therefore a representation of an instant of time, demonstrating the parameters required for the UMAT.

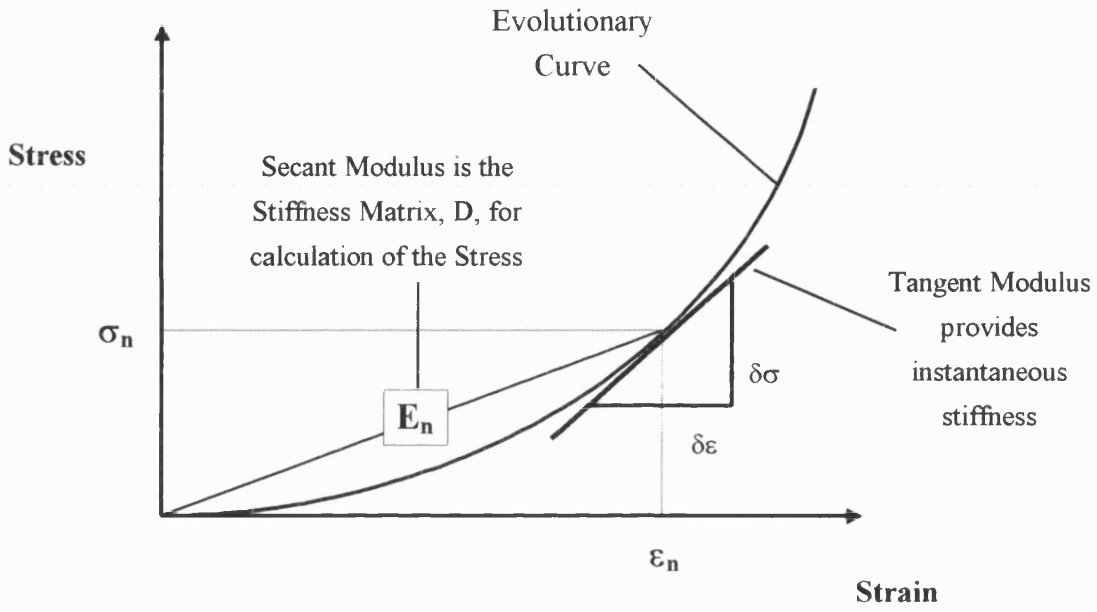

Figure A.3 - Instantaneous stress - strain relationship

In the longer term, each incremental point, once fully converged to a solution via a number of passes through the UMAT, must travel up and down the evolutionary curve, as the entire model attempts to reach convergence. The FE analysis can be considered complete when entire model has reached a long term convergent solution.

Since the UMAT coding must be inherently stable for the solution to guarantee convergence, the coding must be written in a manner that enables the subroutine to run as many times as required, with each pass focusing towards the incremental solution.

A.1.2 Components of a UMAT

In the fundamental format, as described in the previous sections, the UMAT will calculate the material response of a basic elastic element, identical to calling the *ELASTIC command in

the ABAQUS input deck. However, this process allows no modification for modelling specific applications. Before the UMAT can be enhanced, therefore, each of the individual components of the UMAT must be fully understood. The following will describe the basic components of the UMAT.

The UMAT subroutine is called by ABAQUS at least twice for every element and every time increment in the model being examined, since each increment throughout the analysis must converge. The coding may be called as many times as required to ensure convergence. For simple isothermal materials, including the various possible models of cancellous bone, there are three primary variables that need to be defined. These are: -

1. Constitutive Rate Equations (or Jacobian matrix)

The Jacobian matrix (called DDSDDE(i,j) in the UMAT), is perhaps the most difficult parameter to calculate, and defines how the incremental stress varies with the incremental strain for the material.

$$\text{DDSDDE(i, j)} = \frac{\partial \Delta \sigma}{\partial \Delta \varepsilon}$$

Where $\Delta\sigma$ are the stress increments and $\Delta\varepsilon$ are the strain increments.

The Jacobian is described by the gradient of the stress - strain curve, and is hence the tangent modulus (this will be described further in the following section). The Jacobian is thus valid only for the instantaneous time increment for which it is being used, and so must be recalculated for each pass of the UMAT. This parameter is represented in the form of a matrix or array, whose size is dependent upon the number of dimensions of the element (generally 3), making a 6 x 6 matrix.

Since the Jacobian Matrix is the rate of change of stress with strain, its final value for each pass must be the same as the differential of the stress - strain function at that point. Hence any remodelling theory, or other factor which affects the rate of change of stress with strain, must be fully expanded to include all stress and strain terms before differentiation can occur.

2. State Variables

Often called Solution Dependent Variables (SDV), these values define any instantaneous property of the material that is dependent upon the state (often non-linear) or characteristic of the material, e.g. the stress - strain relationship. Within the UMAT, these variables are stored in the STATEV(i) array, and may be given an initial value with the *INITIAL CONDITIONS command.

These variables are defined and used solely by the user, indicating that ABAQUS has no comprehension of their significance i.e. ABAQUS does not change or use their values unless commanded to do so. The value of each SDV is passed into the UMAT at the beginning of the increment, and the magnitude must be altered purely using the UMAT coding before the final value is returned at the end of that increment. There may be any number of State Dependent Variables, and the values of each are stored for each material integration point of every element.

3. Stress Tensor

This is an array containing the stress components, which is passed into the UMAT at the beginning of the increment and must be updated at the end to allow convergence of the solution. The 'Cauchy' or true stress (as discussed in Dieter, 1988) is used in this array which will inherently influence the magnitude of the stress values during successive increments, since the exact area is continually updated. The array is called STRESS(i).

4. Stiffness Matrix, D

The stiffness matrix, [D], describes the secant modulus to any point on the stress - strain curve, and allows calculation of the stress at the following increment. In its simplest one-dimensional form, the matrix demonstrates the stiffness under stretching or compression of an element or bar, where the only component of the matrix is the Young's Modulus. Here, however, the 6 x 6 matrix characterises the full three-dimensional nature of an element or cube of material.

The stiffness matrix is derived from the compliance matrix (discussed in Jones, 1975), [S], where: -

$$[S_{ij}] = \begin{bmatrix} \frac{1}{E_1} & -\frac{\upsilon_{21}}{E_2} & -\frac{\upsilon_{31}}{E_3} & 0 & 0 & 0 \\ -\frac{\upsilon_{12}}{E_1} & \frac{1}{E_2} & -\frac{\upsilon_{32}}{E_3} & 0 & 0 & 0 \\ -\frac{\upsilon_{13}}{E_1} & -\frac{\upsilon_{23}}{E_2} & \frac{1}{E_3} & 0 & 0 & 0 \\ 0 & 0 & 0 & \frac{1}{G_{23}} & 0 & 0 \\ 0 & 0 & 0 & 0 & \frac{1}{G_{31}} & 0 \\ 0 & 0 & 0 & 0 & 0 & \frac{1}{G_{12}} \end{bmatrix}$$

Where E_1 E_2 and E_3 = Stiffness in directions 1, 2, and 3.

υ_{ij} = Poisson's ratio for transverse strain in the j- direction when stressed in the i - direction.

G_{23} G_{31} G_{12} = Shear moduli in the 2-3, 3-1, and 1-2 planes.

For a linear, isothermal, isotropic, homogeneous material, the matrix is symmetric since the values for υ are the same in every direction. In addition the values for E_1, E_2 and E_3 will be identical, as will G_{12}, G_{31} and G_{23}.

The complete stiffness matrix, D, which is obtained by inversion of the compliance matrix, is shown below:

$$D = \begin{bmatrix} \frac{1-\upsilon_{23}\upsilon_{32}}{E_2E_3\varphi} & \frac{\upsilon_{12}+\upsilon_{32}\upsilon_{13}}{E_1E_3\varphi} & \frac{\upsilon_{13}+\upsilon_{13}\upsilon_{23}}{E_1E_2\varphi} & 0 & 0 & 0 \\ \frac{\upsilon_{21}+\upsilon_{31}\upsilon_{23}}{E_2E_3\varphi} & \frac{1-\upsilon_{13}\upsilon_{31}}{E_1E_3\varphi} & \frac{\upsilon_{23}+\upsilon_{21}\upsilon_{13}}{E_1E_2\varphi} & 0 & 0 & 0 \\ \frac{\upsilon_{31}+\upsilon_{21}\upsilon_{32}}{E_2E_3\varphi} & \frac{\upsilon_{32}+\upsilon_{12}\upsilon_{31}}{E_1E_3\varphi} & \frac{1-\upsilon_{12}\upsilon_{21}}{E_1E_2\varphi} & 0 & 0 & 0 \\ 0 & 0 & 0 & G_{23} & 0 & 0 \\ 0 & 0 & 0 & 0 & G_{31} & 0 \\ 0 & 0 & 0 & 0 & 0 & G_{12} \end{bmatrix}$$

where

$$\varphi = \frac{1-\upsilon_{12}\upsilon_{21}-\upsilon_{23}\upsilon_{32}-\upsilon_{31}\upsilon_{13}-2\upsilon_{21}\upsilon_{32}\upsilon_{13}}{E_1E_2E_3}$$

When using simplified isotropic, homogenous material models, the stiffness matrix is greatly simplified since

$$\upsilon_{12} = \upsilon_{21} = \upsilon_{13} = \upsilon_{31} = \upsilon_{23} = \upsilon_{32}$$

and

$$E_1 = E_2 = E_3$$

The Stiffness matrix, [D], therefore becomes:

$$D = \begin{bmatrix} \frac{E(1-\upsilon)}{(1+\upsilon)(1-2\upsilon)} & \frac{E\upsilon}{(1+\upsilon)(1-2\upsilon)} & \frac{E\upsilon}{(1+\upsilon)(1-2\upsilon)} & 0 & 0 & 0 \\ \ddots & \frac{E(1-\upsilon)}{(1+\upsilon)(1-2\upsilon)} & \frac{E\upsilon}{(1+\upsilon)(1-2\upsilon)} & 0 & 0 & 0 \\ \ddots & \ddots & \frac{E(1-\upsilon)}{(1+\upsilon)(1-2\upsilon)} & 0 & 0 & 0 \\ \ddots & \ddots & \ddots & \frac{E}{2(1+\upsilon)} & 0 & 0 \\ \ddots & \ddots & \ddots & \ddots & \frac{E}{2(1+\upsilon)} & 0 \\ \ddots & \ddots & \ddots & \ddots & \ddots & \frac{E}{2(1+\upsilon)} \end{bmatrix}$$

where $\ddots$ represents symmetry of the matrix.

Equation A.1 - Stiffness Matrix

This is the full version of the D matrix used for materials that are homogeneous and isotropic.

A.1.4 Process of programming a UMAT

The UMAT subroutine can be considered a part of a sequence of individual calculations to achieve a full pass of an increment. It follows, therefore, that the identical sequence can be used for the routine to reach convergence in each increment. Since ABAQUS also follows a set method for the order of calculations (e.g. The strain increment is always the only variable with a non-zero value to be carried into the first pass of the UMAT), the UMAT is limited in its order or sequence. The following section will step through the process necessary for a general UMAT.

Consider firstly that the model is at a certain position or increment in time. The first pass of that particular increment is then named as N, and the following passes of the same increment being N+1, N+2...

Figure A.4 graphically demonstrates the process of programming a UMAT. In this case, remodelling in response to compressive strain stimulus, as described previously, has been used for UMAT modification. Each individual numbered step of the process is then described in detail in the following sections.

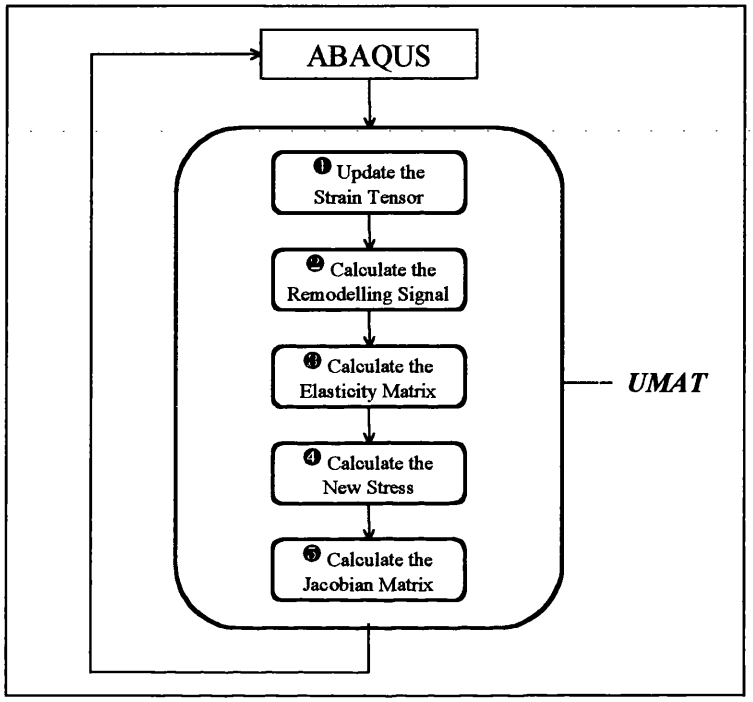

Figure A.4 - The process of programming a UMAT

The following sections relate to their corresponding number in Figure A.4. In addition, this process is shown in Figure A.5 where the action is related to the position of calculation in the graph.

1. *Calculation of the new strain*

Since the present position on the stress - strain curve was known, and the strain increment, $\Delta\underline{\varepsilon}_{(N+1)}$, was passed into the UMAT from ABAQUS, the new strain, $\underline{\varepsilon}_{(N+1)}$ could be calculated:

$$\underline{\varepsilon}_{(N+1)} = \underline{\varepsilon}_{(N)} + \Delta\underline{\varepsilon}_{(N+1)}$$

where underlining represented the column matrix form of the strain array. Expanded, this became:

$$\begin{pmatrix} \varepsilon_1 \\ \varepsilon_2 \\ \varepsilon_3 \\ \gamma_{23} \\ \gamma_{31} \\ \gamma_{12} \end{pmatrix}^{N+1} = \begin{pmatrix} \varepsilon_1 \\ \varepsilon_2 \\ \varepsilon_3 \\ \gamma_{23} \\ \gamma_{31} \\ \gamma_{12} \end{pmatrix}^{N} + \begin{pmatrix} \Delta\varepsilon_1 \\ \Delta\varepsilon_2 \\ \Delta\varepsilon_3 \\ \Delta\gamma_{23} \\ \Delta\gamma_{31} \\ \Delta\gamma_{12} \end{pmatrix}^{N+1}$$

This calculation was referred to as ❶ in Figure A.5, but the actual process was carried out by ABAQUS for the simple models, and so was not included within the UMAT coding. This process related the values to the UMAT using the variables $STRAN(i)_N$, and $DSTRAN(i)_{N+1}$.

2. *Calculation of the remodelling signal*

Assuming the remodelling signal was both a function of strain and fully isotropic, the Young's modulus, E, could be calculated at this point. Hence,

$$\mathbf{E = f(\underline{\varepsilon})_{N+1}}$$

And remodelling to the compressive strain, $\varepsilon_{(3)}$, only

$$\mathbf{E = f(\varepsilon_{(3)})_{N+1}}$$

Alternatively, a simple graph of this relationship allowed interpolation to calculate the values of Young's Modulus. This method involved possible addition of errors since it was an approximation of the exact points defined by the mathematical

relationship. It did, however, provide a simple procedure for complicated, especially non-linear correlations.

3. *Calculation of the elasticity matrix, D*

For the case of the isotropic material element, the stiffness matrix was purely a sequence of calculations involving Poisson's ratio and Young's modulus. For the purposes of easy coding, however, the stiffness matrix could be considered to be made up of two separate components, since the D matrix must be differentiated before finding DDSDDE. Removal of the Young's Modulus allowed the main majority of the matrix (named D*) to remain a constant value, giving:

$$\underline{\mathbf{D}}_{N+1} = \mathbf{E}_{N+1}\ \underline{\mathbf{D}}^*$$

The equation was then programmed as below (Equation A.2) rather than as before, in Equation A.1.

$$\underline{\mathbf{D}}_{N+1} = \mathbf{E}(\varepsilon)_{N+1} \begin{bmatrix} \frac{(1-\upsilon)}{(1+\upsilon)(1-2\upsilon)} & \frac{\upsilon}{(1+\upsilon)(1-2\upsilon)} & \frac{\upsilon}{(1+\upsilon)(1-2\upsilon)} & 0 & 0 & 0 \\ \ddots & \frac{(1-\upsilon)}{(1+\upsilon)(1-2\upsilon)} & \frac{\upsilon}{(1+\upsilon)(1-2\upsilon)} & 0 & 0 & 0 \\ \ddots & \ddots & \frac{(1-\upsilon)}{(1+\upsilon)(1-2\upsilon)} & 0 & 0 & 0 \\ \ddots & \ddots & \ddots & \frac{1}{2(1+\upsilon)} & 0 & 0 \\ \ddots & \ddots & \ddots & \ddots & \frac{1}{2(1+\upsilon)} & 0 \\ \ddots & \ddots & \ddots & \ddots & \ddots & \frac{1}{2(1+\upsilon)} \end{bmatrix}$$

Equation A.2 - Stiffness matrix

The component $\underline{D}^*$ consequently became a constant value array, leaving only the section $E(\varepsilon)$ to be differentiated. This effectively determined line ❸ in Figure A.5, and the routine then moved to point ②.

4. Calculation of the new stress

Once at point ②, the 6 x 1 column stress matrix could be calculated, finding line ❹. Since the three dimensional behaviour of the material was now being considered, the full matrix version of stress, stiffness and strain had to be used, and not simply Young's modulus. Hence:

$$\underline{\sigma}_{N+1} = \underline{\mathbf{D}} \times \underline{\varepsilon}$$

and

$$\underline{\sigma}_{N+1} = \mathbf{E}_{N+1} \times \underline{\mathbf{D}}^* \times \underline{\varepsilon}$$

5. Calculation of the Jacobian, DDSDDE

Since the Jacobian matrix is the rate of change of stress with strain, the evolutionary curve had to be differentiated at point ②. This calculated the tangent modulus, line ❺. To do this, however, all functions of strain were fully expanded before the differentiation. For the simple case, therefore:

$$\frac{\partial \underline{\sigma}_{N+1}}{\partial \underline{\varepsilon}_{N+1}} = \frac{\partial \left[\underline{\mathrm{D}}_{N+1} \underline{\varepsilon}_{N+1} \right]}{\partial \underline{\varepsilon}_{N+1}}$$

And since the D matrix can be expanded,

$$\therefore \frac{\partial \underline{\sigma}_{N+1}}{\partial \underline{\varepsilon}_{N+1}} = \frac{\partial \left[\mathrm{E}(\underline{\varepsilon}) \underline{\mathrm{D}}^*_{N+1} \underline{\varepsilon}_{N+1} \right]}{\partial \underline{\varepsilon}_{N+1}}$$

For ease of comprehension, the equations were written using tensor notation, assuming all the equation components remain identical with regard to their subscripts (e.g. $_{N+1}$). The equation can then be rewritten as

$$\mathrm{DDSDDE}_{ij} = \frac{\partial \sigma_i}{\partial \varepsilon_j} = \frac{\partial \left[\mathrm{E}(\underline{\varepsilon}) \mathrm{D}^*_{ik} \varepsilon_k \right]}{\partial \varepsilon_j}$$

Then, using the chain rule for differentiation,

$$\frac{\partial \sigma_i}{\partial \varepsilon_j} = \frac{\partial E(\varepsilon)}{\partial \varepsilon_j} \mathrm{D}^*_{ik} \varepsilon_k + E(\underline{\varepsilon}) D^*_{ik} \frac{\partial \varepsilon_k}{\partial \varepsilon_j}$$

After simplification, the equation for any component of the DDSDDE matrix

$$\frac{\partial \sigma_i}{\partial \varepsilon_j} = \frac{\partial E(\varepsilon)}{\partial \varepsilon_j} \mathrm{D}^*_{ik} \varepsilon_k + \mathrm{D}_{ij}$$

became:

where $\frac{\partial E(\varepsilon)}{\partial \varepsilon_j}$ is the rate of change of stiffness with strain i.e. the gradient of the remodelling curve.

The full matrix, DDSDDE, therefore becomes:

$$\begin{bmatrix} \mathrm{D}_{11} + \sum_{k=1}^{6} \mathrm{D}^*_{1k} \varepsilon_k \left(\frac{\partial E}{\partial \varepsilon_1} \right) & \mathrm{D}_{12} + \sum_{k=1}^{6} \mathrm{D}^*_{1k} \varepsilon_k \left(\frac{\partial E}{\partial \varepsilon_2} \right) & \cdots & \mathrm{D}_{16} + \sum_{k=1}^{6} \mathrm{D}^*_{1k} \varepsilon_k \left(\frac{\partial E}{\partial \varepsilon_6} \right) \\ \mathrm{D}_{21} + \sum_{k=1}^{6} \mathrm{D}^*_{2k} \varepsilon_k \left(\frac{\partial E}{\partial \varepsilon_1} \right) & \mathrm{D}_{22} + \sum_{k=1}^{6} \mathrm{D}^*_{2k} \varepsilon_k \left(\frac{\partial E}{\partial \varepsilon_2} \right) & \cdots & \mathrm{D}_{26} + \sum_{k=1}^{6} \mathrm{D}^*_{2k} \varepsilon_k \left(\frac{\partial E}{\partial \varepsilon_6} \right) \\ \vdots & \vdots & \ddots & \vdots \\ \mathrm{D}_{61} + \sum_{k=1}^{6} \mathrm{D}^*_{6k} \varepsilon_k \left(\frac{\partial E}{\partial \varepsilon_1} \right) & \mathrm{D}_{62} + \sum_{k=1}^{6} \mathrm{D}^*_{6k} \varepsilon_k \left(\frac{\partial E}{\partial \varepsilon_2} \right) & \cdots & \mathrm{D}_{66} + \sum_{k=1}^{6} \mathrm{D}^*_{6k} \varepsilon_k \left(\frac{\partial E}{\partial \varepsilon_6} \right) \end{bmatrix}$$

Notice that this matrix assumes a remodelling theory based upon strains in all directions and all three planes of shear. For the simple case of stiffness dependence only upon one component of strain (taking ε_3 as the example once again), this matrix becomes vastly simplified with only the third column differing from the previously calculated D matrix. (This occurs due to all the other differentials becoming zero). The full matrix in this case would be as follows:

$$\begin{bmatrix} \mathrm{D}_{11} & \mathrm{D}_{12} & \mathrm{D}_{13} + \sum_{k=1}^{6} \mathrm{D}^*_{1k} \varepsilon_k \left(\frac{\partial E}{\partial \varepsilon_k} \right) & \mathrm{D}_{14} & \mathrm{D}_{15} & \mathrm{D}_{16} \\ \mathrm{D}_{21} & \mathrm{D}_{22} & \mathrm{D}_{23} + \sum_{k=1}^{6} \mathrm{D}^*_{2k} \varepsilon_k \left(\frac{\partial E}{\partial \varepsilon_k} \right) & \mathrm{D}_{24} & \mathrm{D}_{25} & \mathrm{D}_{26} \\ \vdots & \vdots & \vdots & \vdots & \vdots & \vdots \\ \mathrm{D}_{61} & \mathrm{D}_{62} & \mathrm{D}_{63} + \sum_{k=1}^{6} \mathrm{D}^*_{6k} \varepsilon_k \left(\frac{\partial E}{\partial \varepsilon_k} \right) & \mathrm{D}_{64} & \mathrm{D}_{65} & \mathrm{D}_{66} \end{bmatrix}$$

Figure A.5 graphically demonstrates the process described in the above section. Notice that this procedure is similar to a predictor corrector technique for convergence to a solution, and there must be several passes of the UMAT, each using information from the previous increment before the converged incremental solution is achieved. The pass following the one described above will then move onwards to position ③, using the same theory and the process continues until the residual, R, equals zero. The pass has then converged onto the correct position on the stress - strain curve and the process moves to the next increment.

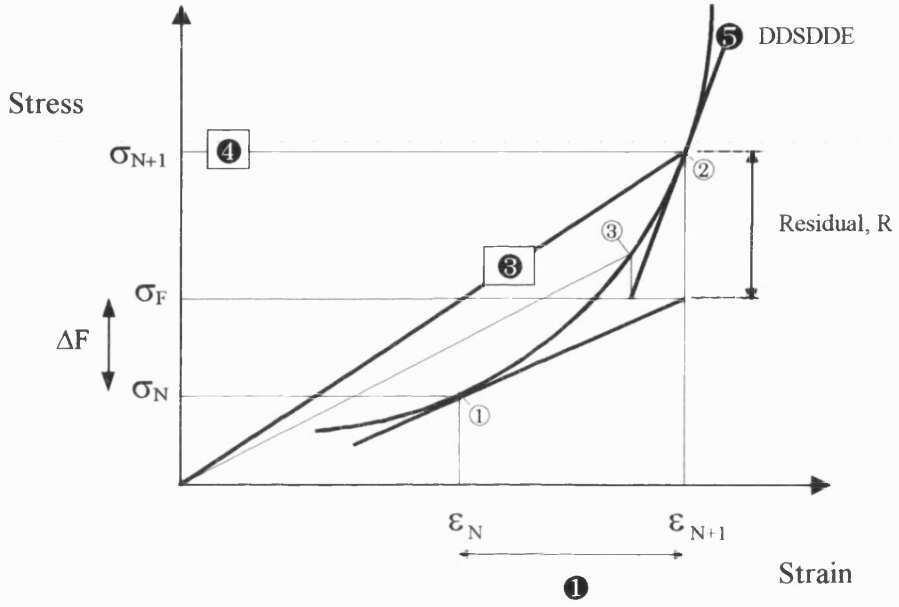

Figure A.5 - Sequential process along incremental stress - strain curve

If the force on the element is supplied as a ramp load, the first pass of the first increment will provide zero values for the stress and strain arrays. In this case, the Jacobian matrix, DDSDDE, will give a value for the tangent gradient as zero, providing an impossible convergence curve. Under these circumstances, boundary conditions must be imposed by specifying a minimum bone density (and hence a minimum stiffness) or a minimum remodelling stiffness at zero strain.

A.1.4 Development of User Material

A single brick element model was created for the purposes of validation of the UMAT. This allowed a faster progression of the model as the solution computational time was greatly

reduced, the boundary conditions could be strictly imposed, and the possibility of detecting errors was greatly increased due to the smaller volume of data to be analysed for each run.

The element was constrained by being simply supported from below (Figure A.6), and loaded with a distributed load from above. One lower corner was built in and the two nearest lower corners constrained, one in the X and one in the Y directions so as to remove all possibility of rotational errors. The figure also shows the element under deformation.

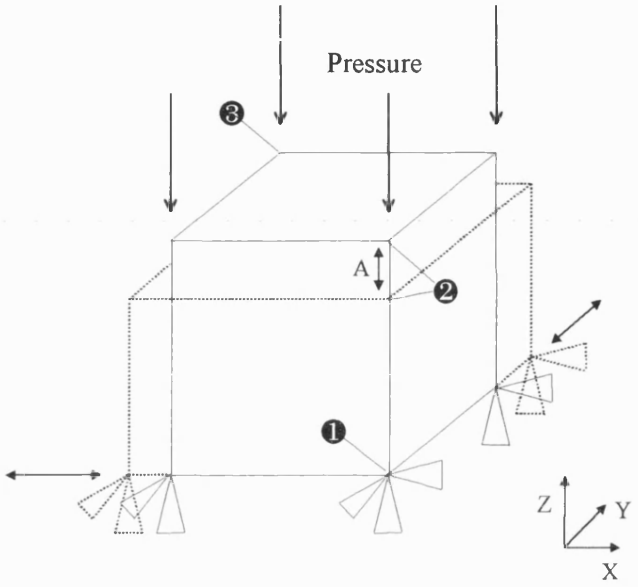

Figure A.6 - Deformation of cubic element model

It was decided that the initial model would be one of stiffness varying linearly only with compressive strain (ε_3) put upon the element. This simple model could represent cancellous bone well for its complexity with the change in element stiffness representing the variation in bone density (Qin 1995). Further models, including von Mises strain remodelling and anisotropies would then simply become expansions of the code to include other directions.

The first model was consequently only a test model, used for verification of the coding and the accurate implementation of the prediction and correction in the UMAT subroutine. As a result, a simplistic view of the initial model was taken with the actual numbers becoming extraneous, and values approximated to cancellous bone were taken (E = 2GPa).

Remodelling of the element was based upon a simple compression graph, shown in Figure A.7, which formed the basis upon which a working model could be based. Notice that the values for strain were negative for this model as the element was in compression.

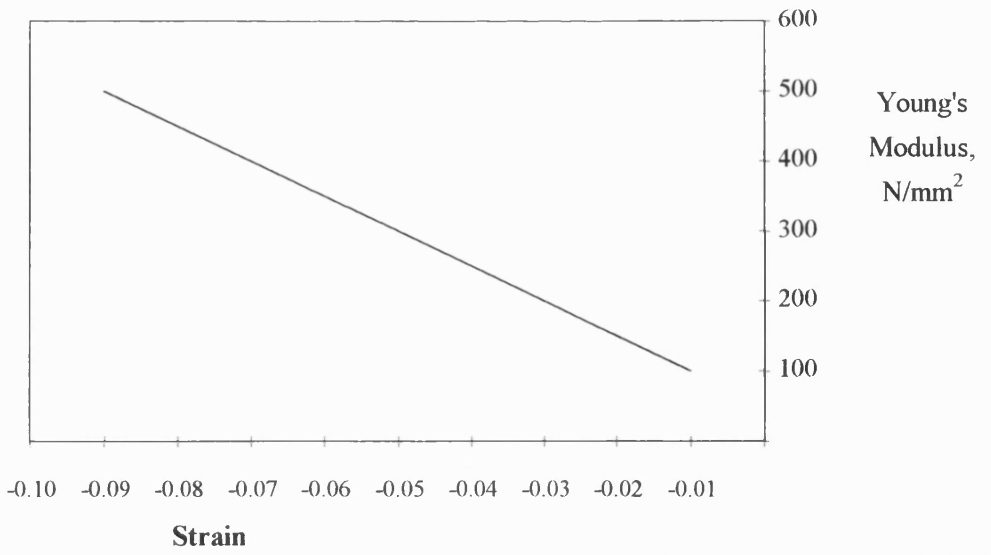

Figure A.7 - Variation of Young's Modulus with strain

The loading on the model was imposed as a two step process, with an initial linear ramp increase directly followed by a short phase of constant pressure (Figure A.8). In order to achieve an initial 5% strain, a pressure loading of 100 N/mm^2 was applied to the upper surface of the element. Since this value fell well within the bounds of the remodelling curve (Figure A.7), ABAQUS was able to calculate a stiffness value for the following increment. The second step of constant loading was included to allow a time period for convergence of the solution, so that any over-shoot in stiffness response of the system to the ramp loading could settle. Time increments were defined initially as a single second each, thereby dividing the loading steps into twenty and ten increments for the first and second steps respectively.

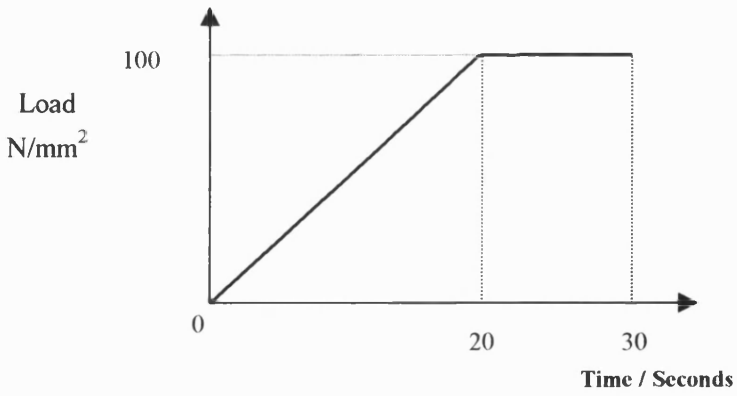

Figure A.8 - Loading on cubic model

The actual magnitudes of the values here were not important, however, merely the process and the given response. Once this was established, a minimum elemental stiffness of 100N/mm^2 was imposed within the UMAT subroutine, ensuring a positive value of DDSDDE at all times.

A.1.5 UMAT results

The loading history defined the ramp increase in compressive force on the element, whilst the UMAT coding both specified the initial stiffnesses and limited the minimum stiffness. The response of the Young's Modulus of the material is shown in Figure A.9.

Figure A.9 - Material stiffness response to compressive loading

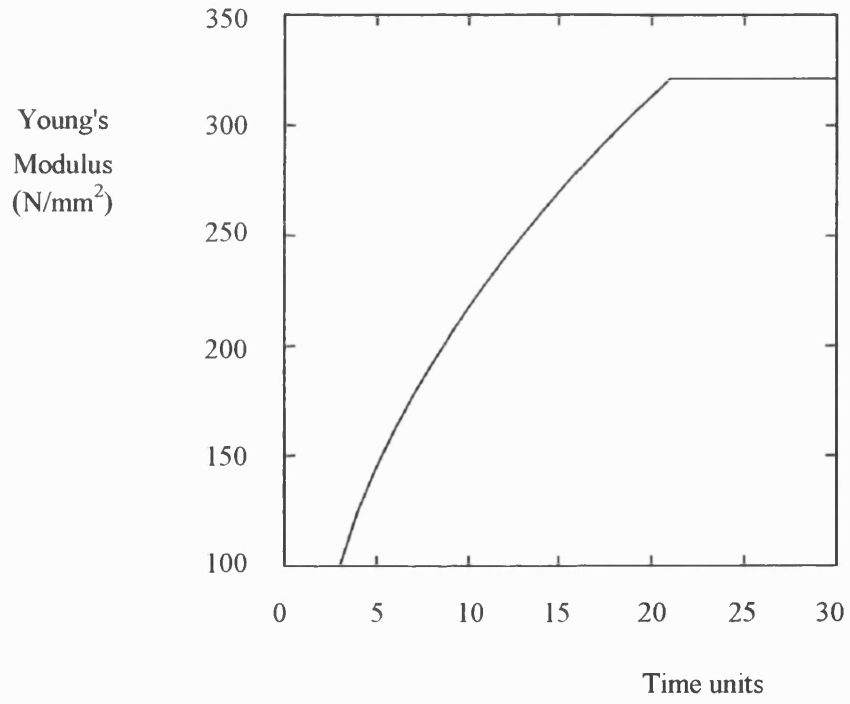

From a time of approximately 3 seconds onwards, the stiffness of the element began to steadily increase non-linearly with time. A progressive reduction in the rate of increasing Young's modulus was seen causing a gradual curvature of the line. The stiffness finally levelled out at a value of 321 N/mm^2 at a time of 21 seconds, a single increment subsequent to the completion of the ramp stage of loading.

The results for the variation of compressive strain with time can be seen in Figure A.10. The curve reflects the increasing stiffness of the element by showing a progressive reduction in the rate of strain with increasing time. The strain then peaked at a value of approximately 5.4 % strain. Both strain histories orthogonal to the direction of loading were identical, peaking at a tensile strain magnitude of approximately 1.6 %. Both of these curves showed a similar progressive reduction of strain with time.

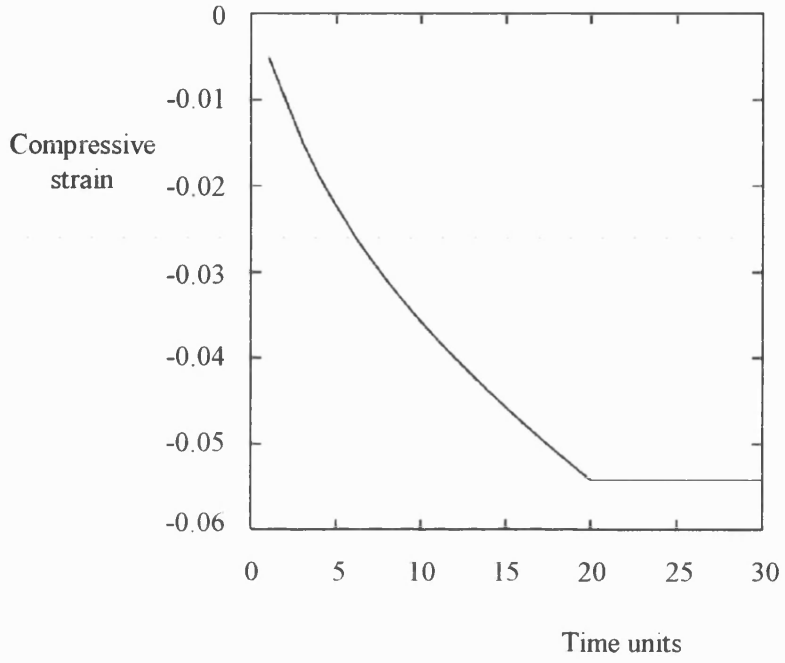

Figure A.10 – Variation of compressive strain

A.1.6 Discussion of results

The Young's Modulus of the material was varied with compressive strain. As the strain on the element increased, the remodelling response was to increase the stiffness, thereby reflecting the shape of the resultant curve.

The initial rise of Young's Modulus above the minimum specified threshold value of 100N/mm^2 was at a time of 3 seconds. This coincided with the first increment in which the load was increased above 15N – the load at which the remodelling curve increased the stiffness to a value above 100 N/mm^2. This implied that the initial definition of stiffness for the element was ignored as a result of remodelling to a strain below that required for the minimum specified stiffness. It should therefore be noted that although the response of

Young's Modulus to compressive strain was correct for the model at any instant in time, Hooke's Law no longer held true over the whole step. The coding has, in effect, modelled a non-linear spring. The value of strain obtained at a time of 20 seconds was in excess of that calculated using Hooke's Law at the same time, since larger deformations occurred under the initial lower stiffness conditions.

This process has not, therefore, completely modelled the process of remodelling, since the change in stiffness was instantaneous and responded to the whole and continual loading history. In order to represent the longer term remodelling correctly, the material must respond over a longer period of time to the stimulus created from numerous loading histories (as discussed in Chapter 6). Nevertheless, what this model does demonstrate is that the technique is capable of producing a change in the material properties of the elements in response to the applied loading.

The coding of the User Material algorithm was highly complex, providing possibilities of user error during coding alterations. These chances would have been increased with the complexity of the remodelling process when including features such as different stimuli and anisotropy. The method described was coded prior to the development of the cortical bone remodelling using the swelling technique. As a result, a second method of modelling the cancellous bone adaptation process was considered. This is described in Chapter 8

TWELFTH UK ABAQUS USER GROUP CONFERECE

10-11th September 1997
Madeley Court Hotel
Telford, Shropshire

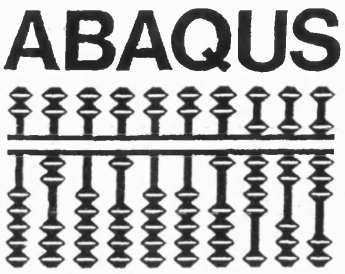

A SIMPLE THREE DIMENSIONAL TECHNIQUE FOR ITERATIVELY MODELLING THE CORTICAL AND CANCELLOUS BONE ADAPTATION PROCESS

W. R. Taylor & S. E. Clift

School of Mechanical Engineering, University of Bath, Claverton Down, Bath, UK.

ABSTRACT

Bone remodelling describes the process whereby bone grows and resorbs in response to the mechanical demands placed upon it. It occurs as bone matrix is laid down or removed in layers from the free surfaces of the bone, and allows optimisation of economic and functional requirements of the bone. Under normal loading conditions, this equilibrium process ensures a constant bone mass by continual deposition and resorption of bone matrix at an equal rate. Under exceptional circumstances, for example following the total replacement of a hip, abrupt changes can occur in the long-term functional loading patterns on the bone. As a result, there can be significant changes in local bone mass, sometimes leading to the long term loosening of the prosthesis.

This paper focuses on the modelling of the bone adaptation process. It demonstrates the potential of ABAQUS as a tool for predicting both the changes in bone geometry and density. A simple four element model is examined using loading conditions with a normalised time scale and the *SWELLING parameter is used in a new technique for representing the growth associated with bone remodelling. The User Routine USDFLD is also employed to read the time dependent values of strain rate, used as the stimulus for bone growth. Whilst the magnitude of the results gained are exaggerated for the purpose of emphasis, a method has been devised to enable the modelling of three dimensional bone growth using finite element analysis as an iterative process.

INTRODUCTION

Total Hip Replacement (THR) has become an increasingly standard surgical procedure in recent years, with very high rates of success measured 10 years postoperatively. A small percentage, approximately 5 - 10%, still fail in the longer term due to loosening of the prosthesis. One of the major causes of this is an effect called stress shielding, which involves the bone that surrounds the implant resorbing from the surface of the implant, leading to pain

caused by small movements of the prosthesis, and ultimately loosening of the new joint. Predictions of the growth patterns that occur in these circumstances will lead to prosthesis design improvements, reducing the need for revision hip operations.

Bone is a remarkable biological material that fulfils a multitude of physiological requirements. Whilst providing the fundamental strength for stanchion, bone also protects internal organs and supplies the leverage to allow muscular action and hence locomotion. Macroscopically, bone appears in two forms. Cortical bone forms the stiff exterior surface or cortex of all vertebral bones. It is deposited in layers, creating one of the body's stiffest substances, and is a key component of structural support. Cancellous or spongy bone is a softer less dense bone found within the cavities of the long bones, and appears as a honeycomb type network (Figure 1).

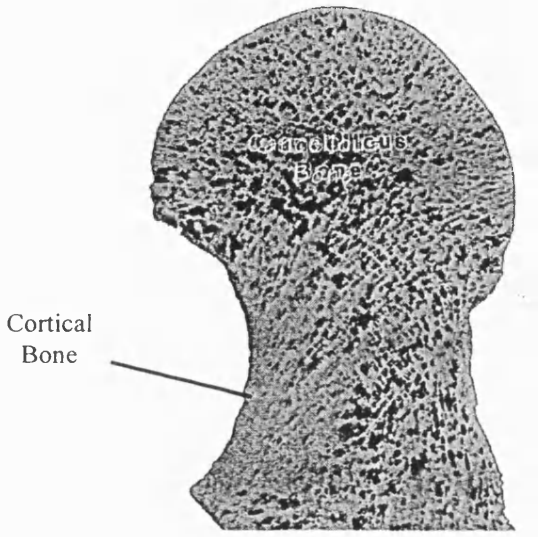

Figure 1 : Slice through femoral head showing both cortical and cancellous bone [Bouvier 1989]

Bone has the ability of self-adaptation to the mechanical demands placed upon it. It is able to both grow and resorb in order to maintain equilibrium between conflicting factors. Large bones are stronger with greater failure loads. Small bones, on the other hand, have a low maintenance cost and require little energy for locomotion and are hence lighter and allow faster movement [Currey 1984]. Bone mass in vertebrates is thus maintained in an equilibrium state, according to the mechanical demands made upon it, by the continual growth and removal of bone matrix from the free surfaces of the bone. This process is called Bone Remodelling and is a direct result of the activity of cells called Osteoclasts and Osteoblasts, which deposit and excavate the bone matrix in response to the changing mechanical stimulus. Whilst the exact form of the remodelling stimulus remains the subject of investigation, it is thought to be some function of strain rather than stress [Carter 1984].

Under 'normal' physiological conditions, the activities of Osteoclastic and Osteoblastic cells are approximately equal, causing no net gain or loss of bone. However, if a change in activity causes a sufficient change in loading conditions from the normal, this biological or remodelling stimulus preferentially activates the rate of the remodelling cells. As a direct result, the balance between bone deposition and resorption is proportionately altered and the overall result is a local gain or loss in bone mass (Figure 2). The resulting change in mass of the bone therefore alters the strain patterns within by the bone, and remodelling continues

until such time as the remodelling stimulus is altered to within the physiologically 'normal' range.

This effect is especially prominent in patients who are subjected to long periods of bed rest where both muscle wastage and bone loss occur, due to the reduction in functional loading. In the case of patients who have experienced THR, the shaft of the implant hides or shields the surrounding bone from its functional loading, causing resorption to occur [Cohen and Rushton, 1995]. This often leads to aseptic loosening of the prosthesis, one of the major causes of long-term failure of implants.

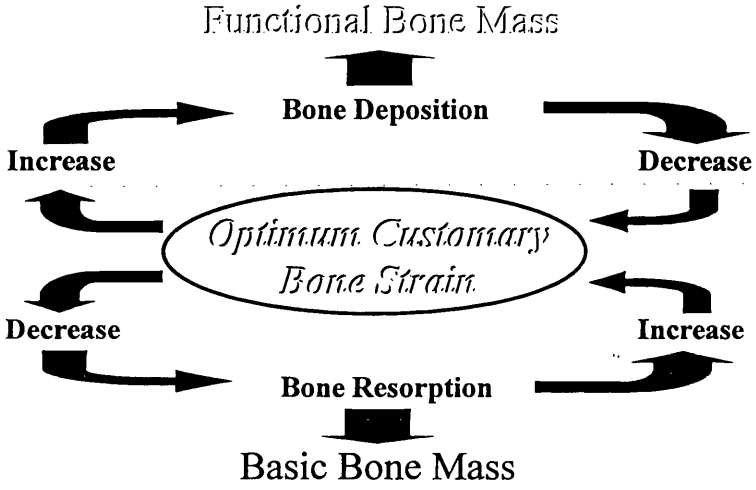

Figure 2 : Functional Bone Remodelling Diagram [Lanyon 1981]

Few previous models have attempted to represent this process of bone growth either in three dimensions or as an iterative process. Van Rietbergen *et al.* [1993] modelled the bone adaptation process in canine femurs using finite element analysis and gained results for the prediction of the change in cortical area and medullary bone fraction. Single iterations were used due to the requirement for mesh refinement.

This study presents the use of the ABAQUS swelling parameter in a new method for modelling the bone adaptation process. Swelling is a phenomenon associated with the change in volume of a solid through the absorption of moisture or surrounding fluid. When taken in a mathematical context, the idea of swelling is simply a measured physical change in volume in response to any quantity or parameter. This paper demonstrates that the growth of bone associated with biological remodelling can be modelled simply by using the Finite Element Method (FEM) and imposing standard swelling strains. In addition, cancellous bone remodelling is calculated using the same coded routines.

MODELLING METHOD

The basic model for the development of the finite element remodelling algorithm code was created using the ABAQUS software. It consisted of four 20 noded cubic elements in a quarter circle construction, using symmetry in the boundary conditions to represent the effect of a full circle. The loading was simply applied on the upper surface of the model, with solid surface support on the lower (Figure 3).

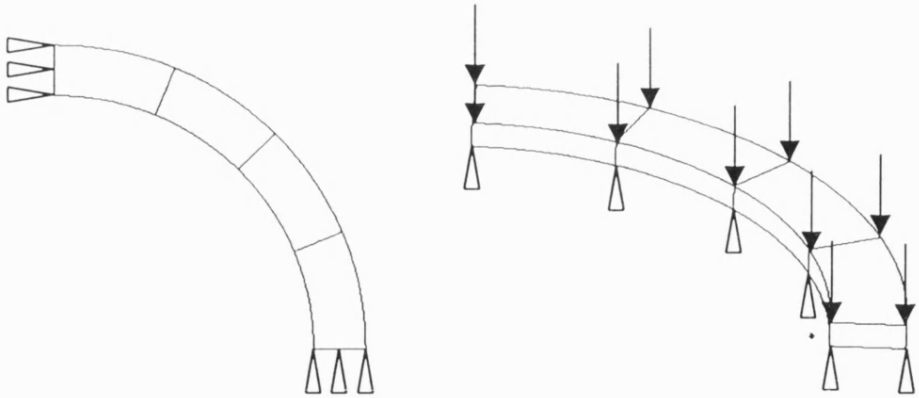

Figure 3 : Basic Element Model, Showing Loading and Boundary Conditions

Any progressive growth pattern will continually change the localised geometry and hence mechanical loading conditions. In order to ensure accuracy in the bone model, an iterative solution is needed. Each element must therefore recalculate its growth requirement at every loading step. In addition, the loading patterns placed upon bone under normal physiological loading conditions are highly complex. Different loading regimes can be seen for every action and position of the skeleton [Cheal *et al* 1992]. To allow for this form of repeated strain stimulated growth, a multiple loading case procedure was constructed, as shown in Figure 4.

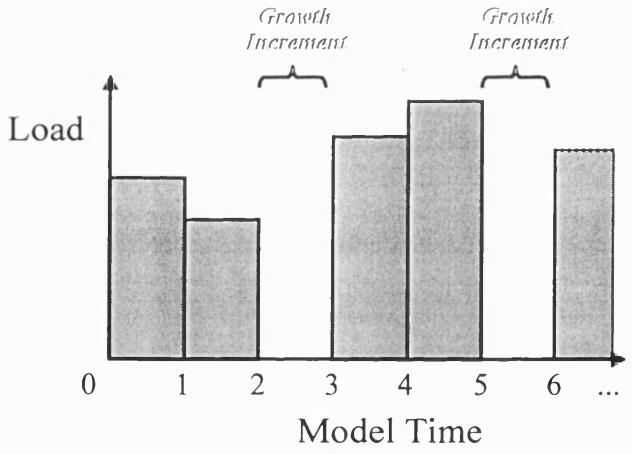

Figure 4 : Model Loading History Diagram

This method of loading involves a number of equal time increments, N+1, per step, (shown as three per step in Figure 4) in which each of the increments imposes the boundary conditions associated with a different set of physiological loading conditions. These loading conditions can vary over each stage, but are only applied over N increments. The final increment in each step is a 'Growth Increment' in which no load is applied, but the growth requirements from the previous increments are calculated and the growth routine is implemented by making the *SWELLING card active. The elements thus swell or 'grow' accordingly. In this manner, the final increment can become equivalent to sleeping and rest

periods, dependent upon the modelling time scale. It must be noted that the loads are all of a unit time, since the *SWELLING routine imposes a time scale which may not be appropriate to the cyclic nature of the loading regime. In this manner, normalisation of the time scale removes the 'rate' from the swelling expansion.

In order for the elements to calculate their local growth requirement, a parameter called the 'Remodelling Stimulus' is determined during the loading increments using the User Subroutine USDFLD. This is a mechanical parameter which gives a quantitative measure of the remodelling requirement produced biologically within the bone. It was decided that *strain rate* should be the mechanical remodelling stimulus [O'Connor *et al.* 1982]; since the time scale on the loading history was normalised, simple strain could be read. Problems arose, however, since enlargement of the elements through the *SWELLING parameter was induced by applying swelling strains to the elements. The strain determined in the following increments therefore included both the strain due to the imposed load and the strain due the previous swelling growth. The calculated value thus became self-perpetuating and increased exponentially. The remodelling stimulus was therefore taken as the difference between the swelling growth induced strain and the load strain. This was equivalent to the inelastic strain.

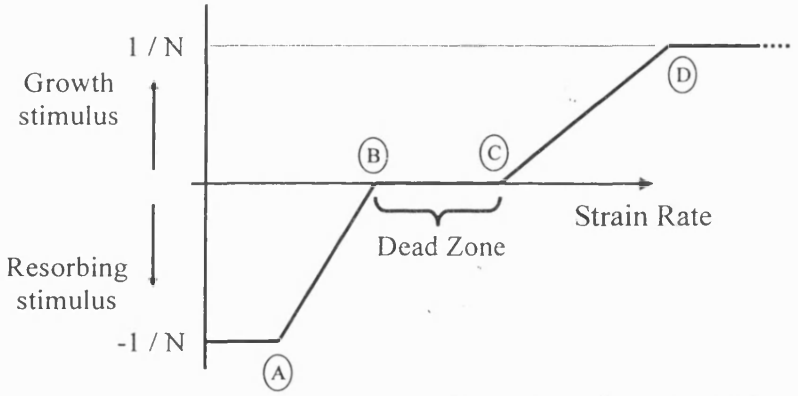

Figure 5 : Trilinear Remodelling Curve

Since an iterative growth solution was required, the utility routine GETVRM was used to access the values of the inelastic strain for each element at the start of each increment. Once these were retrieved they were converted into principal values using the UMAT subroutine SPRIND. A magnitude value was then determined and a remodelling curve was created to convert this value into the Remodelling Stimulus, shown in Figure 5.

The Dead Zone in figure 5 represents the period in which the loading conditions are at physiological equilibrium and no preferential remodelling occurs. If the functional loading on the local bone area increased from this normal dead zone position (towards point D) then a positive growth stimulus would be obtained to a maximum value of 1/N, where N is the number of loading increments. Likewise, after a reduction in load (towards point A), a resorbing stimulus is obtained, to a maximum of –1/N. In this manner, the greatest remodelling stimulus value possible when summed over the whole the step is ± 1. A strain rate constant allows this to be converted into a maximum percentage growth, and hence the rate of model growth can be controlled for both accuracy and convergence criteria. Points A to D were defined in the code, to allow alteration of the remodelling scale.

The stimuli values for each loading increment were retained as State Variables for memory from one increment to the next, but the final Growth Stimulus was saved as a Field Variable and passed into the *SWELLING option. Since the Strain Rate Constant multiplied

by the remodelling stimulus correctly defined the percentage growth required, the swelling parameters were derived from linear correlation (Figure 6). A Field Variable of zero magnitude was passed to the *SWELLING card during the loading increments to ensure no expansion occurred until the final Growth Increment.

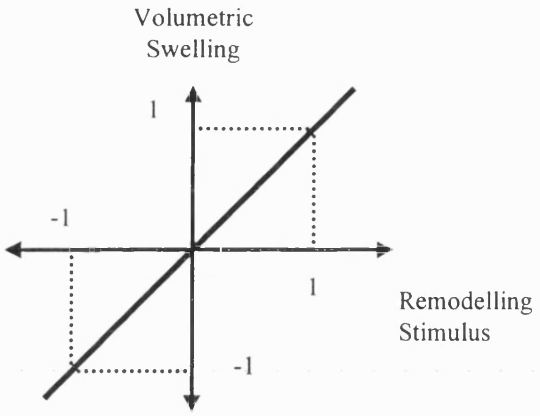

Figure 6 : Swelling Growth Parameters

The swelling subroutine enlarged elements in all three directions, so use of the *RATIOS parameter became essential to ensure unidirectional expansion of the elements. In this manner, growth normal to the free surface could be defined. The elements were initially defined using the OFFSET TO NODES option on the *ORIENTATION card, specifying expansion through the centre nodes, normal to the direction of growth.

RESULTS AND DISCUSSION

Growth of the elements was achieved normal to the free surface in response to the applied loading. The growth occurred in the third increment of each step and continued in progressively decreasing amounts until the Remodelling Stimulus in the elements had entered the Dead Zone period of the curve (Figure 5), and no more expansion occurred. The results of the final growth pattern can be seen below, in Figure 7, where the original model is shown in the lighter shade, and the growth region is shown darker.

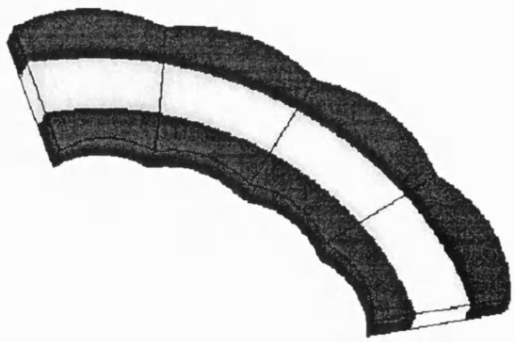

Figure 7 : Preliminary Results of Swelling Growth (cf. Figure 3)

It is clear that the growth of the model was incorrect since smooth expansion of the surfaces should have been achieved. Examination of the results showed that the calculation of the direction of growth was inadequate. Each element had a total of 27 material integration points where the *SWELLING card calculated the magnitude and direction of growth. The OFFSET TO NODES option on the *ORIENTATION card gave each of these points an identical growth direction, which caused the 'rippling' effect.

As a direct result, the ORIENTATION subroutine was used to determine the expansion direction for each material point. Vectors defining the four edges of the element in the direction of growth were derived from the co-ordinates of the corner nodes (Figure 8). This allows the code to be valid for both eight and twenty noded brick elements.

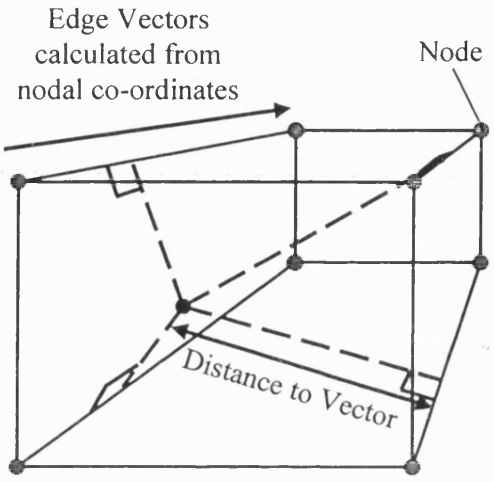

Figure 8 : Calculation of growth direction for each material point

The perpendicular distance from the material point to each edge vector was calculated, giving the material point direction vector :

$$\text{Material Point Direction Vector} = \sum \frac{\text{Edge Vectors}}{\text{Distance to Vectors}}$$

In this manner, every material calculation point had its own growth direction. The results are shown below in Figure 9 where, again, the light areas show the original model.

Figure 9 : Final growth of elements using orientation subroutine

This model demonstrated correct growth patterns and is supported by the growth results shown in Figure 10. The graph shows the growth stages of one of the models' elements. Each peak represents the swelling applied during the growth increments of the loading history. The peaks decrease exponentially as the growth of the model reduces the material strains seen by the applied loading conditions. This produces the self-regulating growth patterns described in Figure 2.

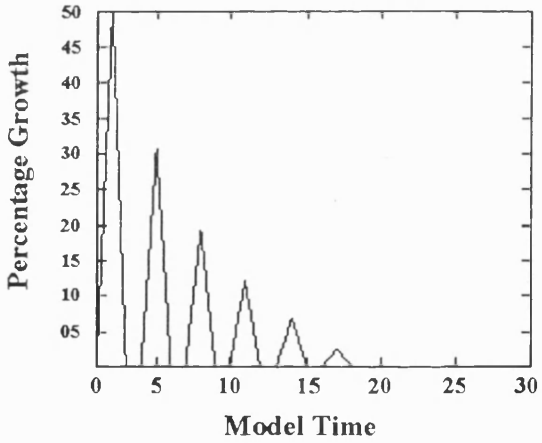

Figure 10 : Graph of Percentage Growth vs Model Time

CANCELLOUS BONE REMODELLING

One of the most promising aspects of this research is the simplicity with which cancellous bone remodelling can be incorporated into the code. On a macro scale, the remodelling of cancellous bone is equivalent to an increase in density of the bone. By using a density constant rather than the strain rate constant, the same code (subroutine USDFLD) can be used to calculate the remodelling stimulus for the Cancellous bone. During the Growth Increment, the Field Variable for the cancellous bone simply varies the Young's Modulus of the material by using the dependencies option of the *ELASTIC card. The two materials are therefore able to use the same remodelling routines, and calculate iterative solutions entirely within

ABAQUS. This allows relatively simple modelling and very fast running times for what can be considered a highly complex biological material.

CONCLUSSIONS

This study has demonstrated that modelling of highly complex bone growth patterns is possible using the ABAQUS software. Like any model, however, simplifications have been made. The growth orientation is a matter of further investigation, especially when modelling geometries more complex than the one presented here. The continual shape changes that could occur may alter the actual direction required from the one defined originally.

In addition, there is continual discussion concerning the actual mechanical remodelling stimulus that relates to the biological bone growth to the functional loading conditions. In reality, it is probable that the remodelling stimulus is a function of a great number of mechanical signals that all interact in an intricate manner. The code has been constructed in such a way that the calculation of the stimulus may be easily altered, and hence various combinations may be compared with experimental evidence.

It must be noted that the magnitudes of the results gained from this model are not significant since the loads and geometries are unrealistic. The process is being elucidated here, since all the final remodelling parameters will vary according to the animal and the actions being modelled. These values will come from preliminary results of the natural bones under normal physiological conditions, since it can be assumed that these bones are in remodelling equilibrium. The positions of the Dead Zone are thus self-defining from the limiting values of the natural model.

FURTHER WORK

The model described in this paper provides a multitude of possibilities and options for the development of bone growth modelling. Extension of this work is paramount to confirm the technique as a large scale modelling method. Initial investigations will include the validation of the basic model against animal experiments. Collaboration has begun with C.T. Rubin and Y. Qin to test and verify the code against turkey ulna remodelling [Brown et al. 1990].

Further developments to the model are also possible. As mentioned previously, the ORIENTATION subroutine is called as a separate routine, and only calculates the growth direction as an initial parameter. The accuracy of the growth could be improved by re-calculating this direction after the swelling routine has occurred.

The final test of the model will be in application to the human hip model, and predicting both the cortical and cancellous bone changes that occur around a variety of implants.

ACKNOWLEDGEMENTS

The authors would like to thank HKS for the provision of the ABAQUS software package. Valuable discussions with Dr. Greg Starke (University of Capetown, SA) and Matt Warner (University of Bath, UK) are gratefully acknowledged.

REFERENCES

1 BROWN T D, PEDERSEN D R, GRAY M L, BRAND R A and RUBIN C T - Toward an identification of mechanical parameters initiating periosteal remodelling: a combined experimental and analytic approach. Journal of Biomechanics, Volume 23, Number 9, pp 893 – 905, 1990

2 BOUVIER M - The biology and composition of bone. Bone Mechanics. CRC Press Inc, Chapter 1, pp 1 – 13, 1989

3 CARTER D R - Mechanical loading histories and cortical bone remodelling. Calcified Tissue International, Volume 36, S19 – S 24, 1984

4 CHEAL E J, SPECTOR M and HAYES W C - Role of loads and prosthesis material properties on the mechanics of the proximal femur after total hip arthroplasty. Journal of Orthopaedic Research, Volume 10, pp 405 – 422, 1992

5 COHEN B and RUSHTON N - Bone remodelling in the proximal femur after Charnley total hip arthroplasty. Journal of Bone and Joint Surgery, Volume 77-B, Number 5, pp 815 – 819, 1995

6 CURREY J D - What should bones be designed to do? Calcified Tissue International, Volume 36, S7 – S10, 1984

7 LANYON L E - Adaptive mechanics – the skeleton's response to mechanical stress. Mechanical Factors and the Skeleton, John Libbey & Company Ltd. pp 72 – 82, 1981

8 O'CONNOR J A and LANYON L E - The influence of strain rate on adaptive bone remodelling. Journal of Biomechanics, Volume 15, Number 10, pp. 767 – 781, 1982

9 VAN RIETBERGEN B, HUISKES R, WEINANS H, SUMNER DR, TURNER TM, and GALANTE J O - The mechanism of bone remodelling and resorption around press-fitted THA stems. Journal of Biomechanics, Volume 26, Number 4/5, pp. 369 – 382, 1993

A SIMPLE THREE DIMENSIONAL TECHNIQUE FOR ITERATIVELY MODELLING THE CORTICAL AND CANCELLOUS BONE ADAPTATION PROCESS

W. R. Taylor & S. E. Clift

School of Mechanical Engineering, University of Bath, Claverton Down, Bath, UK.

ABSTRACT

Bone remodelling describes the process whereby bone grows and resorbs in response to the mechanical demands placed upon it. It occurs as bone matrix is laid down or removed in layers from the free surfaces of the bone, and allows optimisation of economic and functional requirements of the bone. Under normal loading conditions, this equilibrium process ensures a constant bone mass by continual deposition and resorption of bone matrix at an equal rate. Under exceptional circumstances, for example following the total replacement of a hip, abrupt changes can occur in the long-term functional loading patterns on the bone. As a result, there can be significant changes in local bone mass, sometimes leading to the long term loosening of the prosthesis.

This paper focuses on the modelling of the bone adaptation process. It demonstrates the potential of ABAQUS as a tool for predicting both the changes in bone geometry and density. A simple four element model is examined using loading conditions with a normalised time scale and the *SWELLING parameter is used in a new technique for representing the growth associated with bone remodelling. The User Routine USDFLD is also employed to read the time dependent values of strain rate, used as the stimulus for bone growth. Whilst the magnitude of the results gained are exaggerated for the purpose of emphasis, a method has been devised to enable the modelling of three dimensional bone growth using finite element analysis as an iterative process.

INTRODUCTION

Total Hip Replacement (THR) has become an increasingly standard surgical procedure in recent years, with very high rates of success measured 10 years postoperatively . A small percentage, approximately 5 – 10%, still fail in the longer term due to loosening of the prosthesis. One of the major causes of this is an effect called stress shielding, which involves the bone that surrounds the implant resorbing from the surface of the implant, leading to pain caused by small movements of the prosthesis, and ultimately loosening of the new joint.

Predictions of the growth patterns that occur in these circumstances will lead to prosthesis design improvements, reducing the need for revision hip operations.

Bone is a remarkable biological material that fulfils a multitude of physiological requirements. Whilst providing the fundamental strength for stanchion, bone also protects internal organs and supplies the leverage to allow muscular action and hence locomotion. Macroscopically, bone appears in two forms. Cortical bone forms the stiff exterior surface or cortex of all vertebral bones. It is deposited in layers, creating one of the body's stiffest substances, and is a key component of structural support. Cancellous or spongy bone is a softer less dense bone found within the cavities of the long bones, and appears as a honeycomb-type network (Figure 1).

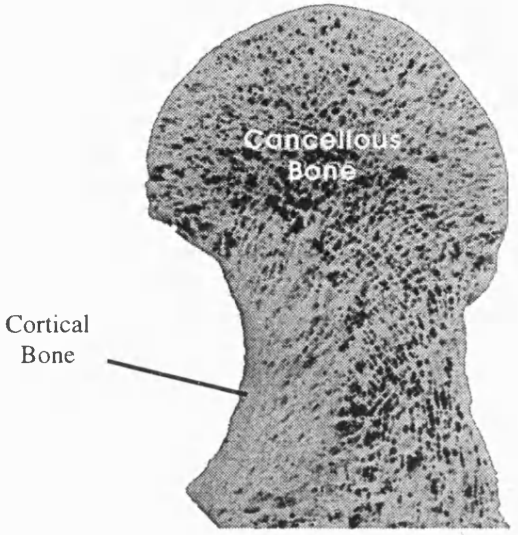

Figure 1 : Slice through femoral head showing both cortical and cancellous bone [Bouvier 1989]

Bone has the ability of self-adaptation to the mechanical demands placed upon it. It is able to both grow and resorb in order to maintain equilibrium between conflicting factors. Large bones are stronger with greater failure loads. Small bones, on the other hand, have a low maintenance cost and require little energy for locomotion and are hence lighter and allow faster movement [Currey 1984]. Bone mass in vertebrates is thus maintained in an equilibrium state, according to the mechanical demands made upon it, by the continual growth and removal of bone matrix from the free surfaces of the bone. This process is called Bone Remodelling and is a direct result of the activity of cells called Osteoclasts and Osteoblasts, which deposit and excavate the bone matrix in response to the changing mechanical stimulus. Whilst the exact form of the remodelling stimulus remains the subject of investigation, it is thought to be some function of strain rather than stress [Carter 1984].

Under 'normal' physiological conditions, the activities of Osteoclastic and Osteoblastic cells are approximately equal, causing no net gain or loss of bone. However, if a change in activity causes a sufficient change in loading conditions from the normal, this biological or remodelling stimulus preferentially activates the rate of the remodelling cells. As a direct result, the balance between bone deposition and resorption is proportionately altered and the overall result is a local gain or loss in bone mass (Figure 2). The resulting change in mass of the bone therefore alters the strain patterns within by the bone, and remodelling continues until such time as the remodelling stimulus is altered to within the physiologically 'normal' range.

This effect is especially prominent in patients who are subjected to long periods of bed rest where both muscle wastage and bone loss occur, due to the reduction in functional loading. In the case of patients who have experienced THR, the shaft of the implant hides or shields the surrounding bone from its functional loading, causing resorption to occur [Cohen and Rushton, 1995]. This often leads to aseptic loosening of the prosthesis, one of the major causes of long-term failure of implants.

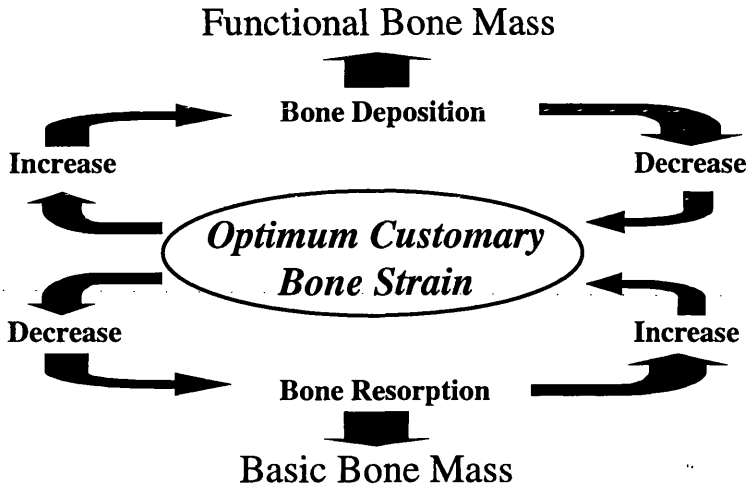

Figure 2 : Functional Bone Remodelling Diagram [Lanyon 1981]

Few previous models have attempted to represent this process of bone growth either in three dimensions or as an iterative process. Van Rietbergen *et al.* [1993] modelled the bone adaptation process in canine femurs using finite element analysis and gained results for the prediction of the change in cortical area and medullary bone fraction. Single iterations were used due to the requirement for mesh refinement.

This study presents the use of the ABAQUS swelling parameter in a new method for modelling the bone adaptation process. Swelling is a phenomenon associated with the change in volume of a solid through the absorption of moisture or surrounding fluid. When taken in a mathematical context, the idea of swelling is simply a measured physical change in volume in response to any quantity or parameter. This paper demonstrates that the growth of bone associated with biological remodelling can be modelled simply by using the Finite Element Method (FEM) and imposing standard swelling strains. In addition, cancellous bone remodelling is calculated using the same coded routines.

MODELLING METHOD

The basic model for the development of the finite element remodelling algorithm code was created using the ABAQUS software. It consisted of four 20 noded cubic elements in a quarter circle construction, using symmetry in the boundary conditions to represent the effect of a full circle. The loading was simply applied on the upper surface of the model, with solid surface support on the lower (Figure 3).

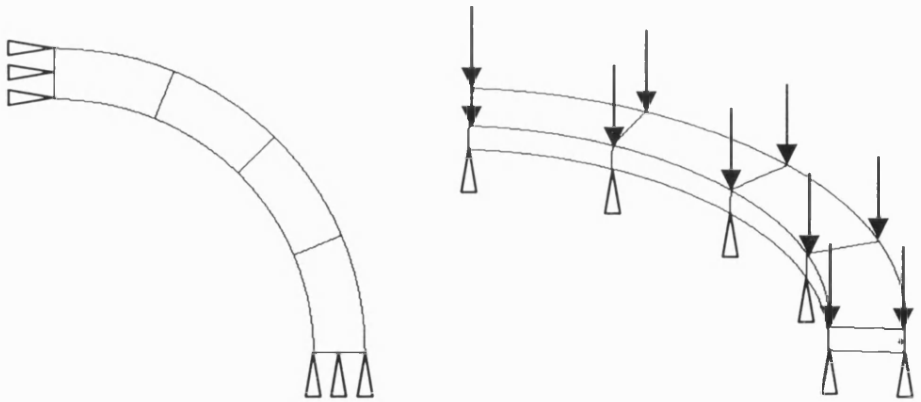

Figure 3 : Basic Element Model, Showing Loading and Boundary Conditions

Any progressive growth pattern will continually change the localised geometry and hence mechanical loading conditions. In order to ensure accuracy in the bone model, an iterative solution is needed. Each element must therefore recalculate its growth requirement at every loading step. In addition, the loading patterns placed upon bone under normal physiological loading conditions are highly complex. Different loading regimes can be seen for every action and position of the skeleton [Cheal *et al* 1992]. To allow for this form of repeated strain stimulated growth, a multiple loading case procedure was constructed, as shown in Figure 4.

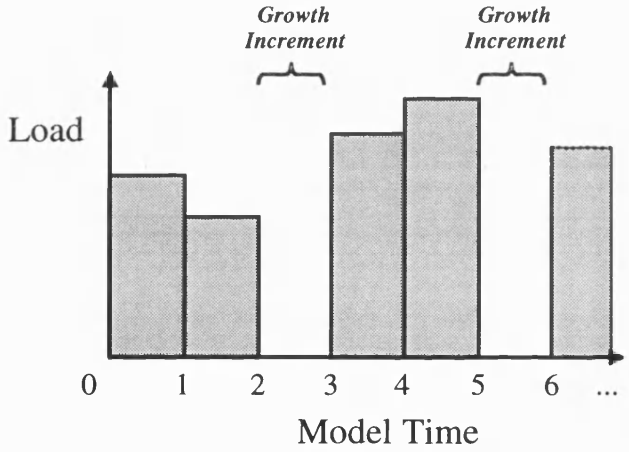

Figure 4 : Model Loading History Diagram

This method of loading involves a number of equal time increments, N+1, per step, (shown as three per step in Figure 4) in which each of the increments imposes the boundary conditions associated with a different set of physiological loading conditions. These loading conditions can vary over each stage, but are only applied over N increments. The final increment in each step is a 'Growth Increment' in which no load is applied, but the growth requirements from the previous increments are calculated and the growth routine is implemented by making the *SWELLING card active. The elements thus swell or 'grow' accordingly. In this manner, the final increment can become equivalent to sleeping and rest periods, dependent upon the modelling time scale. It must be noted that the loads are all of a unit time, since the *SWELLING routine imposes a time scale which may not be appropriate to the cyclic nature of the loading regime. In this manner, normalisation of the time scale removes the 'rate' from the swelling expansion.

In order for the elements to calculate their local growth requirement, a parameter called the 'Remodelling Stimulus' is determined during the loading increments using the User Subroutine USDFLD. This is a mechanical parameter which gives a quantitative measure of the remodelling requirement produced biologically within the bone. It was decided that *strain rate* should be the mechanical remodelling stimulus [O'Connor *et al.* 1982]; since the time scale on the loading history was normalised, simple strain could be read. Problems arose, however, since enlargement of the elements through the *SWELLING parameter was induced by applying swelling strains to the elements. The strain determined in the following increments therefore included both the strain due to the imposed load and the strain due the previous swelling growth. The calculated value thus became self-perpetuating and increased exponentially. The remodelling stimulus was therefore taken as the difference between the swelling growth induced strain and the load strain. This was equivalent to the inelastic strain.

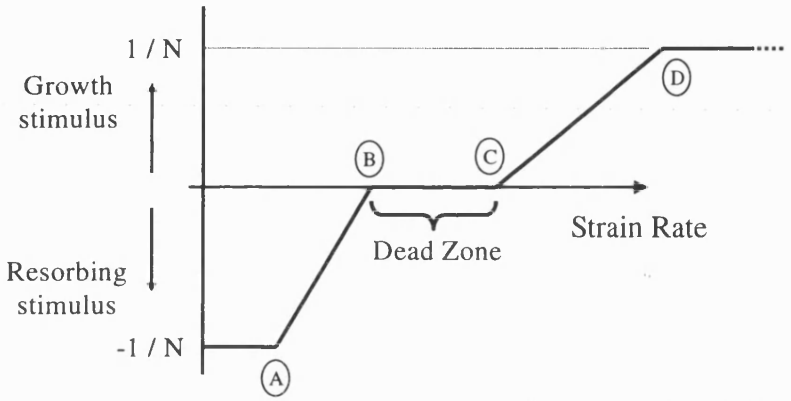

Figure 5 : Trilinear Remodelling Curve

Since an iterative growth solution was required, the utility routine GETVRM was used to access the values of the inelastic strain for each element at the start of each increment. Once these were retrieved they were converted into principal values using the UMAT subroutine SPRIND. A magnitude value was then determined and a remodelling curve was created to convert this value into the Remodelling Stimulus, shown in Figure 5.

The Dead Zone in figure 5 represents the period in which the loading conditions are at physiological equilibrium and no preferential remodelling occurs. If the functional loading on the local bone area increased from this normal dead zone position (towards point D) then a positive growth stimulus would be obtained to a maximum value of 1/N, where N is the number of loading increments. Likewise, after a reduction in load (towards point A), a resorbing stimulus is obtained, to a maximum of –1/N. In this manner, the greatest remodelling stimulus value possible when summed over the whole the step is ± 1. A strain rate constant allows this to be converted into a maximum percentage growth, and hence the rate of model growth can be controlled for both accuracy and convergence criteria. Points A to D were defined in the code, to allow alteration of the remodelling scale.

The stimuli values for each loading increment were retained as State Variables for memory from one increment to the next, but the final Growth Stimulus was saved as a Field Variable and passed into the *SWELLING option. Since the Strain Rate Constant multiplied by the remodelling stimulus correctly defined the percentage growth required, the swelling parameters were derived from linear correlation (Figure 6). A Field Variable of zero magnitude was passed to the *SWELLING card during the loading increments to ensure no expansion occurred until the final Growth Increment.

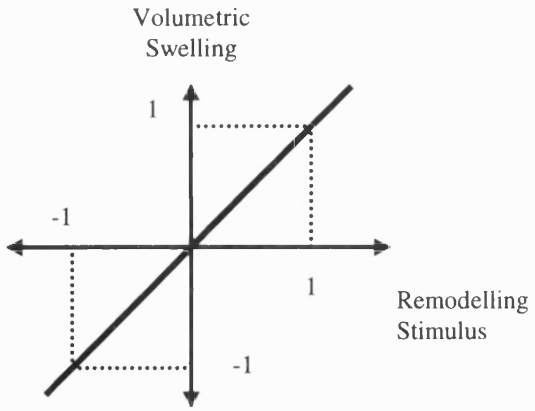

Figure 6 : Swelling Growth Parameters

The swelling subroutine enlarged elements in all three directions, so use of the *RATIOS parameter became essential to ensure unidirectional expansion of the elements. In this manner, growth normal to the free surface could be defined. The elements were initially defined using the OFFSET TO NODES option on the *ORIENTATION card, specifying expansion through the centre nodes, normal to the direction of growth.

RESULTS AND DISCUSSION

Growth of the elements was achieved normal to the free surface in response to the applied loading. The growth occurred in the third increment of each step and continued in progressively decreasing amounts until the Remodelling Stimulus in the elements had entered the Dead Zone period of the curve (Figure 5), and no more expansion occurred. The results of the final growth pattern can be seen below, in Figure 7, where the original model is shown in the lighter shade, and the growth region is shown darker.

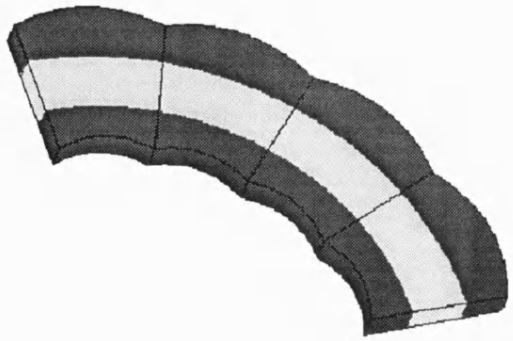

Figure 7 : Preliminary Results of Swelling Growth (cf. Figure 3)

It is clear that the growth of the model was incorrect since smooth expansion of the surfaces should have been achieved. Examination of the results showed that the calculation of the direction of growth was inadequate. Each element had a total of 27 material integration points where the *SWELLING card calculated the magnitude and direction of growth. The OFFSET TO NODES option on the *ORIENTATION card gave each of these points an identical growth direction, which caused the 'rippling' effect.

As a direct result, the ORIENTATION subroutine was used to determine the expansion direction for each material point. Vectors defining the four edges of the element in the direction of growth were derived from the co-ordinates of the corner nodes (Figure 8). This allows the code to be valid for both eight and twenty noded brick elements.

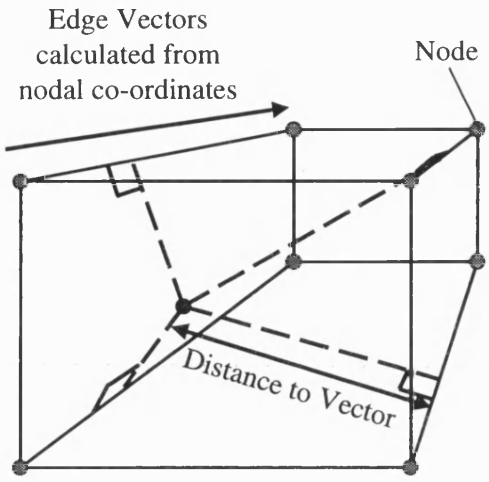

Figure 8 : Calculation of growth direction for each material point

The perpendicular distance from the material point to each edge vector was calculated, giving the material point direction vector :

$$\text{Material Point Direction Vector} = \sum \frac{\text{Edge Vectors}}{\text{Distance to Vectors}}$$

In this manner, every material calculation point had its own growth direction. The results are shown below in Figure 9 where, again, the light areas show the original model.

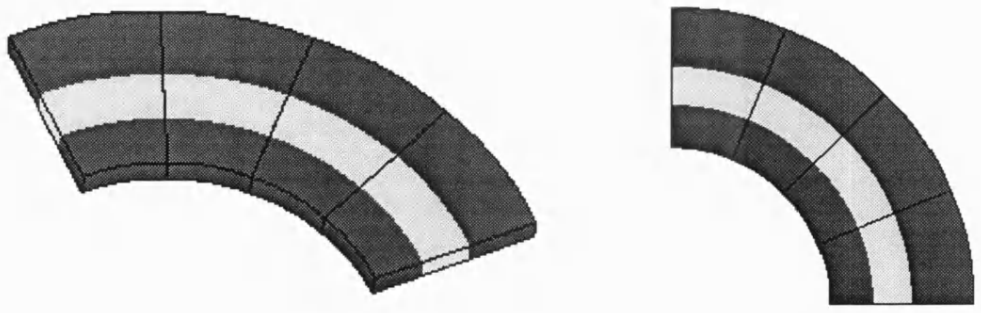

Figure 9 : Final growth of elements using orientation subroutine

This model demonstrated correct growth patterns and is supported by the growth results shown in Figure 10. The graph shows the growth stages of one of the models' elements. Each peak represents the swelling applied during the growth increments of the loading history. The

peaks decrease exponentially as the growth of the model reduces the material strains seen by the applied loading conditions. This produces the self-regulating growth patterns described in Figure 2.

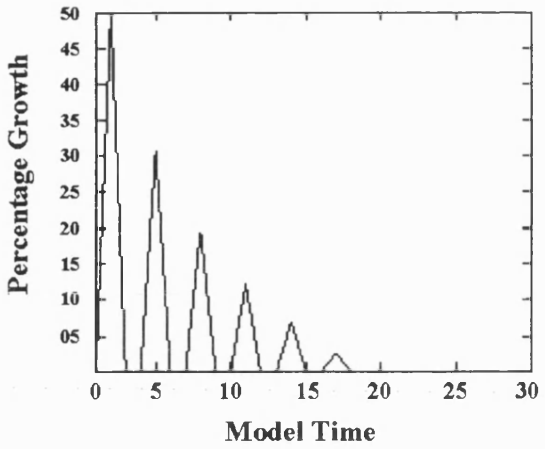

Figure 10 : Graph of Percentage Growth vs Model Time

CANCELLOUS BONE REMODELLING

One of the most promising aspects of this research is the simplicity with which cancellous bone remodelling can be incorporated into the code. On a macro scale, the remodelling of cancellous bone is equivalent to an increase in density of the bone. By using a density constant rather than the strain rate constant, the same code (subroutine USDFLD) can be used to calculate the remodelling stimulus for the Cancellous bone. During the Growth Increment, the Field Variable for the cancellous bone simply varies the Young's Modulus of the material by using the dependencies option of the *ELASTIC card. The two materials are therefore able to use the same remodelling routines, and calculate iterative solutions entirely within ABAQUS. This allows relatively simple modelling and very fast running times for what can be considered a highly complex biological material.

CONCLUSSIONS

This study has demonstrated that modelling of highly complex bone growth patterns is possible using the ABAQUS software. Like any model, however, simplifications have been made. The growth orientation is a matter of further investigation, especially when modelling geometries more complex than the one presented here. The continual shape changes that could occur may alter the actual direction required from the one defined originally.

In addition, there is continual discussion concerning the actual mechanical remodelling stimulus that relates to the biological bone growth to the functional loading conditions. In reality, it is probable that the remodelling stimulus is a function of a great number of mechanical signals that all interact in an intricate manner. The code has been constructed in such a way that the calculation of the stimulus may be easily altered, and hence various combinations may be compared with experimental evidence.

It must be noted that the magnitudes of the results gained from this model are not significant since the loads and geometries are unrealistic. The process is being elucidated here, since all the final remodelling parameters will vary according to the animal and the actions being modelled. These values will come from preliminary results of the natural bones under normal physiological conditions, since it can be assumed that these bones are in remodelling equilibrium. The positions of the Dead Zone are thus self-defining from the limiting values of the natural model.

FURTHER WORK

The model described in this paper provides a multitude of possibilities and options for the development of bone growth modelling. Extension of this work is paramount to confirm the technique as a large scale modelling method. Initial investigations will include the validation of the basic model against animal experiments. Collaboration has begun with C.T. Rubin and Y. Qin to test and verify the code against turkey ulna remodelling [Brown et al. 1990].

Further developments to the model are also possible. As mentioned previously, the ORIENTATION subroutine is called as a separate routine, and only calculates the growth direction as an initial parameter. The accuracy of the growth could be improved by re-calculating this direction after the swelling routine has occurred.

The final test of the model will be in application to the human hip model, and predicting both the cortical and cancellous bone changes that occur around a variety of implants.

ACKNOWLEDGEMENTS

The authors would like to thank HKS for the provision of the ABAQUS software package. Valuable discussions with Dr. Greg Starke (University of Capetown, SA) and Matt Warner (University of Bath, UK) are gratefully acknowledged.

REFERENCES

1 BROWN T D, PEDERSEN D R, GRAY M L, BRAND R A and RUBIN C T - Toward an identification of mechanical parameters initiating periosteal remodelling: a combined experimental and analytic approach. Journal of Biomechanics, Volume 23, Number 9, pp 893 – 905, 1990

2 BOUVIER M - The biology and composition of bone. Bone Mechanics. CRC Press Inc, Chapter 1, pp 1 – 13, 1989

3 CARTER D R - Mechanical loading histories and cortical bone remodelling. Calcified Tissue International, Volume 36, S19 – S 24, 1984

4 CHEAL E J, SPECTOR M and HAYES W C - Role of loads and prosthesis material properties on the mechanics of the proximal femur after total hip arthroplasty. Journal of Orthopaedic Research, Volume 10, pp 405 – 422, 1992

5 COHEN B and RUSHTON N - Bone remodelling in the proximal femur after Charnley total hip arthroplasty. Journal of Bone and Joint Surgery, Volume 77-B, Number 5, pp 815 – 819, 1995

6 CURREY J D - What should bones be designed to do? Calcified Tissue International, Volume 36, S7 – S10, 1984

7 LANYON L E - Adaptive mechanics – the skeleton's response to mechanical stress. Mechanical Factors and the Skeleton, John Libbey & Company Ltd. pp 72 – 82, 1981

8 O'CONNOR J A and LANYON L E - The influence of strain rate on adaptive bone remodelling. Journal of Biomechanics, Volume 15, Number 10, pp. 767 – 781, 1982

9 VAN RIETBERGEN B, HUISKES R, WEINANS H, SUMNER DR, TURNER TM, and GALANTE J O - The mechanism of bone remodelling and resorption around press-fitted THA stems. Journal of Biomechanics, Volume 26, Number 4/5, pp. 369 – 382, 1993